UNIVERSITY OF LEEDS

Continuous Flow Platforms for the Synthesis and Optimisation of Polymeric Materials via RAFT Polymerisation

Sam Parkinson

Submitted in accordance with the requirements for the degree of PhD Chemical Engineering

The University of Leeds

Faculty of Engineering

School of Chemical and Process Engineering

March 2020

Intellectual Property

The candidate confirms that the work submitted is his own, except where work which has formed part of jointly authored publications has been included. The contribution of the candidate and the other authors to this work has been explicitly indicated below. The candidate confirms that appropriate credit has been given within the thesis where reference has been made to the work of others.

The work in Chapter 2 has appeared in: S. T. Knox, **S. Parkinson**, R. Stone and N. J. Warren, *Polym. Chem.*, 2019, 10, 4774-4778. STK and SP contributed to the development of online NMR protocols. The contribution from other authors was performing experiments (STK and RS) and project supervision (NW)

The work in Chapter 3 has appeared in: **S. Parkinson**, N. S. Hondow, J. S. Conteh, R. A. Bourne and N. J. Warren, *React. Chem. Eng.*, 2019,4, 852-861. SP was responsible for performing all experiments and analysis (except TEM). The contribution from other authors was preliminary experiments (JSC), TEM analysis (NSH) and project supervision (NW, RAB)

The work in Chapter 4 has appeared in: **S. Parkinson**, S. T. Knox, R. A. Bourne, N. J. Warren, *Polym. Chem.*, 2020, 20, 3465-3474. SP was responsible for performing all experiments and subsequent analysis of polymers. The contribution from other authors were manuscript writing (STK) and project supervision (NW, RAB)

Acknowledgements

Firstly, I would like to thank my academic supervisors Nick Warren and Richard Bourne for all the guidance and opportunities afforded to me throughout my PhD. Secondly, I'd like to thank everyone I've worked with in the lab throughout my PhD particularly, Calum & Andy in my early PhD years and Charlotte & Ste at the end of my PhD.

Ste, its easy to say that the last years of my PhD would've been much less enjoyable if you hadn't joined the group. My personal highlight is you getting Nick to send me with you to a conference in Germany. All our loud chats about work or (mostly) other topics really helped during the very slow times at end of my PhD. I've never met someone so organised and efficient (and enjoys admin so much!).

Thanks to David, Dewi, Laura, Pete and Charlotte for putting up with me always coming to your offices and distracting you all because I was bored. Especially towards the end of my PhD when I would start bragging that I was bored because my flow 'robot' was doing all my work for me.

Finally, thanks to my family for all their support. Thanks to Mum and Dad for always being so supportive and willing to do anything for me even through your very difficult times.

Abstract

This thesis focuses on the development and use of continuous flow platforms to perform the synthesis and subsequent chain extension of poly(dimethylacrylamide) (PDMAm), via reversible addition fragmentation chain transfer (RAFT) polymerisation, in order to obtain a range of polymeric nanoparticles. Initially, a stainless-steel flow reactor was developed and polymerisation kinetics were obtained for all RAFT polymerisations in both batch and flow reactors. Whilst good control over the polymerisations were observed for both batch and flow reactors slightly accelerated kinetics were observed in flow reactors. A range of poly(dimethylacrylamide)-poly(diacetone acrylamide) based polymerics nanoparticles were then synthesised in the flow reactor. A series of spherical micelles were successfully formed with particle size increasing with PDAAm DP. However, significant fouling was observed during the synthesis of higher order morphologies and no pure phases were obtained. A PFA flow reactor was then developed for synthesising higher order polymeric nanoparticles. At the same time polymerisation kinetics were also accelerated by using an initiator (VA-044) with a significantly higher rate of decomposition. In order to more easily monitor the accelerated reaction kinetics a benchtop NMR was placed at the reactor outlet to allow for continuous online monitoring of the polymerisation. A series of PDMAm-PDAAm spherical nanoparticles were successfully synthesised in the flow reactor in 20 minutes. When targeting higher order morphologies sphere/worm and worm/vesicle mixed phases were succesfully formed. Pure vesicle phases were only formed when high PDAAm DP (> 200) were targeted due to limited chain mobility and poor mixing in the flow reactor. Finally, an automated flow reactor platform that incorporated NMR and GPC was developed and used to monitor and screen reaction conditions for the RAFT solution polymerisations of dimethylacrylamide (DMAm) and *tert*-butylacrylamide. Furthermore, incorporation of an advanced machine learning algorithm (TS-EMO) allowed simultaneous self-optimisation of these polymerisations for both conversion and dispersity.

Contents

List of Figures

Abbreviations

ACVA	4,4-azobis(4-cyanovaleric acid)
AIBN	azobis(isobutyronitrile)
ATRP	atom transfer radical polymerisation
BHT	2,6-di-tert-butyl-4-methylphenol
BPR	back pressure regulator
CCTP	3-((((1-carboxyethyl)thio)carbonothioyl)thio)propanoic acid
CSTR	continuous stirred tank reactor
CTA	chain transfer agent
Đ	dispersity
DAAm	diacetone acrylamide
DCTTC	4-((((2-carboxyethyl)thio)carbonothioyl)thio)-4-cyanopentanoic acid
DLS	dynamic light scattering
DMAm	dimethylacrylamide
DMF	dimethylformamide
DoE	design of experiments
DP	degree of polymerisation
FRP	free radical polymerisation
GPC	gel permeation chromatography
HPLC	high performance liquid chromatography
I.D	internal diameter
IR	infra-red
LAM	less activated monomer
LCST	lower critical solution temperature
LHC	latin hyper cube

LiBr	lithium bromide
MAM	more activated monomer
MMA	methyl methacrylate
M_n	number average molecular weight
MOAL	multi objective active learner
M_p	peak molecular weight
M_w	weight average molecular weight
MWD	molecular weight distribution
NIPAm	*N*-isopropyl acrylamide
NMP	nitroxide mediated polymerisation
NMR	nuclear magnetic resonance
NMSIM	Near-Melder Simplex
OVAT	one variable at a time
PBR	packed bed reactor
PDI	polydispersity index
PET-RAFT	photo-electron transfer reversible addition-fragmentation chain transfer
PEEK	poly(etheretherketone)
PFA	perfluoroalkoxy
PISA	polymerisation induced self-assembly
PTFE	poly(tetrafluoroethylene)
OEGMA	oligo(ethylene glycol) methacrylate
RAFT	reversible addition-fragmentation chain transfer
RDRP	reversible-deactivation radical polymerisation
RI	refractive index
RTD	residence time distribution
S/N	signal to noise ratio
S_NAr	aromatic nucleophilic substitution
SNOBFIT	Stable Noisy Optimization by Branch and FIT
STY	space-time yield
$t_{1/2}$	half life
tBuAm	tertiary-butylacrylamide
TEA	triethylamine

TEM	transmission electron microscopy
THF	tetrahydrofuran
TS-EMO	Thompson Sampling Efficient Multi-objective Optimisation
UV-VIS	ultra violet - visible light
VA-044	2,2'-azobis[2-(2-imidazolin-2-yl)propane]dihydrochloride
ZnTTP	zinc tetraphenylporphyrin

Chapter 1

Introduction

1.1 Flow Chemistry

In recent years, flow chemistry has become a viable alternative to traditional batch chemistry.[4] Flow chemistry offers significant advantages over batch chemistry such as: greater heat transfer, more controlled mixing of reagents, better reproducibility, facile scalibility and improved safety.[4] In flow chemistry, a reaction solution is passed through a tubular reactor, often made from stainless steel or polymeric (perfluoroalkoxy - PFA, poly(tetrafluoroethylene) - PTFE, poly(etheretherketone) - PEEK) tubing, although other reactor geometries such as continuous stirred tank reactors (CSTR) have also been used. The reaction then occurs as the material travels through the reactor, reactant concentration therefore changes along the length of flow reactors instead of changing with time like batch reactors (Figure 1.1). Tubular reactors are often divided into two categories, based on the diameter of tubing used, mesofluidic (500 µm to 5 mm) or microfluidic (10 - 500 µm). The choice of reactor system used is largely application based. Mesofluidic devices have less efficient heat transfer and mixing but are not as prone to blockages and allow for a greater throughput of material, therefore generally have applications where large quantities of material are required.

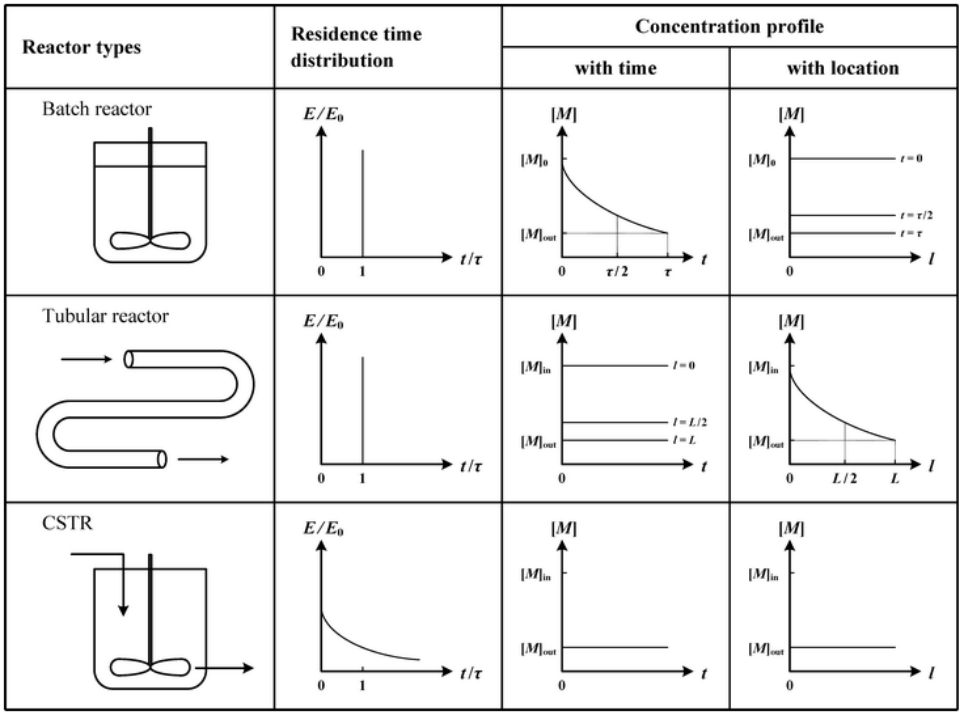

Figure 1.1: Residence time distribution and concentration profiles observed in different types of chemical reactors.[1] Reproduced with permission.

1.1.1 Mixing

Mixing is a diffusion based process and the time to achieve full mixing is therefore proportional to the distance solutions must diffuse across. In a tubular flow reactor, mixing occurs continuously and there are three distinct types of flow regime that affect the mixing: laminar, transient and turbulent (Figure 1.2).[33] Laminar flow is where fluid flows in parallel layers with no disruption between layers. Mixing is poorest in this regime as it has the lowest surface area between layers. Turbulent flow is a much more chaotic regime where small eddie currents form. Turbulent flows have the fastest mixing due to the high surface area between fluid layers in these eddies. Transient flow is the regime between laminar and turbulent, as such it has characteristics of both regimes. The type of flow regime can be determined by calculating the Reynolds number of the system (equation 1.1).[34]

$$Re = \frac{\rho \nu L}{\mu} \tag{1.1}$$

The Reynolds number is a dimensionless parameter that is related to the density (ρ), velocity (ν), viscosity (μ) of a fluid and the channel length (L) which it is passing through. Typically, Reynolds numbers < 2300 indicate laminar flow, where the viscous effects of the fluid are dominating, and Reynolds numbers > 2900 are described as turbulent flow, where inertial

forces dominate. Reynolds numbers in between this are transient flows and the specific amount of laminar and turbulent character in the flow varies depending on how close the Reynolds number is to the transitional boundaries.

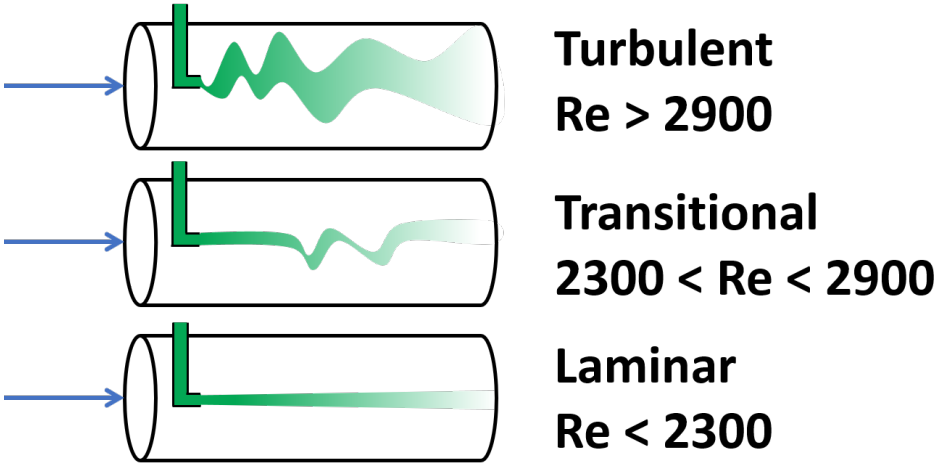

Figure 1.2: Flow profiles typically observed in tubular flow reactors. As Reynolds number increases the flow transitions from laminar to turbulent.

In an ideal tubular reactor all material spends the same amount of time in the reactor.[35] However, tubular reactors do not behave ideally, material flowing close to the wall of the reactor experiences friction from the wall causing a drag effect.[34] This means that the material in the centre of the reactor is flowing faster than the material at the walls. Therefore, as some material is moving faster, all the material will not experience the same residence time, this is described by the residence time distribution (RTD, equation 1.2). Tubular reactor RTDs are affected by variables such as: tubing size, solution viscosity and residence time (Figure 1.3).

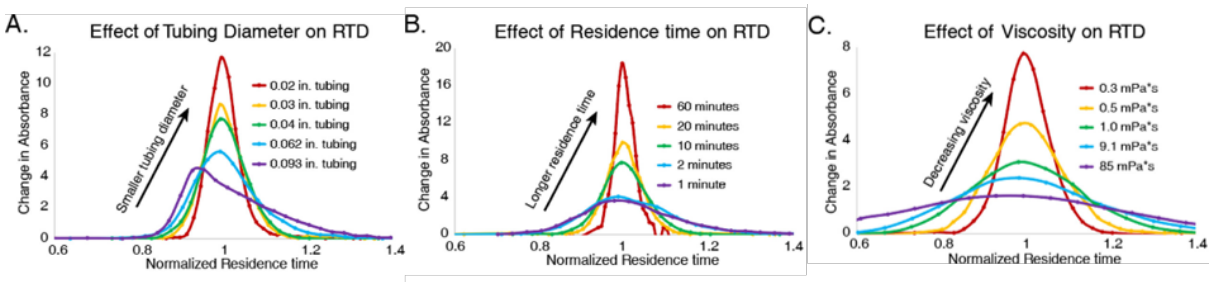

Figure 1.3: Residence time distributions obtained by Reis *et. al.*[2] whilst varying a) tubing diameter, b) residence time and c) solution viscosity. Reproduced with permission.

The residence time distribution of a reactor can be determined experimentally by either injecting a tracer molecule or changing the reaction stream and measuring the change in concentration (C) over time. This can then be converted to give the residence time distribution function, E(t),

which describes in a quantitative manner how much time different fluid elements have spent in the reactor. Using the residence time distribution function the mean residence time, τ, in the reactor can be determined (equation 1.3).

$$E(t) = \frac{C(t)}{\int_0^\infty C(t)dt} \tag{1.2}$$

$$\tau = \int_0^\infty tE(t)dt \tag{1.3}$$

Residence time distribution functions can be used to compare the flow of material in different reactors of similar sizes. However, for the comparison of bigger reactors, E(t) becomes less useful. Therefore, normalised RTD functions ($E(\Theta)$, equation 1.4) and normalised time parameters (Θ, equation 1.5) are often used.

$$E(\Theta) = \tau E(t) \tag{1.4}$$

$$\Theta = \frac{t}{\tau} \tag{1.5}$$

1.1.2 Heat Transfer

When a reactor is heated, the walls of the reactor are initially heated, then conduction or convection transfers heat to the solution inside the reactor. Therefore, the greater the surface area of solution in contact with the reactor walls, the more efficient heating and cooling will be. Excellent thermal control is achieved in flow reactors due to their high surface area to volume ratio (Figure 1.4). The surface area to volume ratio of flow reactors can vary from 10,000 m^{-1} to 50,000 m^{-1} whilst a typical 100 mL round bottom flask has a surface area to volume ratio of less than 1000 m^{-1}. This increased thermal control is ideal for reactions such as nitrations,[36] organometallic alkylations[37] and fluorinations[38] that generate large exotherms, and/or are at risk of thermal runaway and as such have significant safety risks that lead to strict reaction conditions (low temperatures & reactor volumes) when performed in batch.[4,39] Transferring of these reactions to continuous flow processes has allowed for the use of less stringent reaction conditions, due to excellent dispersion of the exotherm as well as, increasing reaction yields.[36–38]

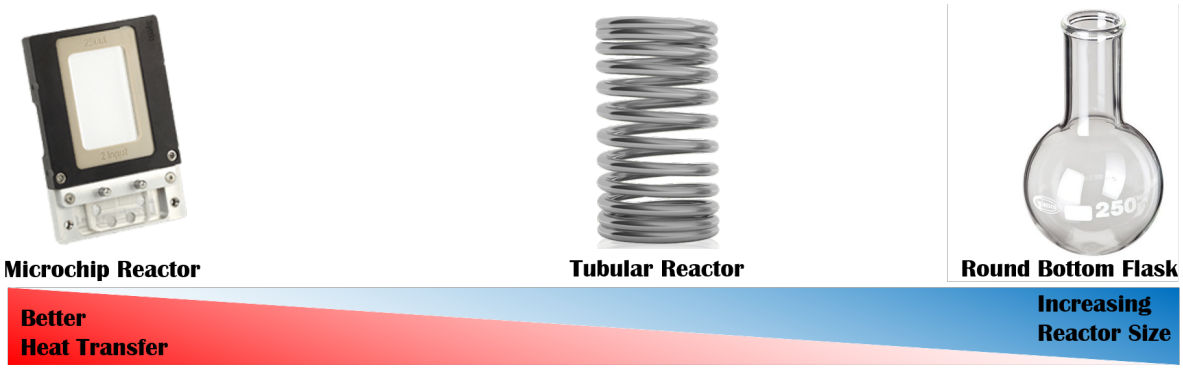

Figure 1.4: Change in volume and heat transfer with different types of reactors.

1.1.3 Safety

The handling of hazardous materials during chemical processes pose significant safety risks, which often limits batch production.[40] For a wide variety of reactions flow chemistry has offered a route to the safe handling and production of these materials.[41] A common safety hazard in batch reactors is the evolution and build up of hazardous or unstable products such as: diazomethane, phosgene and Grignard reagents.[3,37,42,43] In flow chemistry, the small reactor volumes limit the amount of material generated at any given time reducing potential hazards.[44] Additionally, for reactions which generate hazardous intermediates, telescoping of flow reactors allow for instantaneous consumption of intermediates preventing build of such materials (Figure 1.5).[45] For explosive materials the power of any potential explosion is proportional to the cube root of the mass of explosive material.[46] Thus, the small volumes used in flow reactors limits the severity of any potential explosions.[47]

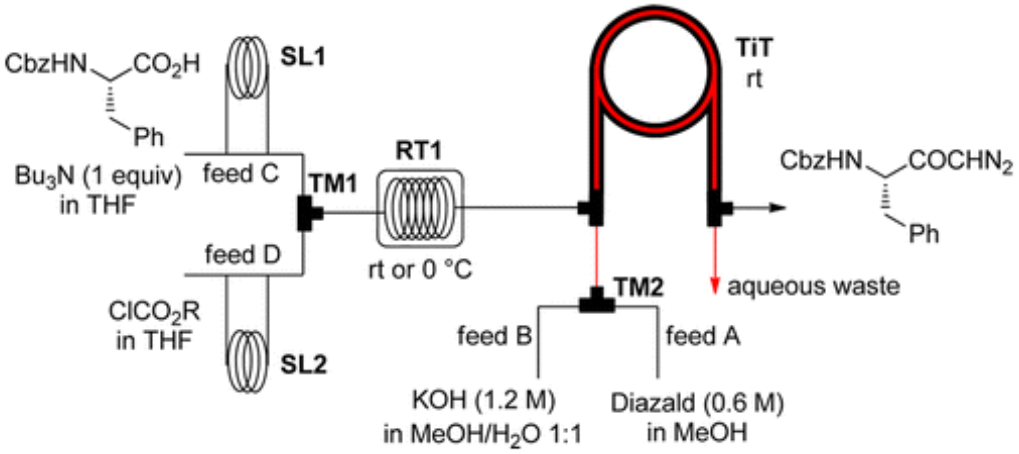

Figure 1.5: Flow system used by Kappe *et. al.*[3] to generated and react diazomethane *in situ*. Reproduced with permission.

Gas–liquid reactions are typically complicated reactions to carry out in a batch reactor.[48] Often gaseous reagents reside in reactor headspaces and are slow to diffuse into reaction solutions, due to poor interfacial area, presenting a significant safety hazard.[49] In batch these hazards are mitigated by reducing gas concentration, which slows the reaction kinetics. Flow reactors can be operated under multiple flow regimes (Figure 1.6) which provide much larger gas-liquid interfacial areas for diffusion, reducing headspace hazards and accelerating reaction kinetics.[50] Thus, a number of gas-liquid reactions have been transferred to flow reactors.[48,51]

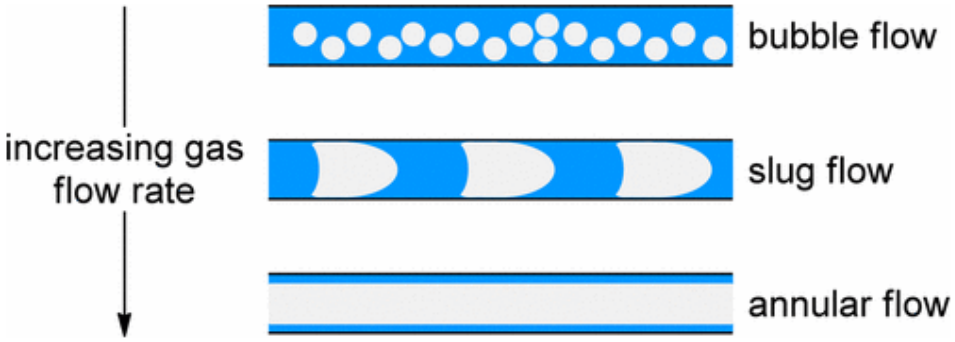

Figure 1.6: Different flow regimes that can be employed during gas-liquid reactions.[4] Reproduced with permission.

1.1.4 Scalability

Scaling of batch reactions is often performed by increasing the size of the reaction vessel. However, modifying reactor dimensions effects heat and mass transfer in the system altering the reaction parameters and therefore products obtained.[52] In flow reactors, material is produced continually over an extended period of time, any quantity of material can therefore be produced.[53] However, if the reaction requires a long residence time or is performed using low volume microreactors, it may still be more productive to perform the reaction in batch.[54] Increasing the size of flow reactors is one possible way to scale production, however lengthening reactors or increasing tubing diameters may affect the residence time distribution, heat or mass transfer of the system.[17] An alternative method to scale up, which maintains the same reaction parameters, is numbering-up (Figure 1.7).[5] This involves simultaneous use of multiple flow reactors in which a process has been optimised. As all reactors are identical the same reaction parameters will consistent across all reactors.[55]

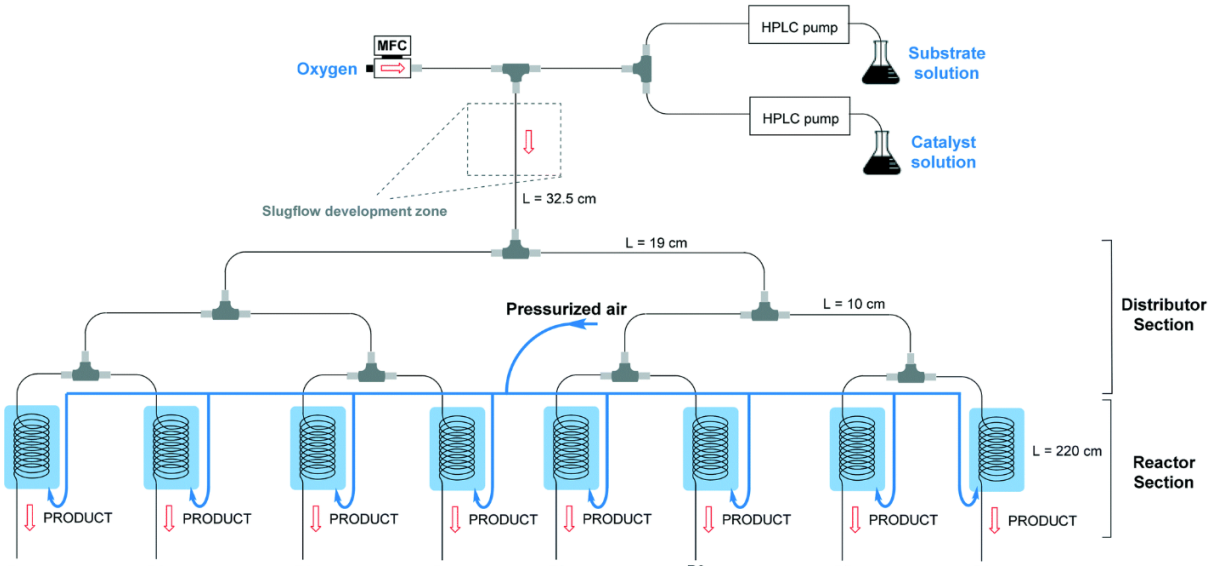

Figure 1.7: Numbered up reactor system used to increase the production of a thiolphenol dimer.[5] Published by The Royal Society of Chemistry.

1.1.5 Online Monitoring

A major advantage of continuous flow chemistry is the ability to integrate analytical techniques into the platform allowing online analysis of the reaction stream.[56] Gathering of real time information about a reaction's progress helps to minimise the time required for reaction screening. A wide variety of analytical techniques have now been incorporated into continuous flow platforms.[6,7,19,57–61] These systems are either incorporated in-line, where the entire reagent stream will pass through the analytical instrument, or at-line, where a sample of the reaction will be taken from the reactor stream via a sampling valve and be analysed. Optical spectroscopy has seen significant incorporation into continuous flow platforms.[6,57] This is mostly due to the ease of which they can be added into platforms, a flow cell simply needs to be placed at the output of the reactor as the techniques are non-destructive. Ley *et al.* have employed inline IR spectroscopy to monitor the progress of hydrogenation reactions and also monitored the formation of highly reactive intermediate compounds (Figure 1.8).[6] Yue *et al.* have integrated UV-Vis spectroscopy into microfluidic devices to monitor particle size during the continuous flow synthesis of gold nanoparticles.[57]

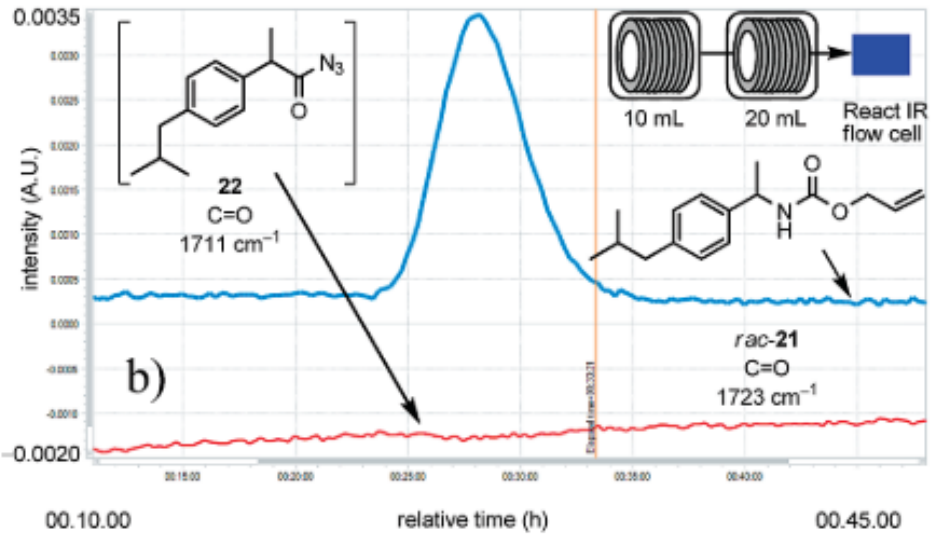

Figure 1.8: Monitoring of a Curtis rearrangement via inline IR reported by Ley *et. al.*[6] Reproduced with permission.

Non-optical analytical techniques have also been incorporated into continuous flow systems. Cronin *et al.* have incorporated a benchtop NMR spectrometer into an automated flow platform (Figure 1.9).[7] The platform was used to monitor a variety of small molecule chemical reactions. Kinetic monitoring, structural characterisation and monitoring stereoselectivity have all been reported on flow platforms via the use of different NMR techniques.[7,58,59] Jensen and coworkers demonstrated the power of online HPLC for monitoring a Heck-type coupling reaction.[60] Using commercially available HPLC apparatus, samples were taken from the reaction stream, via a sampling valve, and analysed to determine yield within a 3 % error margin. Rosenfeld *et al.* incorporated gel permeation chromatography into a continuous flow platform to allow for near real time monitoring of polymer molecular weight and dispersity.[19] Sampling valves were placed at the output of each reactor to take polymer samples from the reactor stream. This platform was used to monitor the polymerisation of styrene and subsequent chain extension with butylacrylate. Holmes *et al.* reported the use of online mass spectrometry to determine to monitor conversion during an amidation reaction.[61]

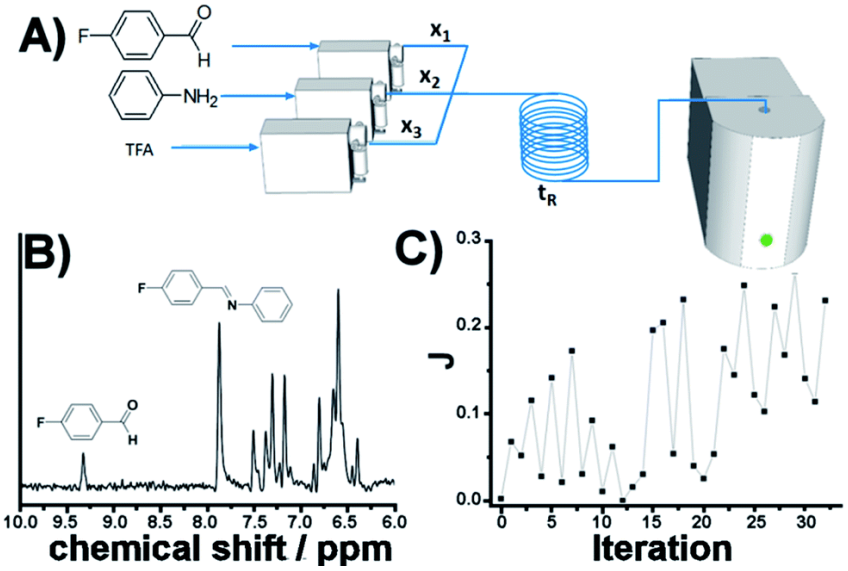

Figure 1.9: Monitoring of imine formation via inline NMR reported by Cronin *et. al.*[7] Published by The Royal Society of Chemistry.

1.2 Reaction Optimisation

Traditional reaction optimisations reported in literature often use a one variable at a time (OVAT) approach.[62] The OVAT approach relies on the assumption that effects of variables on the reaction outcome are independent of each other. Often an OVAT approach will not find the true optimum of a chemical reaction, as it is largely dependant on the starting point (Figure 1.10).[62]

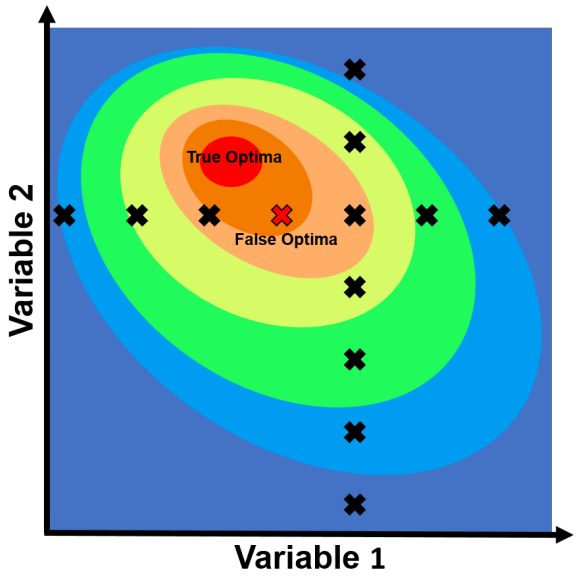

Figure 1.10: The pitfalls of traditional 'one variable at a time' (OVAT) optimisation, the true optimum is missed by assuming reaction variables are independent.

Over the years, there have been numerous statistical algorithms developed for reaction optimisation and parameter screening.[63–65] Often these algorithms are used in tandem with continuous flow platforms.[7,8,10,11,60,66–68] This is mainly due to the facile automation of such platforms compared to batch systems where performing sequential reactions is complex.[69] Combining reaction automation with optimisation algorithms has the potential to greatly increase the development and understanding of chemical processes, through facile collection and analysis of vast quantities of experimental data.[70–72]

1.2.1 Local Optimisations

Design of experiments (DoE) is a well known model-based local optimisation algorithm that has been used for many decades.[66] DoE determines a set of experiments to efficiently identify important variables affecting a chemical process, as well as ascertaining how the differing factors interact with each other. By performing these experiments, response surfaces can be constructed which elucidates the relationship between experimental variables and a response. From these response surfaces optimum regions of experimental space are located for further exploration. The Jensen group first utilised an optimal DoE approach for the optimisation of the alkylation of 1,2-diaminocyclohexane for discrete and continuous variables.[8] A total of 93 experiments led to an optimal yield of 66% (Figure 1.11).

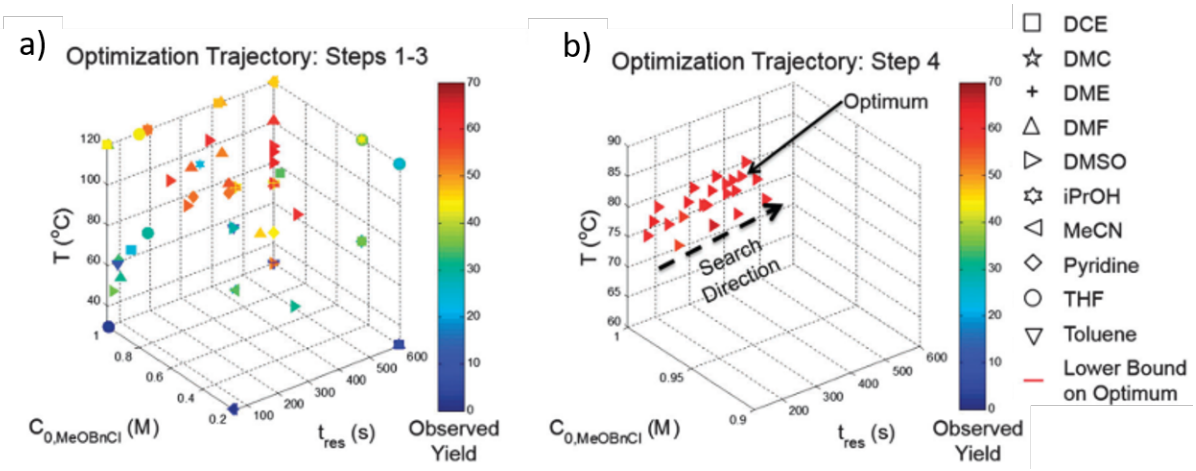

Figure 1.11: a) Optimisation trajectory and observed yield for fractional factorial design and feedback DoE searches. b) Optimisation trajectory and observed yield for gradient search.[8] Reproduced with permission.

Model-based methods such as DoE have some drawbacks. A significant amount of knowledge of the chemical reaction is required to select the reaction conditions and model the reaction

accurately. The need for knowledge of the reaction system could present an issue in kinetically complex systems where either no suitable model exists or multiple models are required.[73] Alternative methods for optimisation which requires no prior knowledge of a reaction are termed black-box methods. The Nelder–Mead simplex (NMSIM) algorithm[63] is an example of a black-box local optimisation method used to determine the maximum (or minimum) of a single-objective. This is achieved by means of using convex polyhedra formed of n + 1 vertices (where n is the number of variables, Figure 1.12).[63] The polyhedron explores the feasible reaction space set by the user. The algorithm begins by conducting n + 1 experiments within a given area of the reaction space. The worst performing experiment is then replaced during each iteration of the algorithm with another experiment via a geometric transformation. This results in a new polyhedron that explores a new point in the reaction space. This approach locates areas with a better response and hence successive simplex iterations converge on a local optimum (Figure 1.12). One of the first times this algorithm was applied to self-optimisation was in the Heck reaction, and represented one of the earliest examples of a self-optimising chemical platform.[60] Since this early report there have been many other chemical reactions optimised using some form of NMSIM.[7,74–76]

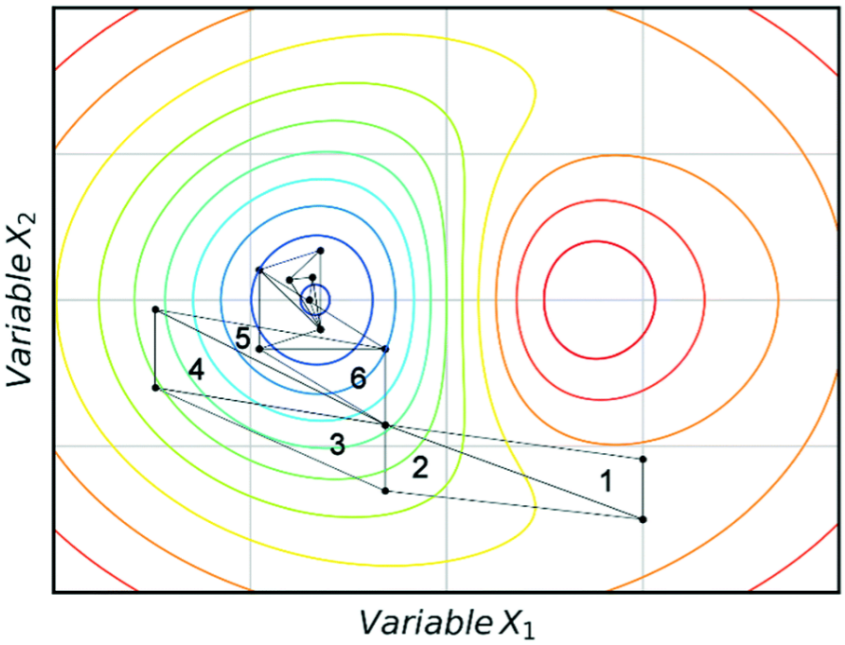

Figure 1.12: An example of a two-variable design space with arbitrary variables and a mapped response surface, showing how NMSIM converges on the minimum. Minima (blue), maxima (red).[9] Reproduced with permission.

Overall, local optimisation algorithms are typically fast to converge on an optimum. The

disadvantage of using local optimisation tools is without *a priori* knowledge about the reaction system then variable–variable interactions can lead to multiple optima. In these cases, there is no guarantee that the global optimum will be found over a local optima before termination. Additionally, any noise (error) in experimental data is not accounted for in local optimisation algorithms, which may lead to false optima.[9]

1.2.2 Global Optimisations

Global optimisation techniques aim to efficiently locate reaction optima despite the inherent experimental noise. These optimisations generate stochastic surrogate models from experimental data and use the models to select new reaction conditions.[77] Stable Noisy Optimisation by Branch and Fit (SNOBFIT) is a global optimisation algorithm for bound constrained noisy optimisation of objective functions.[64] To date, this is the only single-objective global optimiser which has been successfully implemented for the self-optimisation of a chemical reaction.[9] Holmes and co-workers reported using SNOBFIT to optimise the synthesis of AZD9291, an irreversible epidermal growth factor receptor kinase inhibitor (Figure 1.13).[10] A total of 42 experiments were performed by the platform and an optimum yield of 89 % was achieved.

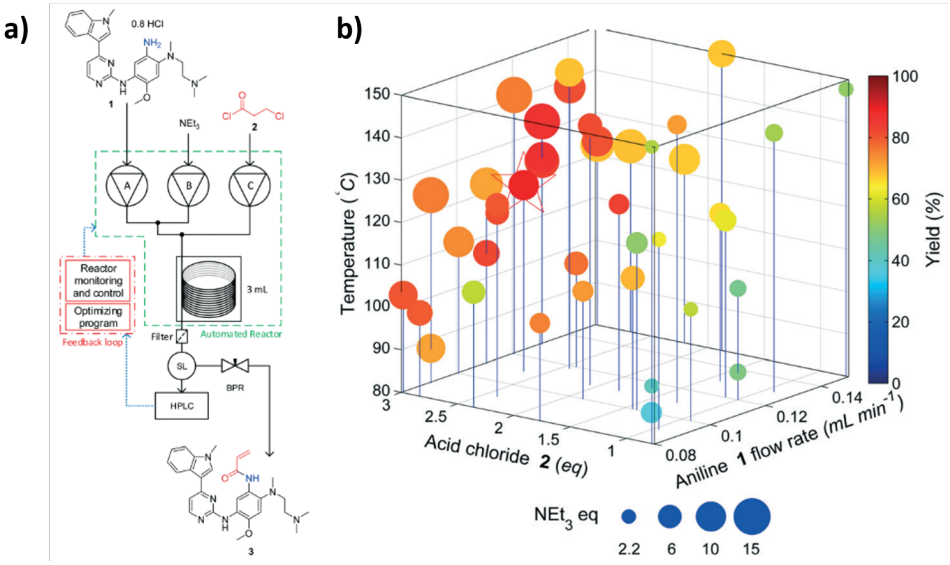

Figure 1.13: a) Continuous flow platform used for the self-optimisation of acrylamide **3** b) Multi-dimensional plot of the optimisation of acrylamide **3**. The three axis flow rate shows the aniline **1** flow rate (x-axis), acid chloride 2 eq. (y-axis) and temperature (z-axis). Optimum conditions are highlighted by the star.[10] Published by The Royal Society of Chemistry.

Currently, all the algorithms discussed only optimise for a singular objective. However, there are often multiple objectives that must be considered in chemical processes.[78] Objectives can

often be conflicting and their optima are located in different regions of reaction space. Various attempts have been made to account for the presence of multiple objectives. One method is to perform single-objective optimisations for each objective .[74,79] However, because this approach does not consider the objectives simultaneously, it can fail to identify a satisfactory compromise. Another approach to multi-objective optimisation is combination of multiple functions into a single objective function. This was used by Fitzpatrick *et al.* to simultaneously optimise throughput, conversion and consumption for an Appel reaction.[75] A similar approach was reported by Krishnadasan *et al.* where a weighted-product objective function was utilised for the optimisation of CdSe nanoparticles.[80] Assigning suitable weightings without substantial *a priori* knowledge is difficult. Additionally, minor changes to these weightings can result in significant changes to the solution obtained.[9] The actual solution to a multi-objective optimisation problem is a set of non-dominated solutions called the Pareto front (Figure 1.14), a non-dominated solution is where one objective cannot be altered without having an effect on another one.[81] Combined objective methods fail to reveal the complete trade-off in a practical number of experiments, as only one Pareto optimal solution is identified per optimisation.[82]

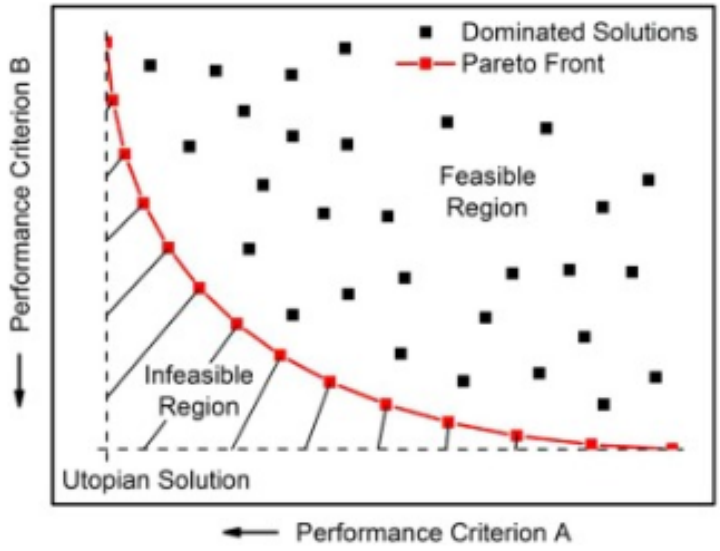

Figure 1.14: An example of a system with two competing minimization performance criteria A and B. It is infeasible to find the utopian point where both A and B are at their optimal values. The points on the Pareto front are non-dominated solutions, as A or B cannot be improved without having a detrimental effect on the other.[11] Reproduced with permission.

Of the multi-objective algorithms that exist only two have been used for the optimisation of chemical processes.[11,67] Houben and co-workers reported the use of the Multi-Objective Active Learner (MOAL) algorithm for the optimisation of an emulsion polymerisation. A total of 14

input variables were optimised to give a conversion of 99 % and particle diameter of 100 ± 10 nm.[67] The other report of using a multi-objective algorithm to optimise chemical processes was by Schweidtmann and co-workers.[11,68] Initially, the Thompson Sampling Multi-objective Efficient Optimisation (TS-EMO) algorithm was used to elucidate a Pareto front for two separate chemical processes with four input variables.[11] A model S_NAr reaction was optimised for E-factor, a measure of how environmentally friendly a process is, and space time yield. A total of 68 experiments were performed by the system and the Pareto front obtained highlighted the trade off between the two objectives (Figure 1.15a). The second chemical reaction optimised was the N-benzylation of benzylamine. Space time yield was maxmised whilst minimising impurites, 78 experiments were performed and a Pareto front of 20 experiments was determined (Figure 1.15b).

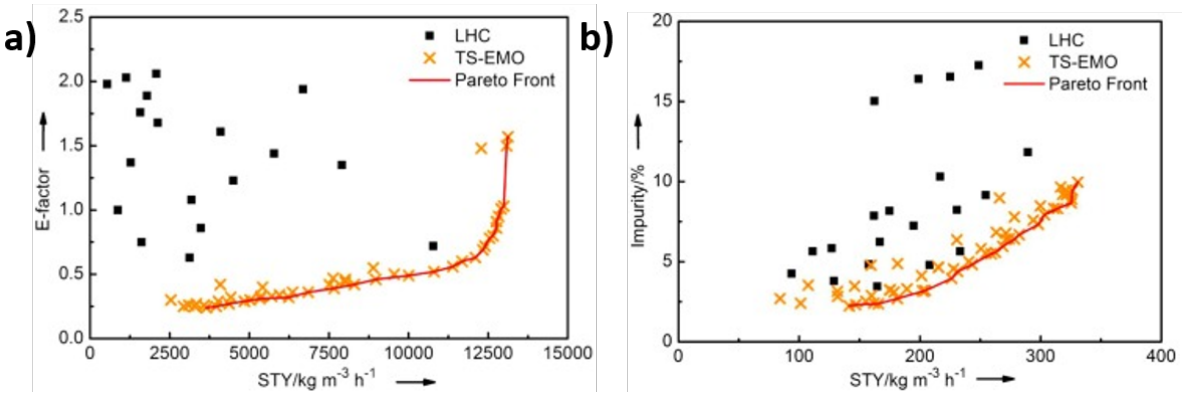

Figure 1.15: a) Results of the four parameter multi-objective self-optimisation of the S_NAr reaction and b) Results of the four parameter multi-objective self-optimisation of an N-benzylation. Both experiments formed a dense Pareto front highlighting the trade-off between their respective objectives.[11] Reproduced with permission.

1.3 Polymer Synthesis

In 1920 Herman Staudinger was the first to report that polymers are made up of large macromolecules consisting of repeating monomer units.[83] There is a wide range of naturally-occurring biomacromolecules such as long chain sugars, hydrocarbons, proteins and nucleic acids. In addition to naturally occurring polymers, there are now also synthetic polymers such as polyurethanes, polystyrene and poly(methyl methacrylate). Typically, polymers exist as mixtures of various chain lengths rather than a uniform chain length. The molecular weight of the mixture of chains is given as either the number average molecular weight (M_n, equation 1.6) where N_i is

the number of chains at a given molecular weight,M_i.

$$M_n = \frac{\sum M_i N_i}{\sum N_i} \tag{1.6}$$

Or weight average molecular weight (M_w, equation 1.7), where higher mass chains have a greater influence.

$$M_w = \frac{\sum M_i^2 N_i}{\sum M_i N_i} \tag{1.7}$$

The distribution of chain lengths is quantified by comparing the two molecular weights to give a dispersity (Đ, equation 1.8)

$$Đ = \frac{M_w}{M_n} \tag{1.8}$$

The mechanical properties of polymers (strength, stiffness, viscosity etc.) can be tuned by altering polymer molecular weight or dispersity. Additionally, mechanical properties can be further tuned by polymerising different monomer units to generate either statistical copolymers, where monomers units are randomly distributed or block copolymers, where different polymer segments are connected by a single covalent bond. The classification of polymerisation reactions has evolved over the past century (Figure 1.16), synthetic polymers were initially formed by either condensation polymerisation or addition polymerisation.[84] The distinction between the two classifications is linked to the products obtained during the reaction. Condensation polymerisation typically generates a polymer and a small molecule whilst only a polymer is generated by addition polymerisation. More recently polymer classification was divided, based on reaction mechanism, into either step polymerisations or chain polymerisations.[85] Step polymerisations occur by reaction of monomer functional groups, to initially form small oligomers before forming long polymer chains at high conversions. Whilst, propagation in chain polymerisations occur at active centres (radical or ionic), meaning long polymer chains can be formed at low conversions. In general, addition polymerisations are chain polymerisations and condensation polymerisations are step polymerisations. Chain polymerisations can subsequently be split into living and non-living polymerisations. In living polymerisations, all polymer chains remain active and can be extended whilst in non-living polymerisations, growing polymer chains are irreversibly terminated preventing further growth.[86]

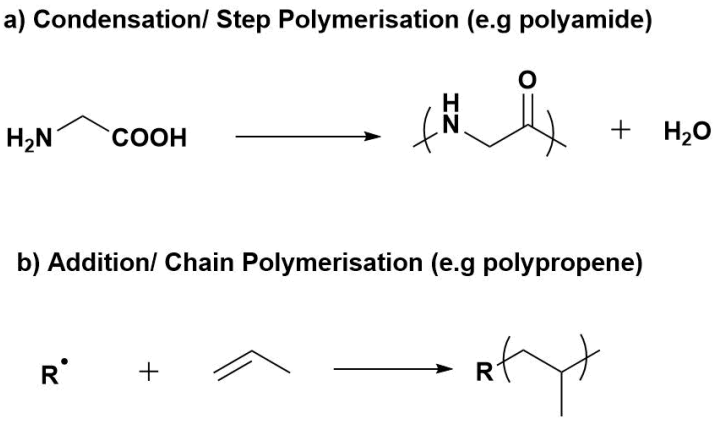

Figure 1.16: Examples of different polymers generated by a) condensation / step polymerisations and b) addition / chain polymerisations.

1.3.1 Anionic Polymerisation

Anionic polymerisation is a type of living polymerisation and the most valuable work done to understand the mechanism of this technique was performed by Szwarc in 1956.[87] Szwarc reported the anionic polymerisation of styrene in anhydrous THF. From Szwarc's work it was found that for anionic polymerisation the number average molecular weight (M_n) of a polymer could be determined by the ratio of monomer to initiator (equation 1.9) and that during anionic polymerisation all chains are initiated at roughly the same time. These features combined with the lack of termination, due to charge repulsion between chains, results in a linear relationship between molecular weight and monomer conversion and near-monodisperse polymer chains (typically $Đ < 1.2$). Anionic polymerisation uses monomers (e.g styrene, epoxide) that contain strong electronegative atoms or vinyl monomers with electron withdrawing groups, to stabilise the anion that is formed.

$$DP = \frac{[M]}{[I]} \tag{1.9}$$

However, one of the main drawbacks to anionic polymerisation is its limited solvent and monomer compatibility. In the presence of protic impurities, termination of anionic end groups will readily occur. As a result, syntheses require rigorous purification of the monomer and solvent, as well as the removal of water. In addition, the polymerisation is also sensitive to numerous protic functionalities limiting the monomers available for polymerisation.

1.3.2 Free Radical Polymerisation

Free radical polymerisation (FRP) is a non-living chain polymerisation which can be used to polymerise a wide range vinyl monomers in a variety of solvents, due to the tolerance of radicals to many functional groups.[86] As such the conditions under which FRP can be performed are much less strict than anionic polymerisation, the only main limit is that oxygen must be purged from the system. The mechanism for FRP (Figure 1.17) can be divided up into 4 categories: initiation, propagation, termination and transfer, each of which can then be further subdivided into different reactions.

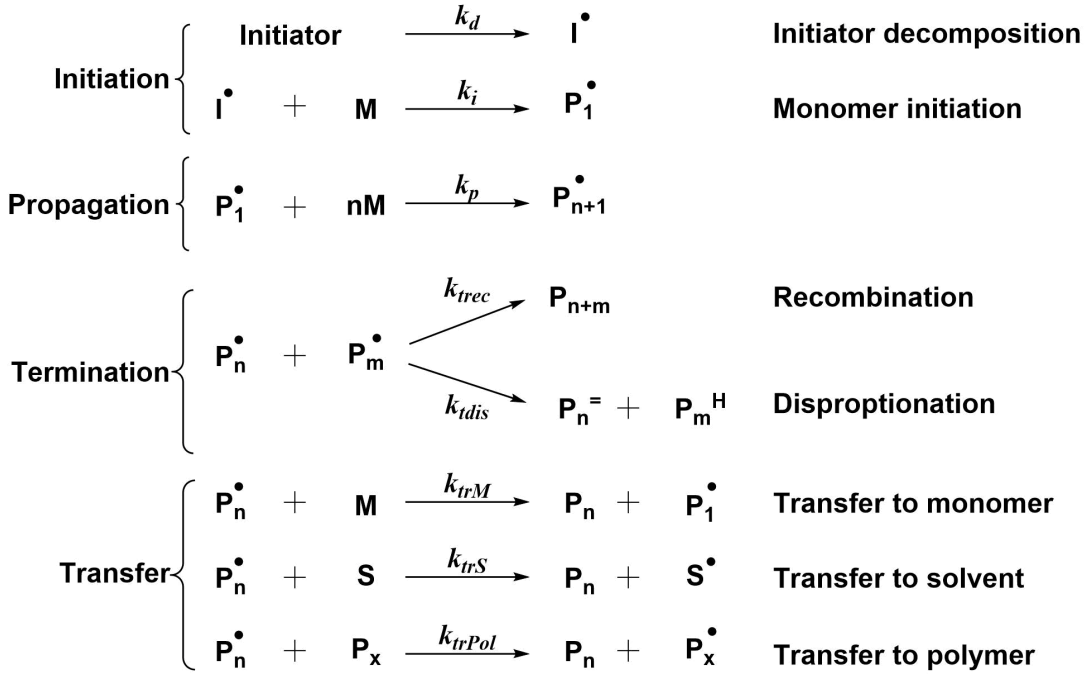

Figure 1.17: Reaction mechanism for free radical polymerisation.

Initiation comprises 2 reactions: firstly, the decomposition of an initiator (either thermal or photolytic), via homolytic cleavage of a covalent bond, generates an initial source of radicals. The formed radical species ($I^\bullet$) then reacts with monomer to form a monomeric radical species ($P_1^\bullet$). The ability of the primary radical to react with the monomer to initiate a polymer chain is defined as the initiator efficiency, *f*. The kinetics of the initiation step are governed by the rate of initiator decomposition (R_d) and the rate of monomer initiation (R_i) according to the following equations:

$$R_d = \frac{d[I]}{dt} = k_d[I] \tag{1.10}$$

$$R_i = 2fR_d = 2fk_d[I] \tag{1.11}$$

After initiation, propagation occurs as this radical species reacts further with monomer to generate a propagating polymer radical ($P_n^\bullet$) which then repetitively reacts with further monomer. In a typical polymerisation reaction, the overall kinetics are governed by the rate of propagation (R_{pr}) according to:

$$R_{pr} = -\frac{d[M]}{dt} = k_{pr}[P_n^\bullet][M] \tag{1.12}$$

Propagation continues until no monomer remains or until all radicals are terminated which can occur via two possible termination reactions (Figure 1.17): recombination and disproportionation. Recombination occurs when two growing radicals react to produce a single, longer polymer chain. Disproportionation involves abstraction of a β-hydrogen atom from another growing chain by a polymer radical. In this case, one of the two subsequent chains contains an unsaturated terminal group. The varying proportion of each of these termination reactions has a dramatic effect on the final dispersity (Đ) of the final polymer. The rates of these reactions are expressed as:

$$R_{rec} = -k_{rec}[P_n^\bullet][P_m^\bullet] \tag{1.13}$$

$$R_{disp} = -k_{disp}[P_n^\bullet][P_m^\bullet] \tag{1.14}$$

The overall rate of termination R_t is expressed as the decrease of the polymer radical concentration:

$$R_t = -\frac{d[P^\bullet]}{dt} = k_t[P^\bullet]^2 \tag{1.15}$$

Additionally to these reactions, the polymer radical can also undergo chain transfer to monomer, polymer or solvent. These side reactions may lead to loss of control over polymer architecture and may cause chain branching and/or increasing the dispersity of the polymer. As these reactions often do not consume radicals and re-initiate the polymerisation quickly they have little effect on polymerisation kinetics. After taking all the reactions present during polymerisation into account and assuming negligible chain transfer, the overall rate of polymerisation is:

$$R_p = k_p[M]\sqrt{\frac{fk_d[I]_0}{k_t}} \tag{1.16}$$

Perhaps the most obvious disadvantage of a non-living polymerisation such as FRP is poor control over the polymer molecular weight and architecture - the resulting polymer chains it produces have a broad molecular weight distribution. In contrast during living polymerisation,

chains grow at the same rate meaning near-monodisperse chains form. Also, in living polymerisations the end groups remain active (no termination step occurs) allowing for more advanced polymer structures to be formed such as block copolymers by further addition of monomer. Whereas in FRP, significant termination occurs preventing further extension of polymer chains.

1.3.3 Reversible Deactivation Radical Polymerisation (RDRP)

In theory, a living FRP would be possible if all termination and chain transfer reactions were eliminated but this is impossible in practice. One method to reduce termination reactions, thus increasing the living character of a radical polymerisation, is to minimise the polymer radical concentration. From equations 1.12 and 1.15 it can be seen that the polymer radical concentration has a much greater effect on the rate of termination ($R_t \propto [P_n^\bullet]^2$) than the rate of propagation ($R_p \propto [P_n^\bullet]$). Thus, by minimising the polymer radical concentration the rate of termination is more significantly suppressed relative to the rate of propagation. This is often described as pseudo-living or controlled radical polymerisation. There are three main criteria required for a polymerisation to be considered living. Firstly, the reaction kinetics must be first order with respect to the monomer assuming a constant radical concentration up to high conversions (> 90 %). This can be determined using the integrated rate equation:

$$R_p = ln\frac{[M]_0}{[M]} = k_p[P^\bullet]t \tag{1.17}$$

If the reaction kinetics are first order there will be a linear relationship between $ln\frac{[M]_0}{[M]}$ and reaction time (Figure 1.18a). A deviation in linearity could indicate either termination, reducing the concentration of polymer radicals, or slow initiation of the polymer radical. The next requirement for a polymerisation to be considered living is a linear evolution in the molecular weight (M_n) with respect to monomer conversion (Figure 1.18b). A linear evolution implies the absence of termination or chain transfer reactions. In comparison, for FRP high molecular weights are only formed at low conversions whilst the rate of termination is low relative to propagation.

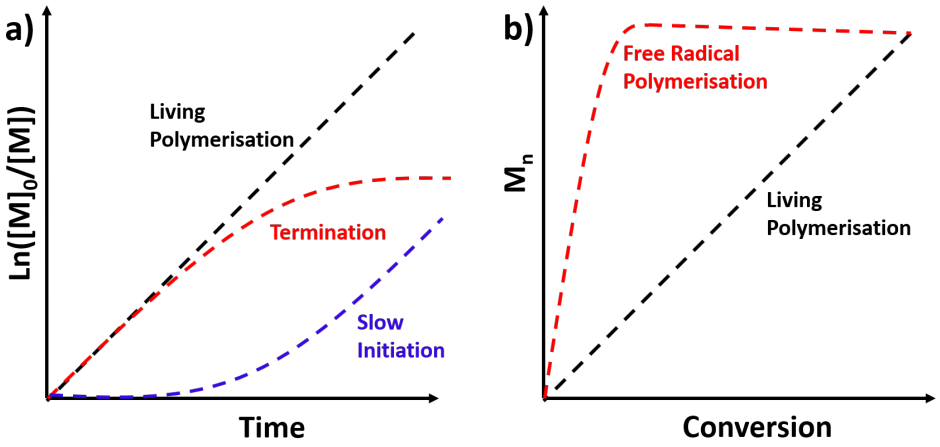

Figure 1.18: (a) Semi-logarithmic plots of $Ln\frac{[M]_0}{[M]}$ vs. time showing the kinetic profiles obtained for a constant $[P^\bullet]$, some degree of termination and slow initiation. (b) Molecular weight evolution for polymers synthesised by free radical polymerisation and living polymerisation techniques.

The final criteria is that a relatively low dispersity is obtained from the polymerisation (Đ < 1.3). For true living polymerisation, such as anionic polymerisation, dispersities are typically less than 1.1. However, CRP techniques have some limitations over true living polymerisation systems because they rely on radical mechanisms that have intrinsic termination reactions which cannot be eliminated. Therefore dispersities less than 1.3 are considered reasonably well controlled.[88] In the 1980s/1990s, obtaining living character in radical systems through controlled radical polymerisations became feasible with techniques such as nitroxide mediated polymerisation (NMP),[89] atom transfer radical polymerisation (ATRP),[90,91] and reversible addition– fragmentation chain transfer (RAFT) polymerisation.[92] These are collectively known as reversible deactivation radical polymerisation (RDRP) techniques because they all contain a dynamic equilibrium between a dormant and propagating radical species. The equilibrium controlling ATRP and NMP is called 'reversible termination' (Figure 1.19a) whilst RAFT polymerisation is controlled by 'reversible transfer' (Figure 1.19b) where the conventional free radical mechanism includes degenerative transfer to a chain transfer agent (CTA). Reversible termination and transfer mechanisms maintain a consistent $[P_n^\bullet]$ thus minimising termination and giving polymerisations living character.

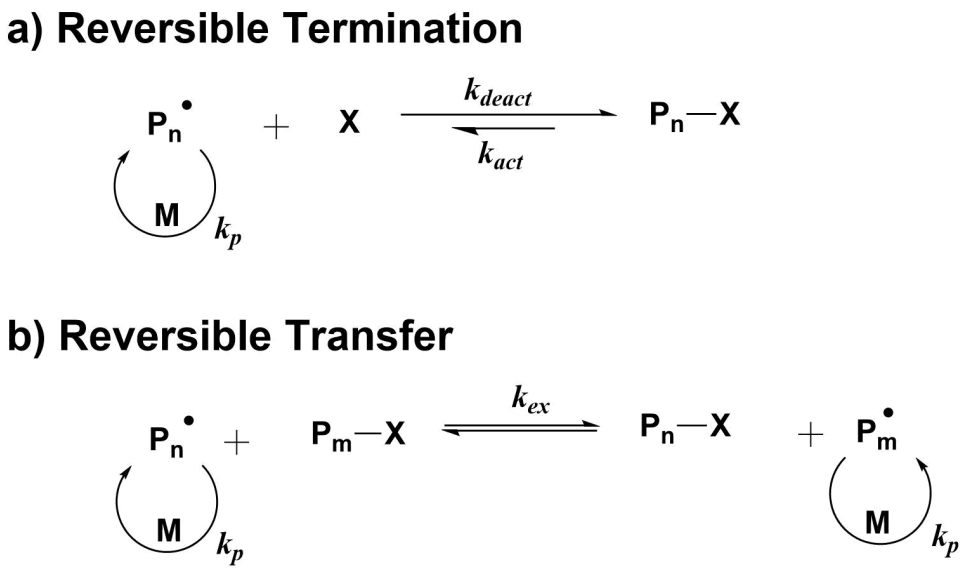

Figure 1.19: General reaction mechanisms for the controlled radical polymerisations

1.3.3.1 Nitroxide Mediated Polymerisation (NMP)

As stated previously, NMP relies on a dynamic equilibrium through reversible homolytic cleavage of a relatively weak covalent bond to generate a growing radical and a less reactive species (also known as the persistent radical). In this case, the radical reacts with a nitroxide spin trap. The development of NMP gained momentum in 1993 after 2,2,6,6-tetramethylpiperidinyloxyl (TEMPO) was used to mediate the controlled polymerisation of styrene.[89]

1.3.3.2 Atom Transfer Radical Polymerisation (ATRP)

ATRP was first reported in 1995 by both Matyjaszewski[90] and Sawamoto.[91] Like NMP, ATRP uses the persistent radical effect to generate a dynamic equilibrium between dormant and propagating radical species. The basic mechanism of ATRP revolves around the formation and breaking of an alkyl halide bond using a transition metal catalyst in order to control the polymer radical concentration. Polymerisation occurs upon addition of the catalyst to a reaction solution containing monomer and an initiator, which contains a labile halogen. The transition metal catalyst undergoes oxidation by extracting the halogen atom from the initiator which generates a radical species ($R^{\bullet}$), which then initiates radical polymerisation.[93] Reversible termination then occurs between the metal-halogen complex and the polymer radicals to maintain a constant propagating radical concentration [$P_n^{\bullet}$]. However, the transition metal catalyst is irreversibly deactivated by termination reactions during the polymerisation, which eventually leads

to a cessation of polymerisation.[94] Initially, this was overcome by using high catalyst concentrations.[94] However recently techniques have been developed to reactivate the catalyst, through a one electron reduction, using light (photo ATRP),[95] reducing agents (ARGET-ATRP),[96] free radical initiator (ICAR-ATRP),[97] electricity (eATRP)[98] and ground state transition metals (SARA-ATRP),[99] although the mechanism for SARA-ATRP is disputed.[99]

1.3.3.3 Reversible Addition-Fragmentation Transfer (RAFT) Polymerisation

RAFT polymerisation was first reported by Rizzardo, Moad, and Thang in 1998,[92] and since then it has emerged as one of the most powerful methods in the field of RDRP.[100] As stated above, RAFT polymerisation operates through a different mechanism to ATRP and NMP. RAFT mainly follows the same mechanism as FRP but the mechanism also features rapid reversible chain transfer mediated by a CTA (Figure 1.20b,d). The ratio of monomer to CTA is used to control the target degree of polymerisation (equation 1.18).

$$DP = \frac{[M]_0}{[CTA]_0} \tag{1.18}$$

The first main difference in the mechanism of RAFT polymerisation compared to FRP is the inital chain transfer (Figure 1.20b). As with FRP, initiation forms a propagating radical ($P_n^{\bullet}$). However, in RAFT this radical then adds to the thiocarbonyl CTA compound to form a radical intermediate. This can either fragment to give the original propagating radical and CTA or another thiocarbonyl compound and a new radical ($R^{\bullet}$). This new radical ($R^{\bullet}$) may then re-initiate polymerisation by reacting with monomer to form a new propagating radical ($P_m^{\bullet}$) or react with the newly formed thiocarbonyl group. The next difference between RAFT and FRP is the chain equilibrium (Figure 1.20d). In this stage propogating polymer radicals ($P_{m/n}$) undergo rapid exchange with the thiocarbonyl capped polymer species in order to keep $[P^{\bullet}]$ constant.

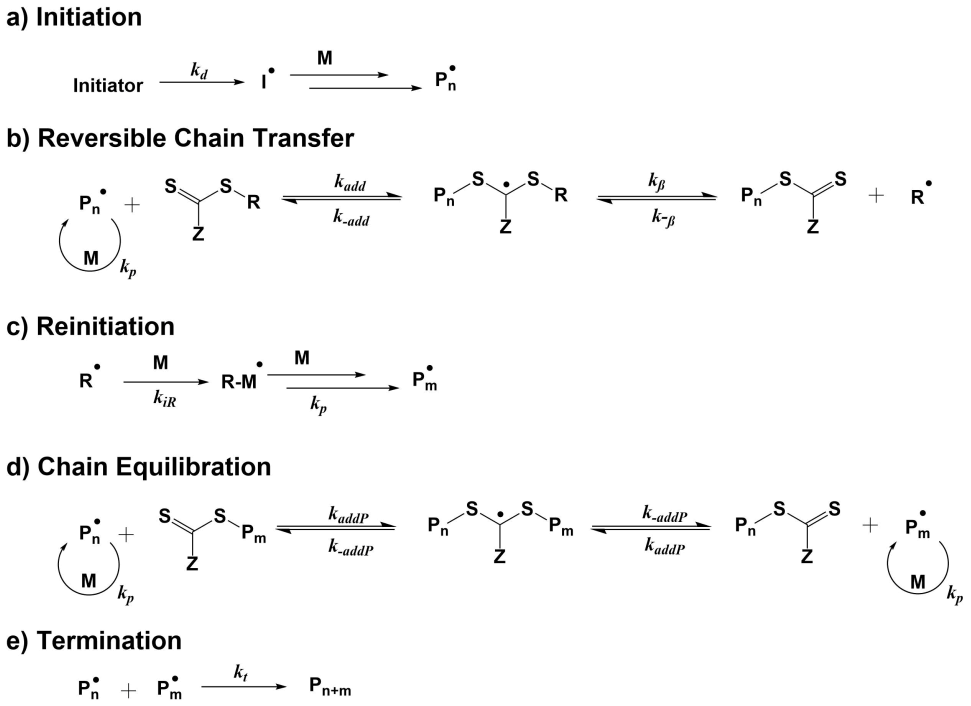

Figure 1.20: Reaction mechanism of RAFT polymerisation showing initiation, propagation, reversible chain transfer, re-initiation, chain equilibration and termination steps.

The main moiety of a RAFT agent (Figure 1.21a), which allows for control over radical polymerisations, is the thiocarbonyl group. However, selection of an appropriate RAFT agent R group is also important for optimal control of a polymerisation.[12] The range of thiocarbonyl RAFT agents continues to expand (Figure 1.21b);[100] currently the main classes of RAFT agent being used are xanthates, dithioesters, dithiocarbamates and trithiocarbonates. The ability of a RAFT agent to control polymerisations varies depends on the monomer being polymerised, the free radical leaving group (R) and the radical stabilising group (Z).[12]

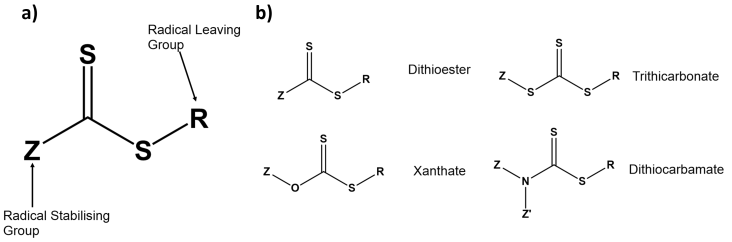

Figure 1.21: a) General structure of RAFT chain transfer agent and b) structures of commonly used RAFT agents.

Most vinyl monomers can be split into two broad classes, "more activated" monomers (MAMs) and "less activated" monomers (LAMs).[12] MAMs are those whose double bond is conjugated to electron withdrawing groups such as: an aromatic ring (e.g. styrene), carbonyl group (e.g.

(meth)acrylates), (meth)acrylamides) or a nitrile (e.g. acrylonitrile). These help stabilise the radical species formed during polymerisation.[101] LAMs do not contain such stabilising groups, but instead contain saturated carbons or heteroatoms with lone pairs (e.g vinyl esters, *N*-vinylpyrrolidone) which cannot conjugate to the radical species.[101] As a result of poor radical stabilisation, LAM monomers propagate much more readily than MAM monomers.

In order to achieve good living control using RAFT polymerisation, the CTA must readily react with propagating radicals to form a stabilised intermediate radical (Figure 1.20b&d). However, this stabilised radical species must also readily decompose to regenerate a propagating radical species otherwise significant retardation of the polymerisation rate will occur. Propagating p(LAM)s are highly reactive and therefore a less stabilised RAFT agent is required to generate the stable intermediate. In contrast, propagating poly(MAM)s are much more stabilised and therefore require a more stabilised RAFT agent in order to form the intermediate. The Z group modifies the rate of addition of propagating radicals to the CTA and the rate of fragmentation of the intermediate species through conjugation to the intermediate radical species.[12] Altering the Z group will alter the monomers than can be polymerised with good control by a RAFT agent (Figure 1.22).

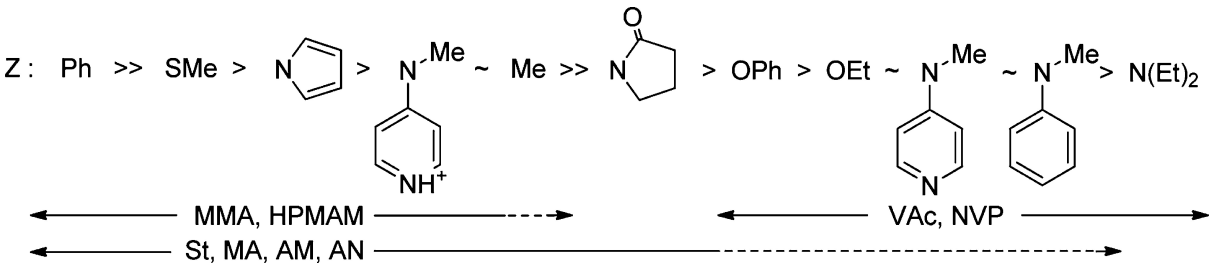

Figure 1.22: Guidelines for selection of the Z group of RAFT agents for various polymerisations. Addition rates decrease and fragmentation rates increase from left to right. A dashed line indicates partial control (i.e., control of molar mass but poor control over dispersity or substantial retardation in the case of MAMs such as St or MA).[12] Reproduced with permission.

The R group (Figure 1.23) needs to be a better homolytic leaving group than the propagating polymer radical as it will then preferentially fragment during the inital chain transfer step to generate $R^{\bullet}$. This new radical must also be able to rapidly re-initiate the polymerisation ($k_{iR} > k_p$, Figure 1.20c) in order to avoid rate retardation.

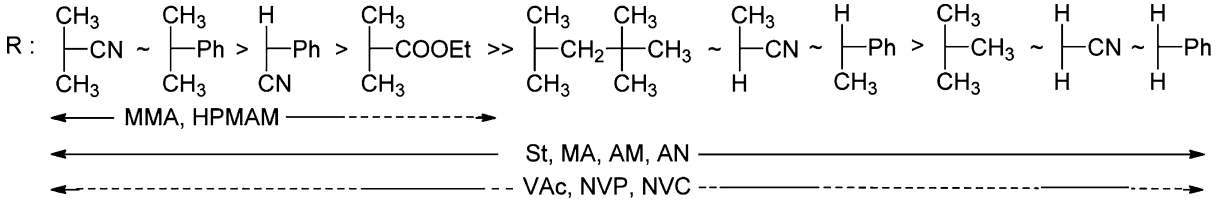

Figure 1.23: Guidelines for selection of the R group of RAFT agents for various polymerisations. Transfer coefficients decrease from left to right. Fragmentation rates also decrease from left to right. A dashed line indicates partial control (i.e., control of molar mass but poor control over dispersity or substantial retardation in the case of VAc, NVC, or NVP).[12] Reproduced with permission.

1.3.4 Heterogeneous Polymerisation

Heterogeneous polymerisations are usually two-phase systems in which either monomer droplets and/or polymer particles are finely dispersed in an immiscible liquid.[86] A typical heterogeneous polymerisation consists of monomer, initiator, solvent and a surfactant, to stabilise monomer droplets and/or polymer particles formed. Heterogeneous polymerisations can be divided into three main types: suspension, emulsion and dispersion.[86] In suspension polymerisation, monomers and initiators are insoluble in the reaction medium and large monomer droplets containing initiator are formed by mechanical mixing. Upon initiation, polymerisation occurs within the monomer droplets.[86] Emulsion polymerisation, involves a monomer which has very limited solubility in the reaction medium. However, unlike suspension polymerisation, the initiator is only soluble in the reaction medium and not soluble in the monomer. After mixing the solution contains monomer droplets, monomer-swollen surfactant micelles and a small amount of dissolved monomer. The soluble initiator then initiates polymerisation of the dissolved monomer. Once the growing oligomers reach a critical length, they become insoluble and enter the monomer-swollen surfactant micelles, and continue to polymerise. Further polymerisation subsequently proceeds within the monomer-swollen polymer particle with monomer gradually transported from the large monomer droplets to the polymerising polymer particles.[86] Dispersion polymerisation differs from suspension and emulsion polymerisation, as all the starting materials are soluble in the reaction medium (Figure 1.24a). However, the polymer is insoluble and upon reaching a critical length during polymerisation polymer particles, stabilised by a surfactant, are formed (Figure 1.24b,c). Monomer then diffuses into these particles and polymerisation continues (Figure 1.24d).[86]

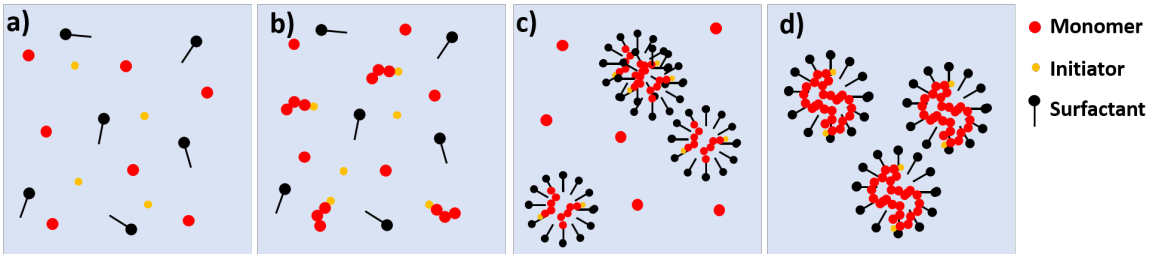

Figure 1.24: Schematic of typical stages in dispersion polymerisation.

1.4 Block Copolymer Self Assembly

1.4.1 Aqueous Self Assembly

Amphiphilic molecules such as detergents, soap and phospholipids comprise both a hydrophilic and a hydrophobic component. When placed in water, the hydrophobic segments aggregate into clusters whilst the hydrophilic segment of the molecule remain solvated. There is a larger enthalpic compensation gained from forming hydrogen bonds with the solvent than if the hydrophilic parts had interacted with each other, leading to short-range repulsion between adjacent hydrophiles. It is the subtle balance between these forces that leads to the formation of various nanostructures. The same is true is for copolymers that comprise defined separate hydrophobic and hydrophilic blocks. The structures generated during the self assembly is dependant on the size and ratio of these blocks. This can be estimated by the packing parameter (p):

$$p = \frac{\nu}{a l_c} \tag{1.19}$$

where ν is the volume of the hydrophobic segment, l_c is the length of the hydrophobic block and a is the effective cross-sectional area of the hydrophilic chain. This simple concept was developed for small molecule surfactants but can be used to estimate the morphology of self-assembled block copolymer amphiphiles. As a general rule, when $p < 1/3$ spherical micelles are formed, cylindrical micelles are produced when $1/3 < p < 1/2$ and when $1/2 < p < 1$ vesicular aggregates are observed.[102] Although a wide range of other morphologies for block copolymers have been reported.[103]

1.4.2 Polymerisation Induced Self Assembly

Traditionally, block copolymer self-assembly has been achieved via post polymerisation methods such as solvent switching or thin film re-hydration. However, these methods require low copolymer concentrations (< 1.0 % w/w) in almost all cases.[13] Polymerisation induced self assembly (PISA) is a method of generating self assembled block copolymer structures at much higher concentrations (up-to 50 % w/w) than post-polymerisation methods.[13] Typically, a soluble homopolymer, which acts as a steric stabiliser, is chain-extended using a second monomer in a suitable solvent such that the growing second block is insoluble, which drives *in situ* self-assembly to form diblock copolymer nano-objects (Figure 1.25).[13]

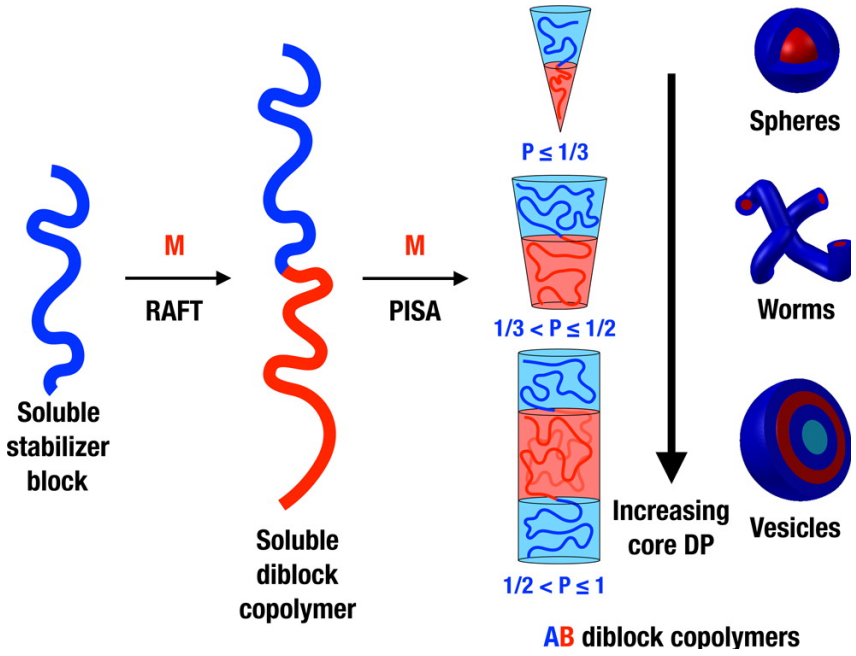

Figure 1.25: Schematic of the Synthesis of Diblock Copolymer Nano-Objects via polymerisation-Induced Self-Assembly (PISA).[13] Reproduced with permission.

As the insoluble core block length increases throughout the polymerisation the nanoparticles undergo transitions to lower curvature morphologies (Figure 1.26). Initially, spherical micelles will fuse together to form anisotropic worms.[104] Worms will then branch and undergo partial coalescence into nascent bilayers with tentacle-like protrusions, leading them to be labelled 'octopi' phases in some literature.[14] These 'octopi' then begin to wrap up to form a vesicle. During this transition hemispherical 'jellyfish' architectures have also been reported.

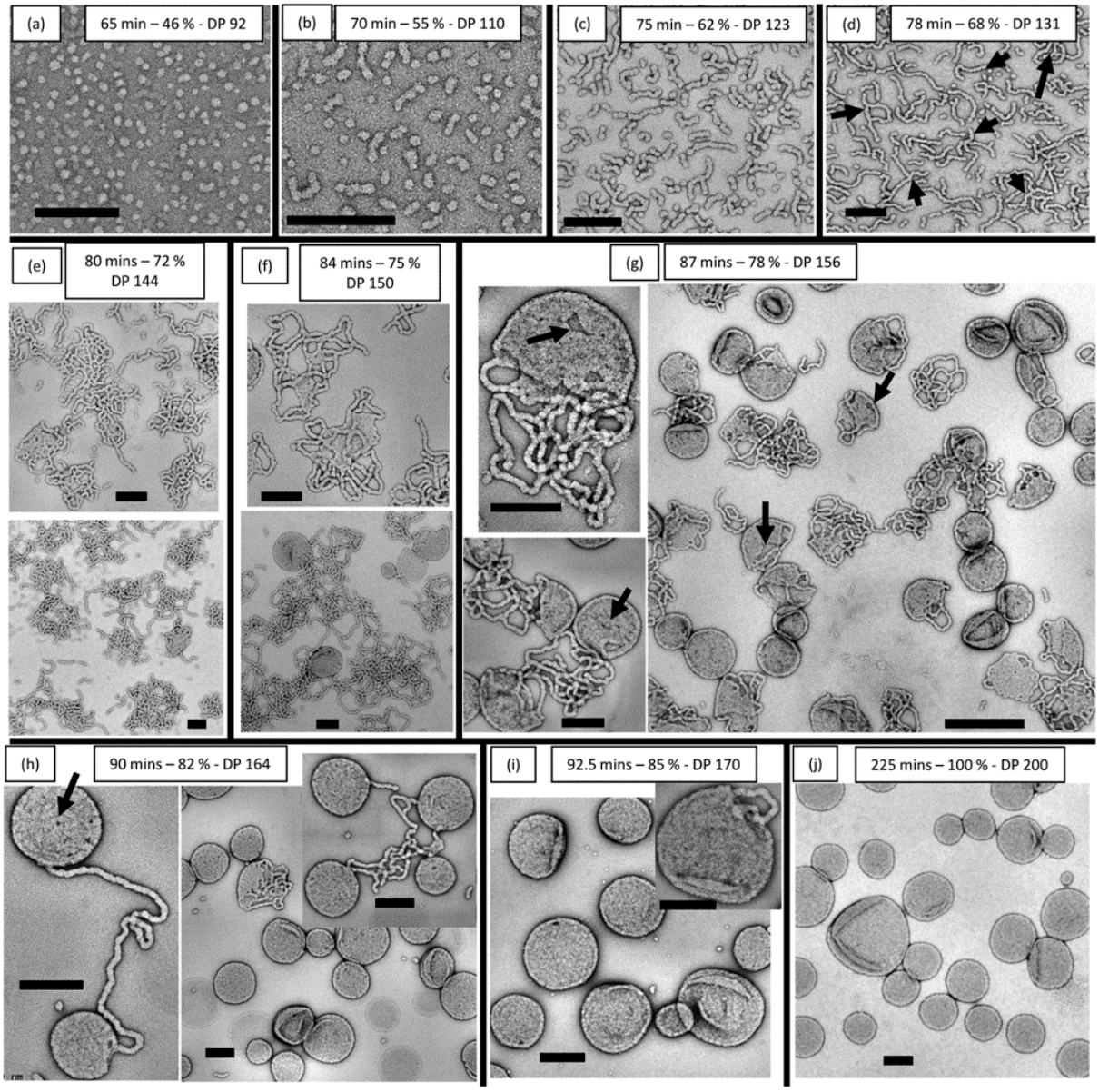

Figure 1.26: Intermediate nanostructures observed during the sphere-to-worm and worm-to-vesicle transitions. Transmission electron micrographs obtained for a) spheres, b) short worms, c) long worms, d) branched worms, e,f) partially coalesced worms, g) jellyfish, and h–j) vesicles generated *in situ* after various reaction times for a target poly(glycerol methacrylate)$_{47}$-poly(2-hydroxy propylmethacrylate)$_{200}$ diblock copolymer prepared by RAFT aqueous dispersion polymerization at 70 °C and 10 w/v % solids. Scale bars = 200 nm.[14] Reproduced with permission

Further research into the self-assembly process during PISA has highlighted factors other than the packing parameter that affect the self-assembly.[15] If the stabilising block is relatively long there is strong steric stabilisation upon micellear nucleation. This prevents sphere-sphere fusion leading to kinetically trapped spherical morphologies.[13] Also, as core block length increases so does its hydrophobicity, limiting chain mobility and therefore *in situ* morphological evolution.[15] For most reported worm and vesicle systems it is expected that un-reacted monomer helps

solubilise the core block, increasing mobility and aiding morphological evolution. The effect of poor chain mobility was demonstrated by Blanazs and co-workers.[15] They synthesised a series of poly(glycerol monomethacrylate)$_{78}$–poly(2-hydroxypropyl methacrylate)$_x$ (PGMAm$_{78}$-PHPMA$_x$) block copolymers at 10 % w/w copolymer concentration and found them all to form spherical micelles. By increasing the copolymer concentration (% w/w) they were able to access a variety of mixed phase and pure phases of spheres, worms and vesicles (Figure 1.27).

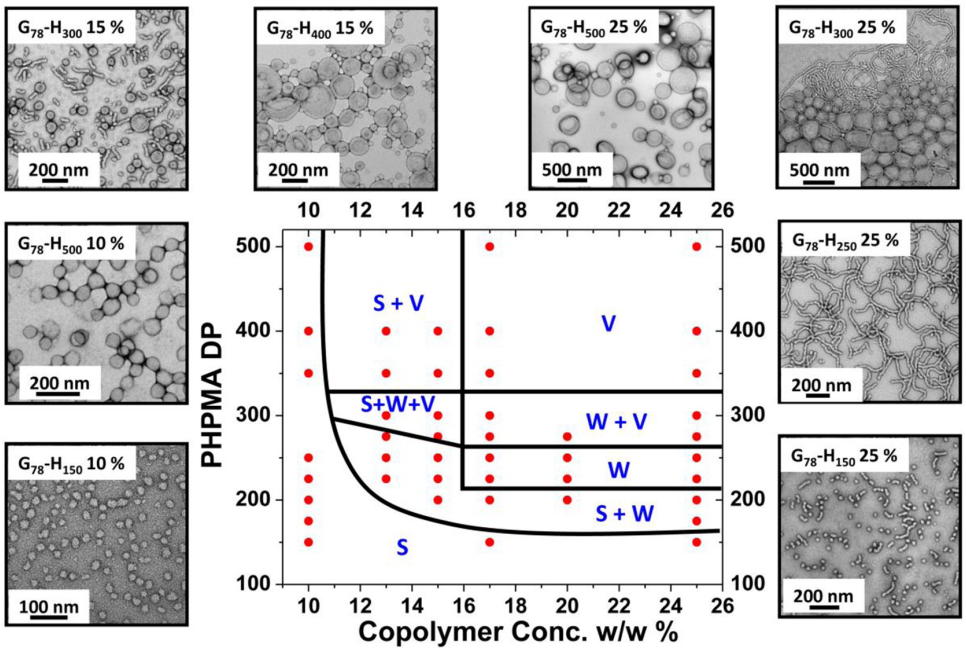

Figure 1.27: Representative TEM images and the corresponding phase diagram for a series of PGMA$_{78}$–PHPMA$_x$ copolymers synthesized by aqueous RAFT dispersion polymerisation at various concentrations ranging between 10 and 25 % w/w. S = spherical micelles, W = worms, and V = vesicles.[15] Reproduced with permission.

At higher copolymer concentrations it is likely that more unreacted monomer diffused into the growing micelles and solubilised the chains allowing morphological evolution. To confirm this limited morphological evolution was due to limited chain mobility Blanazs and co-workers repeated the synthesis of PGMAm$_{78}$-PHPMA$_{500}$ at 10 % w/w copolymer concentration in the presence of ethanol at various concentrations (0-20 % mass).[15] As PHPMA is soluble in ethanol it was believed to solubilise the growing PHPMA chains and allow morphological evolution similar to unreacted monomer at higher copolymer concentrations. As the ethanol concentration increased mixed phases of spheres and vesicles, pure vesicle phases and a worm vesicle mixed phase were observed confirming that self-assembly was linked to hydrophobic chain mobility (Figure 1.28).

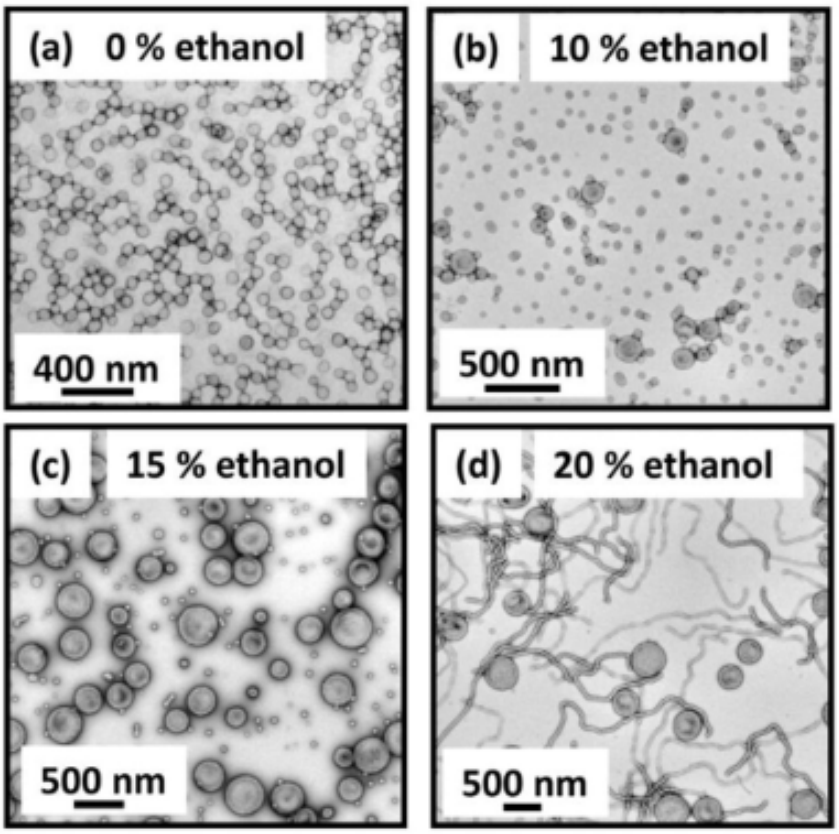

Figure 1.28: Representative TEM images illustrating the effect of adding ethanol cosolvent to the synthesis of $PGMA_{78}$–$PHPMA_{500}$ diblock copolymers by RAFT aqueous dispersion polymerisation at 10 % w/w: (a) no ethanol, (b) 10 % ethanol, (c) 15 % ethanol, (d) 20 % ethanol.[15] Reproduced with permission.

Nano-objects generated by PISA are often prepared using RAFT *emulsion* or *dispersion* polymerisation.[104] For RAFT aqueous dispersion polymerisation, initially all components including monomers, initiators and homopolymer are dissolved in water. At the onset, polymerisation occurs in a homogeneous reaction mixture. However, the formed polymers become insoluble as their molecular weight increases beyond a certain critical value and precipitate to form polymer micelles which are stabilised by the soluble block. After the formation of these polymer micelles, monomer in the aqueous phase diffuses into the micelle core and continues to polymerise. Due to the high local monomer concentration inside the block copolymer nano-objects an increase in the rate of reaction is also observed.[14] In RAFT aqueous emulsion polymerisation, a water soluble homopolymer is used to chain extend a water immiscible monomer (e.g styrene, methyl methacrylate). Initially, after emulsification the monomer resides in large droplets in solution and some monomer will slowly diffuse into the aqueous phase. The soluble homopolymer will react with the monomer in the aqueous phase. Once the insoluble block reaches a critical length

it will drive self assembly into a polymer micelle. More monomer will then diffuse into these micelles from the large monomer droplets and continue to polymerise. Whilst it should be possible to access higher order morphologies using emulsion polymerisation, only few successful reports exist.[105–108]

1.5 Polymerisation in Flow

The development of a broad range of polymerisation techniques means that a wide range of macromolecular structures can now be synthesised.[109] Recently, there has been a drive to improve or find alternative synthetic processes to generate these materials.[109] There has been recent interest in combining polymerisation techniques with flow chemistry.[110] This will hopefully allow production of new macromolecular compounds on a industrially applicable scale. Polymerisations benefit greatly from the increased control over reactor parameters in flow reactors such as temperature, residence time and mixing. Temperature is especially important as polymerisations are exothermic processes and large temperature gradients can be generated when performed in batch reactors.[111] Therefore, scaling up polymerisations in batch is not facile, as heat transfer must be considered in order to maintain the reaction kinetics.[112] If exotherms are not properly dissipated then conversion and quality of the final polymer will be affected.

1.5.1 Anionic Polymerisation in Flow

As stated previously, anionic polymerisations must be performed under strictly dehydrated conditions to avoid termination of the growing polymer chain. In addition, cryogenic conditions are required when anionic polymerisations are performed in polar solvents. These requirements greatly hinder the potential industrial applications of this technique. Therefore, there is great potential in applying continuous flow methodologies. Even in the early reports of anionic polymerisation, continuous processes had been studied and employed to obtain basic kinetic parameters by both Szwarc and Schulz.[87,113] Müller and coworkers demonstrated the preparation of poly(methyl methacrylate) with low dispersities ($Đ = 1.04–1.08$) in a continuous manner using mild reaction conditions (0 °C) in the late 1990s.[114] Employment of a microstructured mixing device in for the anionic polymerisation of amino acid *N*-carboxy anhydrides was reported by Maeda *et al.*.[115] The improved mixing afforded by the micromixing device allowed preparation of poly(glutamine) with much lower dispersities ($Đ = 1.17$) than the equiv-

alent batch polymerisation (Đ = 1.56). Maeda *et al.* extended this technique to the synthesis of poly(amino acid) copolymers synthesising poly(lysine-*co*-alanine) and poly(lysine-*co*-leucine) with much lower dispersities (Đ = 1.64, 1.54) than the respective batch experiments (Đ = 2.56, 2.13).[116] Anionic polymerisations of styrene and its derivatives have been heavily investigated in continuous microreactors.[16,117–119] A range of well-defined styrene homopolymers have been synthesised in seconds using microreactor technology by Nagaki[117] and Frey.[16,119] Frey and co-workers have also reported end group functionalisation of polystyrene by reactor telescoping.[16] This allowed for the preparation of various hydroxyl-terminated polystyrenes. Microreactor telescoping has also allowed the synthesis of complex di- and tri-block copolymers of styrene and alkyl methacrylates (Figure 1.29).[117]

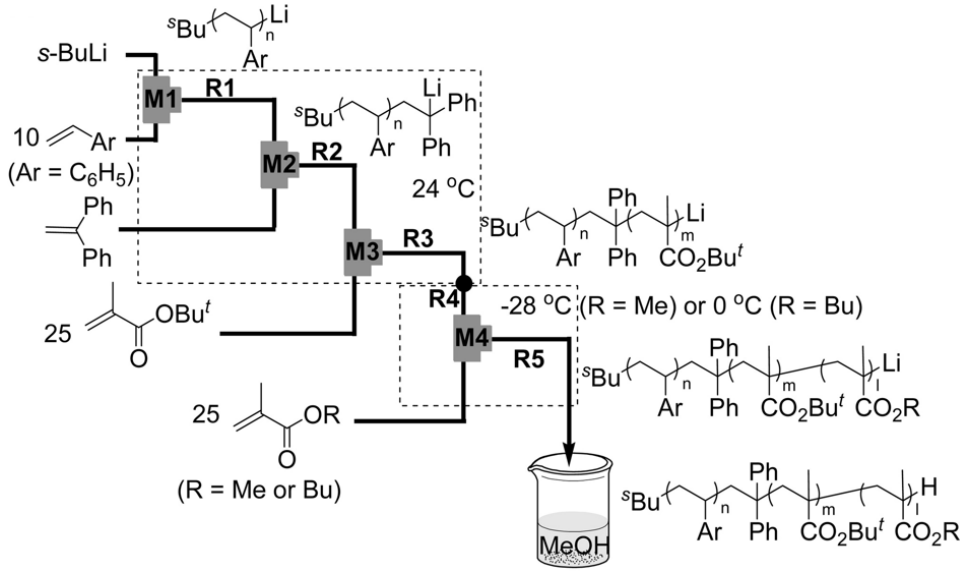

Figure 1.29: Microreactor flow system used for the block copolymerisation of styrene−alkyl methacrylate−alkyl methacrylate.[16] Reproduced with permission.

1.5.2 Free Radical Polymerisation in Flow

The improved heat transfer in flow reactors greatly benefits FRPs, which can often generate large exotherms as polymer viscosity increases.[120] Numerical simulations of different reactor geometries by Serra *et al.* demonstrated the significance of mixing efficiency and characteristic length scales for conversion, molecular weight control and dispersity in FRP.[121] Researchers at Axiva reported that premixing of monomer and initiator via micromixer decreased unwanted high molecular weight polymer fractions.[122] Yoshida *et al.* reported significant improvement for FRP of five different vinyl monomers in flow reactors with respect to molecular weight distribution.[123] Furthermore, by numbering up their microreactor system the synthesis of PMMA

was performed continuously for 6 days. A total of 4 kg of polymer was produced with consistent conversion, M_n and $Đ$.[124] The full effects of mixing in capillary reactors on the FRP of acrylamide were investigated by Su and co-workers.[125] The final polymer conversion, M_n and $Đ$ were all found to be proportional to the capillary diameter. Mechanistic investigations of FRP have also been carried out using flow platforms. Brocken *et al.* used a continuous flow platform for the high throughput screening of the free radical polymerisation of acrylic acid.[126] Monomer and initiator streams were mixed, via T piece, and passed through a heated tubular reactor. Over 100 experimental conditions were screened with multiple variables such as residence time, temperature, monomer concentration and initiator concentration being varied. The obtained data was used to predict reaction conditions to target specific molecular weights. Leibfarth *et. al.* used the precise control over reaction conditions afforded by flow to determine co-monomer reactivity ratios (Figure 1.30).[17]

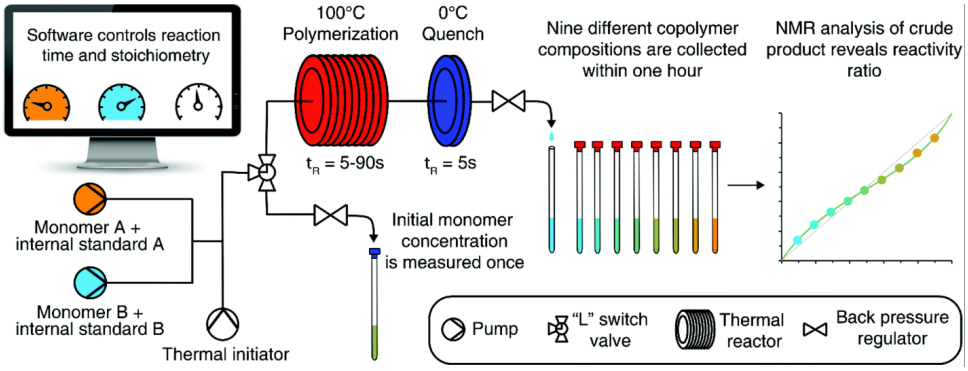

Figure 1.30: The continuous-flow system enabled the collection of nine samples of varying copolymer composition at low conversions in a single experiment. Different internal standards included in each monomer solution allowed accurate determination of monomer conversion by ^{1}H NMR analysis of the crude reaction mixture.[17] Reproduced with permission.

Initial reports of free radical emulsion polymerisation in tubular flow reactors indicated difficulties with fouling inside the reactor.[127,128] Many groups have reported that factors such as mixing rate,[127] surfactant concentration,[129] reactor material,[130] and geometry[131] can effect reactor blocking. Mini-emulsion polymerisations have also been performed in continuous tubular reactors.[18,130] McKenna and co-workers demonstrated that mini-emulsions with moderately high solid contents (up to 60 %) can be obtained under stable operating conditions.[130] Asua *et al.* have demonstrated an alternative method to performing mini-emulsion polymerisation.[18] A mini-emulsion is formed in a batch reactor and then pumped through a tubular reactor (Figure 1.31). Polymerisation occurred through light-mediated radical generation, allowing for high

monomer conversions in under 10 minutes.

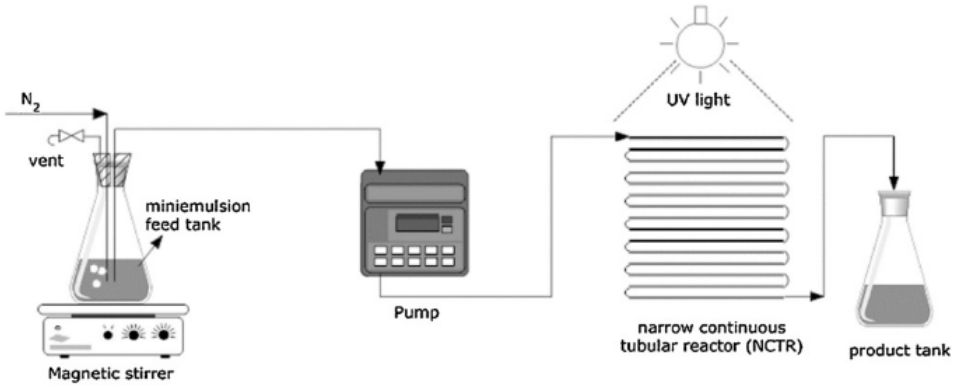

Figure 1.31: Experimental setup used by Asua *et al.*[18] for the free radical miniemulsion polymerisation. Reproduced with permission.

1.5.3 Reversible Deactivation Radical Polymerisation in Flow

1.5.3.1 Nitroxide Mediated Polymerisation in Flow

Often NMP reactions are conducted at high temperature (> 100 °C).[132] Therefore heat transfer is important for handling any exotherms generated during the polymerisation to prevent boiling of solvents. Rosenfeld *et al.* reported the first continuous tubular flow homogeneous NMP.[19] Batch and flow kinetics were obtained for the solution NMPs of styrene and butylacrylate at 140 °C (Figure 1.32). Similar kinetics and molecular weight evolution were observed for batch and flow for the NMP of styrene. Batch and flow kinetics for the NMP of butylacrylate greatly differed, the batch reaction reached near full conversion although the final polymer dispersity was high (Đ = 3), clearly showing loss of control. In the flow reactor, the NMP of butyl acrylate only reached 40 % conversion in the same time, however control of the polymerisation was maintained, indicated by a linear molecular weight evolution and low final disperity (Đ = 1.3). The difference in kinetics were attributed to poor dispersion of large exotherms generated in batch leading to thermal runaway of the polymerisation.[19] Enright *et al.* investigated the polymerisation kinetics of bulk NMP of styrene in a tubular and batch reactors and attributed the differences in final polymer to heat transfer.[133]

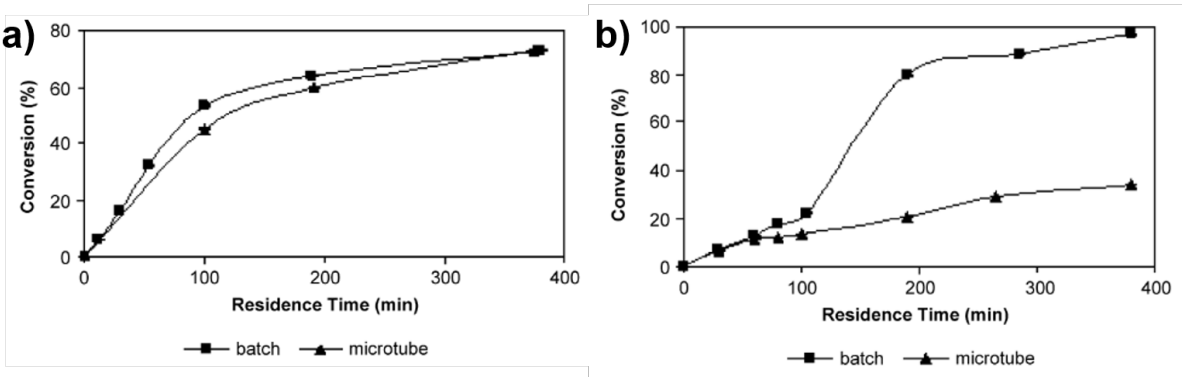

Figure 1.32: Kinetic data obtained for the NMP of a) styrene and b) butylacrylate in batch and flow reactors.[19] Reproduced with permission.

Further comparisons of batch and flow reactors were reported by Fukuyama and co-workers.[134] NMP of styrene and butyl acrylate were found to have higher conversions (87 %, 89 %) and lower dispersities ($Đ = 1.19$, 1.35) in tubular flow reactors than in batch. Fukuyama also reported a telescoped flow reactor system to perform the synthesis of block copolymers via NMP.[134] Styrene was chain extended using a poly(butyl acrylate) macromonomer, high conversion (76 %) and low dispersity ($Đ = 1.26$) was achieved with a residence time of 120 minutes and 140 °C.[134] The effects of mixing and mixer geometry for the telescoped reactor synthesis of the same copolymer system were investigated by Rosenfeld *et al.*[135] Higher conversion and lower dispersities were achieved when a multi-lamination mixer, which splits the reaction stream into multiple parallel streams to increase surface area, was used. Further studies indicated that the length and number of channels present in these mixers allowed for tuning of final polymer properties.[136] The use of continuous flow reactors has not been limited to solution NMP.[133,137] Enright *et al.* investigated the kinetics of the mini-emulsion NMP of styrene and found that both batch and flow reactors possessed similar kinetics.[137] Good control over the polymerisations ($Đ < 1.5$) were observed and both reactors produced similar size latex particles (approx. 170 nm). Enright *et al.* later reported using this mini-emulsion approach to generate di- and tri- block copolymer latexes.[133]

1.5.3.2 Atom Transfer Radical Polymerisation in Flow

There have been many reports of continuous flow reactors being used to perform solution ATRP to produce homo- and multi-block polymers.[114,138–143] Throughout these reports, comparable reaction kinetics and polymer quality between batch and flow reactors has been observed. The synthesis of non-linear polymers via ATRP has also been performed in tubular reactors. Bally

et al. first reported branching polymerisation by ATRP in a tubular reactor.[122] A series of branched polymers were synthesised by copolymerisation through solution ATRP of methyl methacrylate and 2-(2-bromoisobutyryloxy)-ethyl methacrylate in a tubular microreactor. Both the polymerisation rate and branching efficiency were found to be higher in the tubular reactor than in batch. Parida *et al.* also used a tubular flow reactor to synthesise branched poly(2-(dimethylamino)ethyl methacrylate)) by ATRP.[20] Branching efficiency was once again found to be greater in flow compared to batch. Interestingly, it was found that by altering the geometry of the tubular reactor the branching efficiency could be further improved (Figure 1.33).

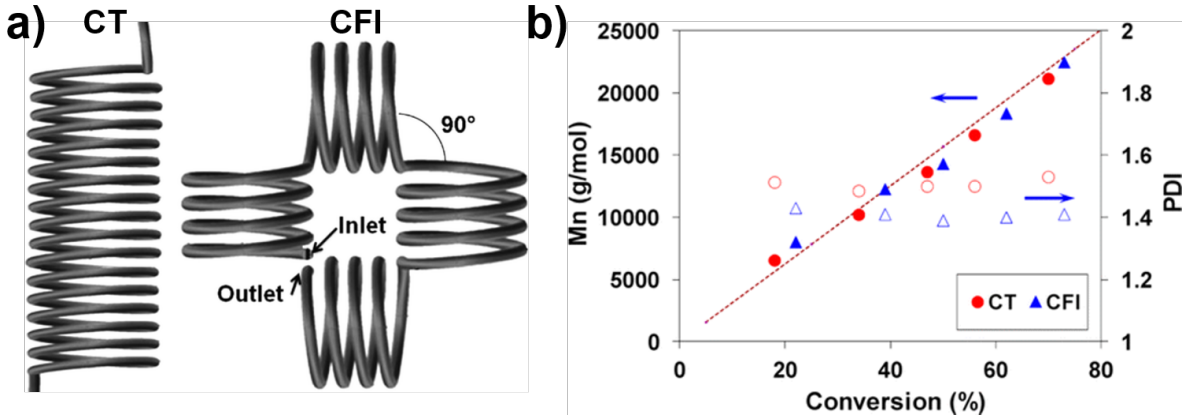

Figure 1.33: a) Coiled tube (CT) and coil flow inverter (CFI) microreactors used for the synthesis of poly(2-(dimethylamino)ethyl methacrylate)). b) Lower dispersity polymers were synthesised in the CFI reactor.[20] Reproduced with permission.

There are a growing number of reports concerning photo ATRP in flow reactors.[21,144–147] The shorter optical path lengths in flow reactors allow for uniform irradiation of the reaction solution, which is often an issue in batch. Increased reaction rates were observed for photo ATRPs in flow reactors compared to batch, likely due to the improved light penetration in flow. The magnitude of the rate increase depended on the transition metal used to mediate the polymerisation.[21,145–147] Kermagoret *et al.* reported a 30-fold increase in reaction rate for the cobalt mediated photo ATRP of vinyl acetate in flow reactors (Figure 1.34).[21] A smaller rate increase (approx. 6-fold) was observed for the copper[145] and iridium[146,147] mediated photo ATRPs of methyl methacrylate in flow reactors.

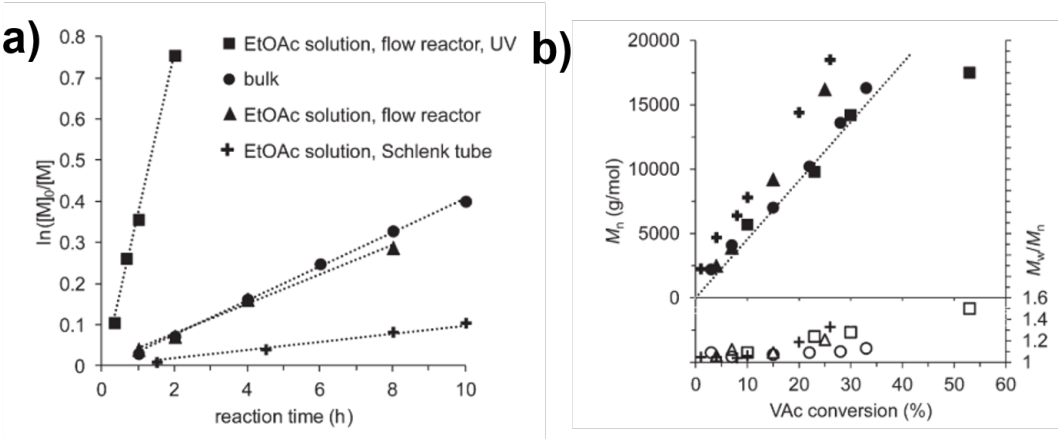

Figure 1.34: a) Semi-logarithmic plot and b) molecular weight evolution for the photo ATRP of vinyl acetate in batch and continuous flow reactors.[21] Reproduced with permission from The Royal Society of Chemistry.

One of the main disadvantages of traditional solution ATRP is the need to remove the metal catalyst from the final polymer solution.[148] Post-polymerisation purification steps add additional costs and waste to the overall process. One way to facilitate the removal of the metal catalyst is to perform ATRP with a heterogeneous catalyst.[149] Shen *et. al.* reported physically adsorbing a copper complex to silica gel and using it to successfully perform ATRP of methyl methacrylate in batch.[149] Following this Shen *et al.* transferred the system to flow by packing the silica supported catalyst into a stainless steel tube to produce a packed bed reactor (PBR).[150,151] ATRP of methyl methacrylate and subsequent chain extension with butyl methacrylate were succesfully performed using the PBR. However, the final polymer dispersities obtained were much higher than those produced in equivalent batch reactions, which they attributed to a broad RTD in the PBR. Another heterogeneous flow system was reported by Chan *et al.*[152] A flow reactor was designed using copper tubing, as solution was flowed through polymerisation occurred at tubing walls whilst also leaching copper into system. Methyl acrylate was successfully polymerised using the copper reactor; high conversion (70 %) and low dispersities (Đ = 1.2) were achieved, although an increase in dispersity was observed during continuous steady state operation of the reactor. This was attributed to a broadening residence time distribution as high molecular weight polymers grow near the tubing walls. This issue was resolved by altering the reactor platform to minimise contact with copper tubing (Figure 1.35).[22] Solution was flowed through a small portion of copper tubing to initiate the polymerisation and leach copper catalyst into solution, then mixed with asorbic acid and passed into stainless steel tubing for the rest of the polymerisation to take place.

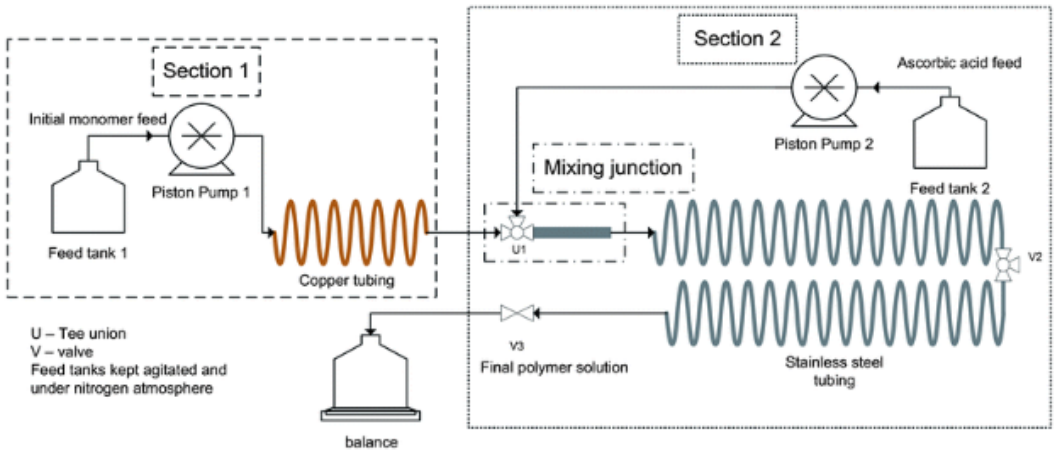

Figure 1.35: Continuous flow reactor system used by Chan *et. al.*[22] to perform the ATRP of acrylate to produce homo- and multiblock copolymers. Reproduced with permission.

1.5.3.3 Reversible Addition-Fragmentation Transfer Polymerisation in Flow

The first report of performing RAFT solution polymerisation in a continuous flow reactor was by Diehl *et al.*[153] The RAFT solution polymerisation of *N*-isopropylacrylamide was performed in both batch and a PFA flow reactor. Both batch and flow reactors gave low dispersity polymers ($Đ < 1.2$) but an accelerated rate was observed in flow with monomer conversion (88 % conversion) much higher than an equivalent batch polymerisation (40 % conversion). They attributed the accelerated rate to isothermal heating in flow. Hornung *et al.* also reported the use of continuous flow reactors for RAFT polymerisation.[23,154,155] Acrylamide, acrylate and vinyl acetate monomers were all successfully polymerised in a stainless steel tubular reactor to give high conversion (> 80 %) and low dispersities ($Đ < 1.3$).[154] A PFA reactor coil was also used for these polymerisations but no conversion was observed. It was determined that oxygen was permeating through the PFA tubing into the reaction solution and that this was preventing polymerisation. Facile incorporation of an inline degasser to the flow platform allowed for successful polymerisation without prior degassing of the reaction solution (Figure 1.36).[23] Hornung *et al.* later telescoped two reactors in order to synthesise block copolymers.[155]

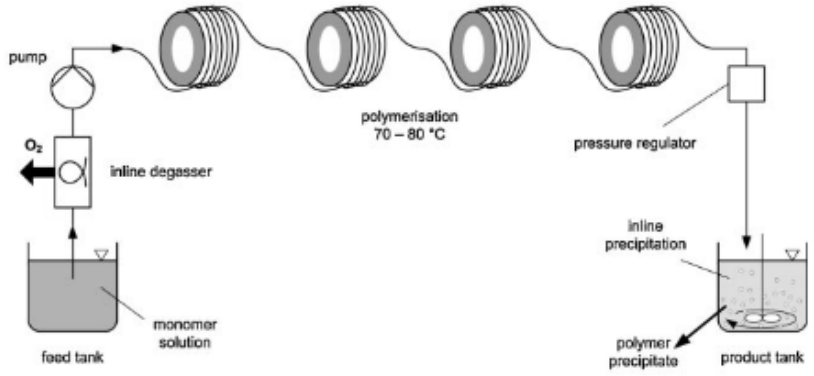

Figure 1.36: Continuous flow reactor system used by Hornung *et. al.*[23] to perform RAFT polymerisations without prior degassing of reaction solutions. Reproduced with permission.

Koch *et al.* reported the RAFT solution and bulk polymerisation of styrene under elevated temperature (120 °C) and pressure (50 bar) in micro-plant scale (25 - 100 mL) flow reactors.[156] The rate of polymerisation increased with concentration of styrene, with bulk polymerisation yielding the highest conversion (22 %) after 40 minutes. All polymerisations were well-controlled under bulk and solution conditions with linear molecular weight evolutions and low dispersites ($Đ < 1.4$) observed. The reactor setup was then employed to chain extend polystyrene with either methyl methacrylate or methyl acrylate by recirculating the polymer along with additional monomer. Kuroki *et al.* designed a "looped" flow reactor to generate multi-block acrylamide copolymers (Figure 1.37).[24] Initially, reaction solution was loaded and recirculated through a reactor coil until high conversion was reached, then more initiator and a different monomer was added to the loop and recirculated. This process was repeated to generate up to hexablock copolymers with high conversions (> 95 %) and low dispersites ($Đ < 1.2$) achieved for all block copolymers.

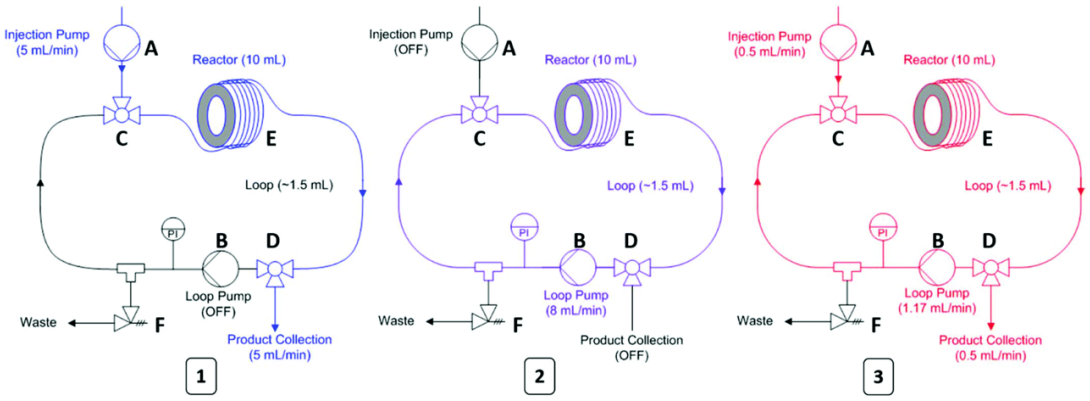

Figure 1.37: The different stages of the loop process: loading (1), loop circulation (2), injection of the following monomer (3) used by Kuroki *et al.*[24] Reproduced with permission.

Junkers and co-workers have also reported the synthesis of multiblock copolymers in flow reactors.[25,157] A premixed reaction solution containing butyl acrylate, 2-cyano-2-propyl dodecyl trithiocarbonate and AIBN was passed through a glass microchip reactor (20 µL) and the resulting polymer was collected, purified and chain extended using the same method.[157] This procedure was used to generate a penta-block copolymer although due to constant re-initiation of polymerisation, an increase in dispersity is observed for each block. However, the polymer dispersities obtained in flow were significantly lower than in batch (for the triblock copolymer synthesis batch Đ = 1.93 , flow Đ = 1.28). Junkers *et al.* later reported a larger telescoped reactor platform, which removed the need for purification steps between each polymerisation (Figure 1.38).[25] A large library of homo-, di-, tri- and tetra- block copolymers were synthesised using the reactor setup. As with the previous work polymer dispersity increased with the number of polymer blocks. Interestingly, polymer dispersity also increased rapidly with target DP which was not observed in their inital work. The final dispersity of a $PBuA_{80}$ differed depending on the reactor used, the microchip reactor (Đ = 1.18) gave a lower dispersity than the larger telescoped reactor (Đ = 1.27).

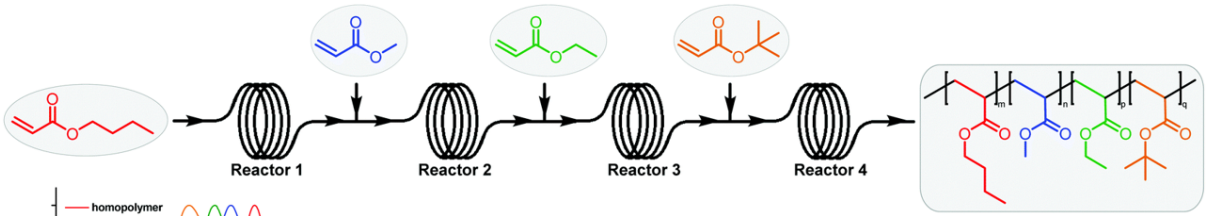

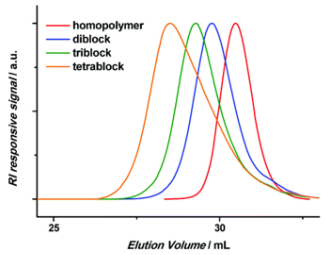

	Conversion / %	Đ	M_n^{app} / g · mol^{-1}	M_p^{app} / g · mol^{-1}	M_n^{theor} / g · mol^{-1}
Homopolymer	95	1.11	1630	1840	1630
Diblock	95	1.23	1960	2490	2490
Triblock	92	1.34	2380	3330	3490
Tetrablock	92	1.47	2990	5030	4780

Figure 1.38: Molecular weight distributions of PnBuA homopolymers with different chain lengths, polymerised in a 0.8 mL tubular reactor, at 100 °C and 16 min residence time reported by Baeten *et al.*[25] M_n^{app} is calculated for full monomer conversion. Determinations of M_n^{app} are based on the Mark–Houwink parameters of PnBuA. Reproduced with permission.

RAFT polymers are coloured because of the thiocarbonyl end groups, which limits their use for applications such as drug delivery, thus end-group removal and modification is necessary.[26] Hornung *et al.* reported a RAFT end group removal in a tubular reactor by aminolysis,[26] thermolysis[158] and a radical induced process[159] to generate polymers with various end groups. For radical induced end-group removal, RAFT polymers were mixed with *N*-ethylpiperidine hy-

pophosphite and passed through a continuous tubular reactor at 100 °C to generate hydrogen terminated polymer chains.[159] Similar processes were also used for aminolysis and thermolysis to generate thiol and alkene terminated polymers.[26,158] Additionally, for aminolysis and thermolysis Hornung *et al.* also reported telescoped reactor platforms for both RAFT polymerisation and end-group removal (Figure 1.39a).[26,158] Vandenbergh and Junkers have also reported end group modification of RAFT polymers via thiol-ene click chemistry in a continuous microreactor (Figure 1.39b).[27,160] Solutions of poly(butyl acrylate) synthesised by RAFT, hexylamine and various acrylates were passed through a micro reactor with a 20 minute residence time to generate various thiol-ene capped polymers.

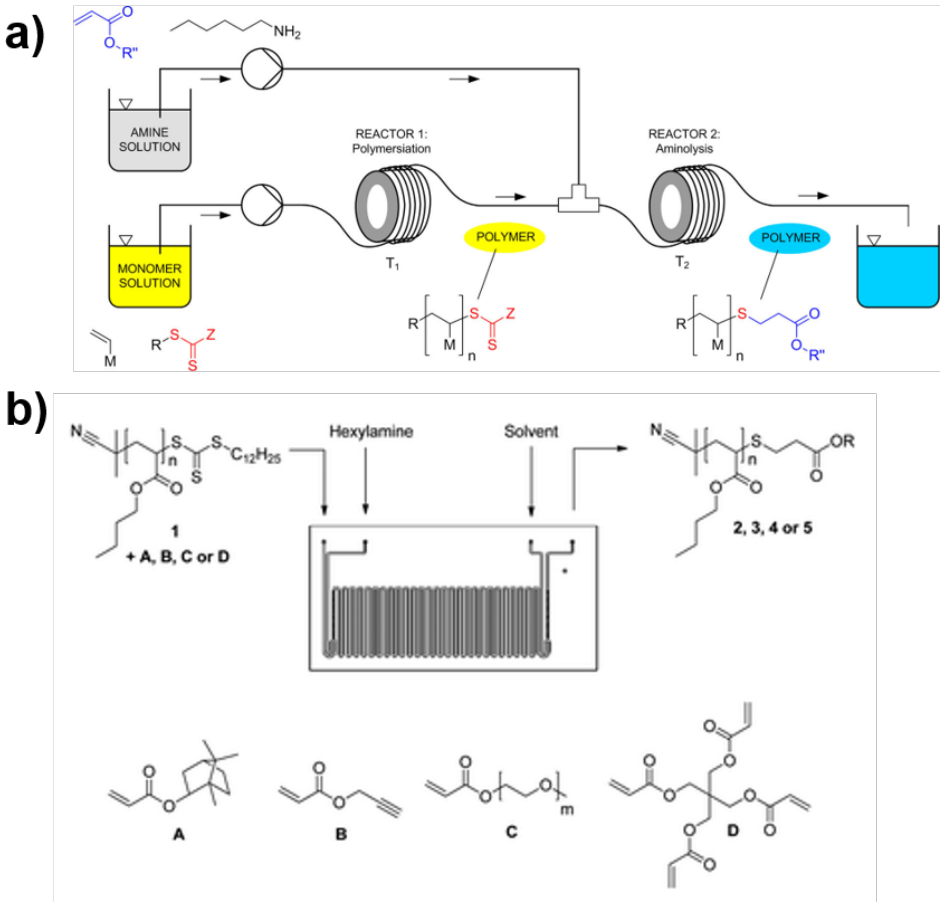

Figure 1.39: a) Telescoped reactor system reported by CSIRO[26] and b) microreactor system reported by Vandenbergh[27] for the end-group modification of RAFT polymers via aminolysis. Reproduced with permission.

Most polymerisations performed in flow reactors operate with a laminar flow regime and therefore have a residence time distribution. The effect of different residence time distributions on polymer dispersity was investigated by Reis and coworkers.[2] Reactors with larger internal diameters had broader residence time distributions which lead to an increased dispersity for the

RAFT polymerisations of *N*-isopropylacrylamide and butyl acrylate. Although it was observed that the impact on dispersity was less noticeable for slower polymerisations, as residence time distribution narrows with increasing residence time. A reactor platform capable of operating under true plug flow was also reported (Figure 1.40).[2] This was made possible by injection of gas into the reactor to generate reaction slugs. Polymerisations performed under plug flow conditions had lower dispersites compared to laminar flow polymerisations.

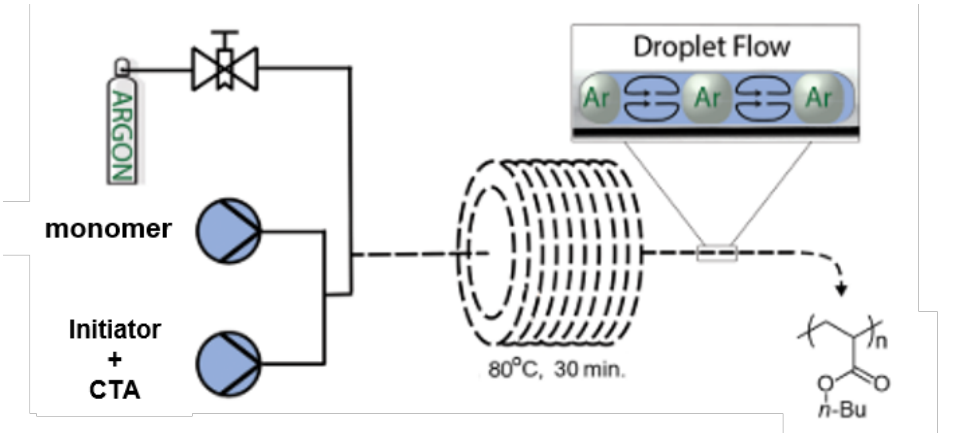

reactor geometry	M_n (g/mol)	$Đ$	conversion(%)
batch (2 mL scale)	13,400	1.14	62
flow (0.04 in. tubing)	13,100	1.17	64
flow (0.093 in. tubing)	13,100	1.26	65
droplet (0.093 in tubing)	13,600	1.15	60

Figure 1.40: Flow reactor developed by Reiss *et. al.*[2] in order to perform the RAFT polymerisation of butylacrylate under plug flow conditions. Reproduced with permission.

As with ATRP, there has been a strong interest in the development flow platforms to perform photo-based RAFT polymerisations.[28,29,32,161–169] Chen *et al.* report a continuous flow reactor with multiple configurations to perform photo-iniferter RAFT polymerisation.[28] Much like photo ATRP, an increased rate of reaction (approx. 4-fold) for the photo RAFT polymerisation of NIPAm was observed in flow reactors compared to an equivalent batch polymerisation. Chen *et al.* also demonstrated strong spatial control over the polymerisation under photoflow conditions (Figure 1.41).[28] By only irradiating specific sections of the reactor, the polymerisation could be halted and restarted. For higher target DPs light induced degradation of the RAFT agent lead to a sharp increase in dispersity. To minimise this degradation the reactor setup was altered to reduce light intensity. The new reactor setup was used to polymerise a range of acrylate and acrylamide monomers with relatively high chain lengths (DP = 250 - 2000) and all

polymers showed narrow dispersities (Đ < 1.3). Wenn *et al.* used photo-initiators to increase the rate of photo RAFT polymerisations in a glass microreactor.[161] Reaction conditions for the photo RAFT polymerisation of butyl acrylate (target DP = 80) using a photo-initiator (benzoin) were screened. Reaction temperature, benzoin concentration and light intensity were all optimised to give a high conversion (83 %) whilst keeping dispersity low (Đ = 1.18). Although it was observed that whilst photo-initiators increased the rate of polymerisation relative to photo-iniferter methods, final polymer dispersities (photo-iniferter Đ = 1.12) were higher due to unwanted termination.

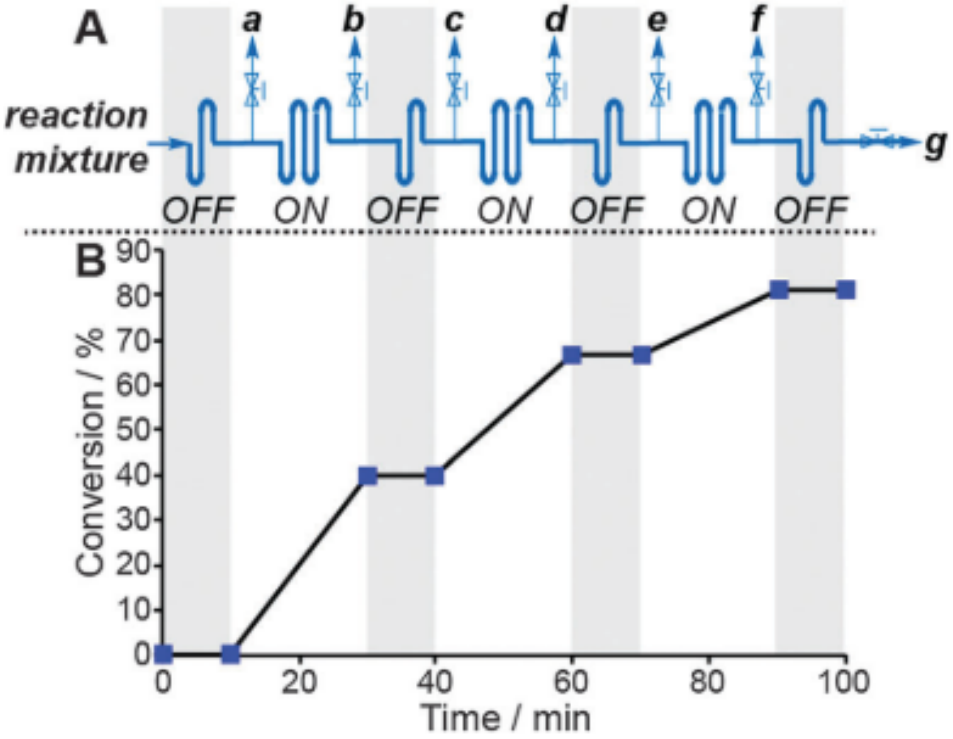

Figure 1.41: Flow reactor system reported by Hornung[28] capable of providing high spacial resolution over photo RAFT polymerisations. Reproduced with permission.

The polymerisation of methacrylate monomers under photoflow conditions was reported by Junkers and coworkers.[162] By performing the photoflow polymerisations at elevated temperature (90 °C) high conversions (> 90 %) and low dispersities (Đ = 1.4) could be achieved for all monomers within 60 minutes. Furthermore telescoping of this reactor system allowed for the synthesis well-defined methacrylate di- and tri-block copolymers. Junkers also reported the use of a high temperature photoflow setup to perform the RAFT polymerisation of isoprene.[163] Using a microreactor a 20-fold rate increase was observed without loss of control over the polymerisation. Successful chain extension with styrene indicated high end group fidelity. The

entire reactor system was scaled up 100-fold to 2 mL without affecting the reaction kinetics, allowing for the generation of 6 g of poly(isoprene) within 6 hours of continuous operation. An alternative photo RAFT process, photo electron transfer RAFT (PET-RAFT) which allowed for oxygen tolerant polymerisation was transferred to flow reactors by Corrigan *et al.*[29,164–166,169] PET-RAFT uses excited zinc tetraphenylporphyrin (ZnTPP) to both deactivate oxygen and act as a photo-redox catalyst to activate the RAFT agent. A flow reactor was used to perform the PET-RAFT polymerisation of diethylacrylamide at numerous residence times and concentrations.[164] High conversions (90 %) were achieved at long residence times (60 minutes) and excellent dispersities ($Đ < 1.2$) were observed for all polymerisations. Corrigan *et al.* later reported automation of this flow platform to enable tailoring of polymer molecular weight distributions (MWD).[165] PET-RAFT of dimethylacrylamide was performed continuously whilst altering reaction parameters (residence time, concentration, light wavelength and intensity). Depending on the conditions a variety of MWDs could be obtained (Figure 1.42). Although, this control over MWD was limited by the laminar flow profile, which allowed for mixing of different experiments in the reactor. This problem was addressed in later work which details the use of a plug flow regime to eliminate mixing between different reaction conditions.[29,166]

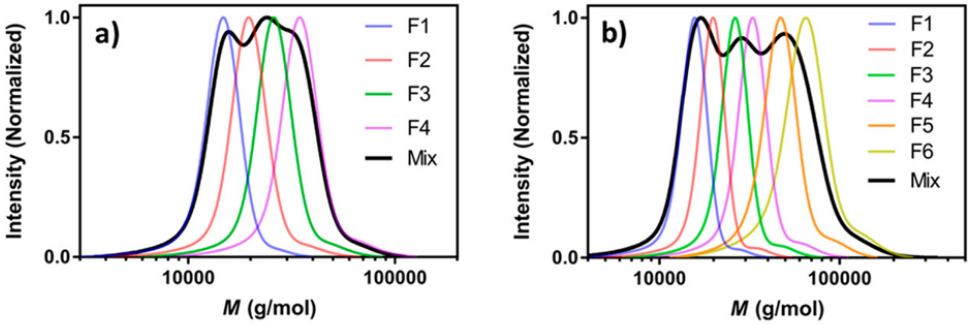

c)

#[a]	Fraction	α (%)[b]	M_p (kg/mol)[c]	M_n (kg/mol)[c]	Đ[c]	Skewness[d]	Kurtosis[d]	FWQM/ FWTQM[e]
1	1	92.5	14.8	13.9	1.07	0.137	5.886	2.34
2	2	94.8	19.6	18.6	1.08	1.075	7.979	2.34
3	3	94.8	26.0	24.6	1.08	0.949	6.829	2.35
4	4	95.2	34.6	32.3	1.10	1.190	7.921	2.38
5	Tailored MWD 1	-	23.9	20.3	1.21	1.472	6.518	1.51
6	Tailored MWD 2	-	17.0	24.6	1.44	2.326	12.72	1.55

Figure 1.42: Tailored MWDs produced in a single pass flow system. a) Tailored MWD 1, composed of four distinct molecular weight polymer fractions. b) Tailored MWD 2, composed of six distinct molecular weight polymer fractions. c) Polymer characteristics for tailored MWDs 1 and 2 and the individual fractions of tailored MWD 1.[29] Reproduced with permission.

The automation and incorporation of analytical techniques into flow reactors for screening

and optimising reactor conditions has been researched by Junkers and coworkers.[30,31,170–173] Initially, an electrospray ionisation mass spectrometer (ESI-MS) was placed at the outlet of a microchip reactor and was used to monitor the RAFT polymerisation of butyl acrylate.[170,171] Using this setup it was possible to observe insertion of single monomer units. The early stages of the RAFT mechanism were also probed using this setup and cross-termination products, often theorised to exist were successfully observed.[172] Another automated flow platform developed by Junkers incorporated GPC allowing the targeting of specific polymer molecular weights (Figure 1.43a).[30] Initially, the platform was used to screen the RAFT polymerisation of butyl acrylate, residence time and target DP were varied and the molecular weight of every sample was determined by GPC. Through incorporation of a bespoke optimisation algorithm the platform was able to identify conditions to give a target molecular weight within ten iterations from startup, subsequent changes were reached in fewer iterations(Figure 1.43b).[30] The versatility of the platform was demonstrated by performing molecular weight optimisation for polymerisation and chain extension of a series of methacrylate and acrylate monomers.

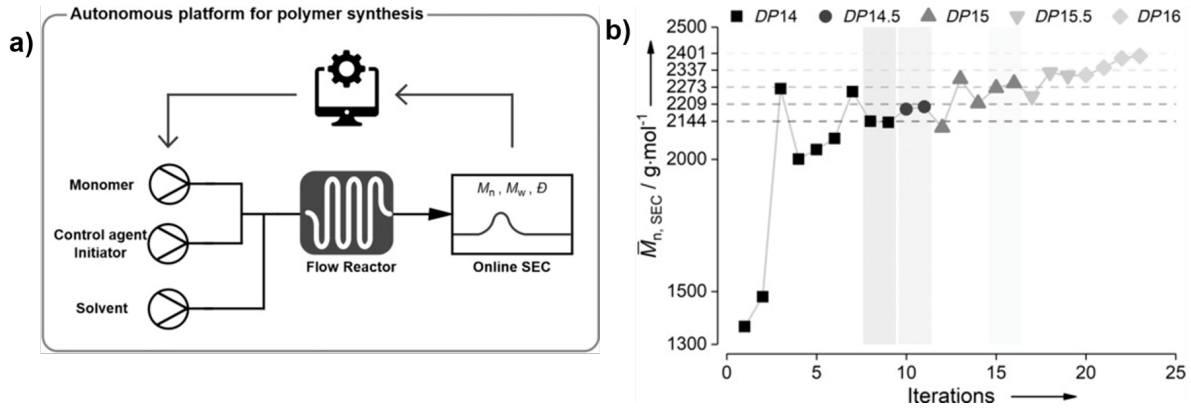

Figure 1.43: a) Experimental setup used by Junkers *et al.* for the b) optimisation for the RAFT polymerisation of poly(butyl acrylate) with target degrees of polymerization: 14, 14.5, 15, 15.5, and 16.[30] Reproduced with permission.

Junkers also recently reported the incorporation of NMR to a continuous flow platform.[31] Using online NMR, monomer conversion and subsequently reaction kinetic could be easily monitored. One large timesweep (10 s to 60 min) was used to collect vast amounts of transient kinetic data for the RAFT polymerisation of methyl acrylate. However, the kinetic profile obtained did not agree with steady state measurements also taken for the polymerisation (Figure 1.44a). As the biggest deviation between the two kinetic profiles was at low conversions, it was assumed that large changes in flow rate led to non-ideal flow behaviour. To eliminate this four timesweeps with

less drastic flow rate changes were performed and the obtained kinetic profile agreed well with the steady state profile. Conversion targeting was then performed for the RAFT polymerisation of methyl acrylate over a range of reaction temperatures (Figure 1.44b). The optimisation algorithm first performed a timesweep to generate a kinetic profile, if the desired conversion was obtained within the timesweep, the kinetic profile is used to determine and set the reactor to the appropriate residence time. If the conversion is not observed then more timesweeps are performed until the desired conversion is observed. Another system for online monitoring of polymer conversion was reported by Lauterbach.[174] Conversion was monitored by inline UV-Vis spectroscopy; as polymerisation progressed a contraction in volume and subsequent increase in concentration was observed. By monitoring the increase in absorbance a conversion value could be obtained provided the response was already calibrated.

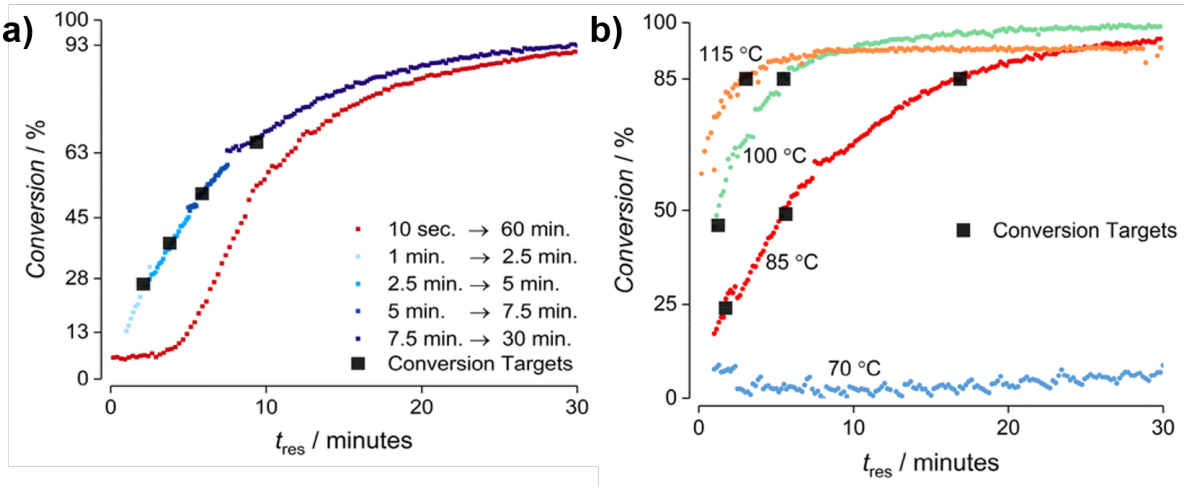

Figure 1.44: a) Wide range timesweeps and b) thermal screens of the RAFT polymerisation of methyl acrylate which were then used to target specific monomer conversions.[31] Reproduced with permission.

Heterogeneous RAFT polymerisation systems have also been performed on continuous flow platforms. Russum *et al.* have reported performing the RAFT mini-emulsion polymerisation of styrene in tubular reactors.[175–177] An emulsion mixture was flowed into a sonication vessel to generate mini-emulsions which where then fed into the tubular reactor.[175] Polymerisation kinetics in the tubular reactor were slightly faster compared to batch. However, higher dispersities were observed for the flow polymerisation likely due to the residence time distribution. High end group fidelity for polymers synthesised in flow was determined by successful chain extension with butyl acrylate in batch.[176] Additionally, Russum *et al.* operated the reactor platform in a plug flow regime, this allowed for polymer dispersities similar to batch reactors to

be obtained.[177] One issue that limits the commercial implementation of continuous emulsion polymerisation processes is the large amount of surfactant required to stabilize the droplets.[1] Recently, Li *et al.* reported a surfactant-free RAFT emulsion polymerisation of MMA in a tubular reactor, where the RAFT agent (4-cyano-4-(thiobenzoylthio)-pentanoic acid) also acted as an emulsion stabiliser.[178] The synthesis of polymeric nanoparticles via PISA in tubular flow reactors was first reported by Peng *et al.* A telescoped reactor system was used to synthesise poly(oligo ethyleneglycol methacrylate) (POEGMA) and chain extend the polymer with methyl methacrylate via RAFT emulsion polymerisation.[179] The mixer geometry was found to effect the nanoparticle size during the formation of the PMMA block. Insufficient mixing when using T-piece mixers gave nanoparticles approx. 30 nm in size regardless of monomer conversion, which is not expected for PISA. Static mixers provided better mixing and as expected nanoparticle size increased with monomer conversion.

The continuous flow synthesis of polymeric nanoparticles via PISA has also been reported by Zaquen and coworkers.[32,167–169] A single reactor photoflow platform was used to perform the RAFT aqueous dispersion polymerisation of 2-hydroxypropryl methacrylate using a poly(ethylene glycol) macro-CTA.[167] On the photoflow platform, a range of block copolymer spheres, worms and vesicles were successfully synthesised at high conversion after 90 minutes. However, TEM analysis of vesicles formed on the photoflow reactor appeared patchy which was not observed for vesicles synthesised in batch. A telescoped photoflow reactor system was also reported for the PET-RAFT synthesis of poly(dimethylacrylamide)-poly(diacetone acrylamide) (PDMAm-PDAAm) nanoparticles.[32] A series of PDMAm-PDAAm nanoparticles were synthesised in both batch and flow (Figure 1.45). Both PDMAm and PDAAm block lengths and polymer concentration were varied in order to generate spheres, worms and vesicles as well as intermediate morphologies. It was observed that synthesising higher molecular weight polymers at high concentrations led to blockages in the reactor. Interestingly, different nanoparticle morphologies were observed for batch and flow reactors, although the authors offered no explanation for this phenomenon.

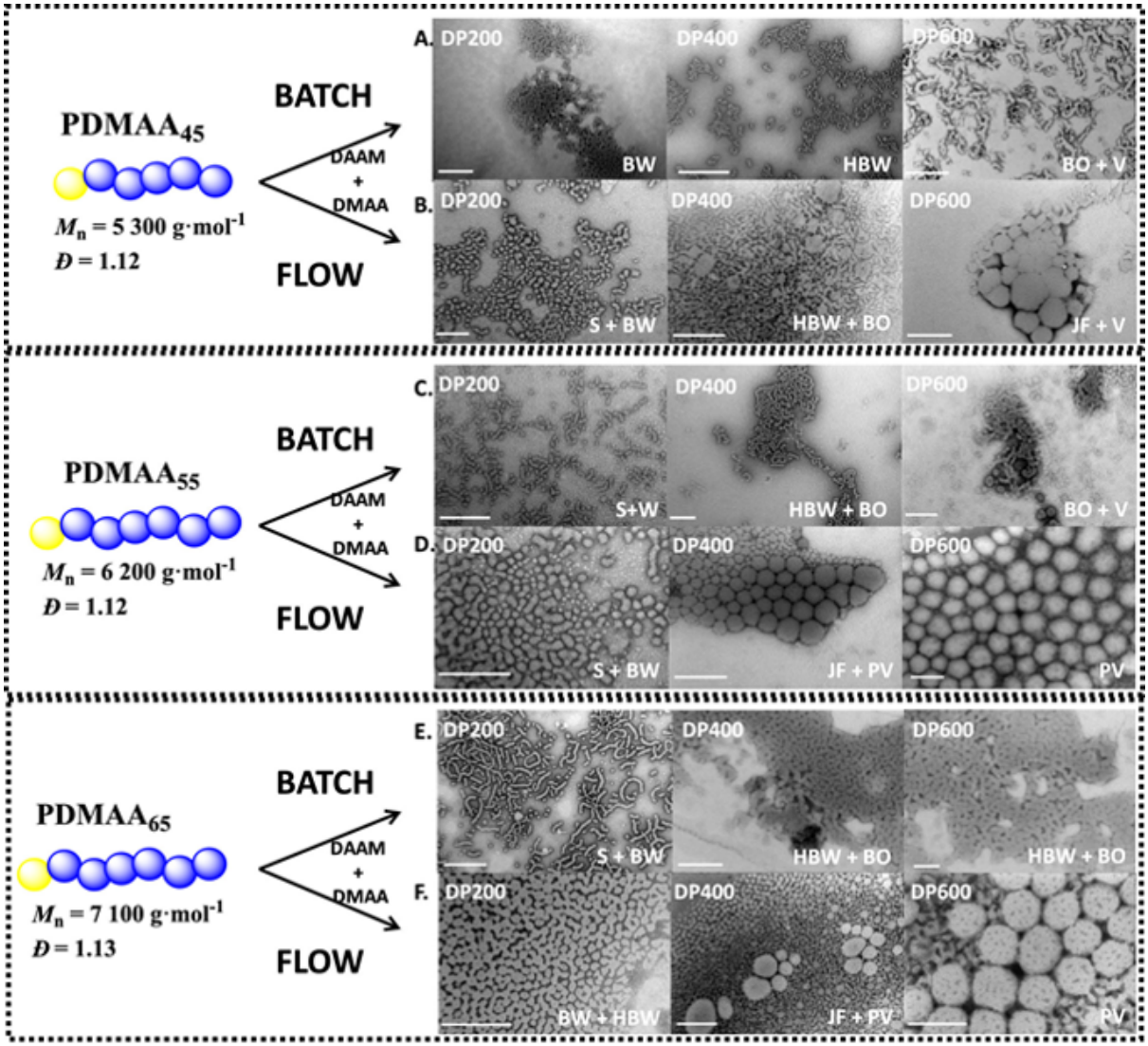

Figure 1.45: TEM micrographs of PDMAA-b-(PDAAm-co-PDMAA) PNPs via aqueous PET-RAFT PISA at [M]:[macroRAFT]:[EY]:[TEtOHA] = x:1:0.01:1 using a batch (header A, C, and E) or flow (header B, D, or F) process. Evolution of morphologies obtained by varying the target degree of polymerisations (DP = 200, DP = 400, and DP = 600) at 17.5 wt % solid content. Scale bars are 0.5 µm, and s = spheres, bw = branched worms, hbw = highly branched worms, bo = bilayer octopi, jf = jellyfish, v = vesicles, and pv = patchy vesicles.[32] Reproduced with permission.

1.6 This Project

These recent developments in continuous flow RAFT polymerisations have aided the growth of this relatively new field of research. This work adds further knowledge of performing and profiling RAFT aqueous and dispersion polymerisations, in a variety of flow reactors, to the current field of research. Furthermore, the ability to perform RAFT polymerisations rapidly and in a continuous manner using flow reactors will hopefully increase the commercial viabil-

ity of the technique. Additionally, work on a new automated reactor platform equipped with multiple analytical techniques capable of monitoring, screening and self-optimising RAFT polymerisations is at the forefront of the field. Automated reactor systems equipped with online analytical techniques also potentially have significant commercial applications either through optimising known polymerisation processes or screening new polymer systems when developing a new process In this work, RAFT polymerisation techniques are combined with continuous flow reactors to synthesise and optimise a series of well-defined homo and block copolymers. Specifically, kinetics for the RAFT polymerisation of dimethylacrylamide and subsequent chain extensions with *N*-isopropylacrylamide or diacetone acrylamide in both batch and flow reactors are obtained and compared. Poly(dimethylacrylamide)-poly(diacetone acrylamide) block copolymer nanoparticles are synthesised by RAFT-PISA in flow reactors to generate a range of particle morphologies. Thereafter, the potential production rate of polymer is improved by increasing the radical flux present during the polymerisation thereby accelerating the reaction kinetics. The ability to generate a range of poly(dimethylacrylamide)-poly(diacetone acrylamide)block copolymer nanoparticle morphologies in flow under these accelerated reaction conditions is then assessed. Finally, a continuous flow platform is developed which incorporates key polymer analytical techniques (NMR, GPC) to allow for the continuous monitoring and screening of polymerisation conditions. Through incorporation of state of the art machine learning algorithms it was possible for the reactor to self optimise the RAFT polymerisations of both dimethylacrylamide and *tert*-butyl acrylamide to both minimise dispersity and maximise conversion.

1.6.1 Project Aims

The specific aims of this project are to:

- Determine the effect performing RAFT polymerisation in flow reactors has on polymerisation kinetics and polymer properties (M_n and $Đ$)
- Optimise the synthesis of block copolymer nano-objects via PISA in flow reactors
- Build an automated flow platform to perform and analyse, via online NMR and GPC, RAFT polymerisations
- Incorporate a machine learning algorithm into an automated flow system to enable autonomous self-optimisation of RAFT polymerisations for multiple objectives

Chapter 2

Continuous Flow Platform Design and Characterisation

This chapter describes the development and characterisation of flow platforms used throughout this thesis. In chapter 3 a basic flow platform, Reactor A, was developed in order to perform RAFT solution and dispersion polymerisations. A transient profiling methodology was also developed in order to obtain polymerisation kinetics using the reactor. In order to be able to adequately assess any differences between polymerisations performed in batch and flow, full characterisation of the flow platforms is required therefore Reactor B was developed. Reactor C was developed in chapter 4 in order to perform and monitor accelerated RAFT dispersion polymerisations to generate polymeric nano-particles. Finally, a fully automated reactor platform, Reactor D, was developed during chapter 5 to screen and optimise reaction conditions the RAFT solution polymerisations.

2.1 Reactor A

Reactor A (Figure 2.1) was the first flow platform developed for this thesis. It was used in chapter 3 to perform the RAFT solution polymerisation of dimethylacrylamide (DMAm) and RAFT aqueous dispersion polymerisation of *N*-isopropylacrylamide (NIPAm) and diacetone acrylamide (DAAm) using a PDMAm macro-CTA. The reactor comprised of a SyringeONE syringe pump or Jasco PU-980 HPLC pump connected to a stainless steel tubular reactor coil (2.1 mm I.D, 5 mL or 20 mL) wrapped around an aluminium heating block on a IKA

hotplate. Initially, the syringe pump was used to acquire transient kinetic profiles for the RAFT polymerisation of DMAm, when production of PDMAm needed to be increased for further experiments the syringe pump was replaced with the HPLC pump and a back pressure regulator (BPR) was added.

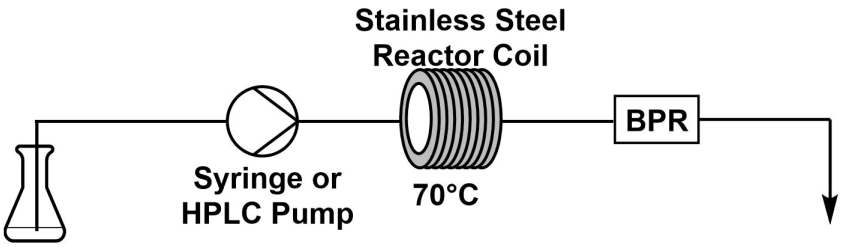

Figure 2.1: Reactor A used in chapter 3 to perform and obtain kinetic data for RAFT solution and dispersion polymerisations.

2.1.1 Transient Kinetic Profiling Method

There are two ways to obtain kinetic data using flow reactors: steady state sampling or transient sampling. Steady-state sampling is often used for kinetic profiling of RAFT polymerisation in flow reactors.[153,154,176] Achieving steady state for every residence time is required to generate a kinetic plot. This requires large volumes of material and is much more time-consuming than a typical batch kinetic study especially when aiming to obtain a similar number of kinetic time points. An alternative approach is to conduct transient state kinetic sampling. During this process, samples are continuously collected from the reactor, but each sample has a different residence time due to specifically controlling pump rates. Under ideal conditions, each sample can be considered to be an individual reaction. Various methods for transient kinetic sampling have been reported in the literature for polymer and small-molecule synthesis.[141,170,180–182] Based on these literature methods, a protocol was developed for transient kinetic sampling which is used throughout this thesis to collect kinetic data for RAFT polymerisations (Figure 2.2).

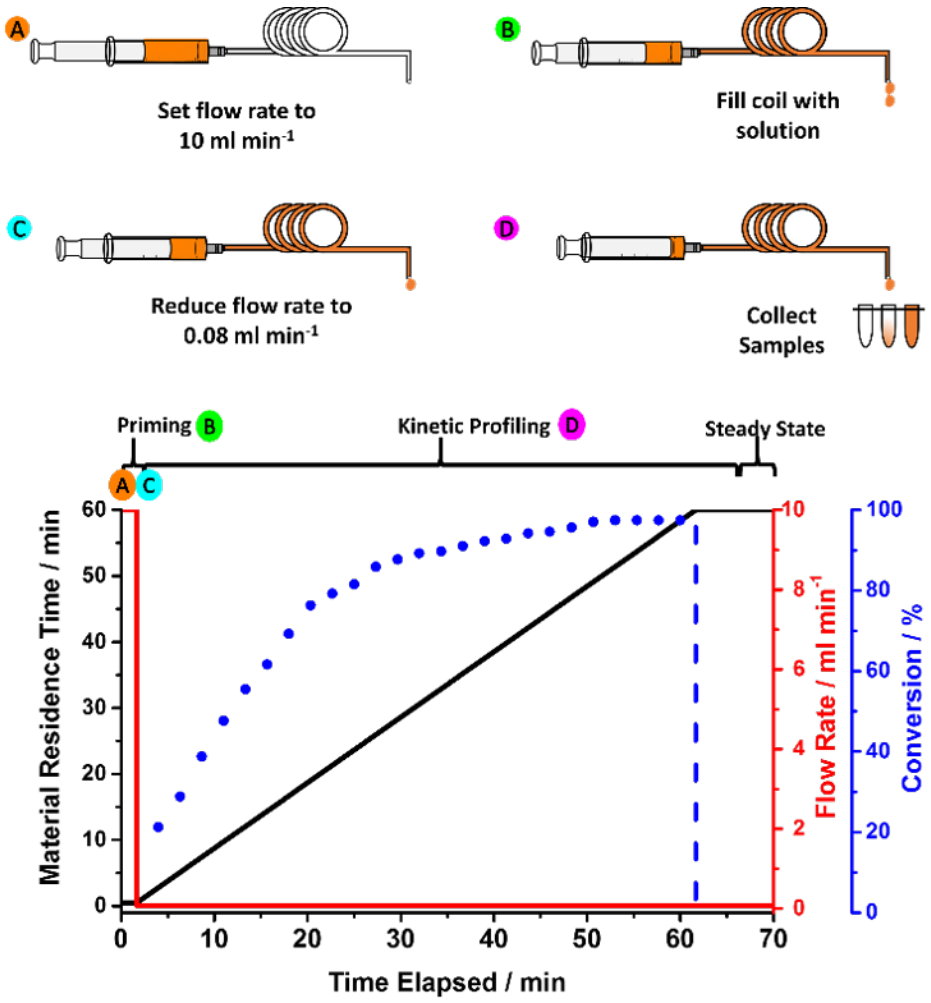

Figure 2.2: Schematic of high resolution kinetic profiling technique used for monitoring the RAFT polymerisation of dimethylacrylamide in chapter 3. (A) the pump flow rate is set to 10 mL min^{-1} and pumping is started, (B) the reactor is then primed with reaction solution (C) and once the reactor is filled with solution the flow rate is reduced to give our desired residence time (0.08 mL min^{-1}). (D) Samples are then collected at set intervals from the reactor outlet. Plot indicates material residence time, flow rate and conversion as a function of the experimental time.

Reactor A was primed with reaction solution at a flow rate of 10 mL min^{-1} until the system reached steady state. The flow rate was then instantaneously reduced to 0.08 mL min^{-1} and samples were collected from the reactor outlet at regular intervals. The sample residence time (t_{res}) is given by:

$$t_{res} = \frac{V_{reactor}}{f_1} + t_m(1 - \frac{f_2}{f_1}) \tag{2.1}$$

whereby t_m is the reaction time of the sample, $V_{reactor}$ is the total volume of the reactor, f_1 is the priming flow rate and f_2 the flow rate after the start of the timesweep. These samples were characterised by ^{1}H NMR and DMF GPC to determine monomer conversion, molecular weight

and molar mass dispersity (Đ).

2.2 Reactor B

One of the main differences between batch chemistry and continuous flow is related to concentration profiles.[4] In a batch reaction the reactant concentration decreases over time and is uniformly distributed throughout the reactor. Conversely in flow, the concentration of starting material decreases along the reactor reaching a minimum at its end. However, concentration also varies across the reactor stream due to the parabolic velocity profile of laminar flow regimes. This leads to a dispersity in the residence times that material experiences often called the residence time distribution (RTD).[183] As stated in Section 1.1, it is important to know the residence time distribution for any given reactor to be able to compare to both batch reactors and other flow reactors. One method for determination of RTD is to inject a tracer pulse into the reactor and monitor its elution from the reactor.[2] Therefore, Reactor B (Figure 2.3) was developed in order to characterise the reactor coils using this method. A sample loop was placed between the HPLC pump and reactor coil to allow a tracer pulse to be injected into the system. The tracer pulse was monitored as it exited the reactor by an RI detector placed at the reactor outlet.

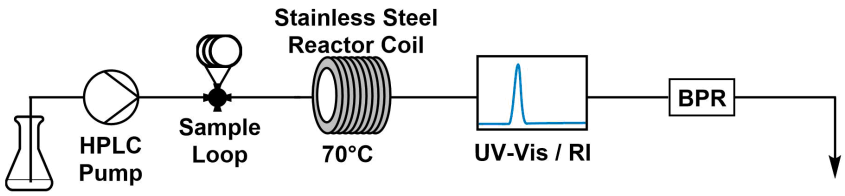

Figure 2.3: Reactor B used to characterise the reactors used in chapter 3 to perform RAFT polymerisations

2.2.1 Determination of Residence Time Distribution

To determine the residence time distribution in both reactor coils (5 mL and 20 mL), a dimethylacrylamide tracer was injected into a water stream (flow rate = 1.0 mL min^{-1}) and monitored at the reactor outlet. The 20 mL reactor coil was shown to have a narrower RTD than the 5 mL coil (Figure 2.4). This is likely due to any flow interruption, such as dead-zones at connecting joints, having more of an influence in the shorter 5 mL reactor.

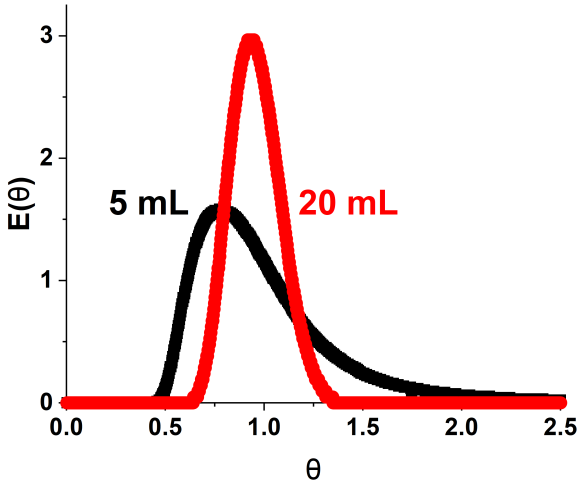

Figure 2.4: Dimensionless residence time distribution plots comparing the behaviour of dimethylacrylamide in 5 mL and 20 mL stainless steel tubular reactors.

Another important factor to consider for polymerisations is that the viscosity of the solution is likely to increase along the reactor coil as polymer chains increase in length. Increases in viscosity reduce the Reynolds number (Equation 1.1) and have been reported to broaden RTDs and polymer dispersity.[2] The largest difference in RTD is likely to be between the start and end of the reactor where the polymer chains are the shortest and longest. To determine any changes in the RTD during polymerisation the RTD tracer experiment for the 5 mL coil was repeated using a $PDMAm_{100}$ tracer (30 % w/w). The RTDs obtained for the DMAm and PDMAm tracers (Figure 2.5) were found to be similar indicating polymer viscosity is not causing an increase in dispersity.

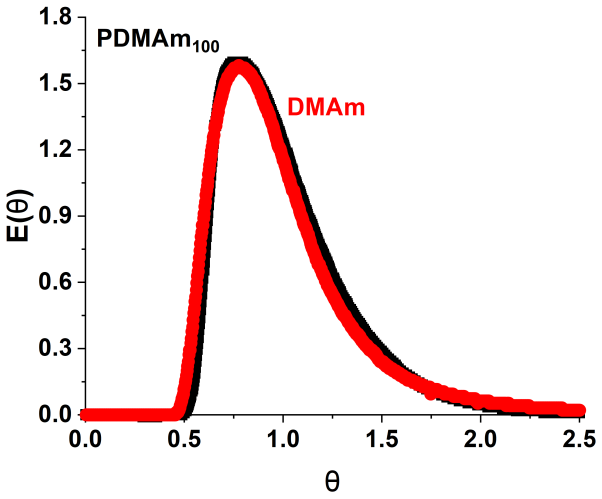

Figure 2.5: Dimensionless residence time distribution plots comparing the behaviour of dimethylacrylamide and poly(dimethylacrylamide) in a 5 mL stainless steel tubular reactor.

2.2.2 Determining Reactor Steady State

Flow reactors typically operate under steady state conditions, where the flow rate is fixed and at any point along the reactor material will experience the same reaction parameters over time. Upon changing reaction conditions there is a time delay to achieving steady state, often a number of reactor volumes.[4] The time to reach steady state conditions in the reactor was determined by pumping a reaction solution through the 5 mL tubular reactor and using a UV-Vis spectrometer to monitor the RAFT agent concentration. After 1.5 minutes (3 reactor volumes) the response became constant (the observed noise is due the decreased signal to noise ratio when using a flow cell); thus steady state was achieved (Figure 2.2.2).

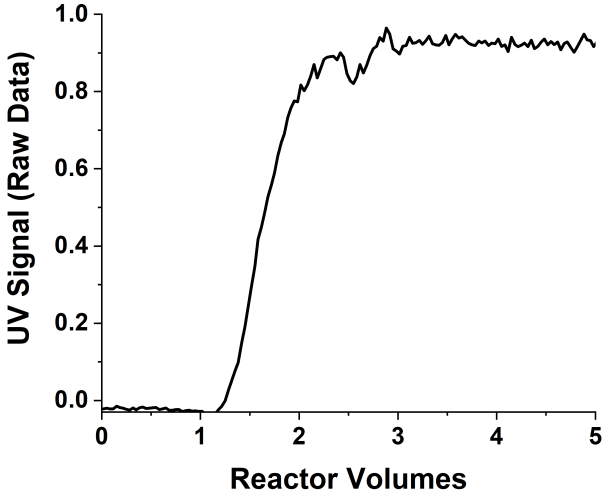

Figure 2.6: UV signal, measuring absorbance at 420 nm, indicating steady state is reached in the reactor after 3 reactor volumes. Reaction solutions were all 30 % w/w solids and [DMAm]:[CTA]:[ACVA] = 100:1:0.1.

2.3 Reactor C

Reactor C (Figure 2.7) was developed in Chapter 4 in order to perform and obtain kinetics for the ultrafast synthesis of PDMAm-PDAAm polymeric nano-particles. To simplify the collection and analysis of kinetic samples generated by the transient profiling method a benchtop NMR instrument was placed at the reactor outlet. Reactor C differs from all other platforms as it contains a 5 mL PFA coil reactor. The reactor material was changed from stainless steel due to fouling observed in chapter 3 when synthesising high order polymeric nano-particles. One of the important factors when choosing the new reactor material was oxygen permeability. Typically, radical polymerisations are highly intolerant to oxygen, a radical scavenger, which will terminate propagating radicals. It is well known that polymeric tubing materials, such as PFA, can be permeated by oxygen.[184] Hornung *et al.* has reported that attempting to perform a RAFT aqueous solution polymerisation within a PFA tubular reactor resulted in no polymerisation.[154] However, the successful synthesis of high order polymer nano-objects in PFA reactors has been reported by Junkers and co-workers,[32,167–169] confirming that PFA is a suitable reactor material for carrying out heterogeneous polymerisations.

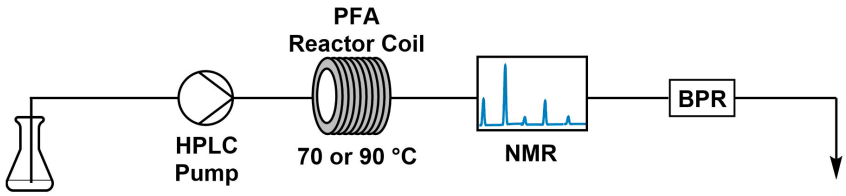

Figure 2.7: Reactor C used in chapter 4 to perform ultrafast RAFT polymerisations and synthesise a range of PDMAm-PDAAm nano-particle morphologies.

2.3.1 Online NMR Analysis

This section includes work from a jointly authored publication.[185] *The work presented here was equally contributed to by Sam Parkinson and Dr. Stephen Knox.*

NMR spectroscopy is one of the most powerful spectroscopic techniques available to polymer chemists due to its ability to generate large detail on chemical structure especially in increasingly complex polymer systems or formulations.[7] Traditional NMR instruments are often large, costly and limited in terms of operating conditions, stifling their uptake into on-line monitoring platforms. However, newer "benchtop" NMR systems that utilise lower field permanent magnets, have allowed for much more rapid uptake into on-line monitoring platforms.[7,58,186] After the NMR was attached to the reactor outlet a protocol was developed that minimised acquisition time whilst maintaining spectra quality.

2.3.1.1 Spectrum Acquisition Time

The time taken to acquire a spectrum is proportional to the number of scans acquired per spectrum. The fewer the number of scans required the faster the spectrum will be acquired however fewer scans will lead to a lower signal to noise ratio (S/N), which may impact spectrum quality. Typically, 32 scans were collected for NMR spectra acquired on traditional high-field instruments such as those obtained in chapter 3. This parameter was optimised by collecting NMR spectra of a low conversion $PDMAm_x$ sample whilst varying the number of scans (2-32). The subsequent conversion calculated from these spectra indicate very little change is observed with conversion always consistently around 35 % (Figure 2.8). Therefore, two scans were performed for all further NMR spectra allowing for the fastest spectra collection without compromising spectra quality.

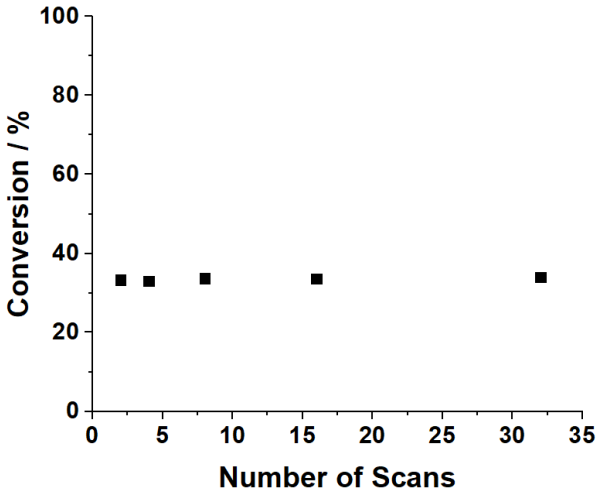

Figure 2.8: Conversion data obtained from NMR spectra of a $PDMAm_{100}$ kinetic sample using either 2, 4, 8, 16 or 32 scans.

2.3.1.2 Pulse Techniques

One major benefit of the incorporated NMR system is the ability to acquire NMR spectra in non-deuterated solvents, which is not possible for traditional high field systems. Therefore reaction solution can be passed directly from the reactor outlet through the NMR for analysis. However, the solvent peaks observed in the spectra are much more intense than with deuterated solvents. This results in significantly broader solvent peaks which can lead to overlap or convolution of other signals in the spectra. One method of removing these large solvent peaks is a technique called presaturation (Figure 2.9), where a long low-power pulse is applied on the solvent resonance before the normal pulse sequence. This long pulse saturates the solvent resonance preventing it from being detected during the following pulse sequence. A minor drawback to using presaturation is the slightly increased time required to collect spectra reducing temporal resolution.

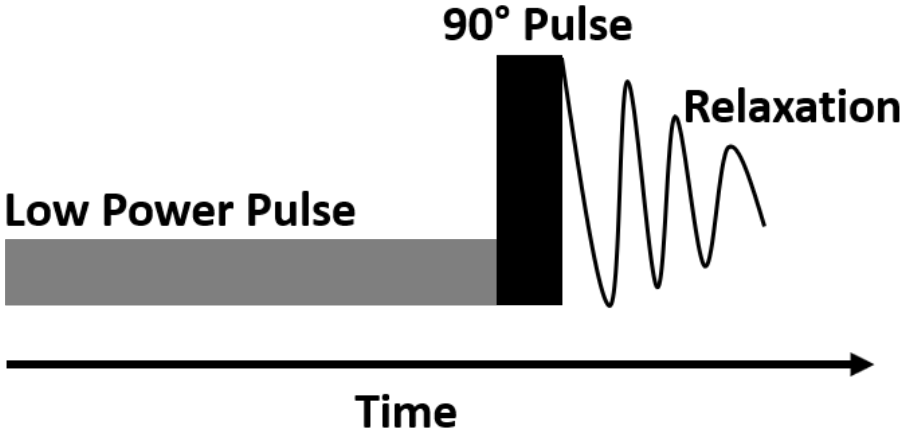

Figure 2.9: NMR pulse sequence used during a presaturation method.

In order to determine if there were any differences in kinetic data using normal and presaturation pulse sequences, transient profiles were obtained using both methods (Figure 2.10). A notable improvement in the kinetic profile when using the presaturation method was observed, particularly after 5 minutes when a sudden deviation from first order kinetics occurred using the normal pulse sequence. This is because as conversion increases, the vinyl peak intensity decreases and thus any phase issues brought about by the large solvent peak, adjacent to the vinyl peaks, are likely to have a greater effect.

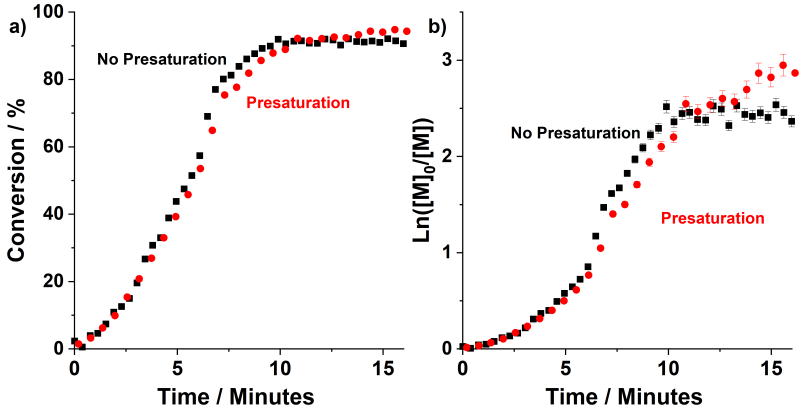

Figure 2.10: a) Conversion vs time and b) Semi-logarithmic rate plots obtained for the RAFT polymerisation of dimethylacrylamide using standard and presaturation NMR pulse sequences. All reactions were performed for at 30 % w/w, 80 °C and [DMAm]:[CCTP]:[VA-044] = 100:1:0.02.

2.3.1.3 Selection of NMR Flow Cell

A way to increase the S/N ratio without lengthening acquisition time, is to increase the sample volume and thus the number of protons observed by the magnet. For the experiments in section 2.3.1.1 PFA tubing (1.6 mm I.D) was used as the flow cell through the NMR. To determine if the quality of NMR spectra could be improved a glass flow cell with a larger internal diameter (4 mm I.D) was used (Figure 2.11).

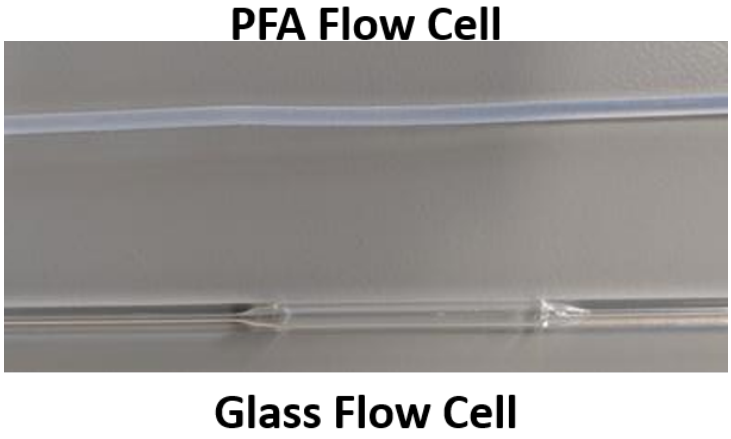

Figure 2.11: PFA and glass flow cells used to collect online NMR spectra

Initially, NMR spectra of a dimethylacrylamide solution were obtained over multiple flow rates in both flow cells (Figure 2.12) and the area of the vinyl proton region were compared relative to a static DMAm spectra obtained in the glass flow cell. A 5-fold increase in vinyl integral area can be observed in the glass flow cell. As well as a higher maximum flow rate (3 mL min^{-1}) before signal is lost compared to the PFA tubing (1 mL min^{-1}). This is expected as a larger internal diameter will reduce the fluid velocity allowing excited material to be in the detection window of the NMR for longer. Increasing the available flow rate ranges would be beneficial when using the transient profiling method developed in chapter 3 as the flow rate limit also limits the time scales which can be monitored. However, at high flow rates ($>$ 1 mL min^{-1}) the relative integral of DMAm increases above 1 in the glass flow cell indicating an increase in the concentration of DMAm in the cell. This may be due to the expansion and contraction of the fluid as it enters and exits the larger area of the flow cell.

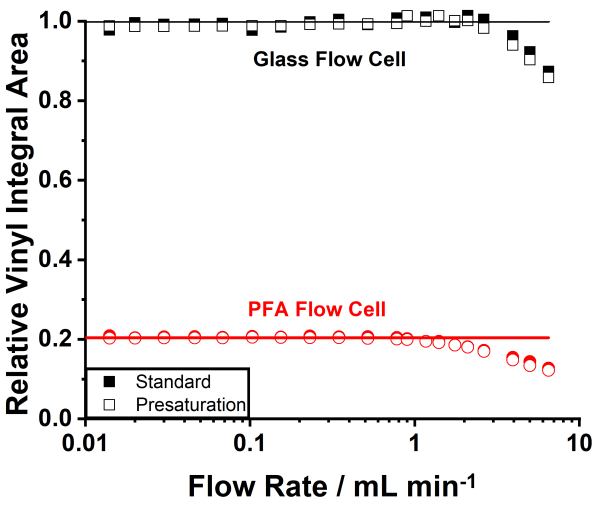

Figure 2.12: Relative integral area for DMAm vinyl protons over multiple flow rates using either a glass or PFA flow cell. Integral areas are relative to static sample in the glass flow cell.

To determine if this expansion and contraction will have an effect on the polymerisation transient kinetic profiles were obtained using both PFA and glass flow cells (Figure 2.13). The kinetic profile obtained using the glass flow cell showed a much reduced rate of reaction compared to PFA tubing. If the concentration of DMAm increased relative to the rest of the reaction solution in the glass flow cell, a stronger peak in the vinyl region would be present leading to a decrease in conversion. As the glass flow cell appeared to lead to inaccurate kinetics when compared to offline kinetic profiles obtained for a similar polymerisation (Figure 4.2), PFA was kept as the NMR flow cell.

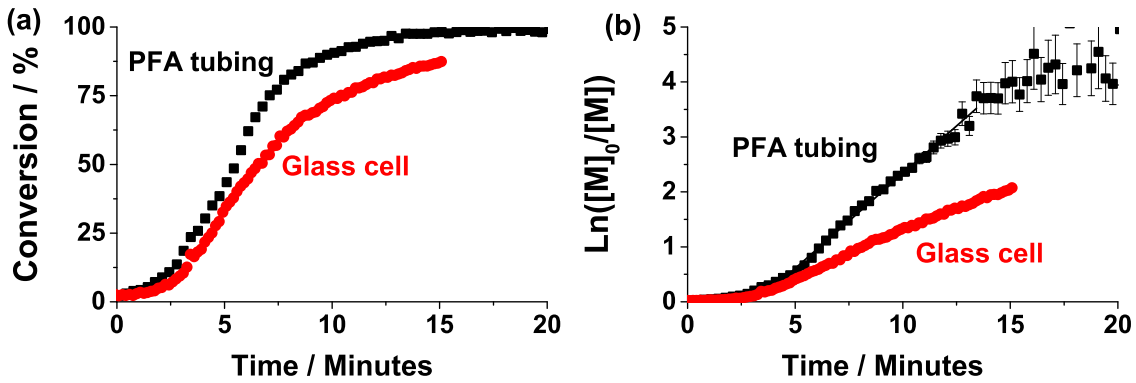

Figure 2.13: a) Conversion vs time and b) semi-logarithmic rate plots obtained for the RAFT polymerisation of dimethylacrylamide using both glass and PFA flow cells. All reactions were performed for at 30 % w/w, 80 °C and [DMAm]:[CCTP]:[VA-044] = 100:1:0.02.

2.4 Reactor D

Reactor D (Figure 2.14) was developed in chapter 5 in order automate the screening and optimisation of RAFT polymerisations. Only homogeneous polymerisations were performed in this chapter thus a stainless steel tubular reactor (PDMAm synthesis: 2.1 mm I.D, 5 mL /PtBuAm synthesis: 0.7 mm I.D, 2 mL) was sufficient. In order to control the reaction temperature a Eurotherm 3210 controller fitted with 2 Elmatic Max K cartridge was used. All modules in the platform (pumps, temperature controller, NMR and GPC) were connected to a PC and using MATLAB software allowed for alteration of reaction conditions and automated analysis to determine conversion, molecular weight and dispersity. The NMR protocol used was the same as for Reactor C. In order to perform GPC analysis a switching valve was installed between the reactor outlet and the NMR allowing for samples to be injected into the GPC for analysis.

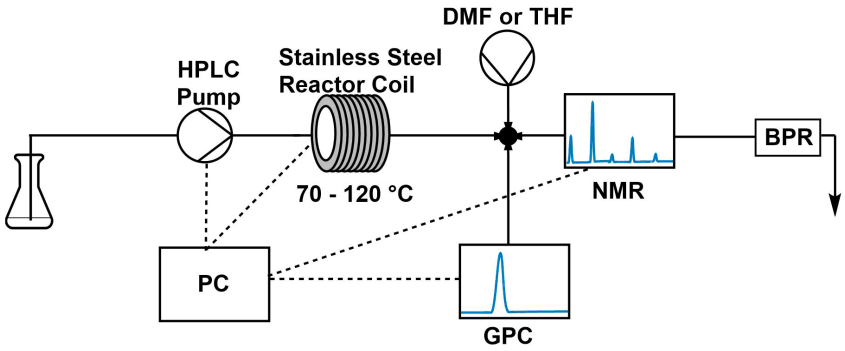

Figure 2.14: Reactor D used in chapter 5 to perform automated reaction screening and self-optimisation of RAFT polymerisations.

2.4.1 Online GPC analysis

Most commercially available GPC systems are quite costly and often have proprietary software which can make integration of systems into a separate automated platform complex. Therefore, a custom GPC system was developed for use in the continuous platform. The GPC consists of 5 parts (Figure 2.15): a HPLC pump (Jasco PU-980), a sample injector (6 Port VICI-EHMA), a guard column (Agilent 5 µm), a separation column (Agilent Rapide M) and a detector (Knauer K2301). Often multiple separation columns are used to achieve a higher resolution chromatogram. Although, this comes with an increase in acquisition time which would reduce the "real-time" quality of data being obtained therefore only one separation column was used.

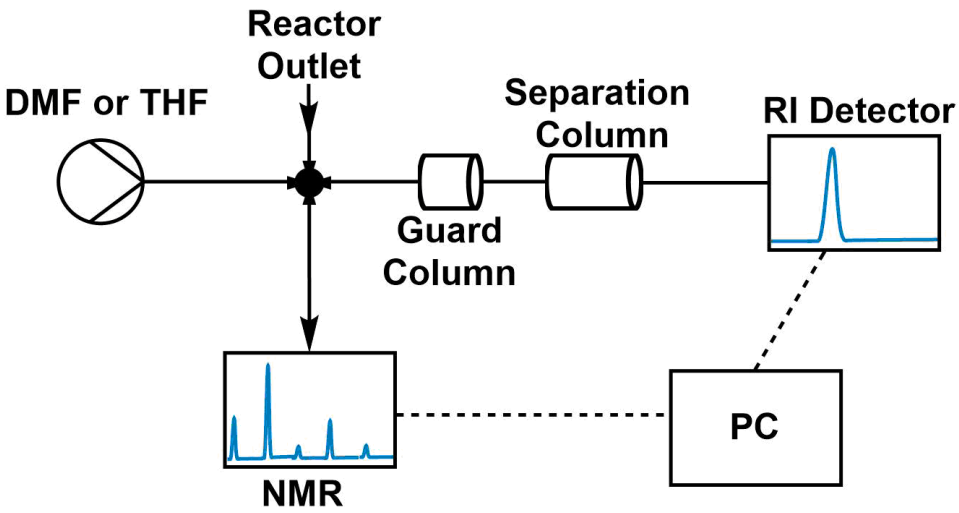

Figure 2.15: GPC setup developed for use in Reactor D to analyse polymer molecular weight and dispersity

2.4.1.1 Calibrating Injection Volume

Samples were taken from the reactor stream via an automated sampling valve attached to both the reaction and GPC eluent streams. As the reaction stream exited the flow reactor it filled a sample loop attached to the valve (Figure 2.16a). As the valve switched into the GPC eluent stream, reaction solution was pushed out of the sample loop and into the GPC eluent stream (Figure 2.16b).

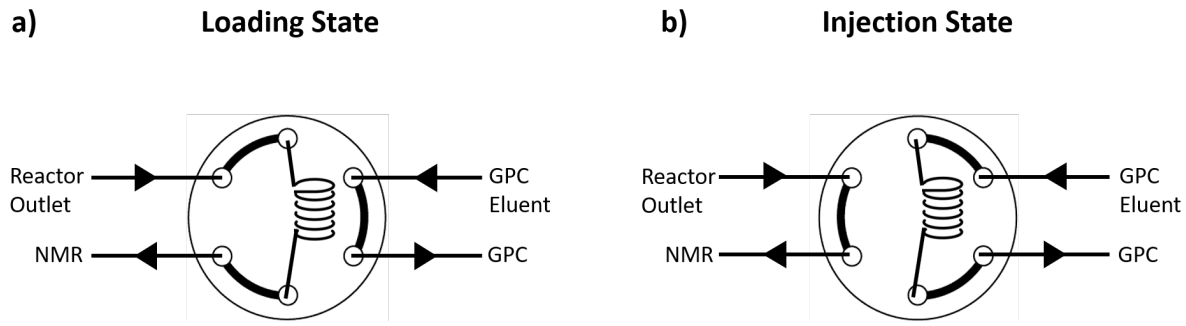

Figure 2.16: The position of the switching valve in either the a) loading state or b) the injection state. When acquiring a sample for GPC analysis the valve will switch to the loading state for a very short period of time (100 ms).

Therefore, the amount of sample injected into the GPC from the reactor stream was determined by the flow rate of the GPC eluent stream. The volume of material injected into the GPC at various flow rates was then determined using a tracer dye (Sudan III) of known concentration (Figure 2.17).

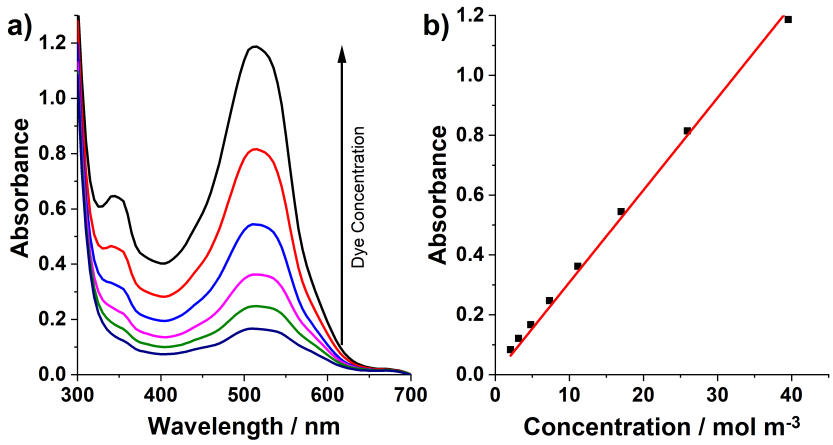

Figure 2.17: a) UV-Vis spectra obtained for Sudan III showing a λ_{max} at 520 nm and b) Calibration curve obtained for Sudan III in DMF at 520 nm used to determine the amount of material injected to online GPC

The sample loop was loaded with a tracer dye and switching was performed with flow rates set at 1, 2 and 3 mL min^{-1} and samples were collected and analysed by UV-Vis spectroscopy. By comparing the concentration of dye before and after switching the volume of material injected could was determined to be 1.5, 3 and 5 µl respectively.

2.4.1.2 GPC Protocol for PDMAm Synthesis

For analysis of the RAFT polymerisation of DMAm performed in Chapter 5 DMF GPC was used to acquire chromatograms in 3 minutes. However, continuous use of this setup led to significant peak broadening. Continuous collection of chromatograms for a pre-made $PDMAm_{100}$ (M_n = 10,000 g mol^{-1}, Đ = 1.17) indicated broadening was worsening as the number of chromatograms collected increased (Figure 2.18a). A subsequent increase in dispersity from 1.5 to over 2.0 was observed as the number of chromatograms obtained increases (Figure 2.18b).

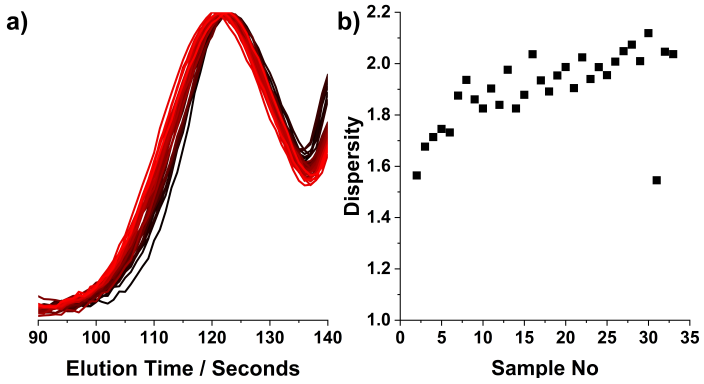

Figure 2.18: a) GPC chromatograms and b) dispersities obtained continuously over 70 minutes for $PDMAm_{100}$ on online platform. As more samples are taken (black to red) increased broadening of chromatograms is observed. 5 µL of sample was injected per measurement.

One possible cause of column degradation was material overload. In order to minimise the amount of material injected whilst still clearly detecting polymer signals, the GPC flow rate was reduced to 1.0 mL min^{-1} for sample injection. No significant broadening over time was observed when using this reduced injection volume (Figure 2.19a). Dispersities for the chromatograms obtained using a reduced injection volume were more consistent with (Đ = 1.20 - 1.25) with small variations caused by baseline noise (Figure 2.19b).

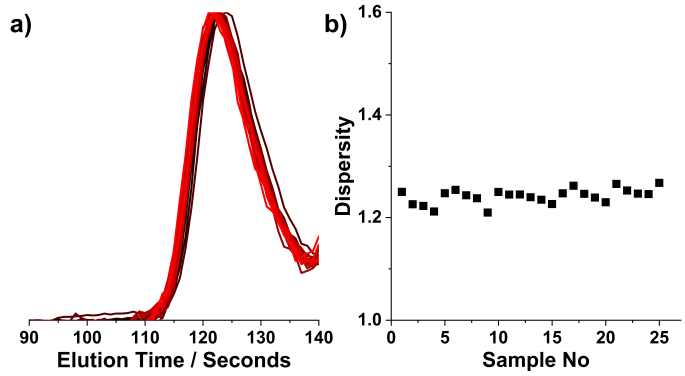

Figure 2.19: a) GPC chromatograms and b) dispersities obtained continuously over 70 minutes for $PDMAm_{100}$ on online platform. As more samples are taken (black to red) no chromatogram broadening is observed. 1.5 µL of sample was injected per measurement.

A well-defined $PDMAm_{200}$ standard was then analysed to ascertain whether reducing the injection volume had a similar effect at higher molecular weight. As with the $PDMAm_{100}$ samples the obtained chromatograms (Figure 2.20a) showed little variation over multiple runs. However, there was a significant variation in the measured dispersities (Đ = 1.6 - 2.1) for these chromatograms (Figure 2.20b).

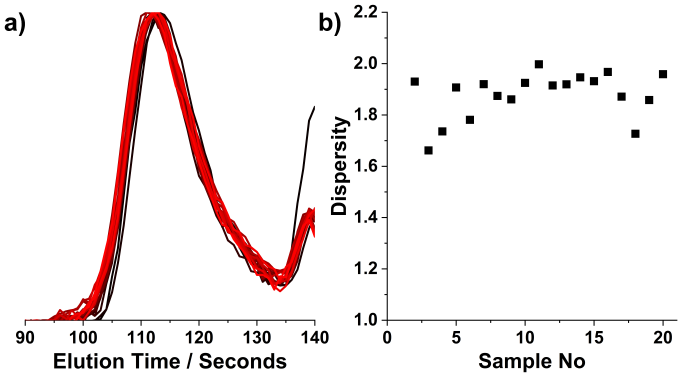

Figure 2.20: a) GPC chromatograms and b) dispersities obtained continuously over 70 minutes for $PDMAm_{200}$ on our online platform. As more samples are taken (black to red) no chromatogram broadening is observed. 1.5 µL of sample was injected per measurement.

Whilst reducing the injection volume improved the consistency of chromatograms, the columns had already been significantly altered from consistent use. A series of PMMA standards, used to calculate molecular weight, were compared over time (Figure 2.21). The gap in elution time between 4 kg mol^{-1} and 265 kg mol^{-1} had decreased from 40 seconds to 30 seconds. The shorter range of elution times led to a larger change in M_n, and therefore dispersity, with respect to time. The shortening of elution times was likely due to a change in the pore size distribution of the column. Due to the reduced elution time observed in the column it was deemed unsuitable for further use and was replaced.

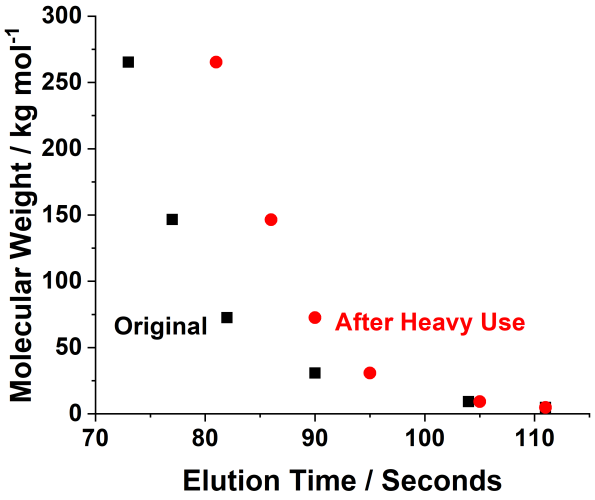

Figure 2.21: Calibration curves obtained for online GPC system highlighting the shortening elution time between high molecular weight polymers after heavy use.

As well as reducing the injection volume, further steps were also taken to try to reduce column

degradation. The flow rate was lowered to 2 mL min^{-1} in order to reduce the pressure in the system. There was also a possibility that radical species, which may react with and alter the column material, were still present in the solution after injection. Therefore, an inhibitor, 2,6-di-tert-butyl-4-methylphenol (BHT) was added to the eluent to quench any lingering radical species.

2.4.1.3 GPC Protocol for PtBuAm Synthesis

For the RAFT polymerisations of *tert*-butyl acrylamide (tBuAm), THF GPC was employed with a flow rate of 2 mL min^{-1} (6 minutes chromatograms) to minimise column degradation. To assess the consistency of THF GPC, chromatograms for the RAFT polymerisation of tBuAm were collected at steady state over 160 minutes (Figure 2.22a). Consistent overlapping chromatograms were obtained, however calculated molecular weight data (Figure 2.22b) showed a slight variation in both M_n and Đ, likely due to noisy baseline data. The small variation was not expected to significantly affect any self-optimisation processes.

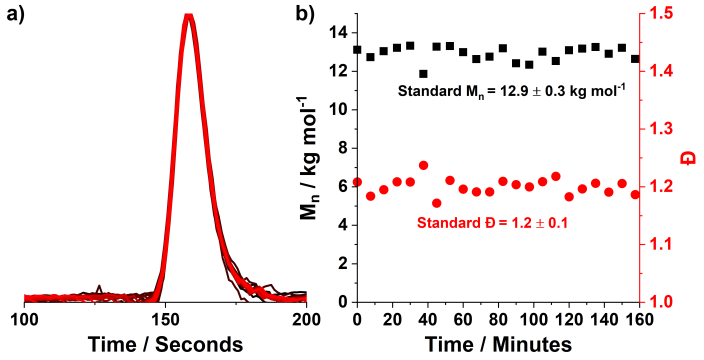

Figure 2.22: a) GPC chromatograms and b) molecular weight data obtained continuously over 160 minutes for $PtBuAm_{200}$ on online platform. As more samples are taken (black to red) no chromatogram broadening is observed. 3 µL of sample was injected per measurement.

2.5 Conclusion

In this chapter a series of flow reactors, with gradually increasing capabilities, and associated methodologies developed throughout this thesis were described. Reactor A was used perform RAFT polymerisations in chapter 3. Furthermore a transient kinetic profiling method was developed using this reactor. Reactor B was used to characterise the reactor coils (5 or 20 mL) used in chapter 3. The 20 mL reactor coil was found to have a narrower residence time distribution than the 5 mL coil due to the reduced impact of dead zones. The number of

reactor volumes required to reach steady state (3 reactor volumes) was also determined using Reactor B. Reactor C was developed in order to perform and kinetically profile, via online NMR, ultrafast RAFT-PISA polymerisations during chapter 4. The number of scans, pulse method and flow cell geometry were all optimised to generate an NMR protocol with a fast spectra acquisition time that maintained high spectra quality. Reactor D was developed to perform the automated multi-objective screening and self-optimisation of RAFT polymerisations using NMR and GPC analysis in chapter 5. DMF GPC protocols for the RAFT polymerisation of dimethylacrylamide allowed for the collection of chromatograms in three minutes. However constant use of this protocol led to broadening of chromatograms due to degradation of the column material. THF GPC protocols for the RAFT polymerisation of *tert*-butylacrylamide allowed for collection of chromatograms in six minutes. Continuous collection of chromatograms over 160 minutes indicated consistent chromatograms with no broadening observed.

Chapter 3

Synthesis and Kinetic Profiling of Block Copolymer Nano-objects via RAFT Polymerisation using a Flow Platform

3.1 Introduction

Flow chemistry is an alternative to batch chemistry, it offers improvements in reaction parameters such as: heat transfer, scale up, reproducibility and safety.[187,188] These benefits have seen uptake of flow chemistry into many areas of chemical synthesis.[4] Given that block copolymers are already present in a vast number of advanced materials,[189] precise control of their structure over a variety of scales is of paramount importance. This can be achieved in batch by using reversible deactivation radical polymerisation (RDRP) technologies such as ATRP,[90] NMP[89] and RAFT polymerisation.[92] Controlled radical polymer syntheses are seeing an increased uptake in the use of flow chemistry.[190] Polymerisations are exothermic reactions and as a result, large temperature increases can be observed when performed in batch reactors.[109,111] Effective dissipation of heat is then dependent on reactor geometry. More severely, the quality of the polymer becomes dependent on the type of reactor chosen, as changing temperature profiles result in altered kinetics which govern chain growth reactions. This reactor depen-

dence and need to dissipate large amounts of heat hinders the scalability of batch polymerisations.[109] The better heat transfer, reproducibility and scalability afforded by flow reactors make them an ideal alternative to batch reactors, which will ultimately allow for the greater control over polymer quality and architecture required for the generation of new advanced polymeric materials. The improved heat transfer and the ability to conduct the reaction at temperatures above the solvent boiling point, by operating at high pressure, has also enabled acceleration of the process.[153] Flow platforms have more recently been combined with new generation RAFT technologies such as photo RAFT[191–193] and oxygen tolerant PET-RAFT,[164] while novel reactor configurations such as looped flow reactors and the ability to telescope processes has also enabled the preparation of multi-block copolymers by sequential polymerisation.[30] Heterogeneous RAFT polymerisation technologies have been widely reported over the last 15 years or so and are popular since they allow rational production of a variety of block copolymer nanoparticles via polymerisation-induced self-assembly (PISA).[13,194,195] Furthermore, the precise nature of the polymerisation enables control not just over the morphology, but the specific dimensions of the resulting nanoparticles.[196,197] This precision could provide additional complementary control over polymer nanoparticles within flow systems. Of the relatively few reports where PISA has been conducted in tubular reactors, surfactant-free RAFT emulsion polymerisation of methyl methacrylate (MMA),[178] and RAFT dispersion polymerisation of MMA using a poly(poly(ethylene glycol)methyl ether methacrylate) macro-CTA in a water/ethanol solvent mixture have both produced well-defined spherical particles.[179] Non-spherical morphologies have also been synthesised via visible light-mediated PISA in a tubular reactor using a poly(ethylene glycol) macro-CTA.[32,167] This chapter focuses on the synthesis and kinetic monitoring of poly(dimethylacrylamide)-based block co-polymers by RAFT aqueous dispersion polymerisation using a flow platform (Figure 3.1). Initially, batch kinetics for all RAFT polymerisations were obtained. Then using Reactor A and the transient profiling method described in chapter 2, kinetic data obtained for the RAFT polymerisation of dimethylacrylamide was compared to traditional sampling methods. Further kinetic profiling of the chain extension of poly(dimethylacrylamide) via RAFT aqueous dispersion polymerisation with both *N*-isopropylacrylamide (NIPAm) and diacetone acrylamide (DAAm) was performed and the subsequent polymer nanoparticles produced were characterised by DLS and TEM.

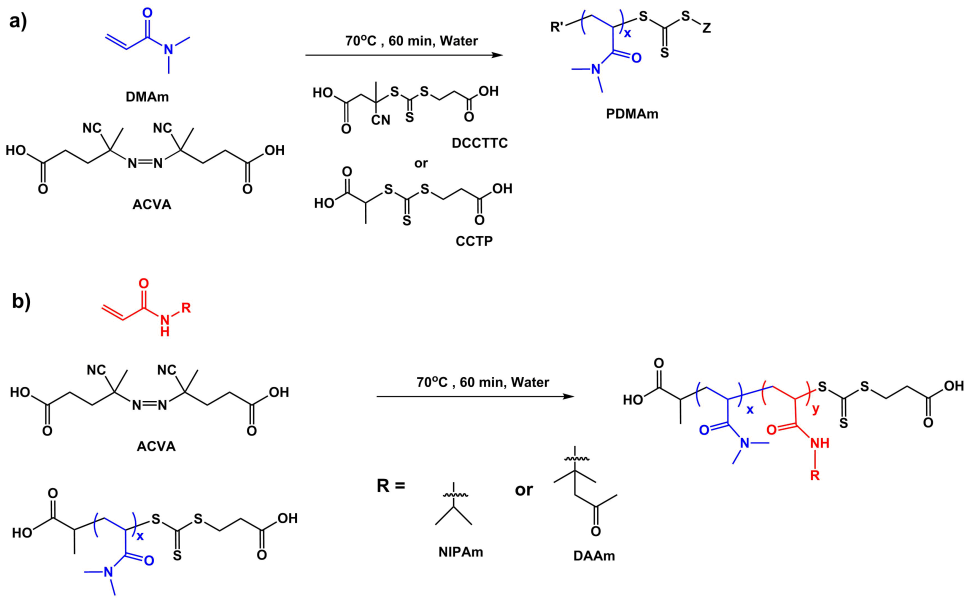

Figure 3.1: Reaction schemes for a) the RAFT solution polymerisation of dimethylacrylamide (DAAm) and b) the RAFT aqueous dispersion polymerisations of *N*-isopropylacrylamide (NIPAm) and diacetone acrylamide (DAAm)

3.2 Experimental

3.2.1 Materials

4,4'-Azobis(4-cyanovaleric acid) (ACVA, 99 %), dimethylacrylamide (DMAm, 99 %), deuterated methanol (CD_3OD, 99.8 %) and deuterium oxide (D_2O, 99.9 %) were purchased from Sigma Aldrich (UK). 3-((((1-Carboxyethyl)thio)carbonothioyl)thio)propanoic acid (CCTP, 90 %) and 4-((((2-carboxyethyl)thio)carbonothioyl)thio)-4-cyanopentanoic acid (DCTTC, 95 %) were purchased from Boron Molecular (Raleigh, USA). Diacetone acrylamide (DAAm, 99 %) was purchased from Alfa Aesar (UK). *N*-Isopropylacrylamide (NIPAm, 98 %) was purchased from TCI Chemicals (UK)

3.2.2 Methods

3.2.2.1 Batch Kinetic Studies of RAFT Polymerisation of DMAm

For a target composition of $DMAm_{100}$: DMAm (2 g, 100 eq), CCTP (0.051 g, 1 eq) and ACVA (0.005 g, 0.1 eq) were added to a round bottom flask and dissolved in water to give 10 - 50 % w/w reaction solution. A stirrer bar was added and then the flask was sealed and sparged with nitrogen for 20 minutes. The flask was then immersed in an oil bath at 70 °C and samples (0.3 mL) were taken every 5 minutes using a nitrogen purged syringe for 60 minutes. Samples

were analysed by ^{1}H NMR spectroscopy and GPC. The same method was employed when using DCTTC and the appropriate masses were used.

3.2.2.2 Batch Synthesis of PDMAm mCTA

For a target composition of $DMAm_{100}$: DMAm (20 g, 100 eq), CCTP (0.51 g, 1 eq) and ACVA (0.05 g, 0.1 eq) were added to a round bottom flask and dissolved in water (48 mL) targeting a final solids concentration of 30 % w/w. A stirrer bar was added and then the flask was sealed and sparged with nitrogen for 20 minutes. The flask was then immersed in an oil bath at 70 °C and left for 50 minutes. Afterwards the flask was removed from the oil bath and quenched by exposure to oxygen. Samples extracted for ^{1}H NMR spectroscopy indicated 93 % monomer conversion and a final DP of 113 via end group analysis. While DMF GPC indicated M_n = 10,700 g mol^{-1} and Đ = 1.09. No further purification was performed and the macro-CTA solution was directly employed for further chain extension experiments as a 30 % w/w solution.

3.2.2.3 Batch Kinetics of $PDMAm_{113}$-$PNIPAm_x$ Copolymers

For a target composition of $DMAm_{113}$-$PNIPAm_{50}$: NIPAm (0.5 g, 50 eq), PDMAm mCTA (0.9 g, 1 eq) and ACVA (0.0025 g, 0.1 eq) were added to a round bottom flask and dissolved in water (12.6 mL) targeting a final solids concentration of 10 % w/w. A stirrer bar was added and then the flask was sealed and sparged with nitrogen for 20 minutes. The flask was then immersed in an oil bath at 70 °C and left for 90 minutes. Samples (0.3 mL) were extracted every 10 minutes using a nitrogen purged syringe for ^{1}H NMR spectroscopy and GPC analysis.

3.2.2.4 Batch Kinetics of $PDMAm_{113}$-$PDAAm_x$ Copolymers

For a target composition of $DMAm_{113}$-$PDAAm_{50}$: DAAm (0.5 g, 50 eq), $PDMAm_{113}$ macroCTA (0.6 g, 1 eq) and ACVA (0.0016 g, 0.1 eq) were added to a round bottom flask and dissolved in water (9.9 mL) targeting a final solids concentration of 10 % w/w. A stirrer bar was added and then the flask was sealed and sparged with nitrogen for 20 minutes. The flask was then immersed in an oil bath at 70 °C and left for 90 minutes. Samples were taken every 10 minutes using a nitrogen purged syringe for ^{1}H NMR spectroscopy and GPC analysis.

3.2.2.5 High Resolution Transient Flow Kinetic Studies

For a target composition of $DMAm_{100}$: DMAm (5 g, 100 eq), CCTP (0.12 g, 1 eq) and ACVA (0.01 g, 0.1 eq) were added to a round bottom flask and dissolved in water (12 mL) targeting a final solids concentration of 30 % w/w. The flask was, sealed, sparged with nitrogen for 20 minutes. A portion of this reaction solution was then taken up into a 20 mL syringe and fitted to a New Era NE-300 syringe pump. The solution was passed through a 5 mL, tubular stainless-steel reactor at a flow rate 10 mL min^{-1} for 90 seconds, the flow rate was then reduced to 0.08 mL min^{-1} giving a retention time of 60 minutes. Kinetic samples (0.2 mL) were collected, in vials, from the reactor outlet changing vials every 144 seconds to give 25 kinetic samples. These samples were then analysed by ^{1}H NMR spectroscopy and DMF GPC.

3.2.2.6 Steady State Kinetic Studies

For a target composition of $DMAm_{100}$: DMAm (20 g, 100 eq), CCTP (0.5 g, 1 eq) and ACVA (0.05 g, 0.1 eq) were added to a round bottom flask and dissolved in water (48 mL) targeting a final solids concentration of 30 % w/w. The flask was, sealed, and sparged with nitrogen for 30 minutes. A portion of this reaction solution was then taken up into a 20 mL syringe and fitted to a New Era NE-300 syringe pump. The solution was then pumped through the 5 mL coil at the appropriate flow rate (either 0.5, 0.25, 0.167, 0.125, 0.1 mL min^{-1}). For each flow rate the reactor was allowed to reach steady state by passing through 3 reactor volumes (15 mL) worth of reaction solution. Three samples (0.3 mL) were then collected from the outlet of the reactor and analysed by ^{1}H NMR spectroscopy to determine monomer conversion.

3.2.2.7 High Throughput Continuous Flow Synthesis of $PDMAm_x$ mCTA

For a target composition of $DMAm_{100}$: DMAm (40 g, 100 eq), CCTP (1.02 g, 1 eq) and ACVA (0.11 g, 0.1 eq) were added to a round bottom flask and followed by water (96 mL) targeting a final solids concentration of 30 % w/w. The flask was sealed and sparged with nitrogen for 20 minutes. A Jasco PU-980 HPLC pump inlet tube was then inserted into the flask and the solution was pumped through a 20 mL stainless-steel tubular reactor at 70 °C with a retention time of 50 minutes (flow rate = 0.4 mL min^{-1}). The polymer was collected at the reactor outlet. ^{1}H NMR spectroscopy indicated > 98 % monomer conversion and a final DP of 113 via end group analysis. DMF GPC analysis indicated M_n = 10,300 g mol^{-1} and Đ = 1.10. No further purification was performed and the macro-CTA solution was employed for further chain

extension experiments as a 30 % w/w solution.

3.2.2.8 Continuous-Flow Kinetics of $PDMAm_{113}$-$PNIPAm_x$ Copolymers

For a target composition of $DMAm_{113}$-$PNIPAm_{50}$: NIPAm (1 g, 50 eq), $PDMAm_{113}$ macroCTA (1.7 g, 1 eq) and ACVA (0.0050 g, 0.1 eq) were added to a round bottom flask and dissolved in water (25.2 mL) targeting a final solids concentration of 10 % w/w. The flask was sealed and sparged with nitrogen for 20 minutes. The HPLC pump inlet tube was then inserted into the flask and the solution was pumped through a 5 mL stainless-steel tubular reactor at 70 °C with a retention time of 50 minutes (flow rate = 0.08 mL min^{-1}). Samples (0.3 mL) were collected at the reactor outlet and analysed by ^{1}H NMR and GPC.

3.2.2.9 Continuous-Flow Kinetics of $PDMAm_{113}$-$PDAAm_x$ Copolymers

For a target composition of $PDMAm_{113}$-$PDAAm_{50}$, DAAm (1 g, 50 eq),$PDMAm_{113}$ macroCTA (1.2 g, 1 eq) and ACVA (0.0033 g, 0.1 eq) were added to a round bottom flask and dissolved in water (19.9 mL) targeting a final solids concentration of 10 % w/w. The flask was sealed and sparged with nitrogen for 20 minutes. The HPLC pump inlet tube was then inserted into the flask and the solution was pumped through a 5 mL stainless-steel tubular reactor at 70 °C at 10 mL min^{-1} for 90 seconds the flow rate was then reduced to 0.08 mL min^{-1} to give a final retention time of 60 minutes. Samples (0.3 mL) were collected at the reactor outlet and analysed by ^{1}H NMR spectroscopy and GPC.

3.2.2.10 Continuous-Flow Synthesis of $PDMAm_{50}$-$PDAAm_x$ Copolymers

For a target composition of $PDMAm_{50}$-$PDAAm_{200}$, DAAm (3 g, 200 eq), $PDMAm_{50}$ macroCTA (0.45 g, 1 eq) and ACVA (0.0025 g, 0.1 eq) were added to a round bottom flask and dissolved in water (13.8 mL) targeting a final solids concentration of 20 % w/w. The flask was sealed and sparged with nitrogen for 20 minutes. The HPLC pump inlet tube was then inserted into the flask and the solution was pumped through a 5 mL stainless-steel tubular reactor at 70 °C at 10 mL min^{-1} for 90 seconds the flow rate was then reduced to 0.08 mL min^{-1} to give a final retention time of 60 minutes. Samples (0.3 mL) were collected at the reactor outlet and analysed by ^{1}H NMR spectroscopy and GPC.

3.2.2.11 ^{1}H NMR Spectroscopy

^{1}H NMR spectra were acquired using a Bruker 500 MHz spectrometer. Samples were dissolved in D_2O or CD_3OD. All chemical shifts are reported in ppm (δ) relative to the lock solvent. The average number of scans accumulated per spectrum was typically 32. For all RAFT polymerisations, conversion was determined by Equation 3.1:

$$Conversion = 1 - \frac{x_n y_0}{y_n x_0} \tag{3.1}$$

where x is the vinyl peak region between 5.6 and 7.0 ppm, y is the overlapping monomer and polymer region between 3.3 to 2.18 ppm (for dimethylacrylamide), 4.2 to 3.8 ppm (for *N*-isopropylacrylamide) or 2.3 to 2.0 ppm (for diacetone acrylamide).

3.2.2.12 Dynamic Light Scattering (DLS)

Dynamic light scattering measurements were conducted at 25 °C using a Malvern Zetasizer Nano series instrument. Light scattering was detected at 173° and hydrodynamic diameters were determined using the Stokes-Einstein equation, which assumes spherical, non-interacting particles.

3.2.2.13 Gel Permeation Chromatography (GPC)

Gel permeation chromatography measurements were conducted using an Agilent 1260 Infinity system fitted with two 5 µm Mixed-C columns plus a guard column, a refractive index (RI) detector and an UV-Vis detector operating at 309 nm. DMF containing 1.0 % w/v lithium bromide (LiBr) was used as eluent. The pump flow rate was set to 1.0 mL min^{-1} and the temperature of the column oven and RI detector were set to 60 °C. A series of ten near-monodisperse poly(methyl methacrylate) standards (M_p ranging from 800 to 2,200,000 g mol^{-1}) were employed as calibration standards in conjunction with an RI detector for determining molecular weights and molar mass dispersities (Đ).

3.2.2.14 Transmission Electron Microscopy (TEM)

Transmission electron microscopy was conducted at 200 kV using a Tecnai F20 FEGTEM. TEM samples were prepared on carbon coated copper grids (400 mesh, continuous film) by adding 20 µL of 0.1 % w/w sample solution and leaving for 1 minute. The excess sample was removed

from the grid by blotting and the same procedure was repeated for staining using a 1 % w/w uranyl acetate solution.

3.3 Results and Discussion

3.3.1 RAFT Polymerisation of Dimethylacrylamide

The RAFT solution polymerisation of dimethylacrylamide (DMAm) was chosen as a model homogeneous polymerisation system for kinetic investigation as acrylamide monomers are known to reach high monomer conversions whilst maintaining living polymer characteristics. Additionally, DMAm forms a hydrophilic polymer which was used for later PISA experiments. Initially, reaction conditions of DMAm with two different RAFT agents (DCTTC or CCTP) were screened to determine a suitable polymerisation system to perform on the flow platform. DMAm conversion was determined using ^{1}H NMR spectroscopy by comparing vinyl protons between 5.5 - 7.0 ppm to the pendant methyl groups between 2.7 - 3.3 ppm (Figure 3.2).

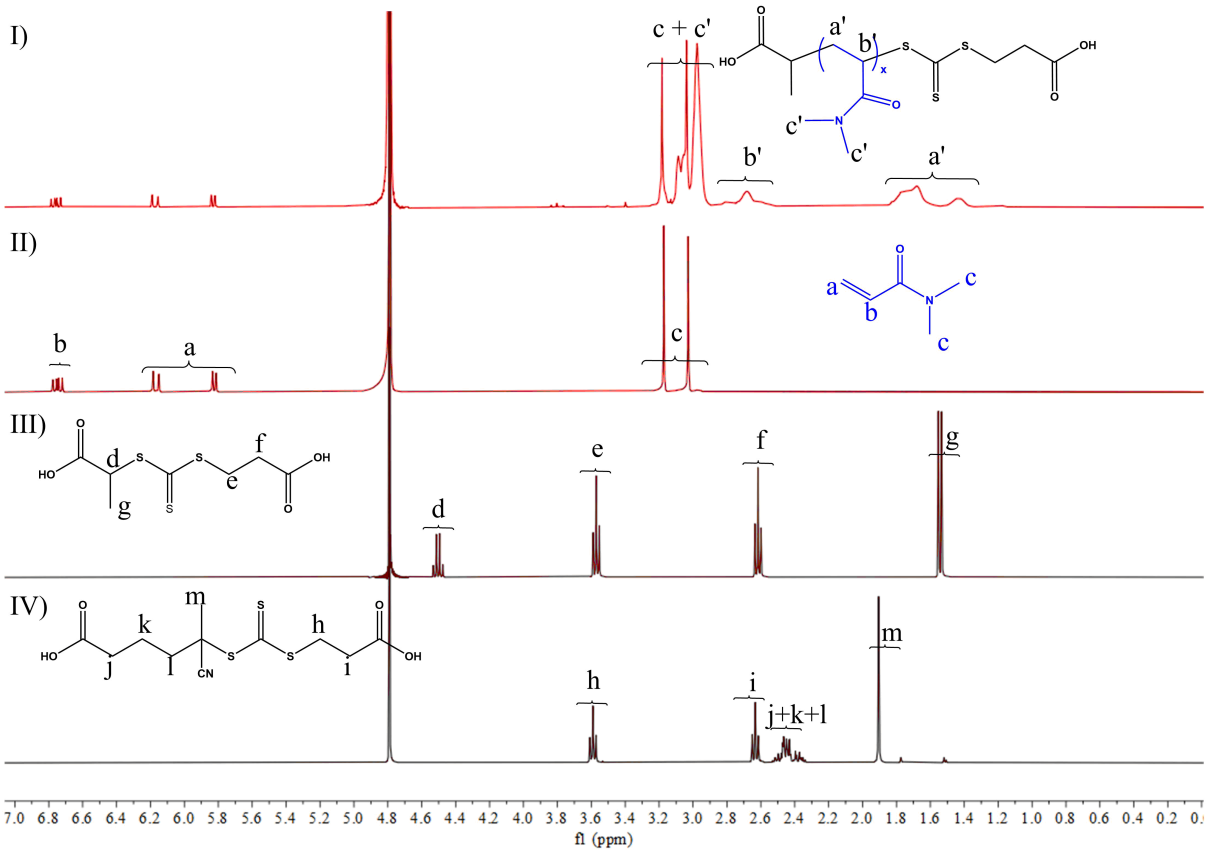

Figure 3.2: ^{1}H NMR spectra obtained during kinetic studies of the RAFT polymerisation of DMAm at I) $t_{120\ min}$ and II) $t_{0\ min}$. ^{1}H NMR spectra were also recorded for the RAFT agents III) CCTP and IV) DCTTC to determine peaks for end-group analysis. Conversion was determined by comparing vinyl protons (a + b) to the pendant methyl groups (c).

The DCTTC RAFT agent NMR kinetics (Figure 3.3) showed high conversions (> 90 %) were achieved after 80 minutes for all concentrations apart from 10 % w/w which took 120 minutes. Linear semi-logarithmic rate plots for 10, 20 and 30 % w/w indicated pseudo-first order kinetics throughout the polymerisations. However, a decrease in rate over the course of the reaction was observed for 40 and 50 % w/w indicating loss of control over the polymerisation likely caused by premature termination reducing the number of propagating polymer radicals. All reactions showed an induction period, with no conversion until 30 minutes, likely due to incompatibility between the RAFT agent and monomer. As discussed in chapter 1, RAFT agent R and Z groups have a large effect on induction periods observed during RAFT polymerisation. There are 3 main ways in which RAFT agent R and Z groups can cause an induction period. Z groups with highly electron withdrawing groups conjugated to the thiocarbonate have been theorised to cause induction periods by stabilising the main and pre-RAFT equilibrium intermediates to such a degree that breaking down to form a new radical species is highly unfavourable.[198,199] However, the DCTTC Z group does not contain any highly electron withdrawing groups so this was unlikely to be the cause of any induction period. The R group causes induction periods by either slow fragmentation due to a poorly stabilised radical or slow re-initiation of the polymerisation due to forming a highly stabilised radical.[200–202] The DCTTC R group contained a cyano group which is known to stabilise radicals making the former unlikely to be the reason for the observed induction period. However, the resulting radical formed will likely have a slow rate of re-initialisation compared to the high rate of propagation of acrylamide monomers. Therefore, the observed induction period was likely slow re-initiation of the polymerisation after the inital chain transfer step. This was later confirmed by using a CTA with a different R group.

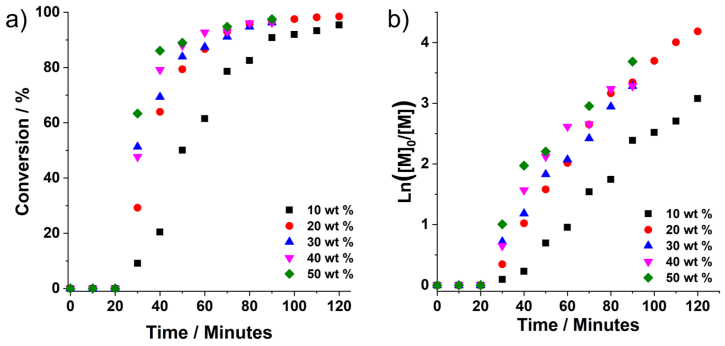

Figure 3.3: a) Conversion vs. time and b) semi-logarithmic rate plots for the RAFT aqueous solution polymerisation of dimethylacrylamide (DMAm) in batch using DCTTC. All reactions were conducted at 70 °C and [DMAm]:[CTA]:[ACVA] = 100:1:0.1.

GPC chromatograms (Figure 3.4) for all polymerisations showed a shift to higher molecular weight with respect to reaction time. For 10, 20 and 30 % w/w a narrowing of the peaks during the shift to high molecular weight was observed. However, for 40 and 50 % w/w a broadening of the peaks during the shift to high molecular weight was observed.

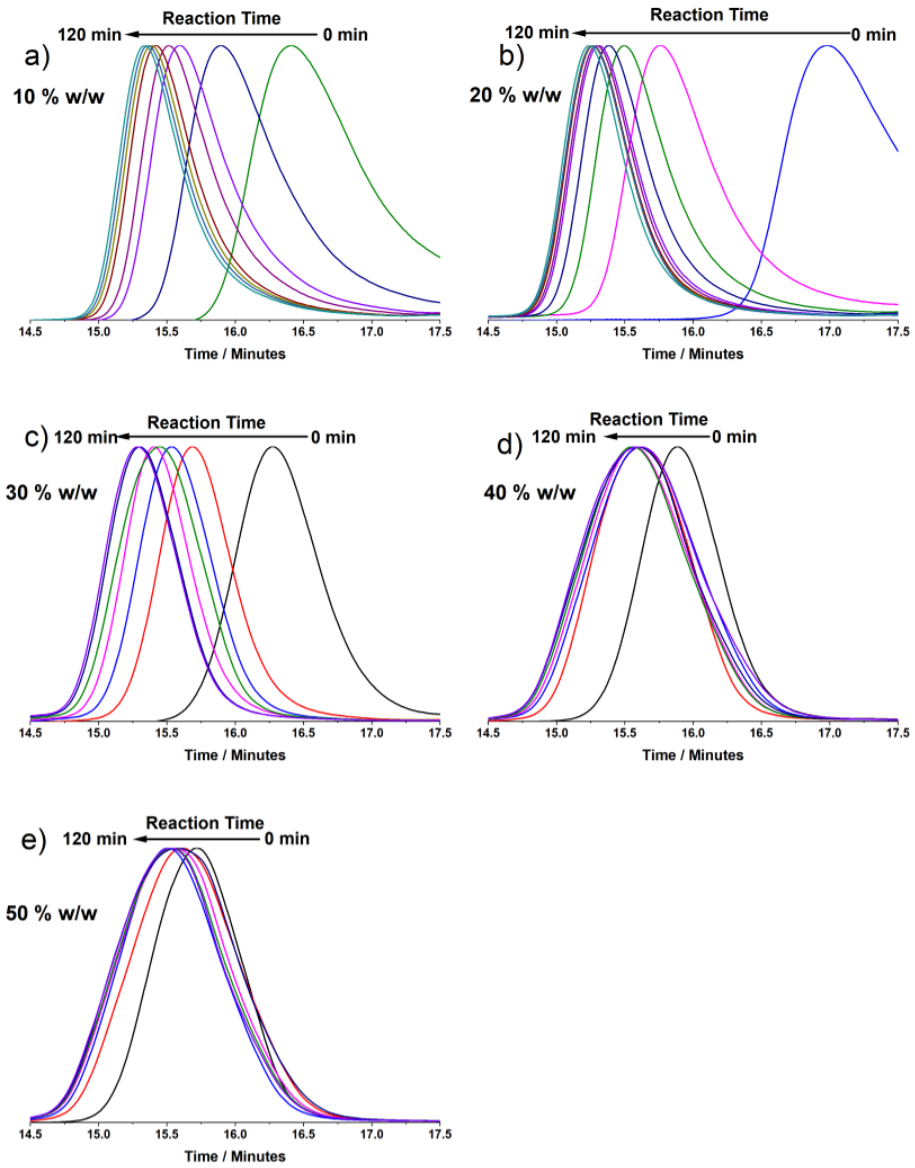

Figure 3.4: GPC chromatograms obtained for kinetic samples extracted from the RAFT polymerisation of dimethylacrylamide (DMAm) in batch using DCTTC. All reactions were conducted at 70 °C with a total solids concentration of a) 10 % b) 20 % c) 30 % d) 40 % or e) 50 % w/w and [DMAm]:[CTA]:[ACVA] = 100:1:0.1.

From the calculated molecular weight data (Figure 3.5), a linear relationship between molecular weight and conversion was observed for 10, 20 and 30 % w/w indicating good control over the polymerisation. However, this linearity was not observed for 40 and 50 % w/w confirming

the loss of control over the polymerisation. In addition to the non-linear relationship between molecular weight and conversion, an increase in dispersity with conversion was also observed. For an ideal RAFT polymerisation with negligible termination, dispersity was expected to decrease with respect to conversion (which was observed for 10, 20 and 30 % w/w).

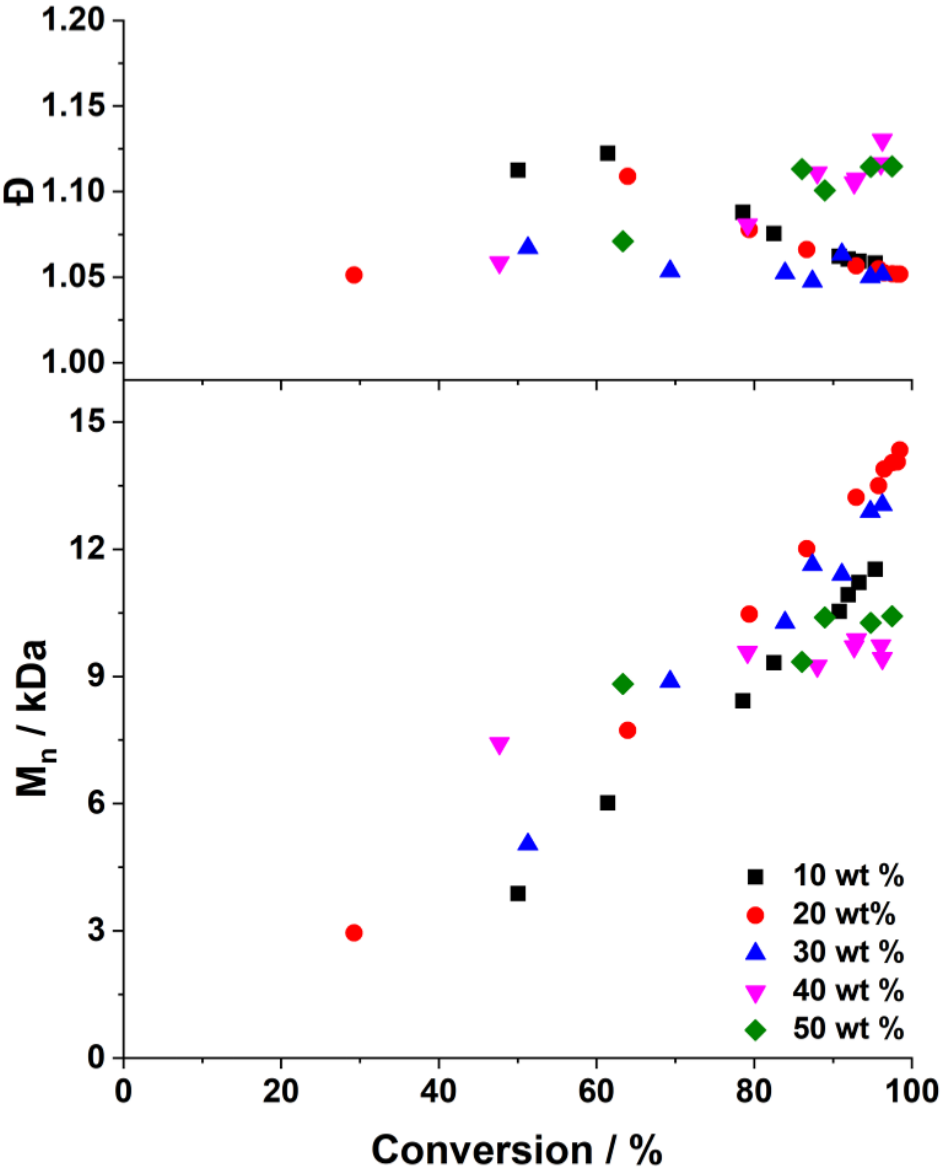

Figure 3.5: Molecular weight and dispersity evolution for RAFT aqueous solution polymerisation of dimethylacrylamide (DMAm) in batch using DCTTC. All reactions were conducted at 70 °C and [DMAm]:[CTA]:[ACVA] = 100:1:0.1.

A RAFT agent (CCTP), with a different R group to DCTTC, was also evaluated. For all polymerisations (Figure 3.6) no induction was observed and as a result high conversions were achieved within 30 minutes for 40 and 50 % w/w, 50 minutes for 20 and 30 % w/w and 90 minutes for 10 % w/w. Linear semi-logarithmic rate plots up to high conversions can be observed for 10

% w/w, 20 % w/w and 30 % w/w indicating pseudo-first order kinetics. A slight decrease in rate was observed for 40 % w/w and 50 % w/w indicating a loss of control over the polymerisation.

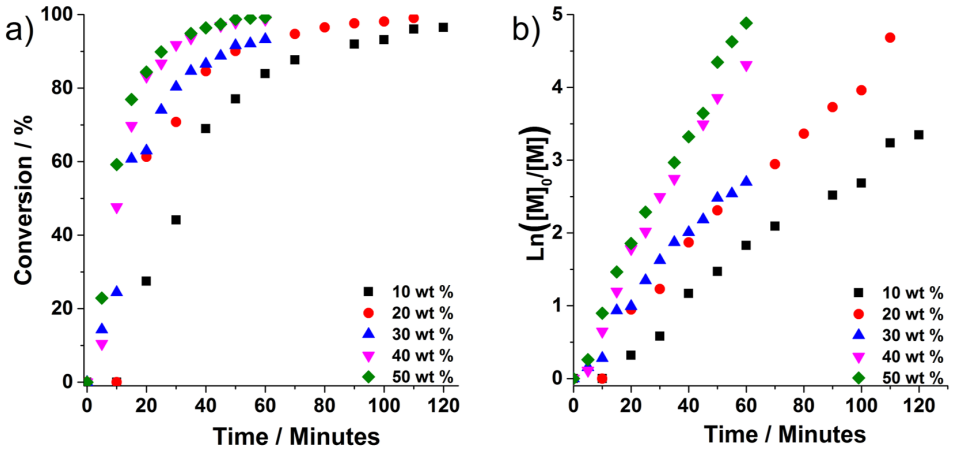

Figure 3.6: a) Conversion vs. time and b) semi-logarithmic rate plots for the RAFT polymerisation of dimethylacrylamide (DMAm) in batch using CCTP. All reactions were conducted at 70 °C and [DMAm]:[CTA]:[ACVA] = 100:1:0.1.

GPC chromatograms (Figure 3.7) for all polymerisations showed a shift to higher molecular weight with respect to reaction time. For 10, 20, 30 and 50 % w/w a narrowing of the peaks during the shift to high molecular weight was observed. However, for 40 % w/w a broadening of the peaks during the shift to high molecular weight was observed. The calculated molecular weight data (Figure 3.8) showed a linear relationship between molecular weight and conversion for 10, 20, 30 and 50 % w/w indicating good control over the polymerisation. However, this linearity was not observed for 40 % w/w further confirming the loss of control over the polymerisation. A decrease in dispersity with respect to conversion was observed for 10, 20, 30 and 50 % w/w whilst 40 % w/w increased. A final dispersity of 1.05 was achieved for all well controlled polymerisations, similar to RAFT polymerisations using DCTTC.

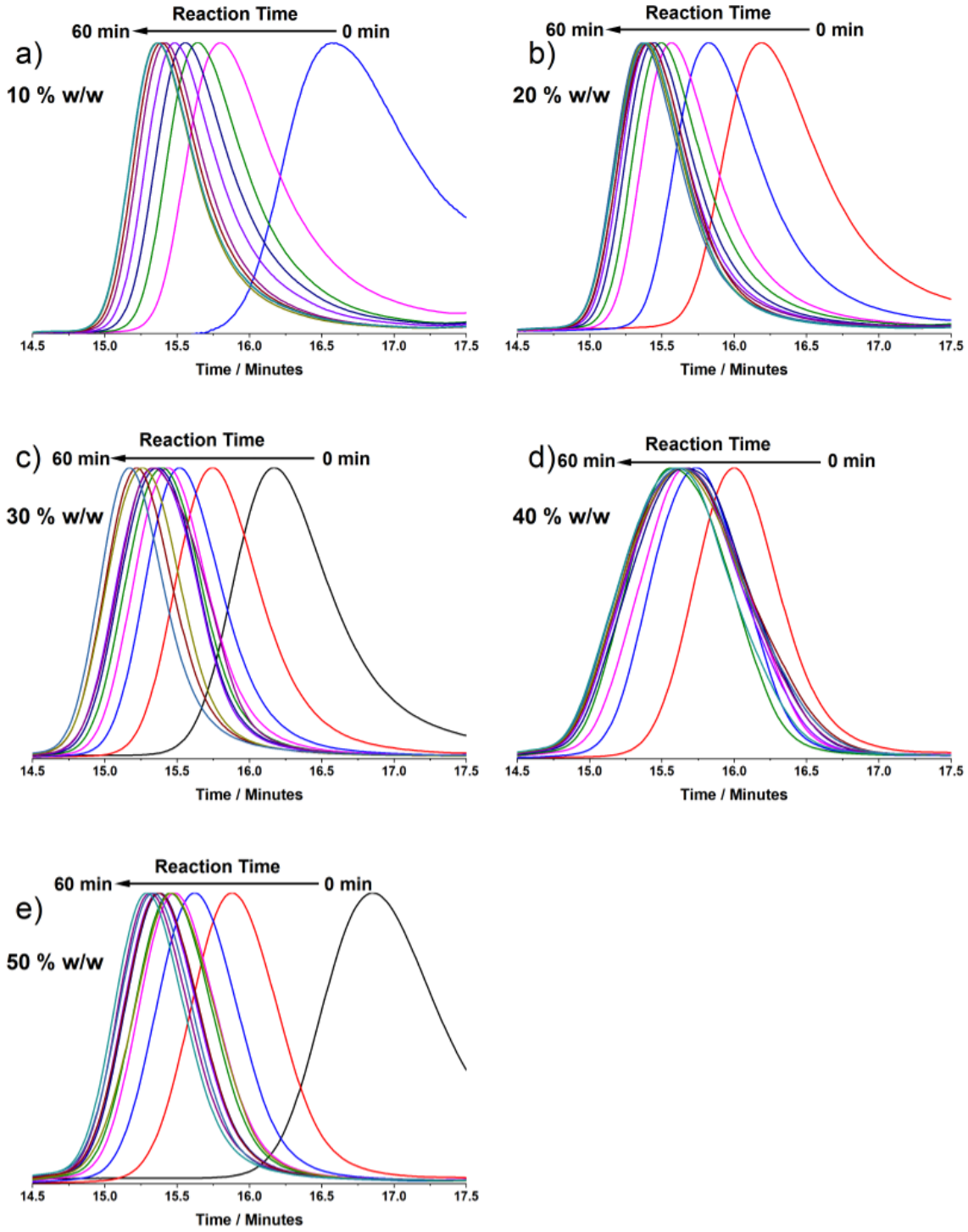

Figure 3.7: GPC chromatograms obtained for kinetic samples extracted from the RAFT polymerisation of dimethylacrylamide (DMAm) in batch using CCTP. All reactions were conducted at 70 °C with a total solids concentration of a) 10 % b) 20 % c) 30 % d) 40 % or e) 50 % w/w and [DMAm]:[CTA]:[ACVA] = 100:1:0.1.

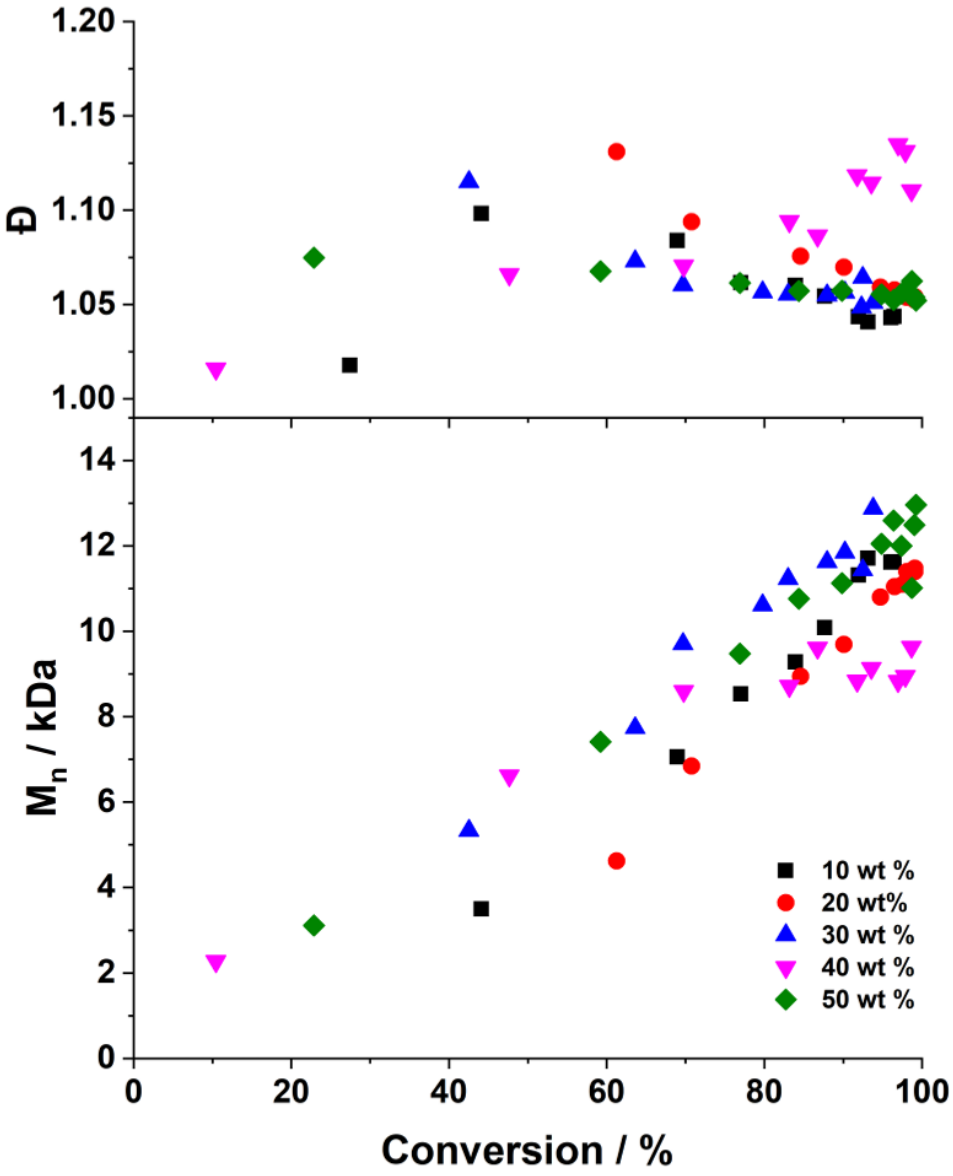

Figure 3.8: Molecular weight and dispersity evolution for RAFT polymerisation of dimethylacrylamide (DMAm) in batch using CCTP. All reactions were conducted at 70°C and [DMAm]:[CTA]:[ACVA] = 100:1:0.1.

After comparing kinetic data, CCTP was chosen as the CTA to be used in flow polymerisations. The kinetic data obtained for DCCTC displayed a large induction period for the polymerisation of DMAm, which was non-ideal and therefore unsuitable to be transferred to the flow reactor. To maximise production of PDMAm the highest concentration that maintained good control over the polymerisation was selected to be performed in flow (30 % w/w). For all RAFT polymerisations a pre-mixed reaction solution was pumped through the system using a syringe pump. Whilst there were multiple reagents present in the reaction which could have been delivered separately, the mixing of multiple streams can be complex and may have affected

both polymerisation kinetics and final polymer dispersity.[203] As further work in this chapter investigated the difference in kinetics between batch and flow reactors, as well as different kinetic profiling methods, using a pre-mixed reaction solution was deemed to be the most suitable method for comparing kinetic data. Kinetic profiling was performed using the transient method described in section 2.1. In order to validate kinetic profiles obtained using the transient method, steady state kinetics were first obtained. Steady state kinetics were performed at five different flow rates. In each case three samples were taken, after 3, 4 and 5 reactor volumes. For all residence times each sample had similar conversions, further confirming steady state (Figure 3.9).

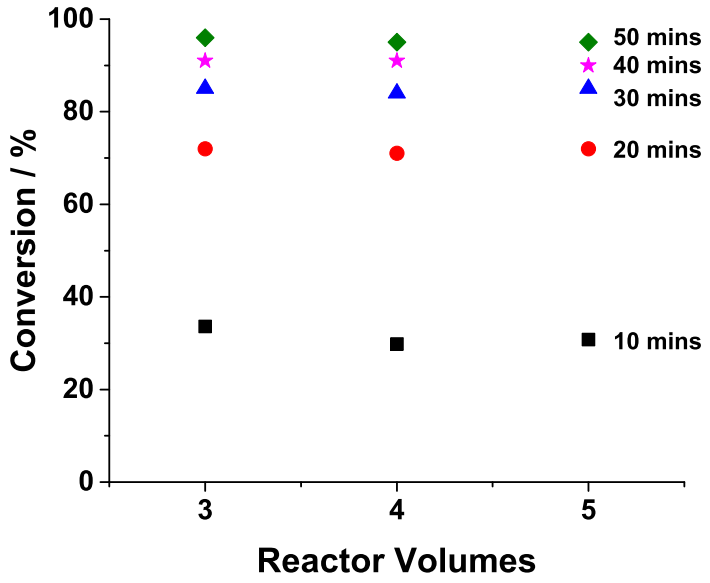

Figure 3.9: Steady state reaction kinetics for the RAFT polymerisation of dimethylacrylamide in flow. For each residence time (10 - 50 minutes) samples were collected, from the outlet, over multiple reactor volumes. All reactions were conducted at 70 °C with total solids concentration of 30 % w/w and [DMAm]:[CCTP]:[ACVA] = 100:1:0.1.

The average conversion values for each residence time were comparable with those obtained during the transient profiling (Figure 3.10), thus validating the transient kinetic method. An overall increased rate was observed for the polymerisation performed using the flow platform. An increased rate has been noted previously for other polymerisations in flow (see section 1.5) and was attributed to the increased heat transfer under flow conditions which may have led to radical decomposition earlier in the reaction.[204] If this was the case, an increased radical flux would result in a faster rate of polymerisation.

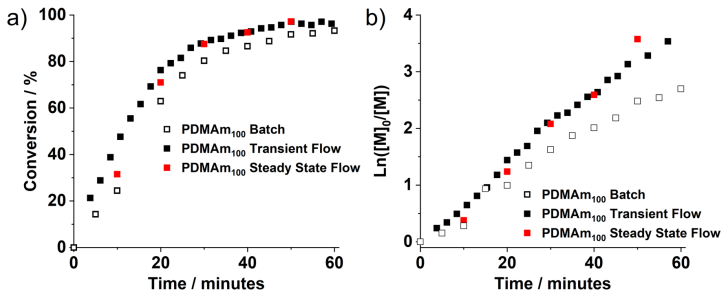

Figure 3.10: (a) Conversion vs. time and (b) semi-logarithmic rate plots for the RAFT polymerisation of dimethylacrylamide (DMAm) using CCTP in batch and flow (steady state and transient). All reactions were conducted at 70 °C with total solids concentration of 30 % w/w and [DMAm]:[CCTP]:[ACVA] = 100:1:0.1.

A large number of kinetic samples were collected using the transient kinetic profiling which allowed for greater resolution of molecular weight evolution. GPC chromatograms (Figure 3.11) for all kinetic samples showed a shift to higher molecular weight with respect to reaction time. For both batch and flow polymerisations, a linear increase in molecular weight with monomer conversion was observed (Figures 3.12). Overall, M_n values in flow were subtly lower than in batch, which was attributed to the discrepancy in dispersity. Nevertheless, the pseudo-living behaviour of RAFT polymerisation was maintained in flow and near equivalent polymers to batch were produced.

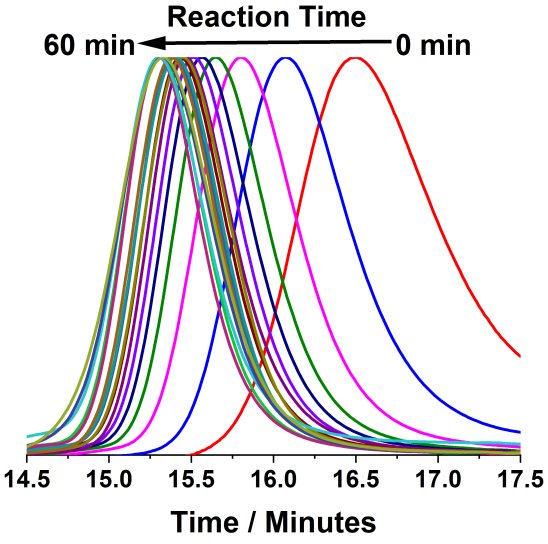

Figure 3.11: GPC chromatograms obtained for the RAFT polymerisation of dimethylacrylamide (DMAm) in flow using CCTP. All reactions were conducted at 70 °C with total solids concentration of 30 % w/w and [DMAm]:[CCTP]:[ACVA] = 100:1:0.1.

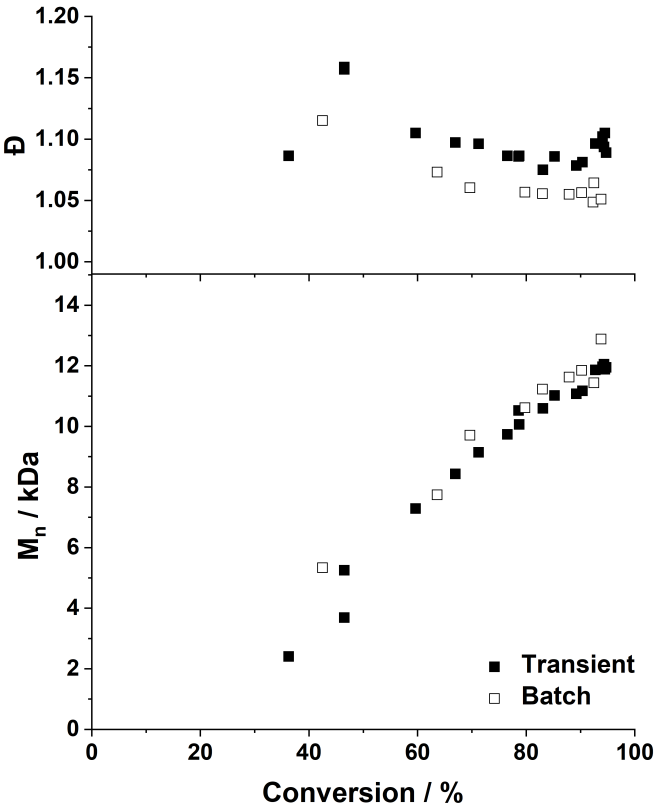

Figure 3.12: Molecular weight and dispersity evolution for the RAFT polymerisation of dimethylacrylamide (DMAm) in batch and flow. All reactions were conducted at 70 °C with total solids concentration of 30 % w/w and [DMAm]:[CCTP]:[ACVA] = 100:1:0.1.

To demonstrate the ability to easily increase product output, a relatively large batch of PDMAm macro-CTA was synthesised. Output was increased by using a 20 mL coil and a HPLC pump set at a flow rate of 0.4 mL min^{-1} providing a residence time of 50 minutes. Approximately 135 g of 30 % w/w polymer solution was obtained and ^{1}H NMR analysis indicated 98 % monomer conversion for this macro-CTA. This conversion was in good agreement with the kinetic profile obtained in the 5 mL flow reactor (Figure 3.10). End group analysis of the polymer via ^{1}H NMR spectroscopy indicated a final DP of 113. Similar molecular weight and dispersities were observed in the 20 mL coil (M_n = 10,300 g mol^{-1}, Đ = 1.10), 5 mL coil (M_n = 10,800 g mol^{-1}, Đ = 1.13) and batch reactor (M_n = 10,700 g mol^{-1}; Đ = 1.09, Figure 3.13). but flow synthesis produced polymers with subtly broader molecular weight distributions.

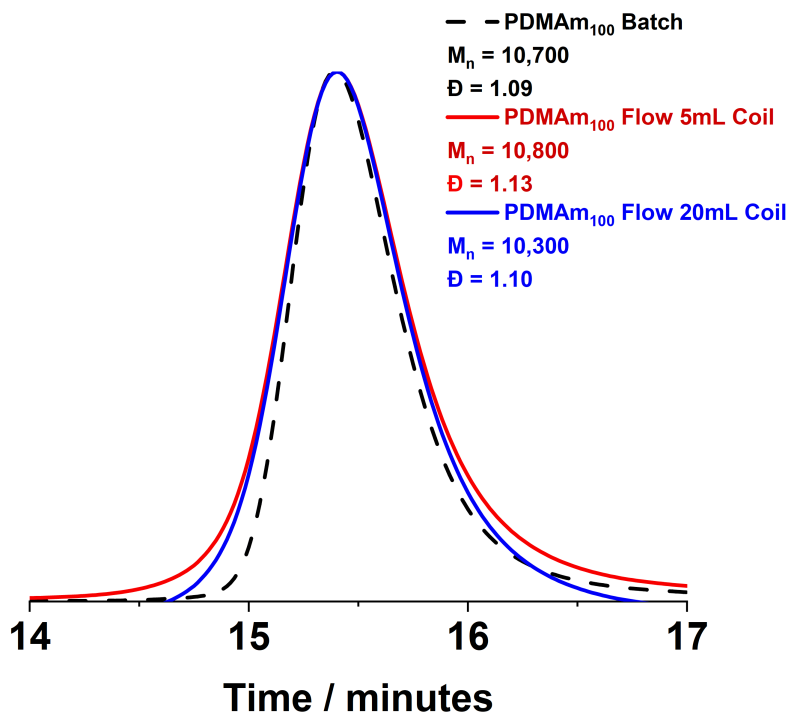

Figure 3.13: GPC chromatograms recorded for PDMAm macro-CTAs synthesised on small scale (batch and flow) and large scale reactor systems (flow only). All reactions were conducted at 70 °C with total solids concentration of 30 % w/w and [DMAm]:[CCTP]:[ACVA] = 100:1:0.1.

It has previously been reported that polymers synthesised in flow have narrower molar mass dispersity due to improved heat transfer minimising the effects of any exotherm.[182] However, subtly broader molecular weight distributions should be expected in non-ideal flow reactors due to the residence time distribution. As described in section 2.2.1 the RTD of the 20 mL coil was narrower than the 5 mL coil and therefore polymers obtained should have a lower dispersity. The dispersity observed for the larger batch was indeed lower (Đ = 1.10 for 20 mL coil vs. Đ = 1.13 for 5 mL coil), but it was not clear whether this small decrease was significant. Nevertheless, the well-defined macro-CTA produced in the 20 mL reactor was used for the preparation of block copolymers without further purification.

3.3.2 RAFT Dispersion Polymerisation of *N*-isopropylacrylamide using a $PDMAm_{113}$ macro-CTA

The RAFT dispersion polymerisation of NIPAm using a PDMAm macro-CTA was selected as example of a polymer system that reversibly undergoes self-assembly to form polymeric micelles. NIPAm forms a thermo-responsive polymer which is insoluble in water above its lower critical solution temperature (LCST), which is reported to be 32 °C.[205] Whilst the LCST

of PNIPAm has been reported to be altered by copolymerisation with other monomers they were all significantly lower than the reaction temperature used (70 °C).[206] Therefore during the RAFT dispersion polymerisation of *N*-isopropylacrylamide using a PDMAm macro-CTA, as the growing PNIPAm block became insoluble it was stabilised by the PDMAm chain, which led to spontaneous self-assembly into polymeric micelles. In order to minimise any potential increase in viscosity as the polymer chains grew, which may have lead to complications upon transfer to the flow reactor, the reaction solution concentration was reduced to 10 % w/w. NIPAm conversion was determined using ^{1}H NMR spectroscopy by comparing vinyl protons between 5.5 - 7.0 ppm to the tertiary hydrogen between 3.8 - 4.2 ppm (Figure 3.14).

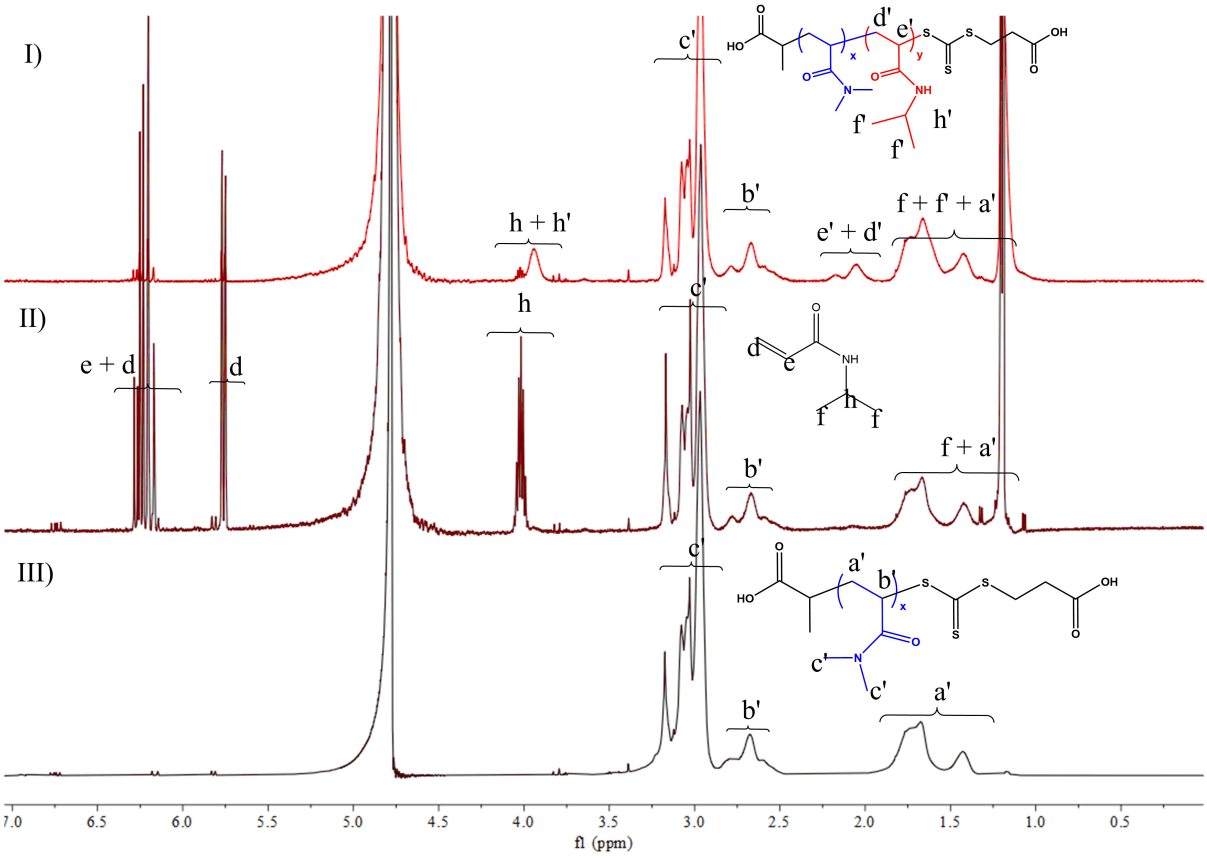

Figure 3.14: ^{1}H NMR spectra acquired for the RAFT dispersion polymerisation of NIPAm at I) $t_{90\ min}$ and II) $t_{0\ min}$. ^{1}H NMR spectra of the III) $PDMAm_{113}$ macro-CTA is also shown. Conversion was determined by comparing vinyl protons (d + e) to the pendant hydrogen (h)

Flow NMR kinetics showed an increased rate of reaction compared to batch. For DP 50 (Figure 3.15a), 83 % conversion was achieved after 60 minutes in flow whilst in batch 83 % conversion was achieved after 80 minutes. Linear semi-logarithmic plots obtained for both batch and flow polymerisations indicated pseudo first order kinetics. For DP 100 (Figure 3.15b), 77 % conversion was reached for in flow after 60 minutes whilst only 72 % conversion was achieved in

batch after 90 minutes. For DP 200 (Figure 3.15c), 83 % conversion was reached for in flow after 45 minutes whilst 86 % conversion was achieved in batch after 90 minutes. A rate acceleration was observed in the semi-logarithmic rate plots after 45 & 25 minutes in flow for DP 100 and 200 whilst in batch the rate acceleration did not occur until 60 & 35 minutes respectively. Rate acceleration is typical of systems undergoing PISA (section 1.4.2). Rate accelerations were caused by diffusion of monomer into polymeric micelles which led to an increased local monomer concentration inside the micelles. This occurred at a critical degree of polymerisation at which the growing amphiphilic polymer chain favoured self-assembly in order to minimise unfavourable polymer-solvent interactions. This degree of polymerisation was estimated by fitting the two kinetic regions, for DP 100 and 200 the onset of particle formation occurs around 45 and 25 % conversion respectively, indicating a critical chain length of 45 - 50 NIPAm units. This explained why no rate acceleration period was observed for DP 50, as the polymer chain never reached a length at which it would self assemble, since the highest conversion reached was 90 % (DP = 40). The ability to take samples over relatively short timescales resulted in much better resolution of the onset of rate acceleration.

GPC chromatograms (Figure 3.16) for all polymerisations showed a shift to higher molecular weight with respect to reaction time. However, evolution of a high molecular weight shoulder was observed for all polymerisations. The development of a high molecular weight shoulder could be due to several factors such as: bimolecular termination where two propagating radical chains react with each other, light branching due to bis-acrylamide impurities or dipole interactions between the polymer and DMF eluent.[207] The high molecular weight shoulder was much more prominent for the flow polymerisations, possibly due to an increased propagating radical concentration. The calculated molecular weight data (Figure 3.17) showed a linear relationship between molecular weight and conversion for DP 50 and 100 in batch and flow indicating good control over the polymerisation by RAFT. For DP 200 deviation from linearity was observed for both batch and flow. Poor overlap of batch and flow molecular weight evolution for DP 200 was due to the large high molecular weight shoulders observed in flow. An increase in dispersity with respect to conversion was observed for all polymerisations caused by the growth of the high molecular weight shoulder as the reaction progresses.

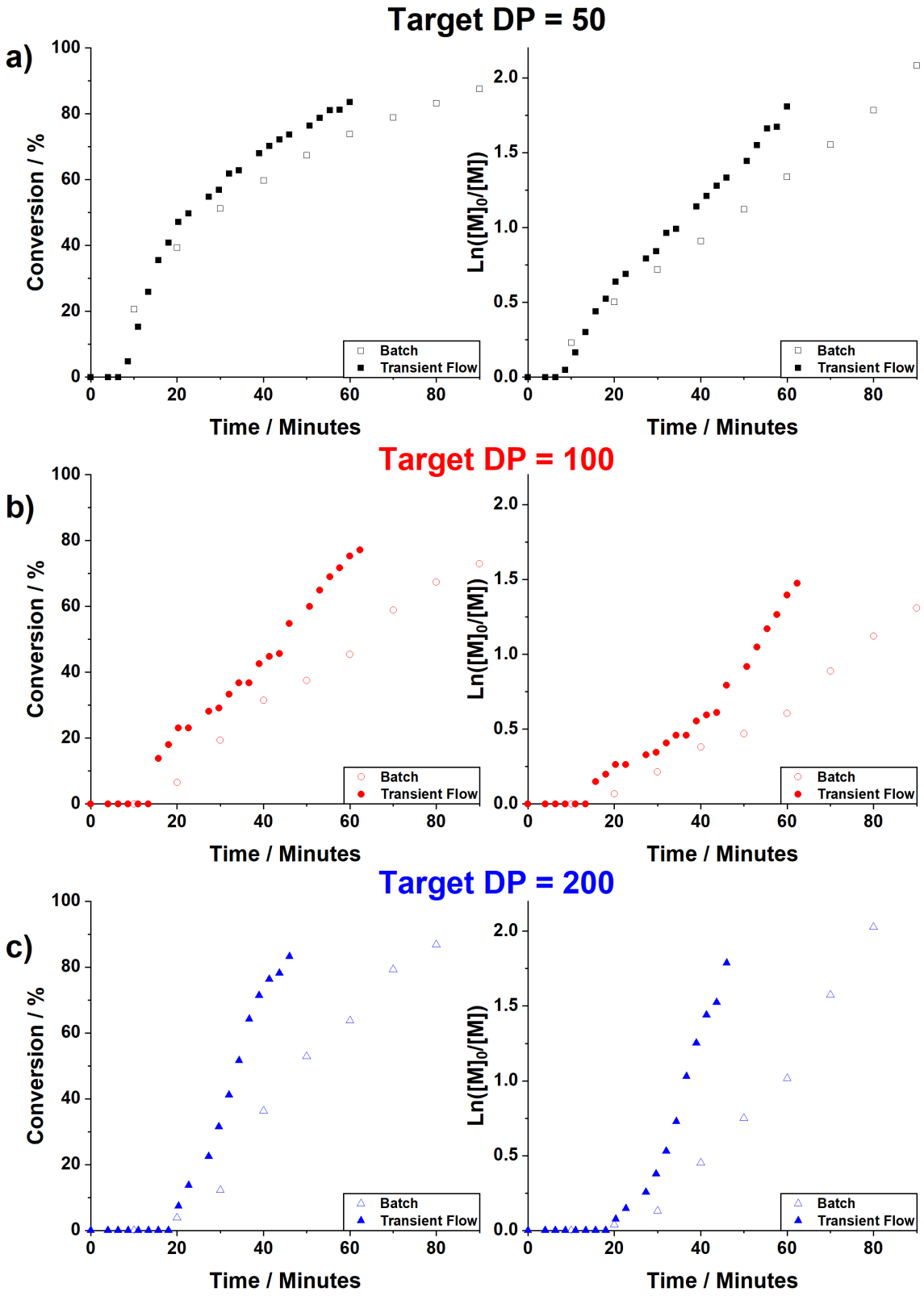

Figure 3.15: Conversion vs. time and semi-logarithmic rate plots for the RAFT aqueous dispersion polymerisation of *N*-isopropylacrylamide (NIPAm) in batch and flow using a $PDMAm_{113}$ macroCTA. All reactions were conducted at 70 °C with total solids concentration of 10 % w/w and [NIPAm]:[$PDMAm_{113}$ macroCTA]:[ACVA] = a)50/b)100/c)200:1:0.1.

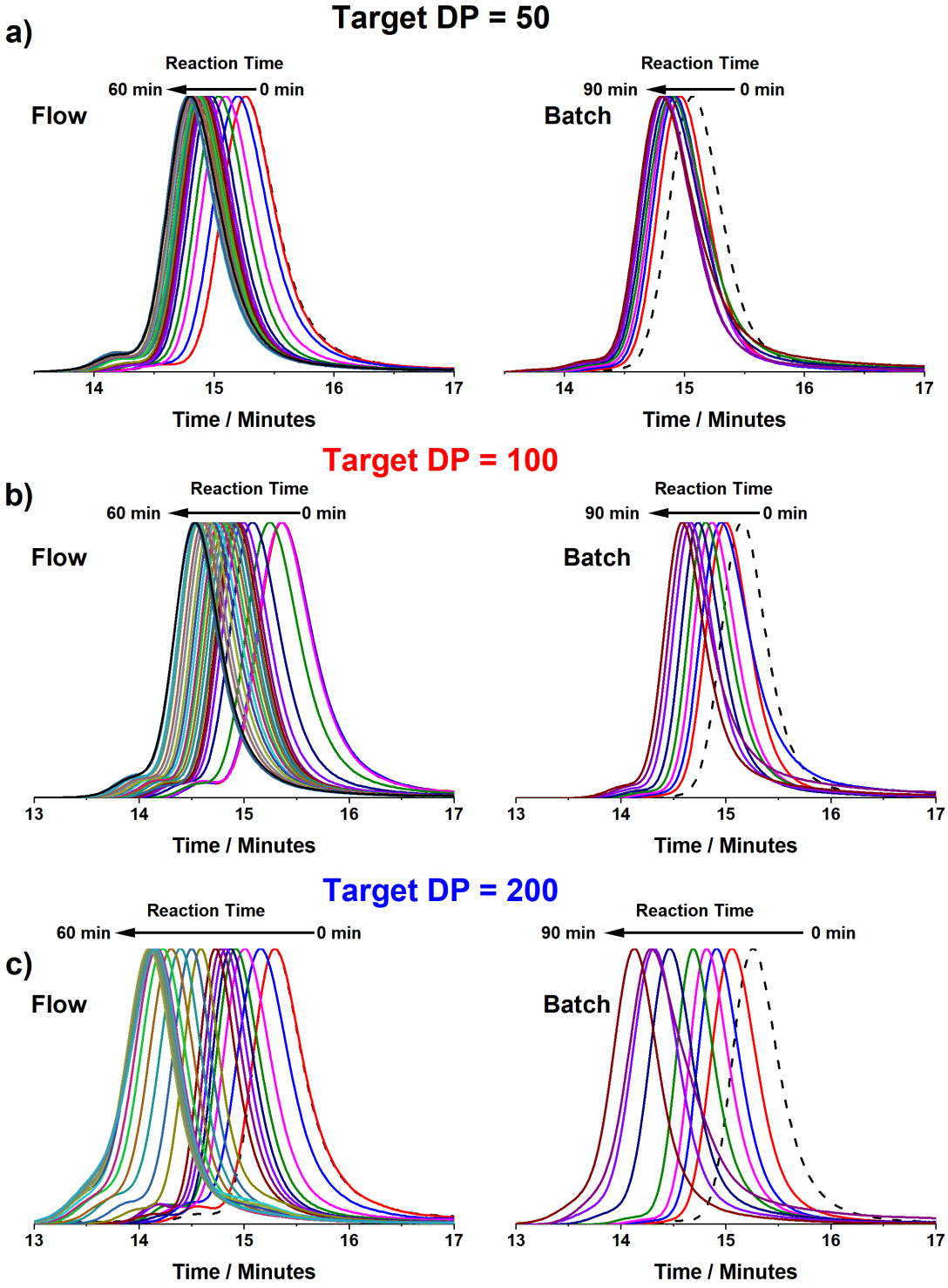

Figure 3.16: GPC chromatograms obtained for a) DP 50 b) DP 100 and c) DP 200 kinetic samples extracted from the RAFT aqueous dispersion polymerisations of *N*-isopropylacrylamide (NIPAm) in batch and flow using a $PDMAm_{113}$ macroCTA. All reactions were conducted at 70 °C with total solids concentration of 10 % w/w and [NIPAm]:[$PDMAm_{113}$ macroCTA]:[ACVA] = 50/100/200:1:0.1.

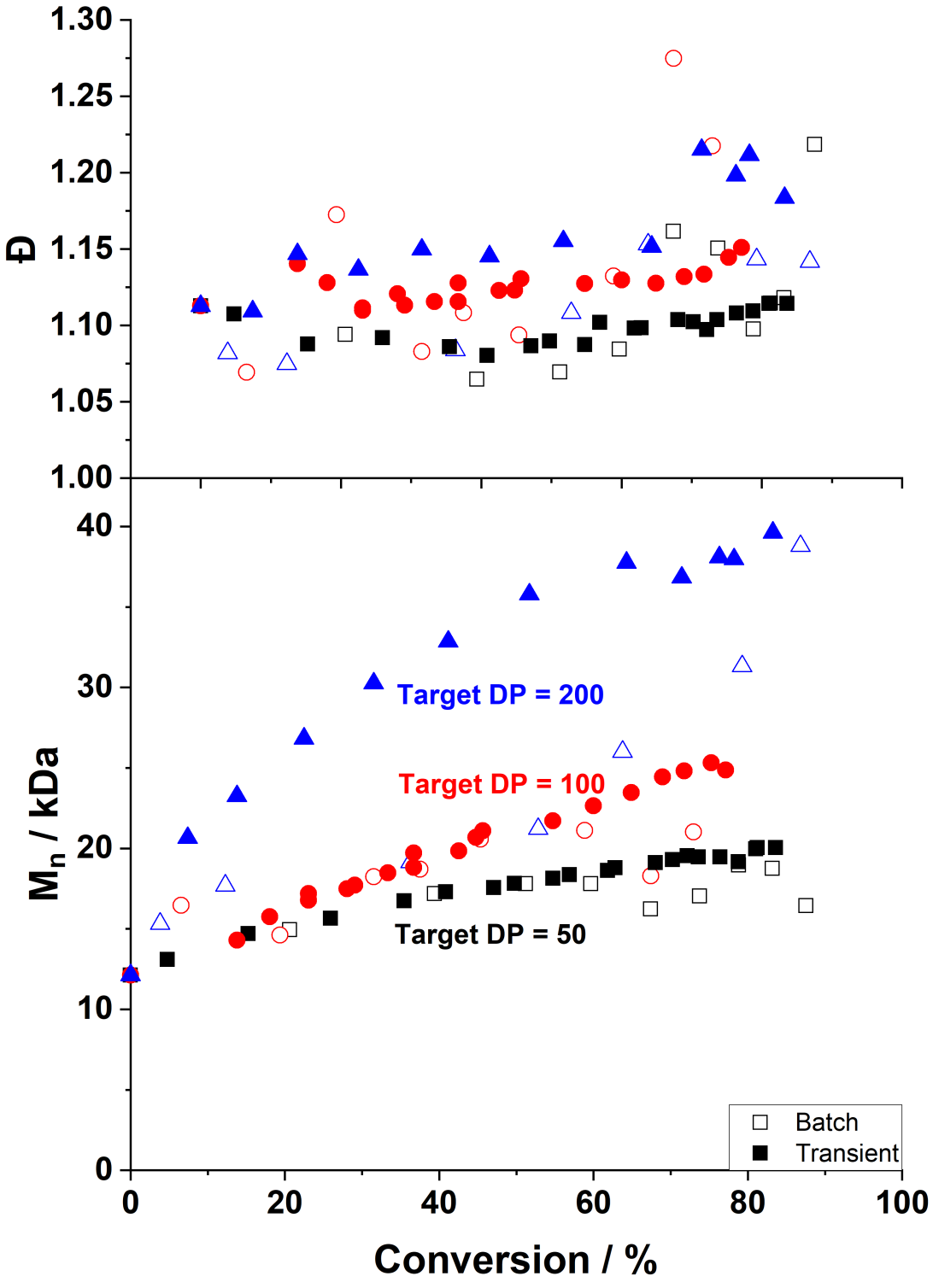

Figure 3.17: Molecular weight and dispersity evolution for RAFT aqueous dispersion polymerisation of *N*-isopropylacrylamide (NIPAm) in batch using a $PDMAm_{113}$ macroCTA (Target DP = 50, 100, 200). All reactions were conducted at 70 °C with total solids concentration of 10 % w/w and [NIPAm]:[$PDMAm_{113}$ macroCTA]:[ACVA] = 50/100/200:1:0.1.

3.3.3 RAFT Dispersion Polymerisation of Diacetone Acrylamide using a $PDMAm_{113}$ macro-CTA

The RAFT dispersion polymerisation of diacetone acrylamide using a PDMAm macro-CTA was chosen as an example of a PISA system for investigation as it is well-studied in literature with multiple self-assembly phase diagrams reported.[208–213] As with the polymerisation of NIPAm a total solids concentration of 10 % w/w was used to minimise potential complications when transferring the system to the flow reactor. DAAm conversion was determined using ^{1}H NMR spectroscopy by comparing vinyl protons between 5.5 - 7.0 ppm to the α-methyl group between 2 - 2.5 ppm (Figure 3.18).

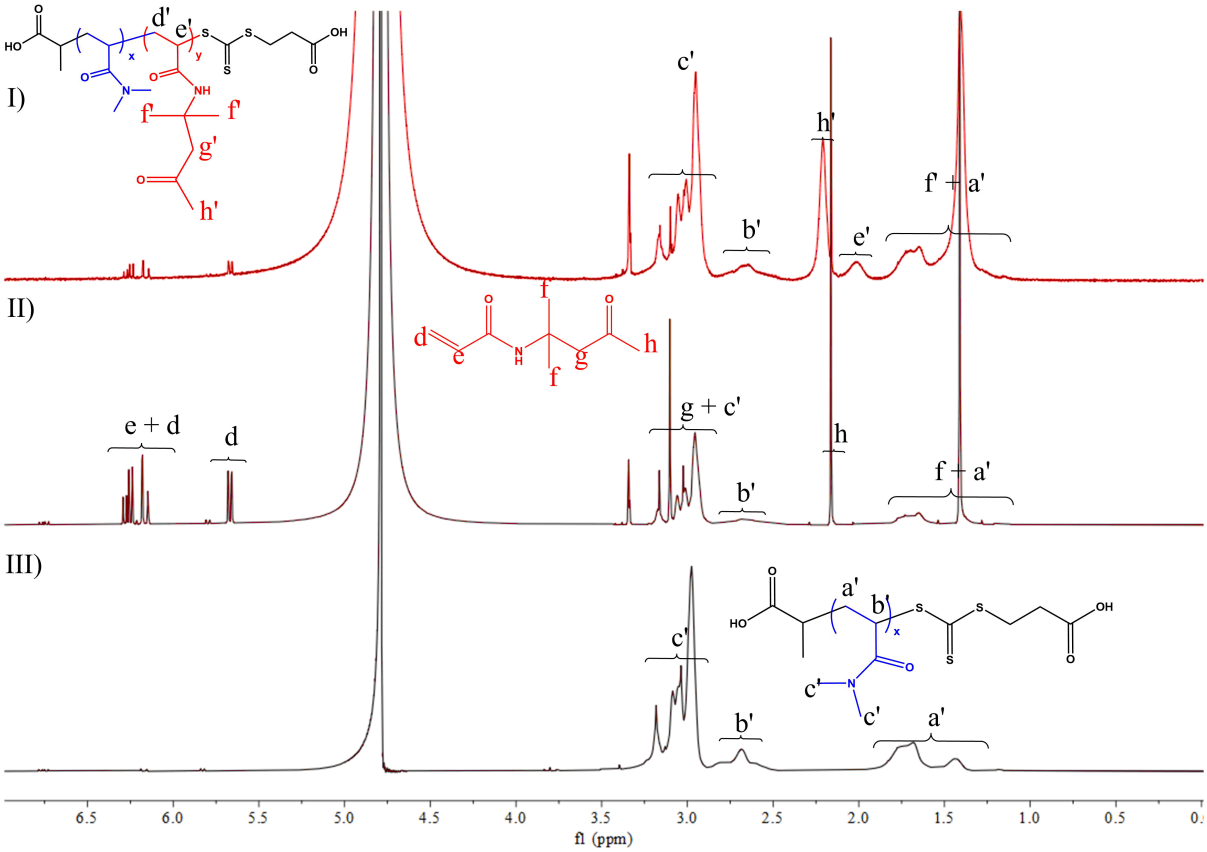

Figure 3.18: ^{1}H NMR spectra acquired for the RAFT dispersion polymerisation of DAAm using a $PDMAm_{113}$ at I) $t_{80\ min}$ and II) $t_{0\ min}$. ^{1}H NMR spectra of the III) $PDMAm_{113}$ macro-CTA is also shown. Conversion was determined by comparing vinyl protons (d + e) to the pendant methyl group (h).

Flow NMR kinetics showed an increased rate of reaction compared to batch. For DP 50 (Figure 3.19a), 95 % conversion was achieved after 60 minutes in flow whilst in batch 95 % conversion was achieved after 70 minutes. For DP 100 (Figure 3.19b), 95 % conversion was reached for in flow after 45 minutes whilst 95 % conversion was achieved in batch after 60 minutes. For

DP 200 (Figure 3.19c), 95 % conversion was reached for in flow after 40 minutes whilst 95 % conversion was achieved in batch after 60 minutes. In contrast to the polymerisation of NIPAm, rate accelerations were observed for all target DPs and the onset of particle formation occurred around 72, 30 and 17 % respectively indicating a critical chain length of 30 - 35 DAAm units. The observed rate acceleration increased with respect to target DP for both flow and batch polymerisations, likely due to monomer concentration increasing, at the moment of self assembly, with target DP . Interestingly, the increase in rate acceleration appeared to be greater in flow than batch with a 4-fold rate increase observed for DP 200 in batch whilst a 5-fold increase was observed in flow, possibly due to an increase in the number of propagating radicals per polymeric micelle.

GPC chromatograms (Figure 3.20) for all polymerisations showed a shift to higher molecular weight with respect to reaction time. Unlike the polymerisation of NIPAm, no high molecular weight shoulder was detected for any target DP. The calculated molecular weight data (Figure 3.21) showed a linear relationship between molecular weight and conversion for DP 50 and DP 100 in both batch and flow. For DP 200 a linear relationship between molecular weight and conversion was observed in flow but a loss of linearity was observed in batch, indicating a loss of control of the polymerisation. For all polymerisations in batch and flow, an increase in dispersity at high conversions was observed indicating radical termination reactions became more prominent at high conversions.

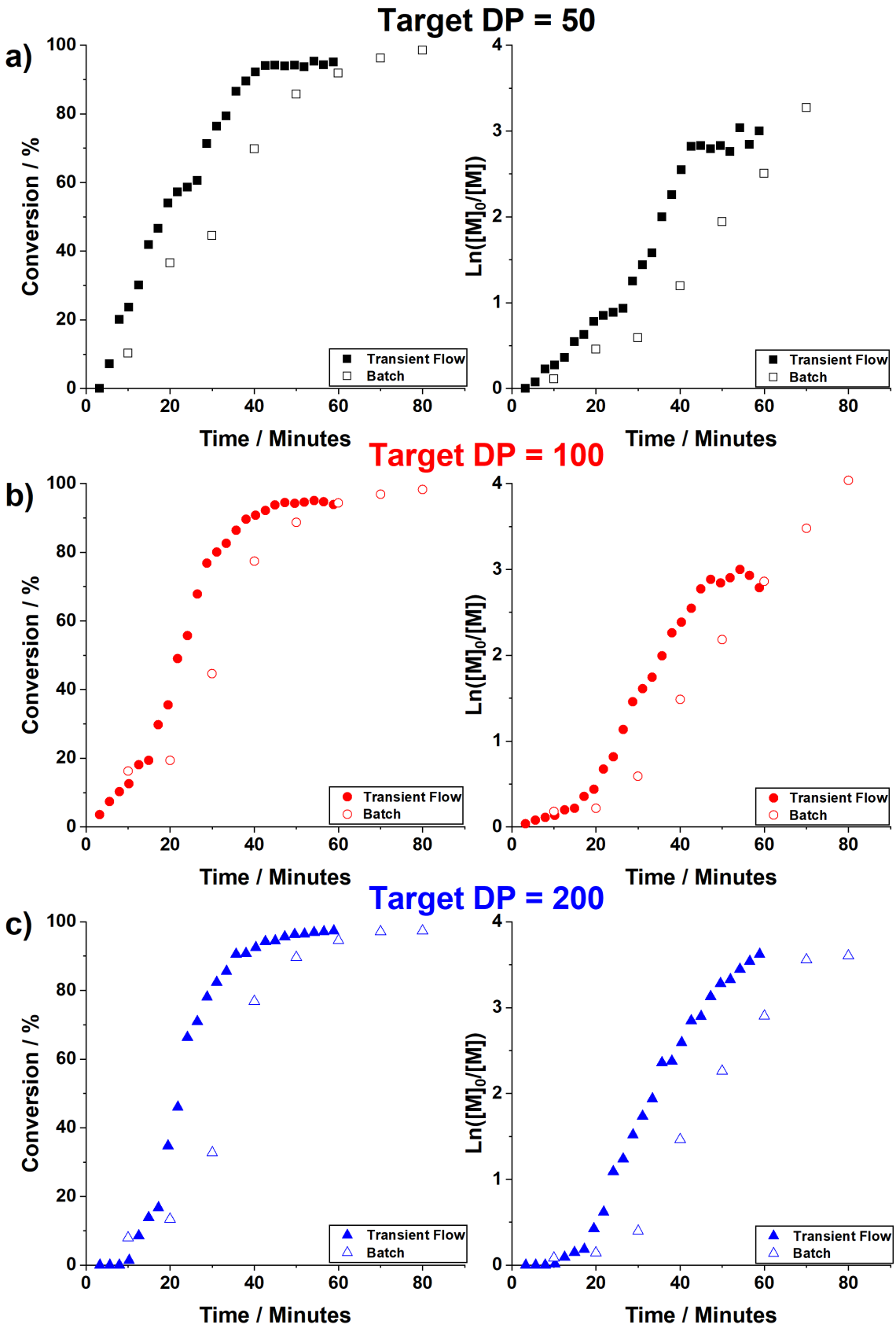

Figure 3.19: Conversion vs. time and semi-logarithmic rate plots for the RAFT aqueous dispersion polymerisation of diacetone acrylamide (DAAm) in batch and flow using aPDMAm$_{113}$ macro-CTA. All reactions were conducted at 70 °C with total solids concentration of 10 % w/w and [DAAm]:[PDMAm$_{113}$ macro-CTA]:[ACVA] = a)50/b)100/c)200:1:0.1.

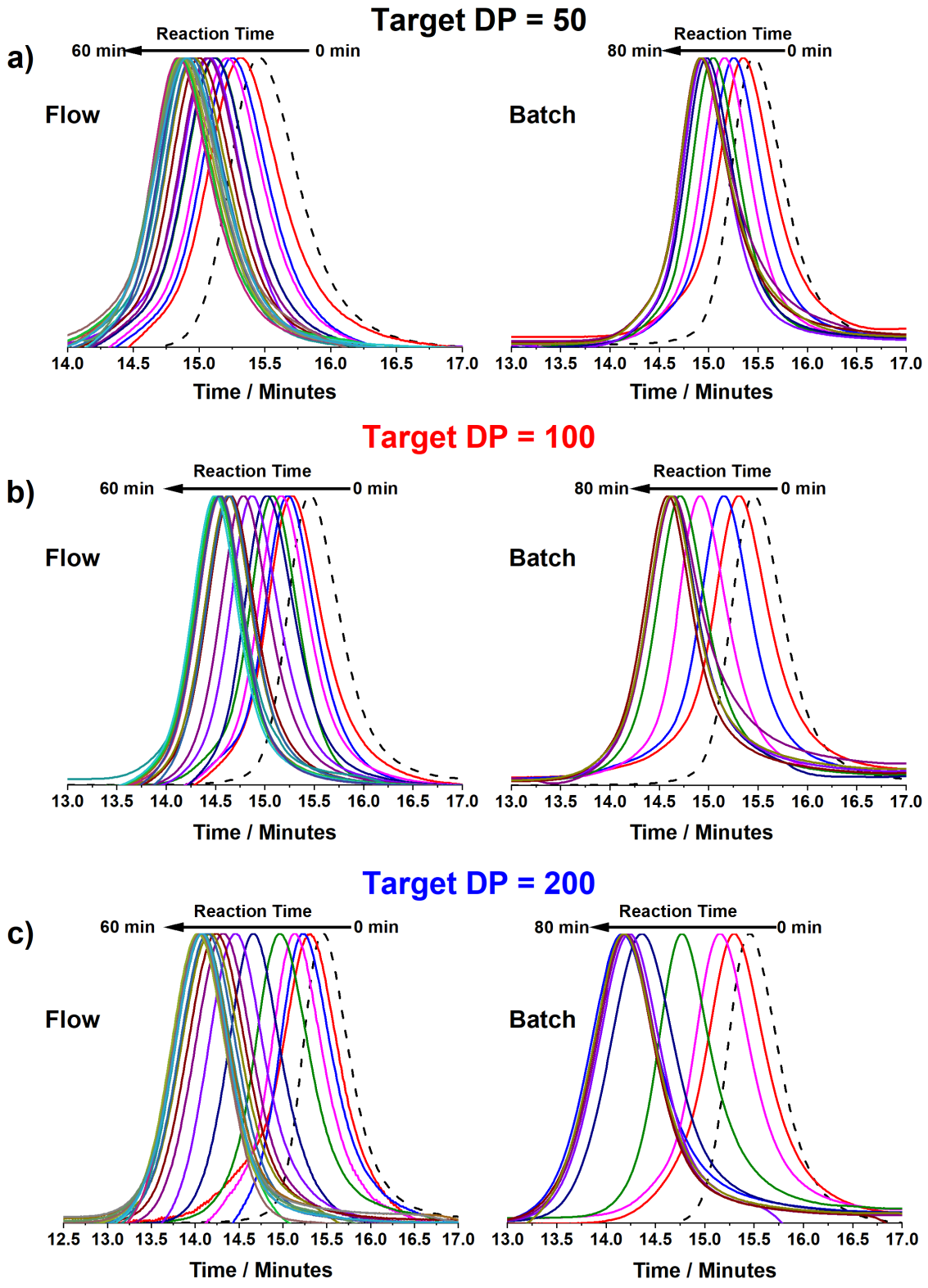

Figure 3.20: GPC chromatograms obtained for a) DP 50 b) DP 100 and c) DP 200 kinetic samples extracted from the RAFT aqueous dispersion polymerisation of diacetone acrylamide (DAAm) in batch and flow using a $PDMAm_{113}$ macro-CTA. All reactions were conducted at 70 °C with total solids concentration of 10 % w/w and [DAAm]:[$PDMAm_{113}$ macro-CTA]:[ACVA] = 50/100/200:1:0.1.

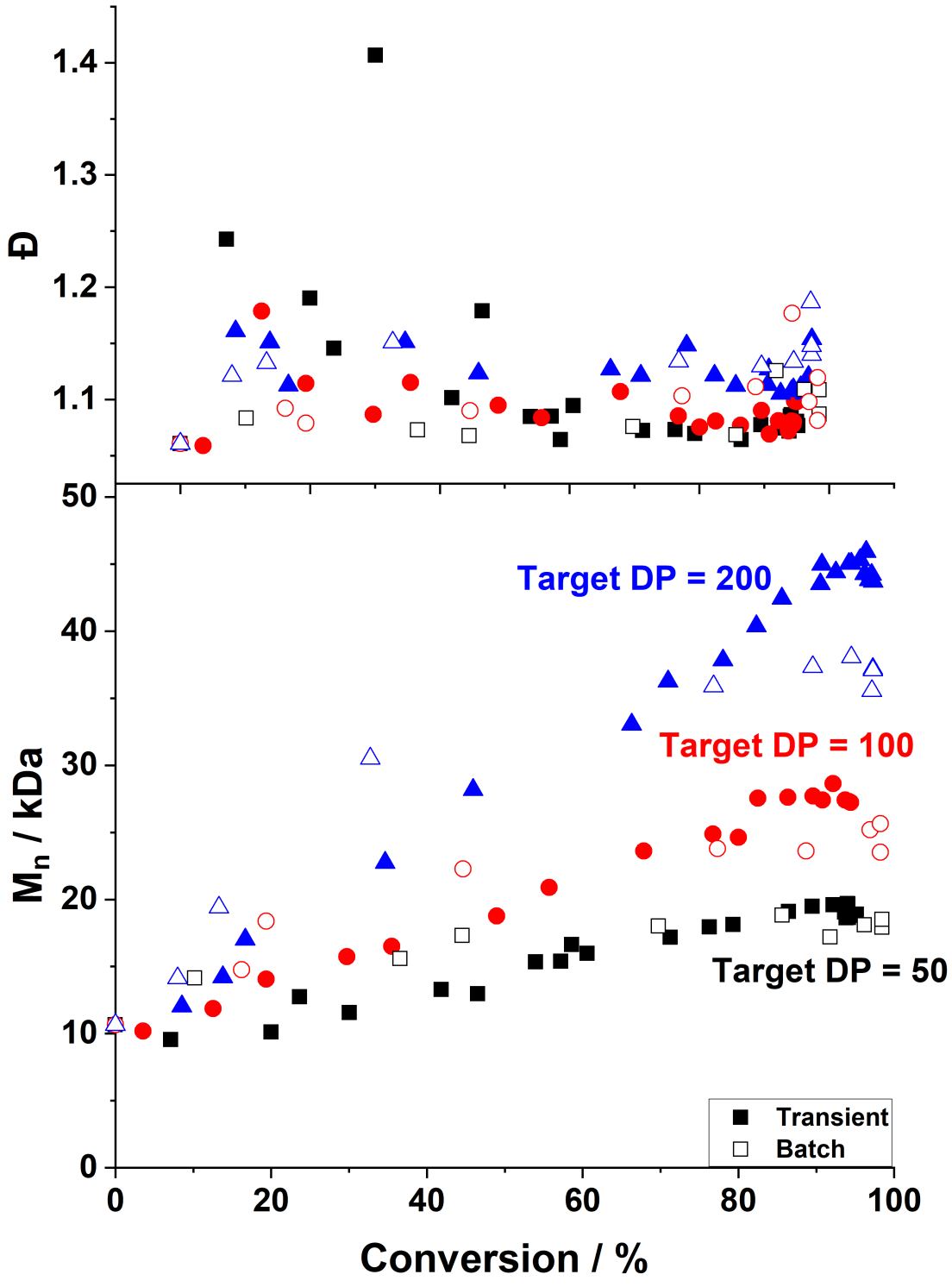

Figure 3.21: Molecular weight and dispersity evolution for RAFT aqueous dispersion polymerisation of diacetone acrylamide (DAAm) in flow using a $PDMAm_{113}$ macro-CTA. All reactions were conducted at 70 °C with total solids concentration of 10 % w/w and [DAAm]:[$PDMAm_{113}$ macro-CTA]:[ACVA] = 50/100/200:1:0.1.

Using the kinetic data acquired, a series of well-defined $PDMAm_{113}$-$PDAAm_y$ copolymers were synthesised using the 5 mL reactor coil and a residence time of 50 min. The resulting diblock copolymer dispersions were characterised using ^1H NMR spectroscopy, GPC and DLS. NMR studies indicated near complete conversion was achieved in all cases while GPC confirmed a systematic increase in molar mass with target PDAAm DP. High blocking efficiencies were observed with monomodal molar mass distributions and low dispersities ($Đ < 1.17$) (Figure 3.22).

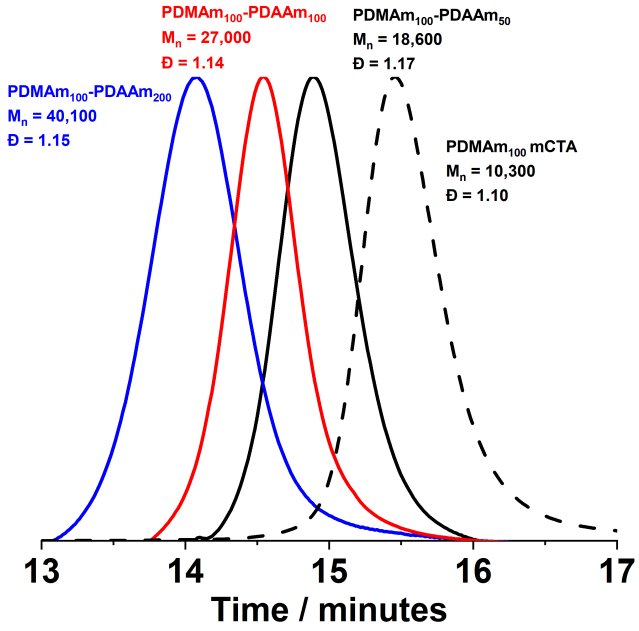

Figure 3.22: GPC chromatograms obtained for the RAFT aqueous dispersion polymerisation of diacetone acrylamide (DAAm) in flow using a $PDMAm_{113}$ macro-CTA. All reactions were conducted at 70 °C with total solids concentration of 10 % w/w and [DAAm]:[$PDMAm_{113}$ macro-CTA]:[ACVA] = 50/100/200:1:0.1.

DLS indicated particles sizes (D_h) of 32, 46 and 55 nm for PDAAm DPs of 50, 100 and 200 respectively. All samples had mono-modal particle size distributions (Figure 3.23) with a PDI of 0.07 for DPs 100 and 200 whilst a slightly broader PDI of 0.13 was observed for DP 50. This DP is only slightly higher than the DP required for micellar nucleation (approx. DP 30) and therefore these particles are likely to comprise more loosely bound diblock copolymer chains. TEM images obtained for $PDMAm_{113}$-$PDAAm_{100}$ and $PDMAm_{113}$-$PDAAm_{200}$ indicated spherical morphologies for both polymers (Figure 3.24) as well as particle sizes of 32 nm and 42 nm respectively, these are slightly smaller than DLS measurements which give intensity average sizes that are skewed towards larger particles that scatter light more intensely.

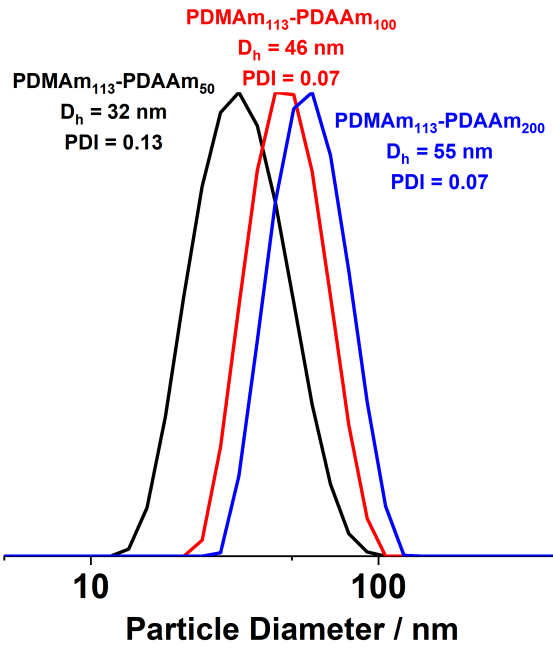

Figure 3.23: DLS size distributions obtained for RAFT aqueous dispersion polymerisation of diacetone acrylamide (DAAm) in flow using a $PDMAm_{113}$ macro-CTA. All reactions were conducted at 70 °C with total solids concentration of 10 % w/w and [DAAm]:[$PDMAm_{113}$ macro-CTA]:[ACVA] = 50/100/200:1:0.1.

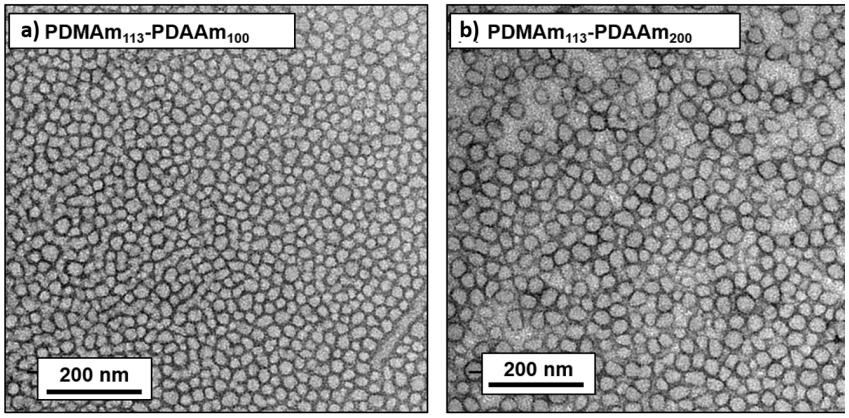

Figure 3.24: TEM images obtained for a) $PDMAm_{113}$-$PDAAm_{100}$ and b)$PDMAm_{113}$-$PDAAm_{200}$ diblock copolymer spheres. All reactions were conducted at 70 °C with total solids concentration of 10 % w/w and [DAAm]:[$PDMAm_{113}$ macro-CTA]:[ACVA] = 50/100/200:1:0.1.

One of the attractive features of PISA is the ability to produce higher order block copolymer nano-objects. To investigate whether this was possible using the flow platform it was necessary to reduce the DP of the PDMAm macro-CTA and raise the total solids to 20 % w/w. According to the phase diagram reported by Byard *et al.*, PDMAm DPs < 58 can produce diblock copolymer worms or vesicles.[209] Hence, a PDMAm macro-CTA with a DP of 50 was prepared and used to mediate the RAFT dispersion polymerisation of DAAm at 20 % w/w in flow. The

target DP of the hydrophobic PDAAm block was raised to 200 targeting a pure vesicle phase. Significant fouling in the reactor was observed for the polymerisation, using a similar protocol for previous experiments. Two diblock copolymers were synthesised by employing two different residence times for the same reaction solution, which attained 31 % and 74 % conversion, equating to $PDMAm_{50}$-$PDAAm_{62}$ and $PDMAm_{50}$-$PDAAm_{148}$ respectively. For both samples large aggregates were observed at the reactor outlet indicating fouling within the reactor. Nevertheless, a systematic increase in M_n with conversion, from 20,900 to 32,600 g mol^{-1} was indicated by GPC (Figure 3.25). GPC also confirmed low molar mass dispersities however, low levels of macro-CTA contamination were observed likely caused by the observed fouling of the reactor.

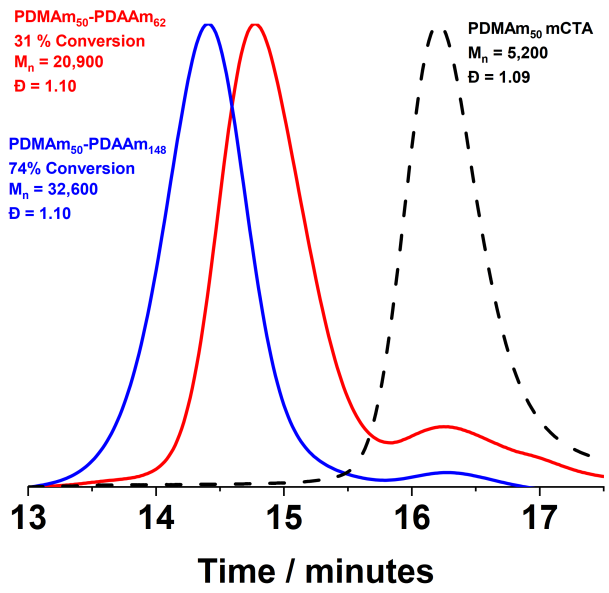

Figure 3.25: GPC chromatograms obtained for the RAFT aqueous dispersion polymerisation of diacetone acrylamide (DAAm) in flow using a $PDMAm_{50}$ macro-CTA. All reactions were conducted at 70 °C with total solids concentration of 20 % w/w and [DAAm]:[$PDMAm_{50}$ macroCTA]:[ACVA] = 200:1:0.1.

Broad and multimodal DLS distributions for the samples (Figure 3.26) suggested the presence of non-spherical morphologies. However, as larger aggregates were present in the outlet stream these may also account for the features corresponding to larger species in the multi-modal DLS traces.

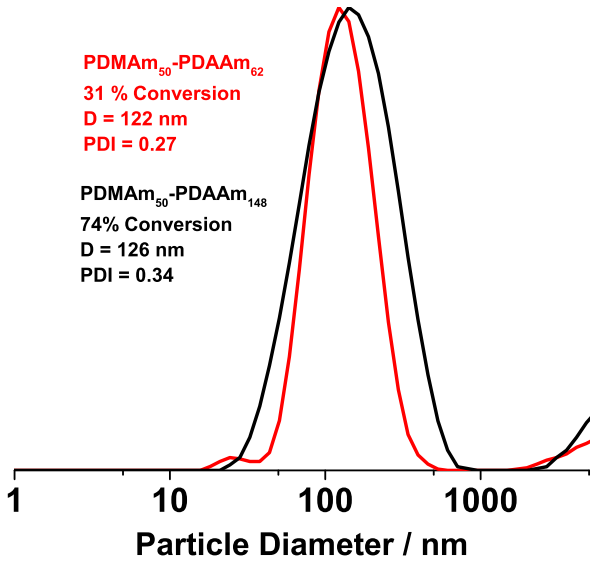

Figure 3.26: DLS size distributions obtained for the chain extension of $PDMAm_{50}$ with DAAm conducted using the continuous-flow reactor. All reactions were conducted at 70 °C with total solids concentration of 20 % w/w and [DAAm]:[$PDMAm_{50}$ macroCTA]:[ACVA] = 200:1:0.1.

TEM images obtained for the two samples (Figure 3.27) indicated that the $PDMAm_{50}$-$PDAAm_{62}$ comprised a majority phase of block copolymer worms (∼180 nm long) whilst the $PDMAm_{50}$-$PDAAm_{148}$ copolymer formed a majority phase of vesicles (∼143 nm). A minor population of spherical particles (∼40 nm and ∼70 nm respectively) was observed in both samples, but it should be noted that the observed reactor fouling was likely to have affected the polymerisation and subsequent self-assembly of the block copolymers. As fouling polymer deposited on the walls of the stainless steel tubing it caused a reduction in internal volume and therefore a decrease in residence time.

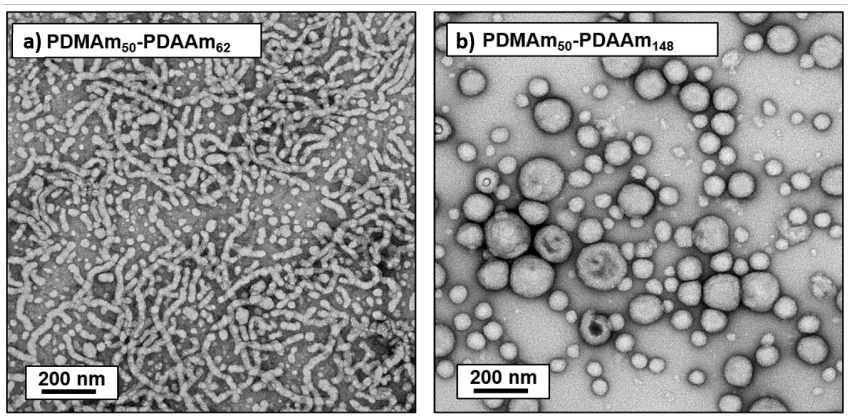

Figure 3.27: TEM images obtained for a) $PDMAm_{50}$-$PDAAm_{62}$ and b)$PDMAm_{50}$-$PDAAm_{148}$ diblock copolymer nanoparticles. All reactions were conducted at 70 °C with total solids concentration of 20 % w/w and [DAAm]:[$PDMAm_{50}$ macroCTA]:[ACVA] = 200:1:0.1.

3.4 Conclusions

In this chapter, homogeneous and heterogeneous RAFT polymerisations were kinetically investigated in both batch and flow reactors. For a homogenous system the RAFT polymerisation of dimethylacrylamide, using two different CTAs, was screened in batch to determine a suitable polymerisation system to transfer to flow. Both CTAs indicated good living control over RAFT polymerisations. However, DCTTC batch kinetics indicated a large induction period which was attributed to the cyano moiety within the DCTTC R group. The non-cyano containing RAFT agent (CCTP) had no induction period and thus was the CTA used in flow experiments. Flow kinetic profiles were obtained using both transient and steady state profiling methods and were found to be comparable, thus validating the transient profiling method. By comparing batch and flow kinetic profiles, it was noted that the rate of polymerisation was faster in flow, which was attributed to improved heat transfer in flow reactors. Both batch and flow polymerisations showed good control over the reaction kinetics and molecular weight distribution. A large batch (40.5 g) of $PDMAm_{113}$ macro-CTA was synthesised using a 20 mL flow reactor and used for further chain extension experiments.

The RAFT aqueous dispersion polymerisation of NIPAm was then investigated and target DP was varied from 50 - 200 in order to investigate the self-assembly behaviour of the system. As with the RAFT polymerisation of DMAm, an accelerated rate of polymerisation was observed in flow but pseudo first order kinetics were observed in both reactors. From the kinetic data, a DP around 50 was determined to be the critical chain length at which self assembly occurred.

High molecular weight shoulders were observed in batch and flow however the shoulder was much more prominent for the flow polymerisation, likely due to the increased reaction rates observed in flow reactors.

Finally, the RAFT aqueous dispersion polymerisation of diacetone acrylamide was investigated. Batch and flow kinetic profiles once again indicated an accelerated rate of polymerisation in flow. A series of $PDMAm_{113}$-$PDAAm_x$ block copolymer spherical nanoparticles were synthesised in flow and nanoparticle size increased with respect to PDAAm block length. Higher order morphologies were targeted by increasing the concentration of the reaction solution and reducing the PDMAm DP to 50. Significant fouling was observed when targeting high conversions for DP 200. Therefore, to succesfully collect samples the polymerisation was performed at two shorter residence times. TEM analysis of the resultant nanoparticles indicated a majority worm phase at the shorter residence time and a majority vesicle phase at the longer residence time. However, both samples contained a population of spherical nanoparticles due to fouling in the flow reactor as the reaction progressed.

Overall these results indicate that flow reactors can be used to perform both homogenous and heterogeneous RAFT polymerisations without detrimentally affecting the polymerisation kinetics. However, the large amount of fouling present during the synthesis of high order polymer nanoparticles is of concern and warrants further investigation.

Chapter 4

Ultrafast Synthesis of Block Copolymer Nano-objects in Flow via RAFT Polymerisation

4.1 Introduction

Block copolymer materials generated by PISA have extremely attractive properties which have resulted in a broad range of applications including as cell storage or growth media,[214–216] viscosity modifiers,[217] friction reducing agents,[218] and as nano-reactors.[219] This rapid growth in applicability means cost effective scale-up of PISA-synthesised polymers is desirable. Otherwise manufacture on the scales required for incorporation in commercial products will be difficult, which is an issue often encountered for controlled radical polymerisations.[109] Radical polymerisations have issues with scale-up in batch such as poor dissipation of large exotherms which affect polymerisation kinetics and the final molecular weight distribution.[109] Transferring polymerisations to flow offers a suitable alternative route to scale up; as the increased heat transfer effectively disperses unwanted exotherms. However, polymerisations with long reaction times ($>$ 1 hour) significantly limit the cost-effective operation of continuous flow processes .[179] As an example for polymerisation that takes one hour, under steady state conditions in flow will take a minimum of 2 hours to collect one reactor volume of product. Any subsequent alterations to the reactor input feeds (i.e changing reagent feed ratios) incurs another time delay.[4] To minimise the impact of these time delays polymerisations must occur on a timescale that

is not limiting to the overall operation. Hence, it is necessary to achieve significant process intensification without any detrimental effects on polymer quality if it is going to be feasible to meet anticipated increase in demand.[109] Therefore, decreasing reaction time (increasing rate of reaction) is as a vital aim towards the cost-effective flow synthesis of polymers. This would allow faster flow rates to be used increasing productivity. Reaction rate increases in flow have been widely reported and are attributed to effects such as heating,[220] mass transfer[221] and light permeability but, the rate increases have often been moderate.[222] An alternative approach is to modify the chemistry of the reaction itself: Gody *et al.* reported an ultrafast method which significantly increased the rate of RAFT polymerisations.[223] The synthesis of soluble multi-block copolymers within 3 minutes was made possible by performing the reaction in the presence of a high k_d thermal initiator (VA-044), as the rate of polymerisation is proportional to k_d (equation 1.16).[101] However, using a high radical flux to increase the rate of RAFT polymerisations (homogeneous or heterogeneous) is only suitable for monomers which have high k_p values relative to k_t, such as acrylamides and acrylates, in order to minimise chain termination reactions..[223] All RAFT polymerisation systems investigated in chapter 3 contain solely acrylamide monomers and are therefore ideal candidates for using the ultrafast RAFT method. This chapter focuses on the ultrafast synthesis of poly(dimethylacrylamide)-b-poly(diacetone acrylamide) nano objects via RAFT aqueous dispersion polymerisation using a flow platform (Reactor C in chapter 2). Transient kinetic profiles are obtained for the ultrafast synthesis of a PDMAm macro-CTA and a PDMAm-PDAAm block copolymer systems. A series of PDMAm-PDAAm copolymers are then synthesised on the flow platform and the resulting nanoparticles were characterised.

4.2 Experimental

4.2.1 Materials

4,4'-Azobis(4-cyanovaleric acid) (ACVA, 99 %), dimethylacrylamide (DMAm, 99 %), deuterated methanol (CD_3OD, 99.8 %) and deuterium oxide (D_2O, 99.9 %) were purchased from Sigma Aldrich (UK). 3-((((1-Carboxyethyl)thio)carbonothioyl)thio) propanoic acid (CCTP, 90 %) was purchased from Boron Molecular (Raleigh, USA). Diacetone acrylamide (DAAm, 99 %) was purchased from Alfa Aesar (UK). 2,2'-Azobis[2-(2-imidazolin-2-yl)propane]dihydrochloride (VA-044, 99 %) was purchased from Wako Chemicals (USA).

4.2.2 Methods

4.2.2.1 Synthesis of $PDMAm_x$ macro-CTA

For a target composition of $PDMAm_{100}$: dimethylacrylamide (20 g, 100 eq), CCTP (0.51 g, 1 eq) and ACVA (0.05 g, 0.1 eq) were added to a 100 mL round bottom flask and dissolved in water (48 mL) to give a 30 % w/w reaction solution. A stirrer bar was added and then the flask was sealed and sparged with nitrogen for 20 minutes. The flask was then immersed in an oil bath at 70 °C and left for 50 minutes. Afterwards the flask was removed from the oil bath and quenched by exposure to oxygen. Samples extracted for ^{1}H NMR spectroscopy indicated 93 % monomer conversion and a final DP of 113 via end group analysis. While DMF GPC indicated M_n = 10,400 g mol^{-1} and Đ = 1.11. No further purification was performed and the macro-CTA solution was used as is for further chain extension experiments.

4.2.2.2 High Resolution Transient Flow Kinetic Studies

For a target composition of $PDMAm_{113}$-$PDAAm_{50}$: diacetone acrylamide (3 g, 50 eq.), $PDMAm_{113}$ macro-CTA (3.6 g, 1 eq), VA-044 (2.3 mg, 0.02 eq) and 3-(trimethylsilyl)-1-propanesulfonic acid sodium salt (0.6 g) were added to a 100 mL round bottom flask and dissolved in water (26 mL) to give a 20 % w/w reaction solution. The flask was sealed and sparged with nitrogen for 20 minutes. The nitrogen stream was left in to provide a positive pressure and a Jasco PU-980 HPLC pump inlet tube was inserted into the flask and the solution was pumped through a 5 mL, tubular PFA reactor at a flow rate 10 mL min^{-1} for 90 seconds; the flow rate was then reduced to 0.25 mL min^{-1} giving a retention time of 20 minutes. Final residence times were calculated using equation 2.1. The outlet of the reactor was connected to the PFA tubing passed directly through the NMR spectrometer.

4.2.2.3 Continuous-Flow Synthesis of $PDMAm_x$-$PDAAm_y$ copolymers

For a target composition of $PDMAm_{113}$-$PDAAm_{100}$: diacetone acrylamide (3 g, 100 eq.), $PDMAm_{113}$ macro-CTA (1.8 g, 1 eq.) and VA-044 (1.1 mg, 0.02 eq.) were added to a 100 mL round bottom flask and dissolved in water (19 mL) to give a 20 % w/w reaction solution. The flask was sealed and sparged with nitrogen for 30 minutes. The HPLC pump inlet tube was then inserted into the flask and the solution was pumped through a PFA tubular reactor at 90 °C with a retention time of 20 minutes.

4.2.2.4 Batch Synthesis of $PDMAm_{46}$-$PDAAm_y$ copolymers

For a target composition of $PDMAm_{46}$-$PDAAm_{500}$: diacetone acrylamide (3 g, 500 eq.), $PDMAm_{46}$ macro-CTA (0.17 g, 1 eq.) and VA-044 (0.2 mg, 0.02 eq.) were added to a 40 mL vial and dissolved in water (13 mL) to give a 20 % w/w reaction solution. A stirrer bar was added and the vial was the sealed. The vial was sparged for 15 minutes and then placed in an oil bath with stirring at either 70 °C or 90 °C for 20 minutes.

4.2.2.5 ^{1}H NMR Spectroscopy

Transient kinetic profiles were obtained using a Magritek Spinsolve Ultra 60 MHz. Analysis was performed on the flowing mixture (in 1/8" PFA tubing) obtained directly from the reactor outlet. A PRESAT method was used to suppress solvent signals at 4.79 ppm (1 s saturation pulse of -65 dB, 7 µs excitation pulse, acquisition time of 6.4 s, repetition time of 10 s & number of scans was 2). All chemical shifts are reported in ppm (δ). Final polymer conversions were acquired using a Bruker 500 MHz. Samples were dissolved in D_2O or CD_3OD. All chemical shifts are reported in ppm (δ). The average number of scans accumulated per spectrum was typically 32. For the RAFT polymerisation of dimethylacrylamide, conversion was determined by Equation 4.1:

$$Conversion = 1 - \frac{2x}{y - \frac{z}{2}} \tag{4.1}$$

where x is the vinyl peak region between 5.6 and 7.0 ppm, y is the overlapping monomer and polymer region between 3.3 to 2.18 ppm and z is the polymer backbone region between 2.18 to 0.0 ppm

For the RAFT dispersion polymerisation of diacetone acrylamide, conversion was determined by by Equation 4.2:

$$Conversion = 1 - \frac{a_n b_0}{a_0 b_n} \tag{4.2}$$

where a is the vinyl peak region between 5.6 and 7.0 ppm and b is the internal standard peak at 0.1 to -0.1 ppm

4.2.2.6 Gel Permeation Chromotgraphy

Gel permeation chromatography measurements were conducted an Agilent 1260 Infinity system fitted with two 5 µm Mixed-C columns plus a guard column, a refractive index detector and an

UV-Vis detector operating at 309 nm. DMF eluent contained 1.0 w/v % lithium bromide (LiBr) at a flow rate of 1.0 mL min^{-1} at a temperature of 60 °C. A series of ten near-monodisperse poly(methyl methacrylate) standards (M_p ranging from 800 to 2,200,000 g mol^{-1}) were employed as calibration standards in conjunction with an RI detector for determining molecular weights.

4.2.2.7 Dynamic Light Scattering

Dynamic light scattering measurements were conducted at 25 °C using a Malvern Instruments Zetasizer Nano series instrument. Light scattering was detected at 173° and hydrodynamic diameters were determined using the Stokes-Einstein equation, which assumes spherical, non-interacting particles.

4.2.2.8 Transmission electron microscopy (TEM)

Transmission electron microscopy was conducted at 200 kV using a Tecnai F20 FEGTEM. TEM samples were prepared on carbon coated copper grids (400 mesh, continuous film) by adding 20 µL of 0.1 % w/w sample solution and leaving for 1 minute. The excess sample was removed from the grid by blotting and the same procedure was repeated for staining using a 1 % w/w uranyl acetate solution.

4.3 Results and Discussion

4.3.1 Transient Ultrafast RAFT Polymerisation Kinetics

The transient kinetic profiling method developed in chapter 2 was used to generate kinetic profiles for all polymerisations. To maintain the resolution of the profile at shorter reaction times the time between sampling needed to be reduced, which would have increased user workload and potential for error. Therefore, a benchtop NMR spectrometer was added to a flow platform (Reactor C), which allowed for even greater temporal resolution and reproducibility when collecting transient kinetic profiles (see section 2.3.1).

4.3.1.1 Ultrafast RAFT Polymerisation of Dimethyacrylamide

A major difference between traditional NMR spectrometers and the benchtop one used in this thesis is magnetic field strength, which affected the resolution of peaks in NMR spectra. The off-line NMR spectrometer used a 400 MHz magnet whilst the benchtop system used a 60 MHz

magnet. The lower magnetic field strength of the benchtop NMR spectrometer meant that it was no longer possible to distinguish the growing polymer backbone peaks from the pendant methyl groups for the polymerisation of dimethylacrylamide (Figure 4.1). Yet, this loss of resolution did not affect the ability to determine monomer conversion. However, it was not possible to distinguish any peaks from the RAFT agent preventing end-group analysis.

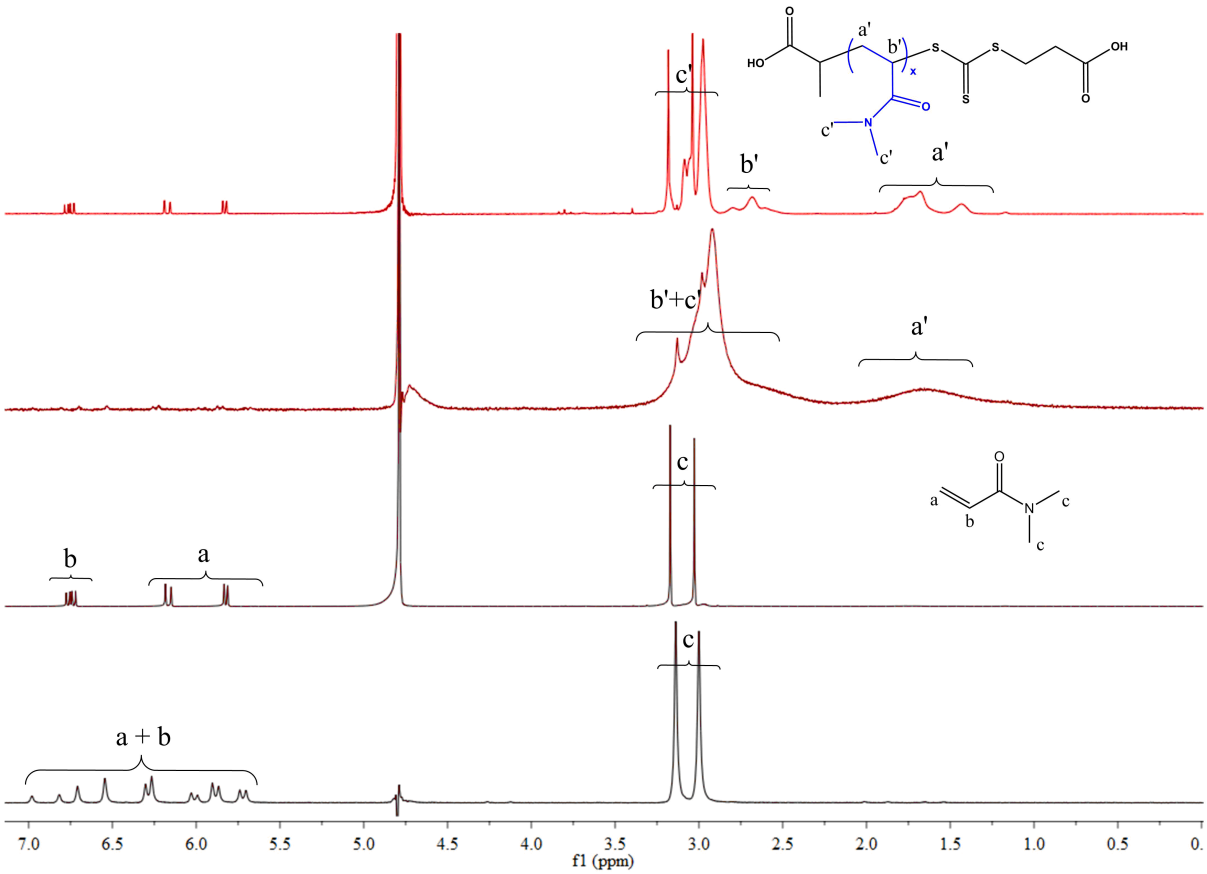

Figure 4.1: ^{1}H NMR spectra recorded for DMAm and PDMAm on 400 MHz and 60 MHz spectrometers.

The transient kinetic profile (Figure 4.2) confirmed the accelerated rate of polymerisation with high conversion achieved (> 90 %) within 10 minutes compared to 40 minutes for the equivalent polymerisation in chapter 3. The observed rate increase (approx. 6-fold) agreed with the expected increase predicted by equation 1.16. Due to the high temporal resolution achieved using the transient profiling method a short induction period (~ 2 min) was observed in the semi-logarithmic plot followed by a linear relationship which indicated first order kinetics throughout the polymerisation until high conversions where some termination may have been present.

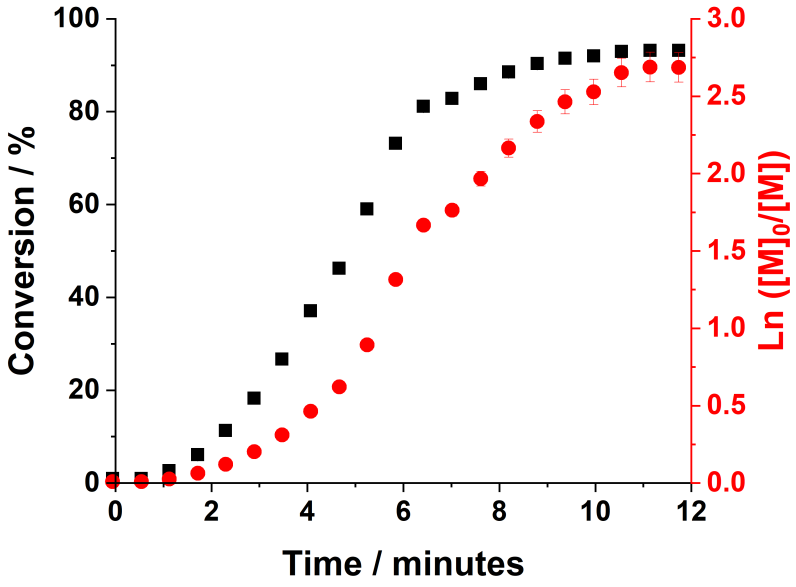

Figure 4.2: Conversion vs. time and semi-logarithmic rate plot for the RAFT solution polymerisation of dimethyl acrylamide (DMAm) in the flow platform. All reactions were conducted at 90 °C with total solids concentration of 30 % w/w and [DMAm]:[CCTP]:[VA-044] = 100:1:0.02.

4.3.1.2 Ultrafast RAFT Aqueous Dispersion Polymerisation of Diacetone acrylamide using a $PDMAm_{113}$ macro-CTA

Polymerisation kinetics for the chain extension of $PDMAm_{113}$ macro-CTA with 50, 100 and 200 equivalents of DAAm were also obtained. As this polymerisation system underwent PISA, NMR spectra acquired online differ significantly from off-line. Samples for off-line NMR spectra were dissolved in d^4-methanol which solvated both PDMAm and PDAAm blocks. This allowed signals from both polymer blocks to be observed in the spectrum. Online NMR spectra were measured directly from the reactor outlet so only the PDMAm block was solvated. As a result, the PDAAm block could not be detected using online NMR (Figure 4.3). Additionally, the reduced resolution of the online spectrometer caused DAAm monomer and PDMAm peaks to overlap thus equation 3.1 could not be used to calculate conversion. In order to determine conversion an internal standard (3-(trimethylsilyl)-1-propanesulfonic acid sodium salt) was added to the reaction mixture. Conversion was then calculated by comparing the integrals of the signals resulting from three vinyl protons between 5.6 and 7.0 ppm with the peak from the internal standard at 0 ppm, where the initial conversion (t = 0 minutes) is assumed to be 0 % (equation 4.2).

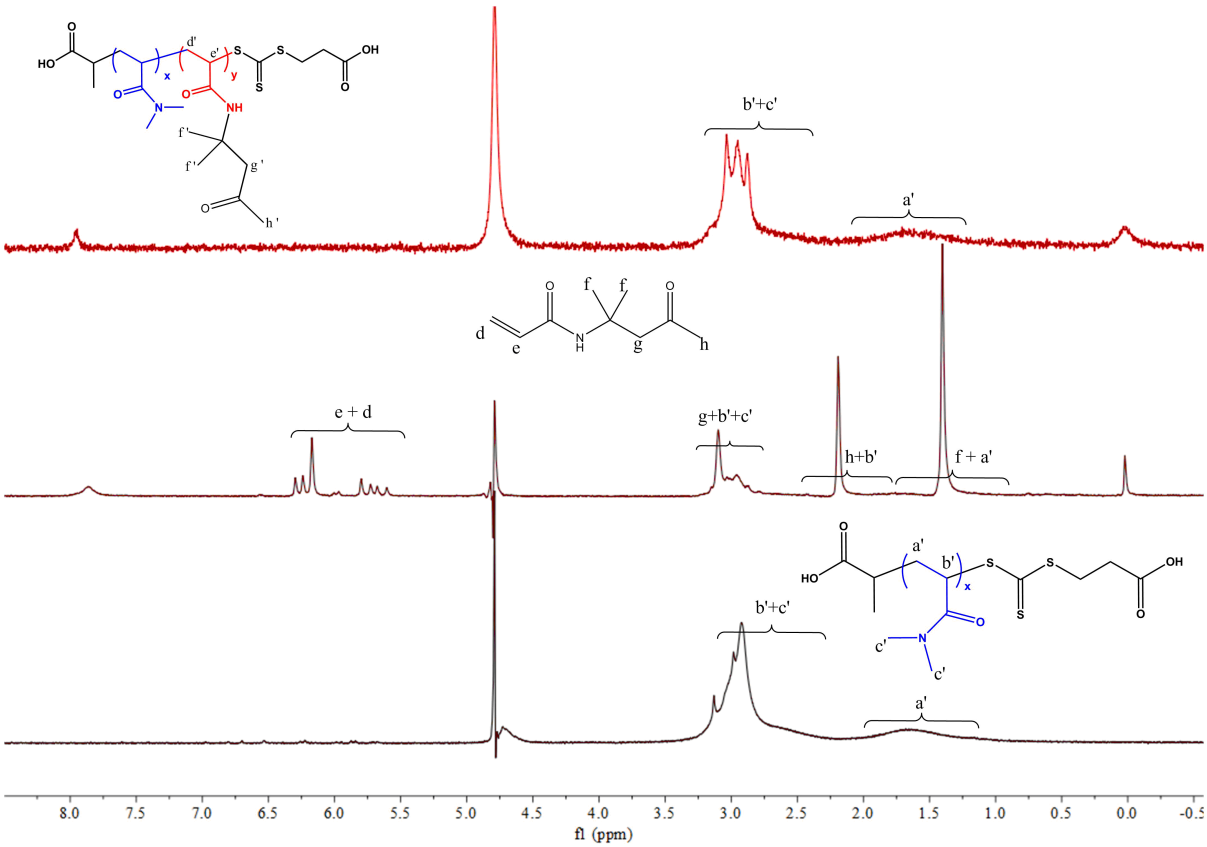

Figure 4.3: Online 60 MHz spectrometer ^{1}H NMR spectra recorded for the chain extension of PDMAm (bottom) with diacetone acrylamide (middle) to form PDMAm-PDAAm block copolymers (top).

From the obtained kinetic data an accelerated rate of polymerisation was observed with high conversions achieved within 8 minutes (Figure 4.4). For DP 50 and 100 the observed rate increase (approx. 5-fold) was slightly below the expected increase predicted by equation 1.16 whilst the rate increase for DP 200 (approx. 2-fold) was much lower than expected. Despite the accelerated kinetics, the high temporal resolution afforded by the flow-NMR clearly showed the characteristic rate enhancement of RAFT dispersion polymerisation at 70, 30 and 17 % conversion respectively during the onset of micellisation.[195] All profiles indicated this occured at a PDAAm DP of approximately 35 which corresponded to the DP indicated in section 3.3.3. The characteristic RAFT-PISA profiles along with similar critical DP lengths observed for multiple DPs indicated good control over the polymerisation was still maintained when using an increased radical flux to increase the polymerisation rate.

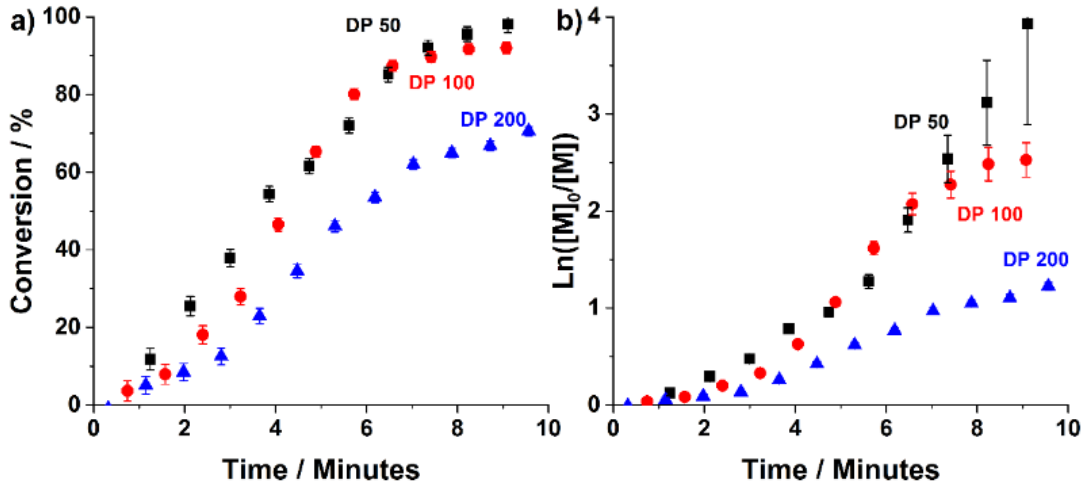

Figure 4.4: (a) Conversion vs. time and (b) semi-logarithmic rate plots for the RAFT aqueous dispersion polymerisation of diacetone acrylamide (DAAm) using a $PDMAm_{113}$ macroCTA in flow. All reactions were conducted at 90 °C with total solids concentration of 20 % w/w and [DAAm]:[$PDMAm_{113}$ macroCTA]:[VA-044] = 50/100/200:1:0.02.

A slower rate of polymerisation was observed with increasing DP, presumably due to initiator concentration decreasing as target DP increased, leading to a reduction in propagating radical concentration (Figure 4.5). For DP 100 and 200 a third region of rate deceleration is observed, and again this related to radical concentration in the reaction mixture. Whilst the magnitude of the decrease in radical flux would not usually alter the course of polymerisation (and indeed at short times showed a limited impact), the oxygen permeability of PFA tubing meant that there was a critical radical flux below which the reaction was affected, this was particularly relevant once a significant portion of the initiator had been consumed. Diffusion of oxygen into the reactor also affected the rate increase of the polymerisations.

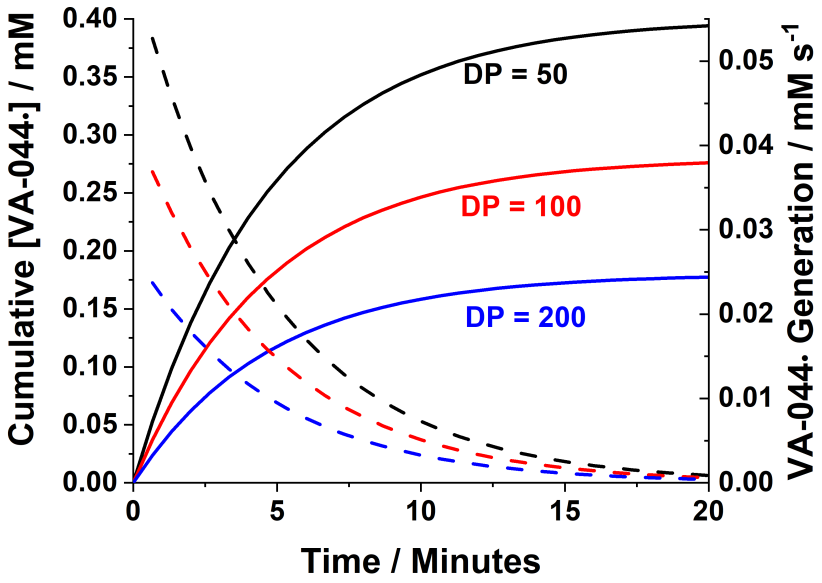

Figure 4.5: Cumulative (solid) and instantaneous (dash) radical concentration generated during the RAFT polymerisation of diacetone acrylamide using a $PDMAm_{113}$ macroCTA. All reactions were conducted at 90 °C with total solids concentration of 20 % w/w and [DAAm]:[$PDMAm_{113}$ macroCTA]:[VA-044] = 50/100/200:1:0.02.

4.3.2 Spherical Nanoparticle Synthesis via RAFT Aqueous Dispersion Polymerisation of Diacetone Acrylamide using a $PDMAm_{113}$ macro-CTA

After confirming that the kinetic profiles of the ultrafast polymerisations were typical of RAFT dispersion polymerisation, the formation of block copolymer nanoparticles under ultrafast conditions was then investigated. To determine whether increasing the rate of reaction affected polymer self-assembly, a series of $PDMAm_{113}$-$PDAAm_y$ diblock copolymers were synthesised. To ensure high monomer conversions were attained in all reactions, the residence time was set to 20 minutes, after which the product was collected at the reactor outlet and characterised by ^{1}H NMR spectroscopy, GPC, DLS and TEM. ^{1}H NMR studies indicated a high conversion (> 90 %) was achieved for target DPs of 50 and 100, however only 83 % conversion was achieved for $PDMAm_{113}$-$PDAAm_{200}$, which was attributed to lower radical concentrations. GPC chromatograms showed a systematic shift to higher M_n with narrow dispersities and good blocking efficiency for all polymers (Figure 4.6) further demonstrating the good RAFT control achieved despite accelerated reaction kinetics.

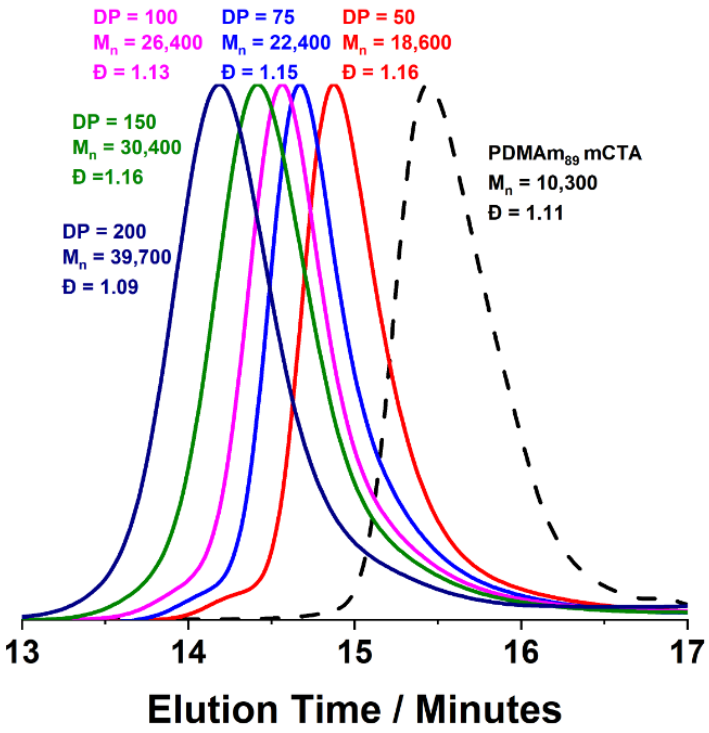

Figure 4.6: DMF GPC chromatograms for a series of $PDMAm_{113}$-$PDAAm_y$ polymer nano-objects synthesised in a flow tubular reactor where y = 50 to 200. Polymerisation was conducted at 90 °C , 20 % w/w solids and [$PDMAm_{113}$ macroCTA]:[VA-044] = 50:1. GPC data was calibrated against a series of ten near-monodisperse poly(methyl methacrylate) standards.

Analysing these polymers by DLS (Figure 4.7) showed that D_h (31, 38, 40, 45 and 52 nm respectively) increased with PDAAm DP, whilst low PDIs (< 0.05), indicating a near-monodisperse population of particles, were observed for all samples. All D_h values obtained are similar to those obtained for non-ultrafast RAFT-PISA polymerisations in chapter 3. This indicated that there was no effect on the PISA self-assembly process from increasing the rate of polymerisation. TEM images (Figure 4.8) confirmed spherical morphologies and particle sizes (25 nm, 29 nm, 35 nm, 42 nm, 47 nm respectively) increasing with PDAAm DP. Despite spherical particle morphologies being confirmed by TEM, during collection from the reactor outlet a cloudy liquid was obtained for DP 200, for all other chain lengths clear gels were extruded. This gelling of spherical dispersion in PISA systems has previously been explained by colloidal interactions between the nano-sized particles.[224]

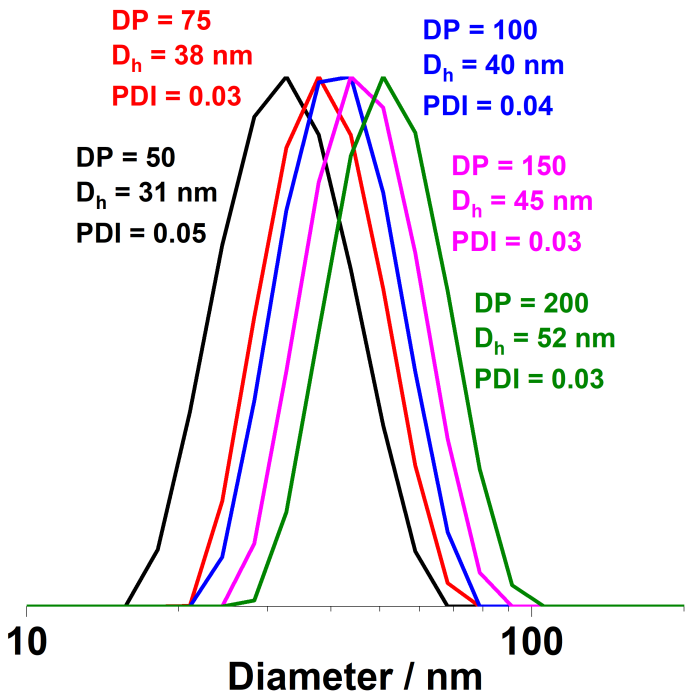

Figure 4.7: DLS size distributions obtained for a series of $PDMAm_{113}$-$PDAAm_y$ polymer nano-objects synthesised in a flow tubular reactor where y = 50 to 200. Target DPs are stated for each polymerisation. All reactions were conducted at 90 °C with total solids concentration of 20 % w/w and [$PDMAm_{113}$ macroCTA]:[VA-044] = 1:0.02.

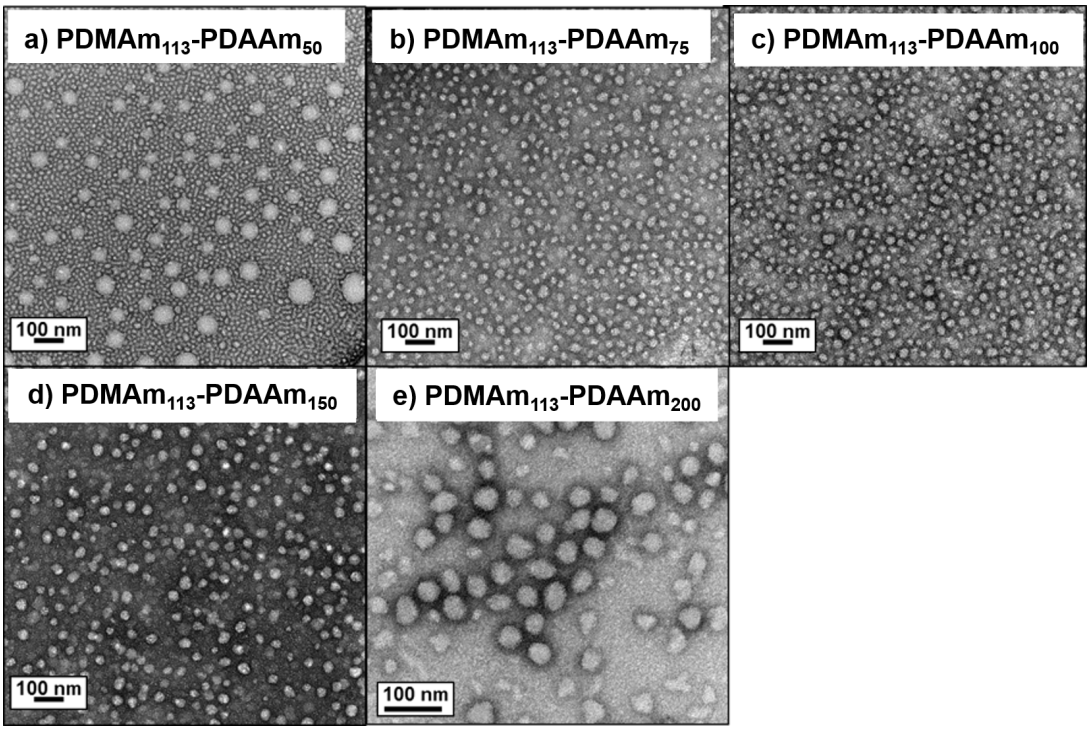

Figure 4.8: Transmission electron microscopy images for $PDMAm_{113}$-$PDAAm_y$ block copolymers where y = a) 50 b) 75 c) 100 d) 150 e) 200. All images were obtained using 0.1 % w/w of diblock copolymer at pH 3.

4.3.3 High Order Morphology Nanoparticle Synthesis via RAFT Aqueous Dispersion Polymerisation of Diacetone Acrylamide using a $PDMAm_{46}$ macro CTA

As with section 3.3.3, in order to synthesis higher order morphologies the DP of the PDMAm macro-CTA was reduced ($PDMAm_{46}$) and a series of polymers were synthesised. High conversions (> 90 %) were reached in 20 minutes for all polymers synthesised up to a PDAAm DP of 100 after which the conversion began to decrease significantly down to 79 % for a target PDAAm DP of 200, analogous to earlier observations with the $PDMAm_{113}$ macro-CTA. For all polymers synthesised, a systematic shift to higher M_n was observed with low dispersities and good blocking efficiency (Figure 4.9).

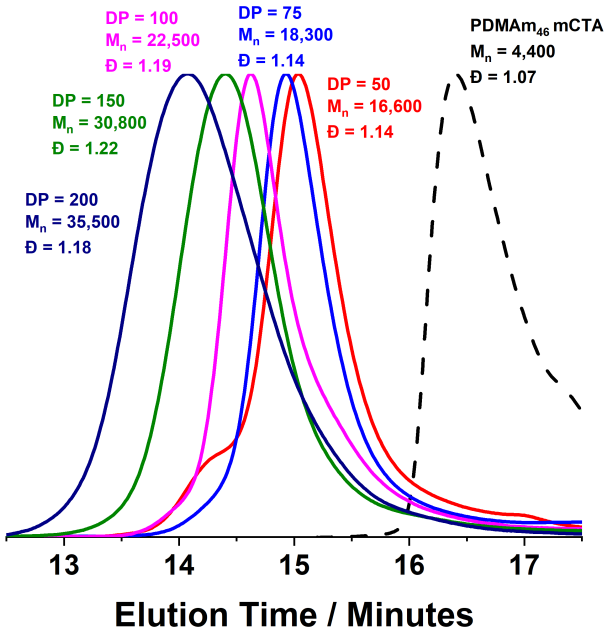

Figure 4.9: DMF GPC chromatograms for a series of $PDMAm_{113}$-$PDAAm_y$ polymer nano-objects synthesised in a flow tubular reactor where y = 50 to 200. All reactions were conducted at 90 °C at 20 % w/w solids and [$PDMAm_{113}$ macroCTA]:[VA-044] = 50:1.

DLS analysis of these polymers (Figure 4.10) showed an increase in D_h and PDI with increasing DAAm DP. Whilst DLS analysis assumes spherical morphologies, rendering obtained D_h values irrelevant, the increased PDI of samples likely indicated the presence of different morphologies[225] although, TEM imaging was required for final morphological classification. Additionally, DLS analysis of target PDAAm DPs of 150 and 200 polymers was only possible by filtering the samples due to the presence of large aggregates.

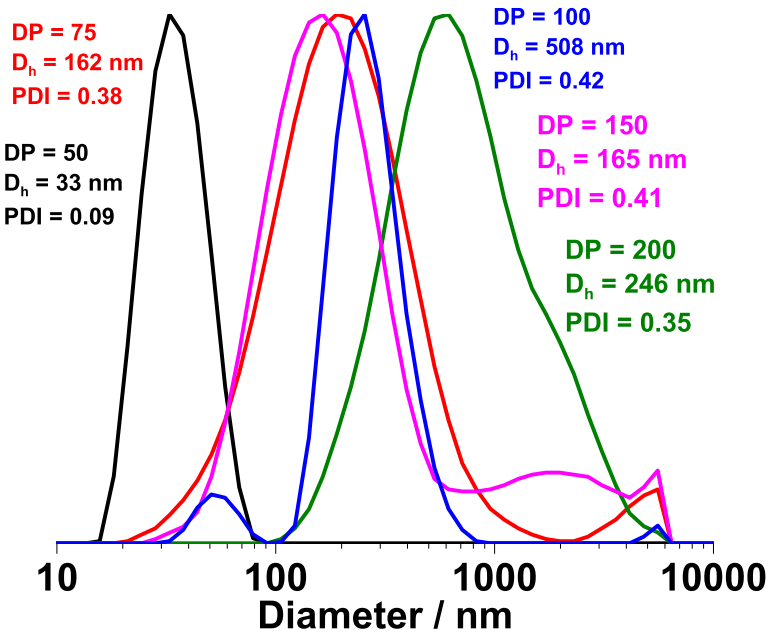

Figure 4.10: DLS size distributions obtained for a series of $PDMAm_{113}$-$PDAAm_y$ polymer nano-objects synthesised in a flow tubular reactor where y = 50 to 200. Nano-objects formed are likely to be non-spherical and therefore the D_h stated is not representative of the true size. All reactions were conducted at 90 °C with total solids concentration of 20 % w/w and [$PDMAm_{46}$ macroCTA]:[VA-044] = 1:0.02.

TEM images indicated a pure sphere phase (∼ 30 nm) at DP 50, a majority worm phase (∼ 300 nm) at DP 75 and a mixed worm-vesicle phase (∼ 500 nm vesicles) at DP 100 (Figure 4.11). This was in agreement with the reported phase diagram for this system which predicted the phases observed.[209] Yet for DP 150 and 200, predicted to be pure vesicle phases, mixed phases consisting of worms, vesicles and lamella were observed. The polymers synthesised have low dispersities and the anticipated M_n indicating good control over the polymerisation. However, the inability to synthesise a pure vesicle phase and the formation of aggregates indicated a loss of control during the polymer self-assembly.

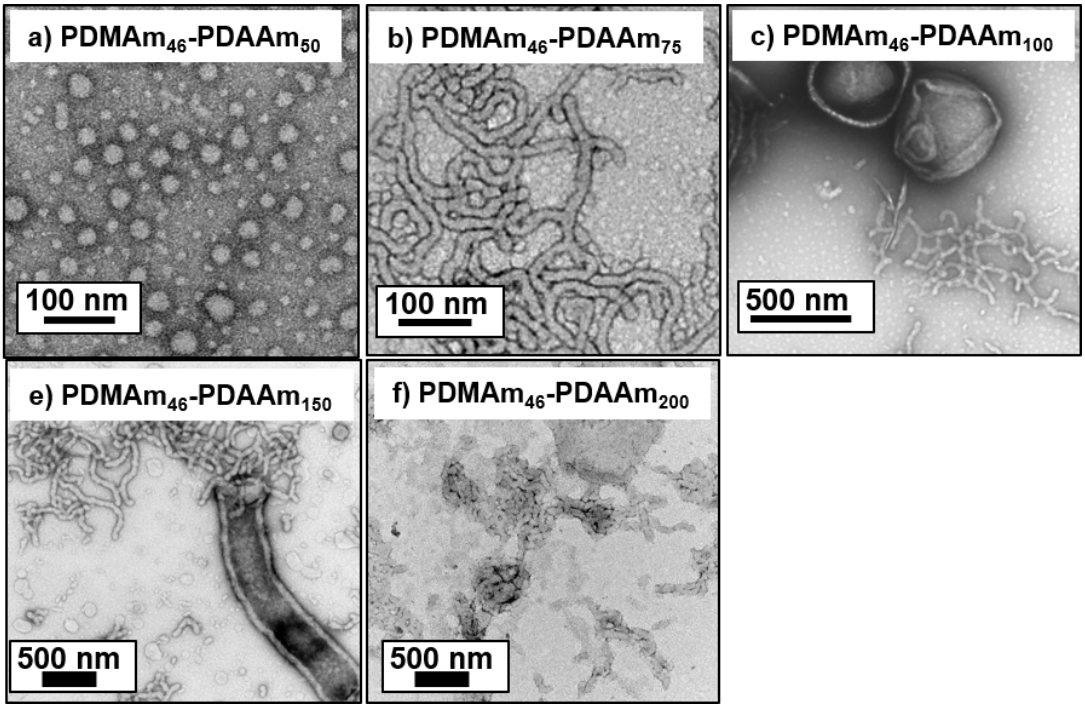

Figure 4.11: Transmission electron microscopy images for a series of $PDMAm_{46}$-$PDAAm_y$ polymer nano-objects synthesised in a flow tubular reactor where y = a) 50 b) 75 c) 100 d) 150 e) 200. All images were obtained using 0.1 % w/w of diblock copolymer at pH 3.

4.3.4 Optimisation of Vesicle Synthesis

4.3.4.1 Reaction Temperature

To determine the cause of the loss of control over the polymer self-assembly, a series of control experiments were performed. First, to determine whether conducting the polymerisation in a flow reactor was the cause, the synthesis was performed in batch under the same conditions (i.e. 90 °C). During this synthesis, phase separation occurred; where aggregates of polymer precipitated from solution (Figure 4.12). Given the volume of material in any given area of the flow reactor was very low, the appearance of precipitate differed from batch, with no large aggregates observed – though phase separation was observed along the tubing in flow and the polymer aggregates formed were smaller. Temperature responsive behaviour has been reported previously for PDMAm-PDAAm block copolymer systems, generally involving transitions between worm and lamella phases from 20 - 70 °C.[208] Therefore, the reaction temperature was reduced to 70 °C to attempt to eliminate any unwanted temperature responsive behaviour. The resulting reaction solution was a homogeneous white liquid, which was expected for a vesicular dispersion.

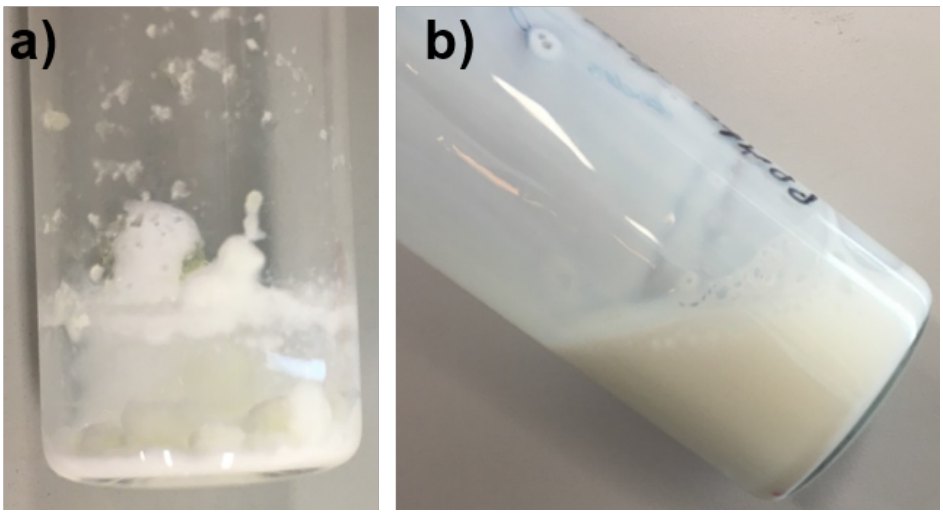

Figure 4.12: $PDMAm_{46}$-$PDAAm_{500}$ vesicle batch synthesis using RAFT-PISA at a) 90 °C and b) 70 °C after 20 minutes. Polymer vesicles appear to aggregate and phase separate when the polymerisation is performed at 90 °C. polymerisations were performed at 20 % w/w solids with [$PDMAm_{46}$ macroCTA]:[VA-044] = 50:1.

4.3.4.2 Initiator Concentration

After confirming no precipitation occurred at lower temperature, the synthesis was then repeated in flow at a lower temperature (70 °C). However, the sample collected at the reactor outlet was completely clear suggesting that no polymerisation had occurred (Figure 4.13a). GPC analysis (Figure 4.13b) showed a decrease in M_n, potentially caused by polymer degradation, confirming no polymerisation occurred.

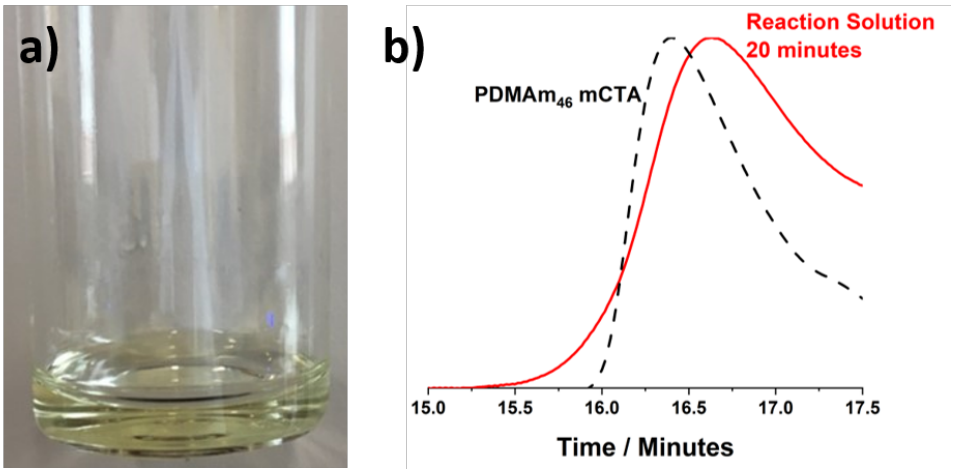

Figure 4.13: a) Photograph of product collected at outlet of flow reactor. Transparent sample indicates no polymerisation has occured. b) GPC chromatogram for the polymerisation of $PDMAm_{46}$-$PDAAm_{200}$ performed in the flow reactor in the continuous reactor platform indicating no polymerisation has taken place. Polymerisations were conducted at 70 °C using RAFT aqueous dispersion polymerisation at 20 % w/w solids and [$PDMAm_{46}$ macroCTA]:[VA-044] = 50:1.

PFA was chosen as the reactor material as it was reported to be suitable for the fouling free synthesis of block copolymer nano-objects. However, there are conflicting reports on the suitability of this material for performing RAFT polymerisations. In contrast to Junkers and co-workers findings,[167] Hornung *et al.* reported the inability to perform RAFT polymerisation in PFA tubing even though polymerisation occurred when performed in stainless steel tubing and batch reactors.[154] PFA is a widely used material in industry due to its high chemical tolerance, low friction surface and good mechanical properties. Yet, as with other types of polymer tubing, PFA allows oxygen to permeate through its walls.[184] This permeating oxygen will quench the radical species formed during RAFT polymerisation. Although a difference between this work and Hornung's reported use of PFA tubing, is that initially successfully polymerisations were performed when the reactor was at 90 °C. The reactor was set at high temperature in order to increase the radical flux in the system and thus accelerate the reaction rate. A high radical flux will lead to fast consumption of dissolved oxygen and as long as a sufficient concentration of radicals remain once all the oxygen is consumed, polymerisation will occur.[226] Oxygen tolerance via an increased radical flux has been well reported for many polymerisations.[227] Conversely, as the temperature of the reactor is reduced, in order to form successfully form vesicle morphologies, the radical flux is also reduced (Figure 4.14). This reduces below the level required to remove oxygen as well as initiate polymerisation, since oxygen will readily react with carbon-centered radicals to form peroxy-centered radicals, which do not participate in the polymerisation process.[228] As the rate of peroxy radical formations is reported to be much faster than propagation,[229] the concentration of oxygen must be reduced for polymerisation to occur. Initiator concentration and therefore radical flux was increased in order to reduce the concentration of oxygen in the system. A VA-044 concentration of 10:1 (0.25 mM) was used for all further experiments performed at 70 °C to enable successful polymerisation.

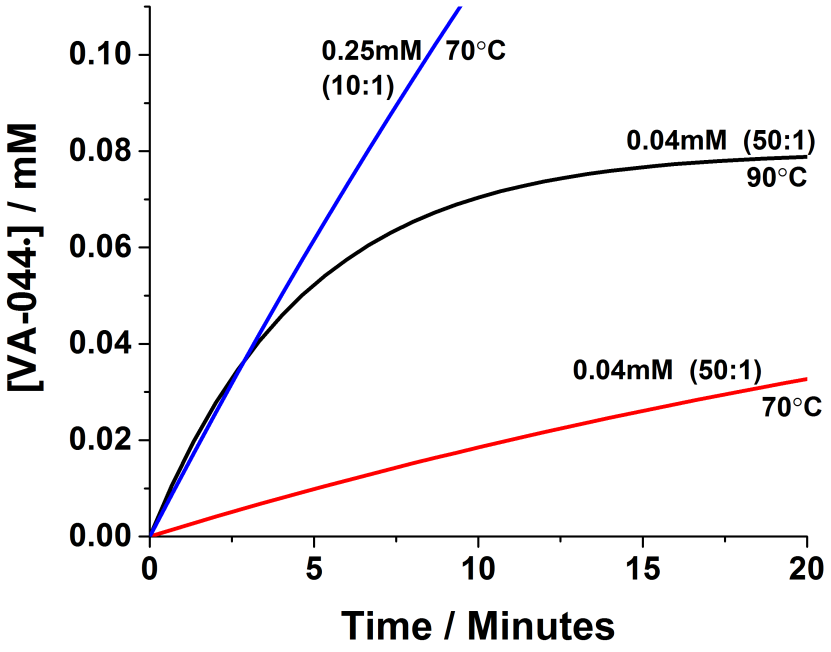

Figure 4.14: Calculated temperature dependence on VA-044 initiator radical generation at various concentrations. Performing polymerisations at different temperatures has a pronounced effect on the radical concentration. Using the flow platform, due to the oxygen permeability of the reactor material (PFA), synthesising $PDMAm_{46}$-$PDAAm_{500}$ at 70 °C with [$PDMAm_{46}$ macroCTA]:[VA-044] = 50:1 is not possible as the radical flux (red) is insufficient to quench oxygen. Whilst performing the reaction at higher temperature (black) or higher $[VA\text{-}044]_0$ (blue) allows for a successful polymerisation.

4.3.4.3 Optimised Vesicle Synthesis

Using a VA-044 concentration of 0.25 mM, a series of polymers were synthesised at 70 °C, with target DPs corresponding to a pure vesicle phase.[209] High conversions were obtained for all polymers in 20 minutes (> 90 %) until high target DPs (> 500). GPC chromatograms showed a shift to higher M_n (Figure 4.15) with good blocking efficiency for all polymers. Molar mass dispersity initially increased up to 1.36 (at DP 200), but then decreased to 1.17 (at DP 600). At a target DP of 1000, a much higher molar mass dispersity indicated a loss of RAFT control.

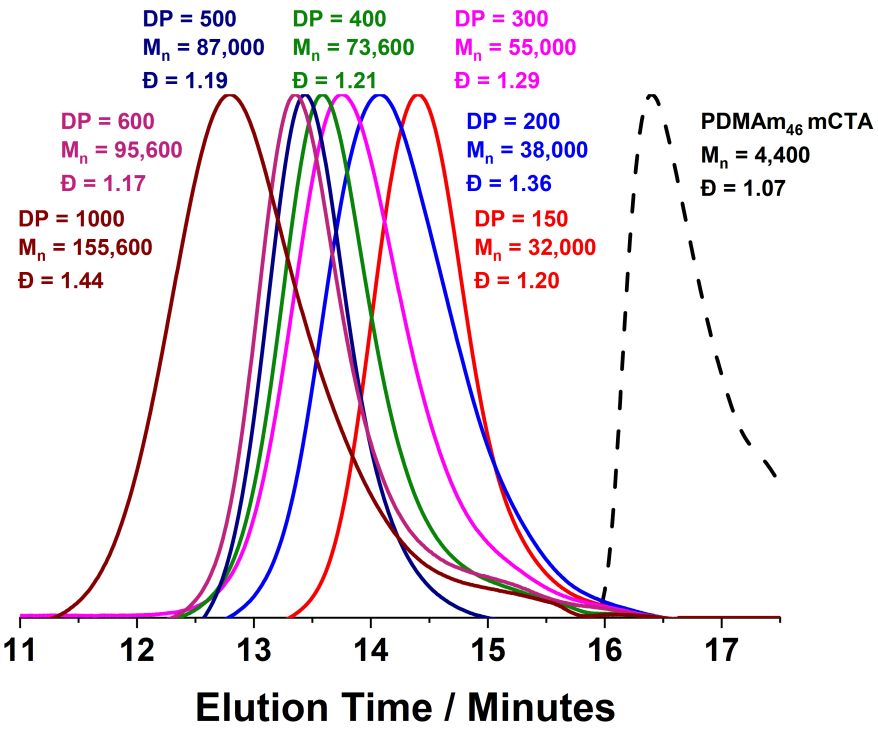

Figure 4.15: DMF GPC chromatograms for a series of $PDMAm_{46}$-$PDAAm_y$ polymer nano-objects synthesised in a flow tubular reactor where y = 150 to 1000. Polymerisation was conducted at 70 °C using RAFT aqueous dispersion polymerisation at 20 % w/w solids and [VA-044] = 0.25mM.

DLS analyses of these polymers once again showed unexpected behaviour for DP 150 and 200, yet as DP increased > 400 nm particles were observed with PDI typical for similarly reported vesicle systems (Figure 4.16).[209] Again, the target DP 1000 sample produced larger particles according to DLS, which is similar to observations for traditional (slower) PISA systems.[197,230] TEM images were obtained to confirm particle morphologies (Figure 4.17). Similarly to the experiments at 90 °C, target DP 150 and 200 polymers only contained large aggregates. However, pure vesicle phases (300 nm, 342 nm, 307 nm , 355 nm and 570 nm respectively) were observed for all other target DPs. The mechanisms through which block copolymers self-assemble offered some explanation for the observed aggregate formation between DP 150 - 200. It is well reported that evolution from spherical morphologies to worm/vesicle morphologies is driven by a reduction in the surface curvature,[231] which occurs during PISA as the hydrophobic chain grows.[195] However, as the hydrophobic chain increases in length it becomes more dehydrated and the mobility of the chain is reduced[15] and this limited mobility can inhibit morphological evolution.

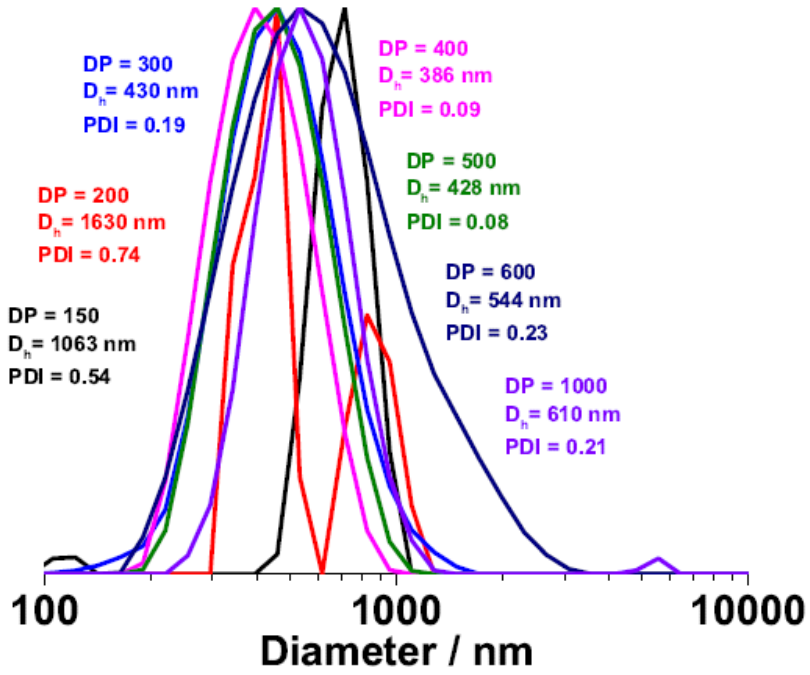

Figure 4.16: DLS size distributions obtained for a series of PDMAm$_{46}$-PDAAm$_y$ polymer nano-objects synthesised in a flow tubular reactor where y = 150 to 1000. All reactions were conducted at 70 °C with total solids concentration of 20 % w/w and [VA-044] = 0.25 mM.

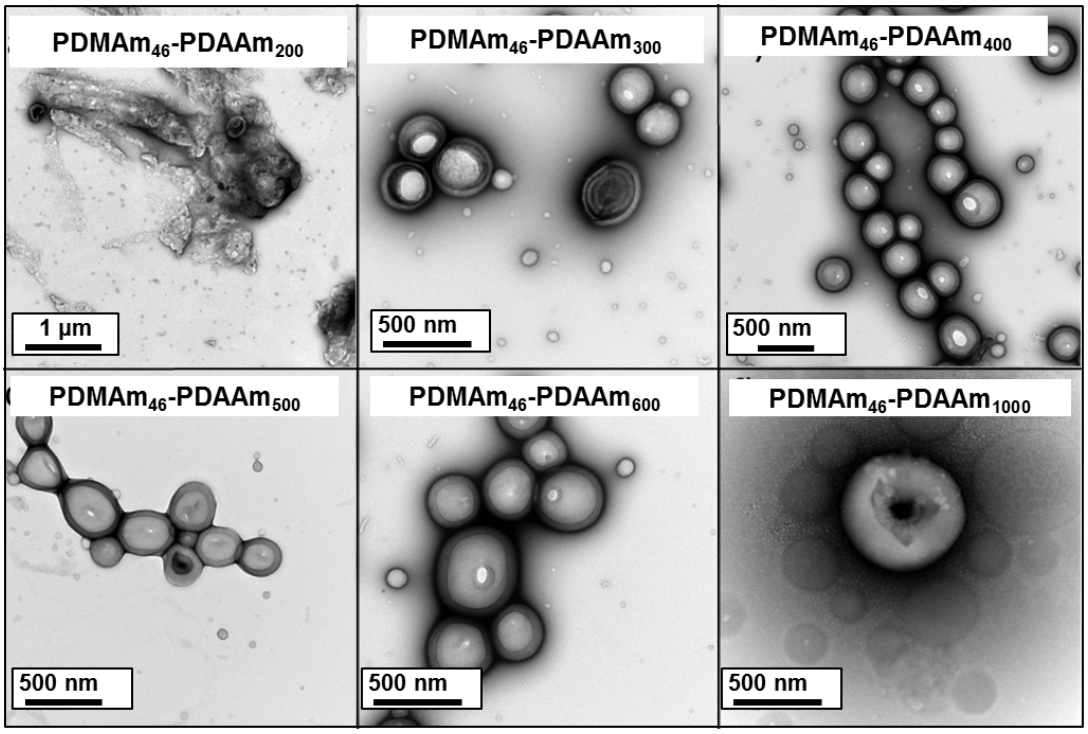

Figure 4.17: Transmission electron microscopy images for a series of PDMAm$_{46}$-PDAAm$_y$ polymer nano-objects synthesised in a flow tubular reactor where y = a) 200, b) 300, c) 400, d) 500, e) 600 and f) 1000. All images were obtained using 0.1 % w/w of diblock copolymer at pH 3.

This can be mitigated by adding a co-solvent;[15] in typical PISA systems, un-reacted monomer

acts as a co-solvent facilitating morphological change. Poor hydrophobic chain solvation was likely a factor in the aggregate formation occurring for the target DP 200 system. However as the target DP of the hydrophobic chain increased, as the polymerisation reaches the worm-vesicle phase transition the concentration of un-reacted monomer also increased and vesicle morphologies were formed. Hence, it was concluded that poor hydrophobic solvation contributed to aggregate formation in the system. However, aggregate formation for this block copolymer composition was not reported in batch. Therefore, there must have been another factor contributing to aggregate formation in the system.

4.3.4.4 Determination of Polymer Fouling

Trends in $PDMAm_{46}$-$PDAAm_y$ molar mass evolution (Figure 4.18) offered insight into further causes of polymer aggregation in the system. As PDAAm block length increased, a linear increase in molecular weight was observed, indicating good RAFT polymerisation control. However, the expected decrease in dispersity with increasing DP was not present in the system – instead a local maximum in dispersity was observed at DP = 200. This initial increase in dispersity was uncharacteristic of the RAFT process and may have been caused by poor mixing as a result of an increase in viscosity. As discussed above, a viscous worm like phase was expected to exist at DP 200 which will have led to a reduction in diffusive mixing,[232] which tubular reactors are reliant upon. Furthermore, poor mixing is known to cause increased dispersity in flow reactors.[233] Hence, the initial increase in dispersity was attributed to poor mixing in the flow reactor and the subsequent decrease to improved mixing due to a reduction in viscosity following the transition of polymeric worms to vesicles.

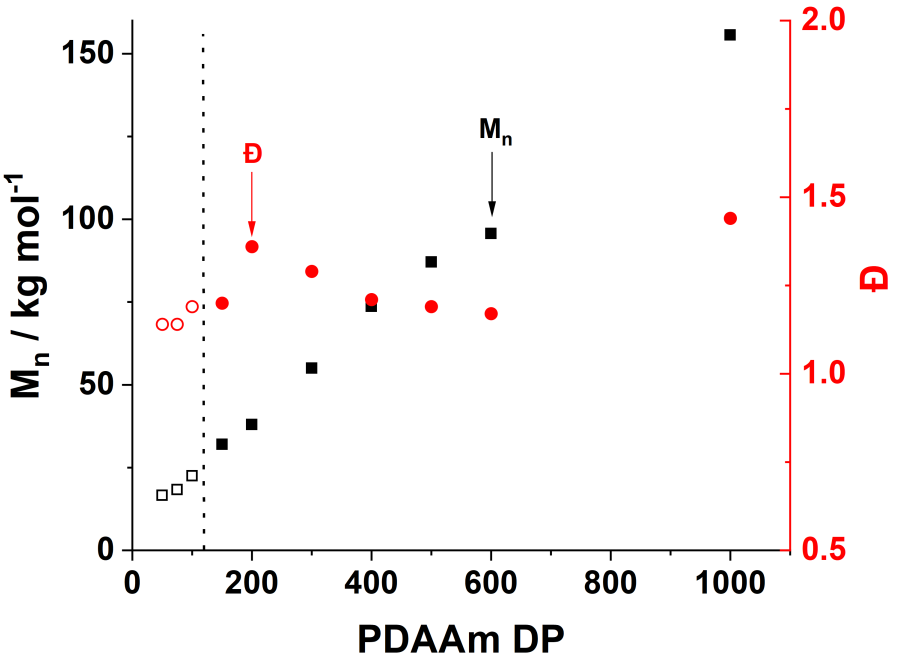

Figure 4.18: Evolution of molar mass and dispersity of $PDMAm_{46}$-$PDAAm_y$ polymers synthesised on the flow platform with respect to increasing PDAAm DP. All polymerisation has a retention time of 20 minutes and were performed at 70 °C (filled) or 90 °C (hollow). Reaction solution were made at 20 % w/w solids and adjusted to pH 3.

Poor mixing, due to increased viscosity, was also likely to be a factor in aggregate formation observed in the flow reactors. The flow reactor relied on diffusive mixing whereas, batch reactors were continuously mixed through agitation by a stirrer. This continuous agitation in batch provided additional kinetic energy which helped the system overcome the barrier for the worm-vesicle transition caused by poor hydrophobic core mobility. Due to this lack of additional energy in the flow reactor the polymeric nanoparticles may have gotten trapped in one of the worm-gel transition phases when there was insufficient monomer to solubilise the hydrophobic block. Aggregation must have then occurred as an alternative pathway to minimise the energy of the system. To confirm the importance of mixing, the synthesis of $PDMAm_{46}$-$PDAAm_{200}$ was repeated in batch with both diffusive (no stirring) and continuous (stirring) mixing. Upon dilution for DLS analysis aggregates were observed for the diffusively mixed sample whereas, no aggregates were observed for the stirred sample (Figure 4.19).

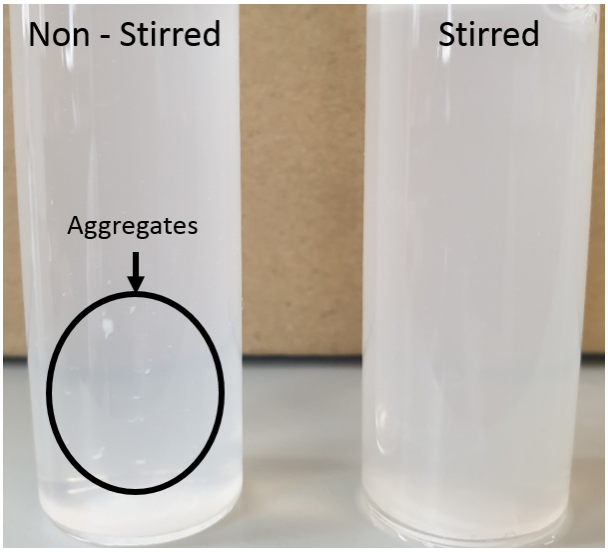

Figure 4.19: Diluted samples from the batch polymerisations of $PDMAm_{46}$-$PDAAm_{200}$ with or without stirring. Aggregates were found to be present in the non-stirred sample. Polymerisations were conducted at 70 °C, 20 % w/w solids and [DAAm]:[$PDMAm_{46}$ macroCTA]:[VA-044] = 200:1:0.02.

GPC analysis (Figure 4.20a) indicated very similar polymers were produced regardless of diffusive or continuous mixing methods. However, DLS analysis (Figure 4.20b) shows a significant disparity in D_h was observed: the non-stirred polymerisation (550 nm) was nearly double that of the stirred polymerisation (350 nm). As a result, it can be concluded that under flow conditions both inadequate mixing in the reactor and poor hydrophobic core mobility contribute to aggregate formation when synthesizing block copolymers with compositions near the worm-vesicle phase boundary.

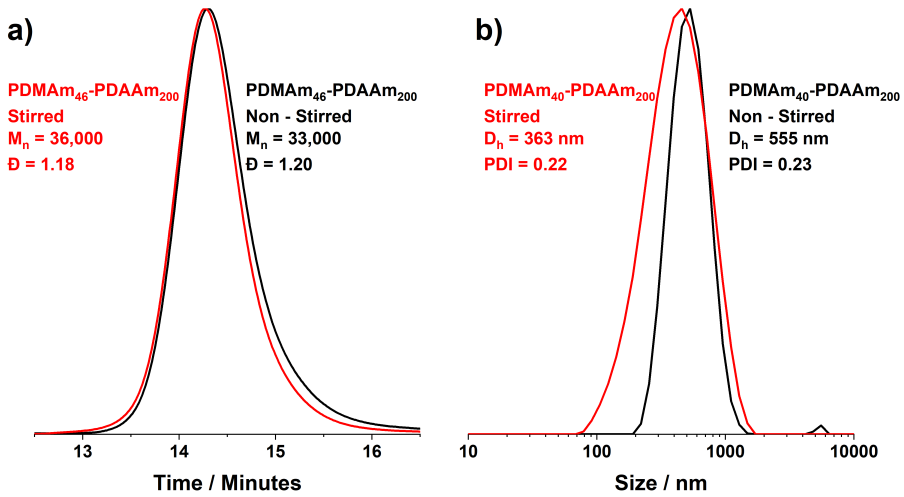

Figure 4.20: a) GPC chromatograms and b) DLS size distributions obtained for the batch polymerisations of $PDMAm_{46}$-$PDAAm_{200}$ with or without stirring. Polymerisations were conducted at 70 °C, 20 % w/w solids and [DAAm]:[$PDMAm_{46}$ macroCTA]:[VA-044] = 200:1:0.02.

4.4 Conclusions

In this chapter, an ultrafast synthesis method was applied to both RAFT aqueous solution and RAFT aqueous dispersion polymerisations. Kinetic profiles for these reactions were obtained using the previously developed transient profiling method alongside an in-line NMR spectrometer, which allowed for increased temporal resolution of the profile. The rate of polymerisation for the synthesis of a PDMAm macro-CTA and its subsequent chain extension with DAAm, to form $PDMAm_x$-$PDAAm_y$ nano-objects, was significantly increased when using VA-044 at 90 °C. High conversions were achieved within minutes for low DPs. Kinetic profiles obtained for RAFT aqueous dispersion polymerisations were characteristic of RAFT-PISA polymerisations and a DP of approximately 35 was determined to be the critical chain length for self-assembly. A series of well-defined $PDMAm_x$-$PDAAm_y$ block copolymers were synthesised with high conversions (> 90 %) in 20 minutes using the flow platform. These polymers underwent PISA to form spherical, worm and mixed phase nano-objects, as determined by DLS and TEM, depending on their composition. However, it was not possible to produce pure vesicle phases under these reaction conditions, this was attributed to a temperature responsive behaviour upon formation of the vesicle phase. Lowering reaction temperature of the flow reactor for vesicle synthesis caused an inhibition of the polymerisation, which was attributed to the reduced radical flux not being able to quench oxygen permeating the system through the PFA reactor walls. By simply increasing the concentration of VA-044, polymerisations were successfully performed at 70 °C and formed pure vesicle phases in under 20 minutes with no detrimental effect on molar mass dispersity. Yet, loss of control over particle formation and aggregate formation was still observed for polymer compositions around the reported worm-vesicle phase boundary. Through observation of molecular weight trends, aggregate formation was attributed to a complex amalgam of both the PISA mechanism and mixing in the flow reactor system. Overall these results indicated the ability to perform ultrafast RAFT polymerisations for the synthesis of block copolymer nanoparticles in flow. However, poor mixing in tubular reactors leading to the presence of polymer aggregates when targeting certain block copolymer compositions is likely to be of concern for commercial implementation of the flow system and further investigation into reactor design is needed.

Chapter 5

Optimisation of RAFT Polymerisations using an Automated Flow Reactor Platform

5.1 Introduction

The automation of chemical reactions will offer a great deal of opportunities for the research and development of chemical syntheses and production. Increased uptake in reactor automation will allow for a paradigm shift in the way in which chemists operate. Instead of allocating resources to manual lab work, chemists will be able to focus on higher level tasks. Flow chemistry is a key technology in the development of automated chemical reactors, largely down to its reproducibility, increased control over reaction variables and scalability.[4] To truly benefit from the automation of flow platforms, the incorporation of online analytical techniques is necessary. Online analytical techniques allow for facile and rapid acquisition of reaction data compared to offline methods. Recent advances in online monitoring have allowed for some of the most powerful analytical techniques available to chemists such as IR,[234] UV-Vis spectroscopy,[235] NMR spectroscopy,[236] HPLC,[181] mass spectrometry,[237] and GPC[238] to be incorporated into flow platforms. Furthermore, incorporation of machine learning algorithms into these automated platforms allowed them to become more autonomous and capable of performing self-optimisations with minimal user input. Small molecule synthesis has seen large interest in the use of autonomous flow reactors, with a wide range of reactions having been

self-optimised.[7,10,11,239–242] However, the development of online monitoring platforms for polymerisations were initially limited to batch systems.[186,243–245] Nevertheless, more flow platforms that incorporate online monitoring techniques have been recently developed.[6,170,246] This increasing number of automated flow platforms is a positive step towards fully automating polymer synthesis and development, although the integration of optimisation algorithms into these automated systems has been limited. However, the uptake of autonomous flow platforms for polymer synthesis is relatively low compared to small molecule synthesis.[30,31] The quality of synthetic polymers can vary drastically if there any small deviations in reactant ratios, impurities and temperature. This is due to the complex kinetics of chain growth, fast reaction rates of individual processes and the exotherms generated during chain-growth. Therefore, batch to batch reproducibility can be limited. Although more advanced precision polymerisation techniques, such as RAFT, have been developed, the reproducibility in batch can still often vary. Hence, enhanced precision and reproducibilty afforded by flow offers significant benefits.[109] To date there have been few reports of an autonomous flow platform capable of optimising polymerisation conditions.[30,31] In this chapter, a fully automated flow reactor platform (Reactor D from chapter 2) was used to screen reaction conditions of the RAFT polymerisation of dimethylacrylamide (DMAm). Furthermore, by incorporating an advanced machine learning algorithm in the platform it evolved into an autonomous system capable of performing a multi-objective self-optimisation of the RAFT polymerisation of DMAm. The autonomous system was then employed to screen and self-optimise the RAFT polymerisation of *tert*-butylacrylamide (tBuAm).

5.2 Experimental

5.2.1 Materials

2,2'-Azobis[2-(2-imidazolin-2-yl)propane]dihydrochloride (VA-044, 99 %) was purchased from Wako Chemicals (US). 4,4 -Azobis(4-cyanovaleric acid) (ACVA, 99 %), 2,2 -azobis(2-methylpropionitrile) (AIBN, 98 %), dimethylacrylamide (DMAm, 99 %), *tert*-butylacrylamide (tBuAm, 97 %), lithium bromide (LiBr, 99 %) and triethylamine (TEA, 99 %) were purchased from Sigma Aldrich (UK). 3-((((1-Carboxyethyl)thio)carbonothioyl)thio) propanoic acid (CTTP, 90 %) and 4-((((2-carboxyethyl)thio)carbonothioyl)thio)-4-cyanopentanoic acid (DCTTC, 95 %) was purchased from Boron Molecular (Raleigh, USA). 2-(((methylthio) carbonothioyl)thio)phenyl acetic

acid (CPMT, ∼90%) was synthesised by Thomas Howell using a previously reported literature method.[12] HPLC grade dimethylformamide (DMF) and tetrahydrofuran (THF) were purchased from Fisher Scientific (Loughborough, UK).

5.2.2 Methods

5.2.2.1 On-line ^{1}H NMR spectra

^{1}H NMR spectra were obtained using a Magritek Spinsolve Ultra 60 MHz NMR spectrometer. NMR spectra were collected as the reaction solution passed directly from the reactor outlet into a 1/8" PFA flow cell placed inside the NMR spectrometer. A PRESAT method was used to suppress solvent signals at 3.3 ppm for methanol or 4.79 ppm for water (1 s saturation pulse of -65 dB, 7 µs excitation pulse, acquisition time of 6.4 s, repetition time of 10 s & number of scans was 2). All chemical shifts are reported in ppm (δ). For the RAFT polymerisation of dimethylacrylamide conversion was determined by Equation 5.1:

$$Conversion = 1 - \frac{2x}{y - \frac{z}{2}} \tag{5.1}$$

where x is the vinyl peak region between 5.6 and 7.0 ppm, y is the overlapping monomer and polymer region between 3.3 to 2.18 ppm and z is the polymer backbone region between 2.18 to 0.0 ppm. For the RAFT polymerisation of *tert*-butylacrylamide conversion was determined by Equation 5.2:

$$Conversion = 1 - \frac{6x}{y + 1.5x} \tag{5.2}$$

where x is the vinyl peak region between 5.8 and 6.4 ppm, y is the overlapping monomer and polymer region between 2.3 to 0.0 ppm.

5.2.2.2 On-line Gel permeation chromatography

On-line gel permeation chromatography measurements were conducted using a custom built instrument comprised of a Jasco PU-980 HPLC pump, a single Agilent Rapide M column plus a guard column and a Knauer 2301 refractive index (RI) detector. For analysis of DMAm polymers, DMF containing 1.0 % w/v lithium bromide (LiBr) was used as eluent. The pump flow rate was set to 3.0 mL min^{-1} and the all equipment was kept at room temperature. A series of near-monodisperse poly(methyl methacrylate) standards (M_p ranging from 1,000 to

265,000 g mol^{-1}) were employed as calibration standards in conjunction with an RI detector for determining molecular weights and molar mass dispersities (Đ).

For analysis of tBuAm polymers, THF containing 1.0 % w/v triethylamine (TEA) and 0.05 % ww/w butylated hydroxytoluene (BHT) was used as eluent. The pump flow rate was set to 2.0 mL min^{-1} and the all equipment was kept at room temperature. A series of near-monodisperse poly(methyl methacrylate) standards (M_p ranging from 1000 to 265,000 g mol^{-1}) were employed as calibration standards in conjunction with an RI detector for determining molecular weights and molar mass dispersities (Đ).

5.2.2.3 Off-line Gel permeation chromatography

Off-line gel permeation chromatography measurements were conducted using an Agilent 1260 Infinity system fitted with two 5 µm Mixed-C columns plus a guard column, a refractive index (RI) detector and a UV-Vis detector operating at 309 nm. DMF containing 1.0 % w/v lithium bromide (LiBr) was used as eluent. The pump flow rate was 1.0 mL min^{-1} and the temperature of the column oven and RI detector were 60 °C. A series of near-monodisperse poly(methyl methacrylate) standards (M_p ranging from 800 to 2,200,000 g mol^{-1}) were employed as calibration standards in conjunction with an RI detector for determining molecular weights and molar mass dispersities (Đ).

5.2.2.4 High resolution Transient Data Collection

For a target composition of $PDMAm_{100}$: dimethylacrylamide (5 g, 100 eq.), CCTP (0.12 g, 1 eq.) and VA-044 (0.01 g, 0.1 eq.) were added to a round bottom flask and dissolved in water (12 mL) to give a 30 % w/w reaction solution. The flask was, sealed, sparged with nitrogen for 20 minutes. The solution was passed through a 2 mL tubular stainless-steel reactor at a flow rate 10 mL min^{-1} for 90 seconds, the flow rate was then reduced to 0.08 mL min^{-1} giving a retention time of 60 minutes. Online ^{1}H NMR spectra were collected every 20 seconds and GPC samples were taken and measured at-line every 180 seconds.

5.2.2.5 Steady State Data Collection

For a target composition of $PDMAm_{100}$: dimethylacrylamide (20 g, 100 eq.), CCTP (0.5 g, 1 eq.) and VA-044 (0.05 g, 0.1 eq.) were weighed into to a round bottom flask and dissolved in water (48 mL) to give a 30 % w/w reaction solution. The flask was, sealed, and sparged with

nitrogen for 30 minutes. The solution was then pumped through a 2 mL stainless steel coil at the appropriate flow rate. For each flow rate the reactor reached steady state by passing through 3 reactor volumes (6 mL) of reaction solution. Online ^{1}H NMR spectra and GPC measurements were taken online after the reactor had achieved steady state.

5.3 Results and Discussion

5.3.1 Automated Transient Kinetics

An algorithm was developed in order to allow for the automation of the transient kinetic profiling methods stated in chapter 2 (see appendix). The polymerisation of dimethylacrylamide using ACVA performed in chapter 3 was repeated three times using the automated flow platform. Automating this process significantly reduced the manual work required compared to previous the transient kinetics profiling. However, the kinetic profiles (Figure 5.1) obtained displayed irregular regions at 10, 30 and 40 minutes, which deviated from first order kinetic behaviour observed for this polymerisation in chapter 3. NMR spectra were obtained using a standard pulse sequence, described in chapter 2, as such the water peak was clearly observed. In the regions of irregular conversion at 10, 30 and 40 minutes, a splitting of the water peak was observed (Figure 5.2), which likely caused phase issues near the vinyl peak region skewing conversion. One possible cause for solvent peak splitting was sample inhomogeneity, as the polymer chains grew, due to poor mixing in the flow cell. This was similar to the altered kinetics seen in chapter 2 when using a glass flow cell.

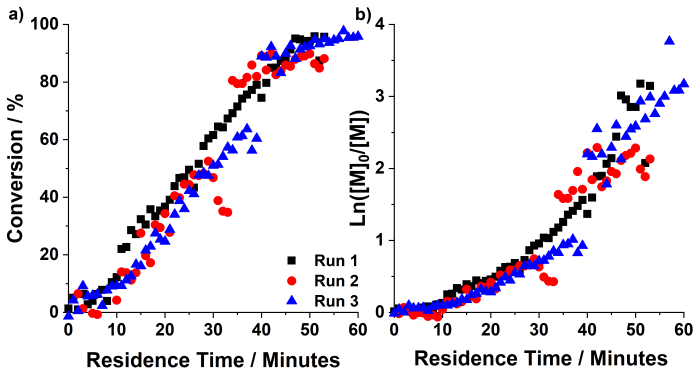

Figure 5.1: a) Conversion vs time and b) Semi-logarithmic plots obtained for the RAFT polymerisation of dimethylacrylamide. All reactions were performed for at 30 % w/w, 70 °C and [DMAm]:[CCTP]:[ACVA] = 100:1:0.1.

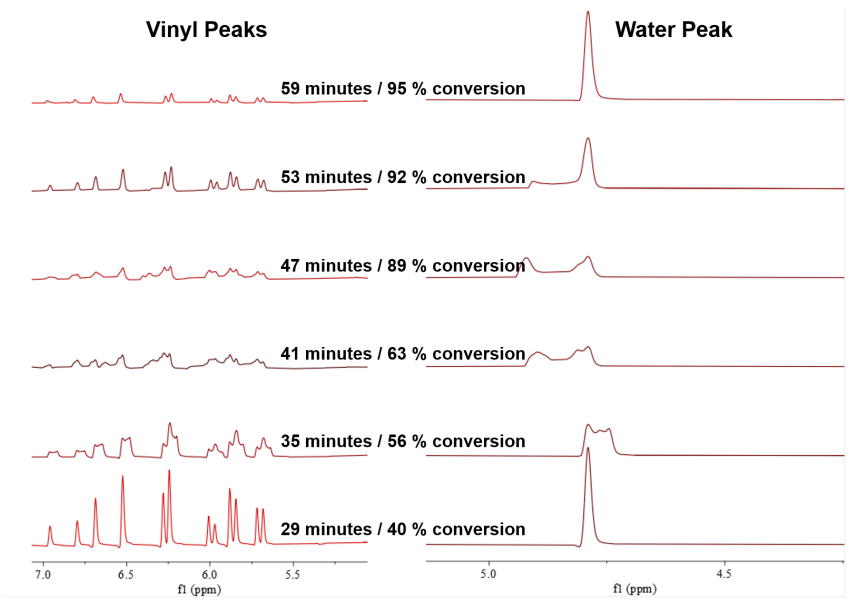

Figure 5.2: NMR stack obtained for the RAFT polymerisation of dimethylacrylamide (Run 3). Splitting of the water peak between 40 - 50 minutes indicated inhomogeneity in the sample. The reaction was performed for at 30 % w/w, 70 °C and [DMAm]:[CCTP]:[ACVA] = 100:1:0.1.

Whilst increasing the flow rate was expected to improve mixing and therefore improve the conversion profile, a faster flow rate will lead to partial loss of the kinetic profile as it corresponds to a shorter residence time. Therefore, the polymerisation reported in chapter 4, which had faster kinetics, was employed to allow for the use of a faster final flow rate (0.2 mL min^{-1}). The kinetic profile (Figure 5.3) obtained showed no irregular regions of conversion and pseudo-first order kinetics that are typical for RAFT polymerisation were observed.[247]

Online GPC analysis (Figure 5.4a) yielded no polymer peak after 3 & 6 minutes, likely due to low polymer concentrations as well as the limited resolution of the GPC at low molecular weight. A polymer peak (M_n = 6,500 g mol^{-1}) was detected after 9 minutes and a shift to higher molecular weight with increasing reaction time was observed for every subsequent chromatogram. From the obtained molecular weight data, a linear relationship between molecular weight and conversion was observed indicating good living control over the polymerisation (Figure 5.4b). Transient kinetic profiling is a powerful tool, allowing for rapid collection of large amounts of kinetic data. However whilst the technique is useful, when the flow platform performed both in-line and at-line analysis limitations were apparent such as: usable flow rate range and temporal control over GPC collection. Therefore this method was not used for further experiments and a new sampling method more suitable for the flow platform was developed.

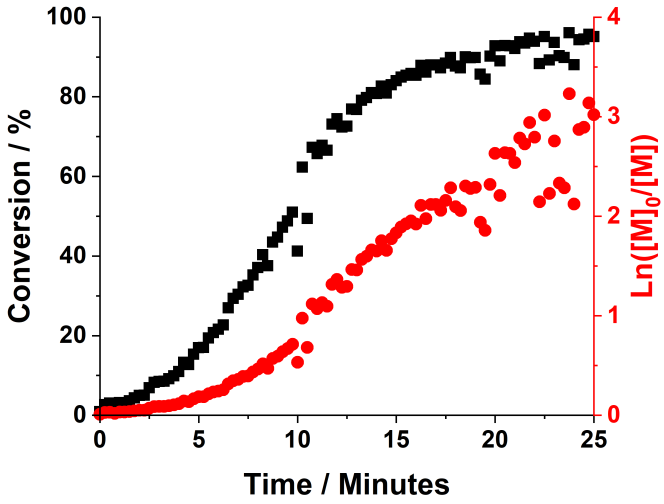

Figure 5.3: NMR kinetic plots obtained through transient sampling for the RAFT polymerisation of dimethylacrylamide. All reactions were performed for at 30 % w/w, 70 °C and [DMAm]:[CCTP]:[VA-044] = 100:1:0.02.

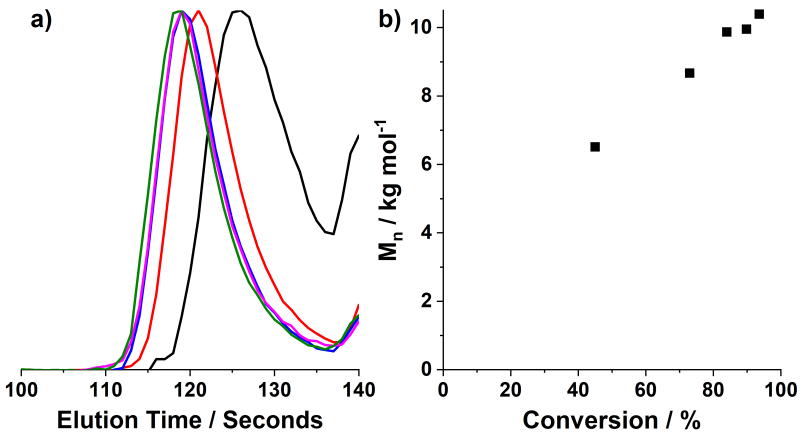

Figure 5.4: a) GPC chromatograms and b) molecular weight evolution obtained through transient sampling for the RAFT polymerisation of dimethylacrylamide. All reactions were performed for at 30 % w/w, 70 °C and [DMAm]:[CCTP]:[VA-044] = 100:1:0.02.

5.3.2 Automated Steady State Kinetics

An automated steady state sampling method (see appendix), that better suited the flow platform, was developed as an alternative to transient profiling. As discussed previously in chapter 3, to achieve a similar temporal resolution to transient profiling a significant time and material cost was incurred. However, automating the process mitigated the time cost as the actual operator time required was relatively short and the system was able to continuously run experiments, which was often not feasible during manual operation.

The RAFT polymerisation of DMAm performed in section 5.3.1 was repeated using steady state sampling. Samples were taken at 5, 10, 15, 20 and 25 minutes giving an overall run time of 225 minutes, significantly longer than the transient method. Whilst the temporal resolution of the steady state profile was significantly lower than the transient profile, the linear semi-logarithmic plot clearly indicated pseudo-first order kinetics (Figure 5.5). Conversions obtained via steady state were noticeably higher than the transient profile at 5 (55 %) and 10 (80 %) minutes. It has been reported recently, that performing wide time sweeps for online transient profiling led to significantly lower conversions.[31] Poor thermal contact between the tubing and the heating block may have led to inadequate heating at high flow rates affecting the initiator decomposition and therefore the reaction kinetics.[248]

GPC chromatograms (Figure 5.6a) for the polymerisation showed a shift to higher molecular weight with respect to reaction time. Although, evolution of a high molecular weight shoulder was observed as reaction time increased. However, measured molecular weight data for the polymerisation showed a linear increase with respect to conversion (Figure 5.6b).

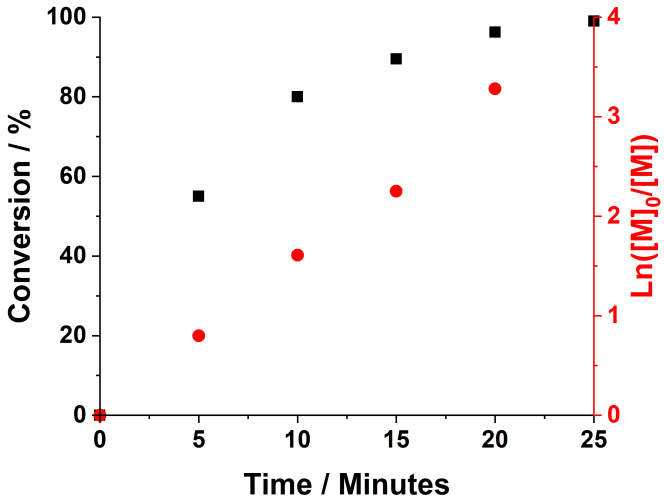

Figure 5.5: NMR kinetic plots obtained through steady state sampling for the RAFT polymerisation of dimethylacrylamide. All reactions were performed for at 30 % w/w, 70 °C and [DMAm]:[CCTP]:[VA-044] = 100:1:0.02.

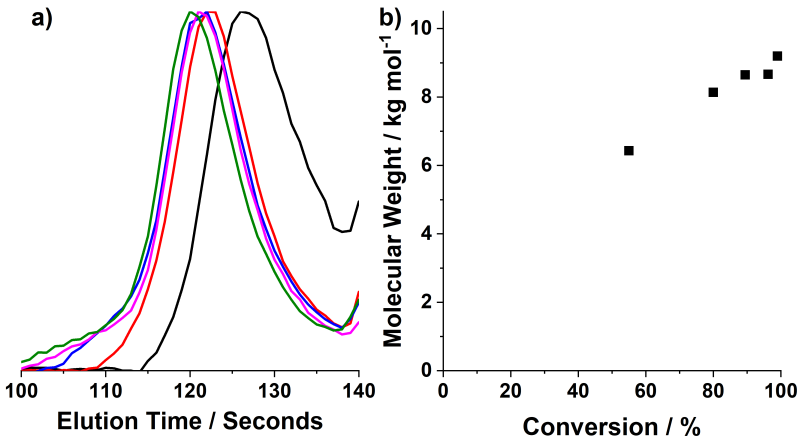

Figure 5.6: a) GPC chromatograms and b) molecular weight evolution obtained through steady state sampling for the RAFT polymerisation of dimethylacrylamide. All reactions were performed for at 30 % w/w, 70 °C and [DMAm]:[CCTP]:[VA-044] = 100:1:0.02.

5.3.3 Automated Reaction Screening and Optimisation of the RAFT polymerisation of Dimethylacrylamide

5.3.3.1 Automated Reaction Screening

With the successful development of a robust automated profiling method, reaction conditions for the synthesis of a new polymer ($PDMAm_{200}$), of which there was no prior kinetic data available, were screened by the platform. The reaction space was screened using a design of experiments (DoE) between residence times of 1 - 5 minutes and temperatures of 80 - 120 °C in 5 °C increments. A total of 45 experiments were performed with a run-time of approximately 20 hours, although total operator time amounted to less than 1 hour.

Conversion and dispersity were the two important criteria monitored by the platform (Figure 5.7a). Molecular weight was also measured (see appendix) but as it increased linearly with conversion was deemed to not be important and a linear increase was assumed for optimisation experiments. Screening of the reaction space yielded an optimum set of reaction conditions to perform the polymerisation (5 minutes, 95 °C). At these conditions conversion was maximised (88 %) and dispersity was very near to its minimum (Đ = 1.23). Fitting a response surface to the reaction data allowed for easier visualisation of trends in the reaction space (Figure 5.7b). Expected trends in RAFT polymerisations are observed such as dispersity decreasing with respect to conversion and conversion increasing with both temperature and time.[249] However, above a certain temperature (95 °C) an overall increase in dispersity, decrease in conversion and loss of pseudo-first order kinetic behaviour were observed as temperature increased. As stated

previously the rate of reaction in a RAFT polymerisation is proportional to the concentration of propagating radicals.[101] As temperature increased, the number of propagating radicals increased and initially the rapid rate of reaction yielded high conversion at short residence times at higher temperatures. However, at very high temperatures (> 100 °C), near full decomposition of VA-044 was achieved within the residence time (Figure 5.8). Similar to kinetics observed in chapter 4, once the majority of VA-044 was consumed no new radicals were generated to drive the RAFT polymerisation, hence the apparent stagnation of conversion at long temperature and residence times. Additionally, an increased radical concentration will have caused an increase in k_t explaining the increased dispersity for similar conversions at higher temperatures.

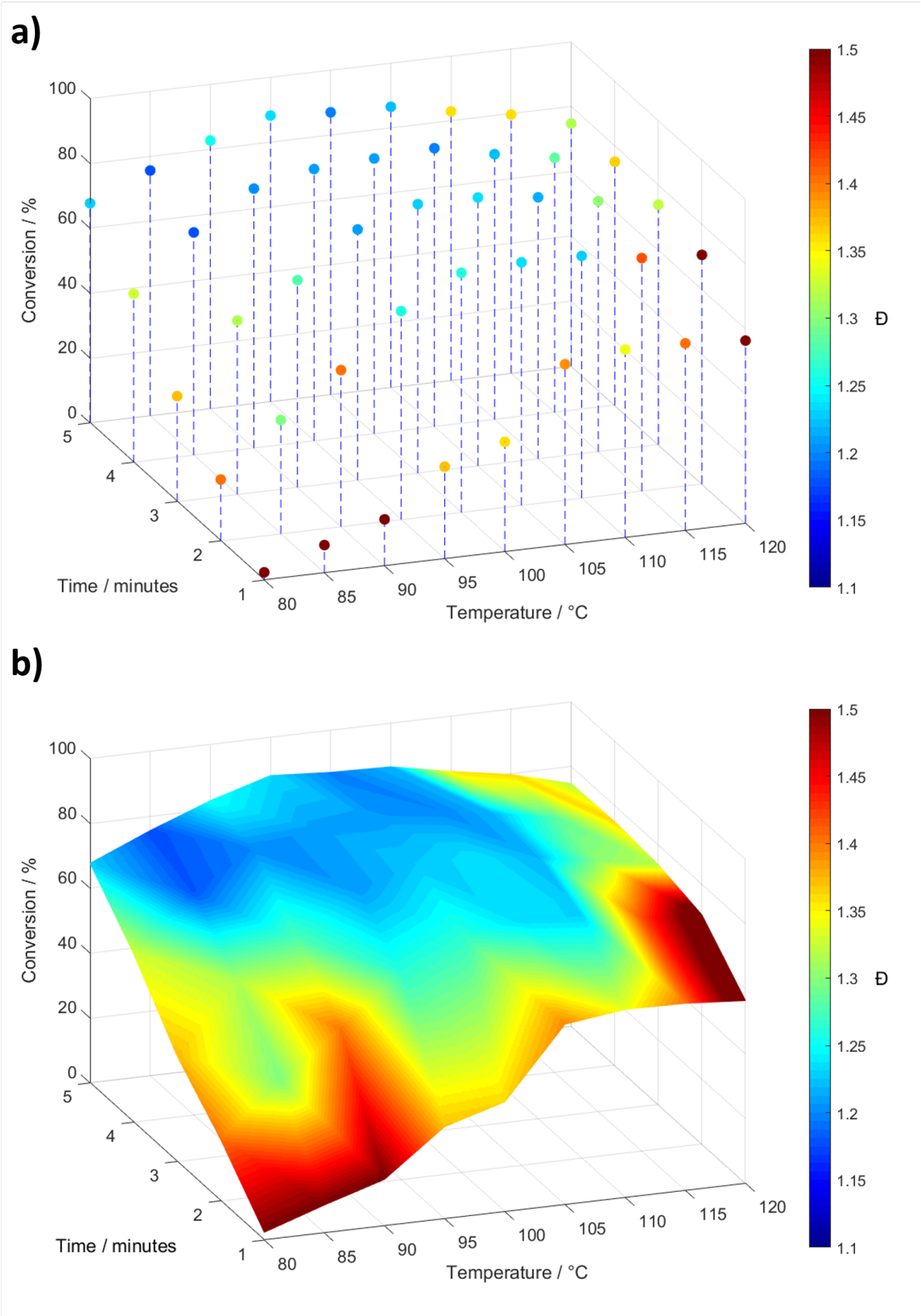

Figure 5.7: a) 3-D plot and b) response surface generated from the obtained data for the reaction screening of the RAFT polymerisation of dimethylacrylamide. All reactions were performed for at 30 % w/w and [DMAm]:[CCTP]:[VA-044] = 200:1:0.02.

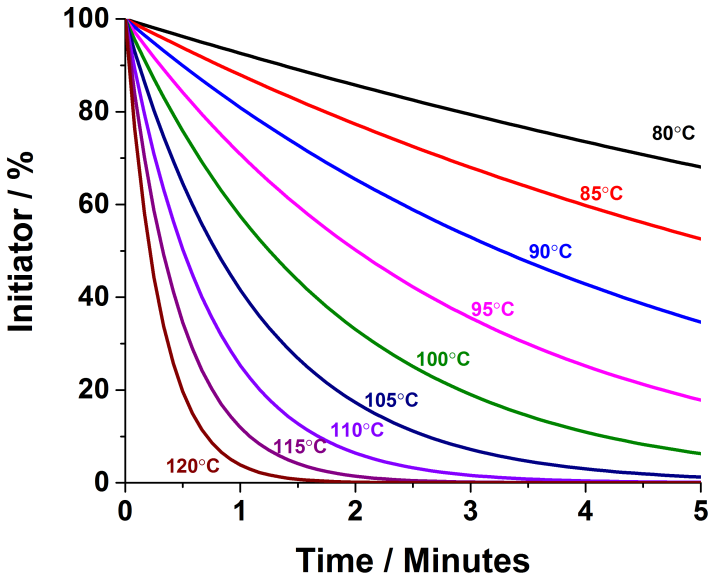

Figure 5.8: Calculated decomposition of VA-044 across temperatures used for screening the RAFT polymerisation of $PDMAm_{200}$.

5.3.3.2 Self-optimisation

The automated continuous flow platform was initially developed for the screening of polymerisations. The next step was to make the system capable of examining data and to predict new experiments without human intervention. This was achieved through the incorporation of a self-optimisation algorithm, Thompson Sampling Efficient Multi-objective Optimisation (TS-EMO), into the platform.[250] There are a variety of optimisable objectives in a chemical reaction and their, often, non-linear responses to reaction conditions make optimisations difficult.[11] Common optimised objectives for small molecule syntheses include yield, process costs, impurity levels stereo-selectivity, environmental impact and productivity. Polymerisation reactions differ to small molecule reactions and as such their optimisable objectives differ. Conversion, molecular weight, dispersity, polymer composition, end-group fidelity, polymer particle size and morphology are all potential objectives to optimise. As discussed in Chapter 1 many single objective algorithms have been successfully employed for the optimisation of small-molecule reactions. Reports of self-optimisations of RAFT polymerisations using flow platforms are beginning to emerge. Junkers *et. al.* have reported two flow platforms for single objective optimisations of RAFT polymerisations.[30,31] One flow reactor platform was able to optimise polymerisation conditions for a pre-specified molecular weight within a 1.5 % error margin. Whilst the other used transient profiling to target specific conversions. However, to date there are currently no

reports of a multi-objective self-optimisation of RAFT polymerisations using an automated flow platform. Of the few multi-objective algorithms reported for chemical reactions, TS-EMO was selected and integrated into the platform (see appendix). The polymerisation of $PDMAm_{200}$, screened previously in section 5.3.2, was optimised for both dispersity and conversion. Additionally, the reaction space was expanded in order to test the efficiency of the algorithm. The overall efficiency of the self-optimisation compared to the reaction screen was apparent when comparing the run time of each method. The screening method took 20 hours to perform a total of 45 experiments whilst the self optimisation took seven hours to perform 28 experiments in a larger reaction space.

Ten initial training reactions were performed, with conditions selected through Latin hypercube (LHC) sampling. The data obtained was used to train the algorithm and four new reaction conditions (10 min, 84 °C / 9.6 min, 85 °C / 9.4 min, 109 °C / 9 min, 120 °C) were generated and employed, this was repeated until a total of 28 experiments had been performed. The initial LHC experiments gave data in regions of high dispersity ($Đ > 1.6$) with varying conversions (Figure 5.9). The subsequent 18 experiments elucidated a Pareto front (Figure 5.9a - dashed lined) consisting of 6 points. The Pareto front showed that large increases in conversion with minimal increase in dispersity were possible until high conversions where the opposite became true. Dispersities observed for this experiment were much higher than those obtained in the previous screening experiment due to the column degradation described during chapter 2. Whilst absolute values for dispersity were higher, the trends in dispersity observed should have remained unaffected. The optimal dispersity was 1.43 at 50 % conversion whilst the optimal conversion was 99.9 % with a dispersity of 1.7. Similar to the screening experiment, the optimum reaction conditions (5.2 minutes, 92 °C) chosen were at highest conversion (99.0 %) before a large dispersity increase ($Đ = 1.45$). These optimal conditions were almost identical to the previous screening experiment (5 minutes, 95 °C). Whilst in a larger reaction space the algorithm identified that the optimum conversions and dispersities were likely to reside in the reaction space used for the screening experiment (Figure 5.9b). The majority of the reaction conditions generated by the algorithm were within the smaller reaction space ($\frac{11}{18}$ experiments).

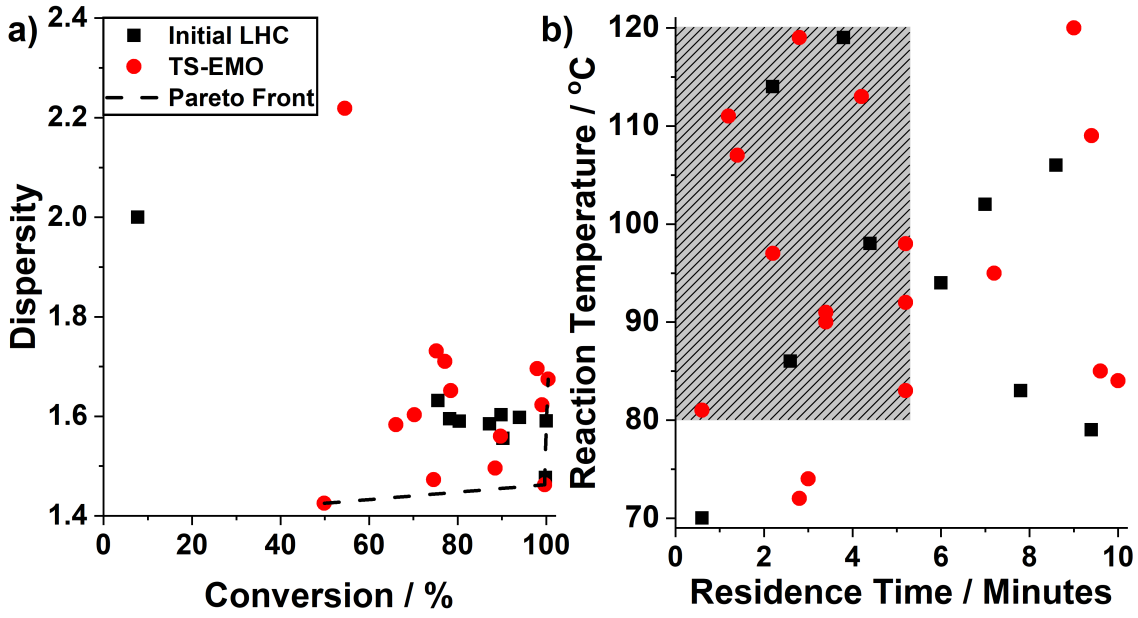

Figure 5.9: a) Experimental data and b) experimental conditions generated during the multi-objective optimisation of the RAFT polymerisation of dimethylacrylamide. A Latin hypercube (LHC) generated 10 inital experiments after which the TS-EMO algorithm generated new reaction conditions based current reaction data. The grey area is the reaction space used during previous automated screening experiments. All reactions were performed for at 30 % w/w and [DMAm]:[CCTP]:[VA-044] = 200:1:0.02.

Additionally models generated by the TS-EMO algorithm included hyper parameters (Θ_i, Figure 5.10), which qualitatively highlighted the relevance of input variables to the model, where lower values equated to a greater relevance. Conversion model hyper parameters indicated temperature had a greater contribution than reaction time, this was likely linked to the increased generation of radicals at higher temperatures. In contrast, dispersity model hyper parameters indicated that residence time had the greater contribution, likely due to the increased probability of termination reactions occurring as radical species remain active for longer.

	GP1 (Conversion)	GP2 (Dispersity)
$\Theta_{\text{Residence Time}}$	0.109	0.032
$\Theta_{\text{Temperature}}$	0.049	0.137

Figure 5.10: Hyper parameters generated by the TS-EMO algorithm for the multi-objective optimisation of the RAFT polymerisation of $PDMAm_{200}$. Lower values indicate a higher contribution to the model.

5.3.4 Automated Reaction Screening and Optimisation of the RAFT polymerisation of *tert*-butylacrylamide

5.3.4.1 Automated Reaction Screening

After screening and self-optimising the RAFT polymerisation of DMAm the platform was employed to screen the RAFT polymerisation of *tert*-butylacrylamide (tBuAm). A new solvent needed to be selected as tBuAm is insoluble in water. The choice of solvent strongly affected the feasibilty of using NMR for conversion measurements. A solvent ideally would have as few peaks as possible but importantly, needed to have no peaks in regions used for monomer conversion. Methanol was selected as it solubilised both tBuAm and PtBuAm and contained only 1 peak in ^{1}H NMR (Figure 5.11, 3.3 ppm). This also demonstrated the versatility of flow as using methanol to perform batch polymerisations at the reaction temperatures used (80 - 120 °C) would be impractical considering its boiling point (66 °C) is well below the reaction temperatures used. Reducing reaction temperatures would drastically decrease radical flux and reaction rates. However, the flow platform was operated under a pressure of 100 psi (7 bar), generated by the back pressure regulator. The increased pressure raised the boiling point of methanol to 120 °C making it possible to perform experiments at elevated reaction temperatures in order to maintain a high radical flux.

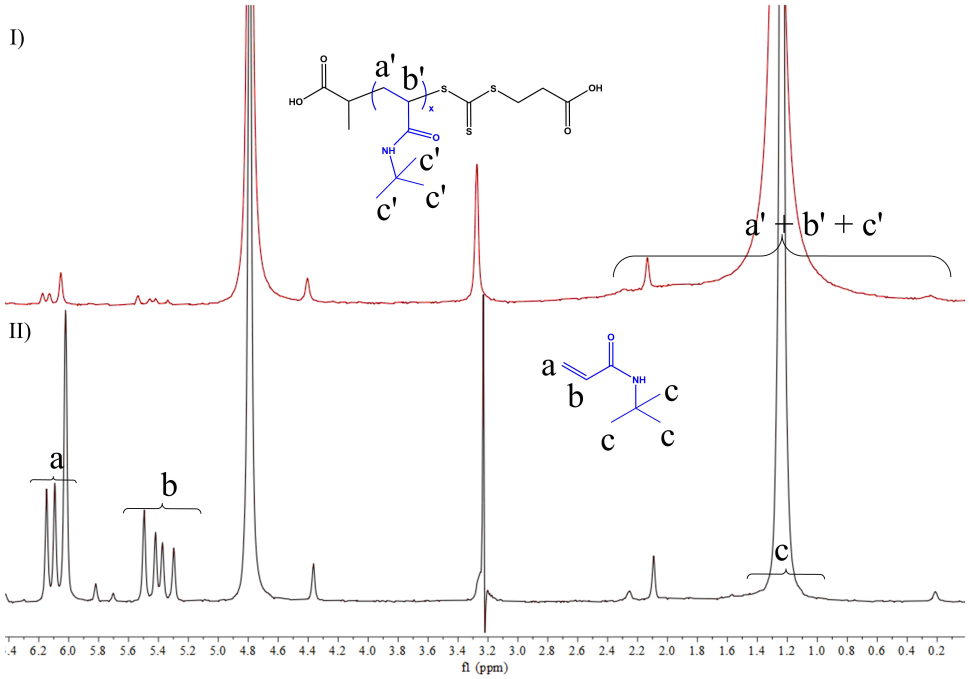

Figure 5.11: ^{1}H NMR spectra during reaction screening of the RAFT polymerisation of tBuAm at I) $t_{20\ min}$ and II) $t_{0\ min}$. Conversion was determined, using equation 5.2, by comparing vinyl protons (a + b) to the pendant methyl groups (c) and polymer backbone (a' + b') .

Initially, the reaction space screened, using the DoE approach, was between 4 - 20 minute residence times, in 4 minute increments, and temperatures of 80 - 120 °C, in 10 °C increments. A total of 25 experiments were performed, with a run-time of approximately 25 hours. The reaction surface obtained was purposefully less data rich than the one obtained for the synthesis of $PDMAm_{200}$ in order to demonstrate the efficiency of the TS-EMO algorithm. From the screened reaction space (Figure 5.12a) an optimum set of conditions were estimated for the polymerisation (16 minutes, 100 °C). Where conversion was almost maximised (89 %) and dispersity was at a local minimum (Đ = 1.32). However due to the limited detail in the screen it was feasible that better optimum conditions existed. Once again, fitting a response surface to the reaction data obtained allowed for facile observation of trends in the reaction (Figure 5.12b). Expected trends of RAFT polymerisation were observed such as dispersity decreasing with respect to conversion and conversion increasing with both temperature and time.[249] Similar to the screening for $PDMAm_{200}$, after a certain temperature (100 °C) an overall increase in dispersity, a slight decrease in conversion and a loss of pseudo first order kinetic behaviour as temperature increased was observed. As with the screening of $PDMAm_{200}$, the observed trends were linked with the decomposition of the initiator. For the polymerisation of tBuAm, AIBN was employed as the initiator, as VA-044 was insoluble in methanol. As AIBN has a lower k_d than VA-044, the overall radical flux and therefore reaction rate was slower. To compensate for this reduced radical flux the initiator concentration was increased (1 mmol L^{-1}, [CCTP]:[AIBN] = 10:1) allowing for radical generation similar to VA-044 at low reaction temperatures (Figure 5.13). As with VA-044 at high temperatures (> 100 °C) the majority of AIBN was consumed within the maximum residence time screened (20 min), explaining the stagnation of the reaction kinetics.

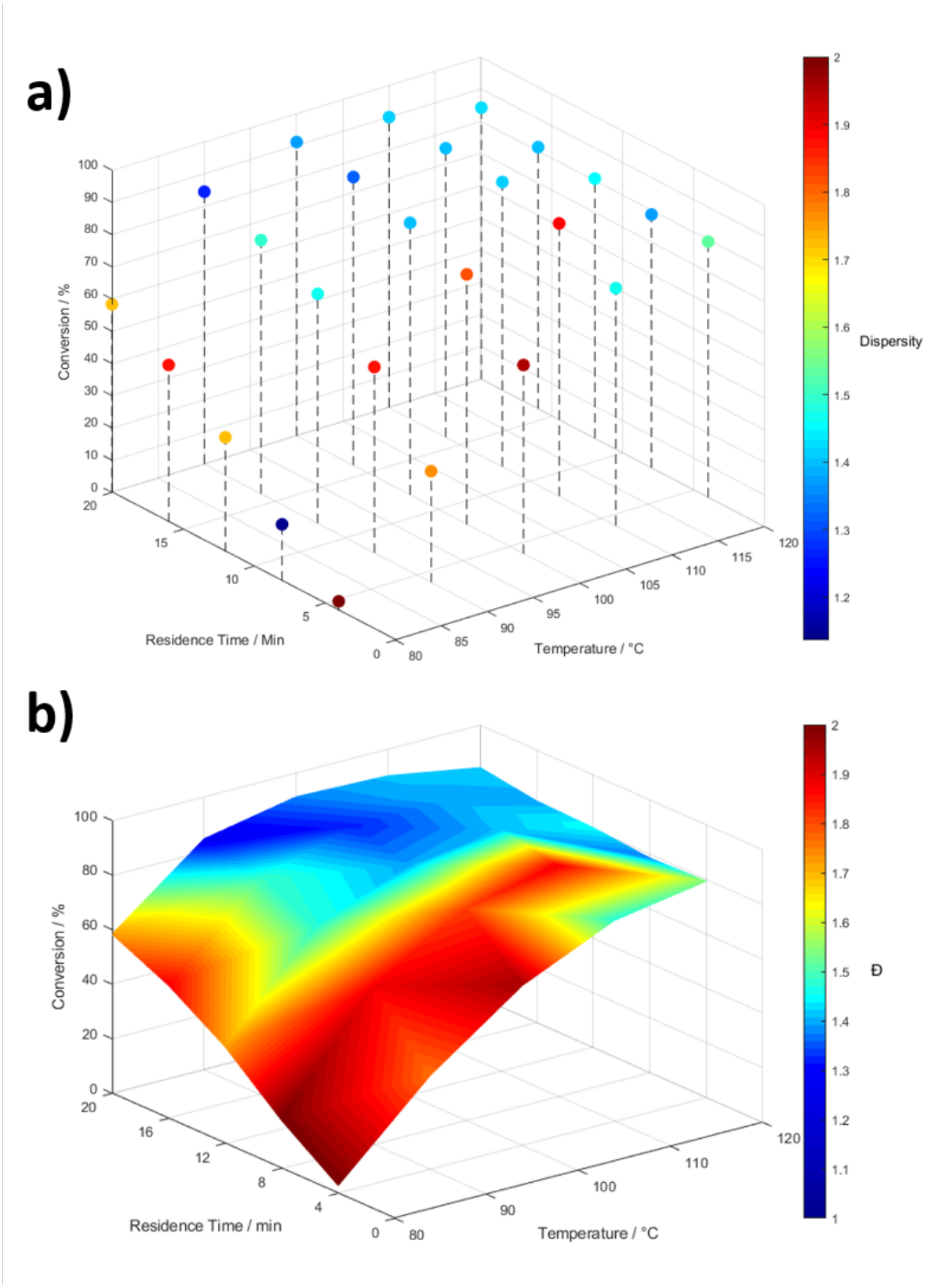

Figure 5.12: a) 3-D plot and b) response surface generated from the obtained data for the reaction screening of the RAFT polymerisation of *tert*-butylacrylamide. All reactions were performed for at 30 % w/w and [tBuAm]:[CCTP]:[AIBN] = 200:1:0.1.

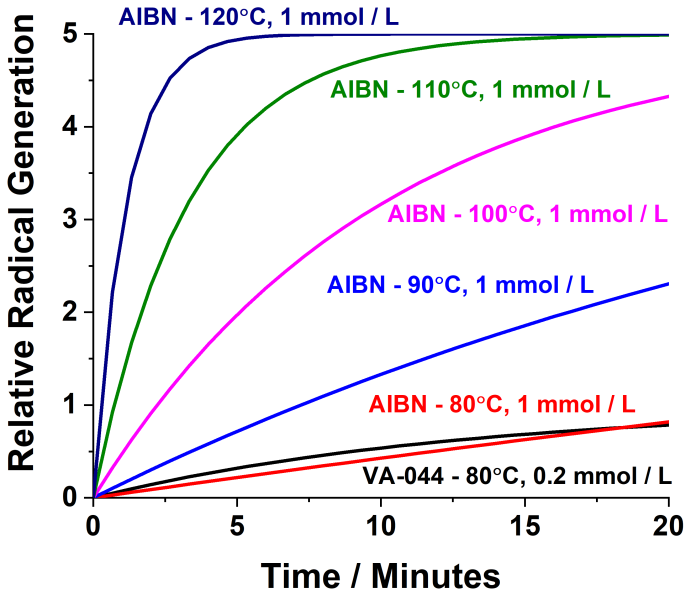

Figure 5.13: Calculated radical generation of VA-044 and AIBN, relative to VA-044, across reaction temperatures used for screening the RAFT polymerisation of $PtBuAm_{200}$. The concentration of AIBN (1 mmol L^{-1}) was 5 times higher than VA-044 (0.2 mmol L^{-1})in order to mimic a similar radical flux at 80 °C.

5.3.4.2 Self-Optimisation

Self-optimisation of the polymerisation of tBuAm was performed for 3 different RAFT agents (CCTP, DCTTC and CPMT). For all optimisations, the same reaction space used for the previous screening experiment was employed. The platform operated similarly to the optimisation of $PDMAm_{200}$, initially ten training experiments were generated by LHC sampling and performed. The TS-EMO algorithm then repeatedly predicted and employed four new sets of experimental conditions until a Pareto front was elucidated (30, 36 and 25 total experiments respectively for CCTP, DCTTC and CPMT). Similar to the optimisation of $PDMAm_{200}$, Pareto fronts obtained for CCTP and DCTTC showed large increases in conversion with minimal increased in dispersity until high conversions where the opposite became true. For CCTP, the lowest dispersity was 1.27 at 74 % conversion whilst the highest conversion was 90 % with a dispersity of 1.47 (Figure 5.14a). The optimal reaction conditions (20 minutes, 92 °C) were at the highest conversion (89.0 %) before a large dispersity increase ($Đ = 1.34$). It was noted that these optimum conditions differed from conditions estimated during the data poor screen, which were found to be within the obtain Pareto front. For DCTTC, the highest conversion was 80 %, lower than the CCTP RAFT agent, with a dispersity of 1.32 whilst the lowest dispersity was 1.21 at

40 % conversion (Figure 5.14b). The optimal reaction conditions (19.5 minutes, 102 °C) were the same as conditions for the highest conversion. Whilst for CPMT, low NMR conversions and no polymer signals were observed for a large number of reaction conditions meaning no relationship between objectives could be ascertained. The highest conversion was 40 %, much lower than other RAFT agents, with a dispersity of 1.22 whilst the lowest dispersity was 1.18 at 37 % conversion (Figure 5.14c). Due to the small number and similarity of the data points obtained it was not possible to discern optimal reaction conditions. Dispersity was well controlled in all optimal polymerisations with little variation across all CTAs (Đ = 1.2 - 1.3) however conversion significantly varied with CTA (40 % - 90 %). It was also observed that TS-EMO generated reaction conditions tended towards higher temperatures and longer residence times as optimal conversion decreased. It was determined that decreasing optimal conversions were due to the different CTA R groups. As observed in chapter 3 R groups that form stabilised radical species ($R^{\bullet}$) led to induction periods during the RAFT polymerisation of acrylamides. When comparing the CTA R groups used to literature it was found that CPMT formed the most stable $R^{\bullet}$ whilst CCTP formed the least stable $R^{\bullet}$.[12] Therefore as different CTAs were used increasing induction periods led the TS-EMO algorithm to select more extreme reaction conditions in order to achieve high conversion.

The hyper parameters generated by the TS-EMO algorithm identified temperature as the key reaction parameter for CCTP and DCTTC with the temperature hyper parameter orders of magnitude lower than residence time (Figure 5.15a,b). A significant number of experimental conditions generated by the algorithm ($\frac{13}{20}$ & $\frac{20}{26}$) were within small reaction temperature windows, 95 - 105 °C for CCTP and 100 - 105 °C for DCTTC. It is likely that temperature was much more significant for this polymerisation compared to the polymerisation of DMAm due to the higher concentration of initiator used. As temperature increased, the concentration of propagating radicals and therefore k_t greatly increased, compared to the DMAm polymerisation. When the optimal conversion decreased using CPMT, the relevance of the residence time hyper parameter increased being only a few times larger than temperature (Figure 5.15c), due to the large induction periods preventing polymerisation.

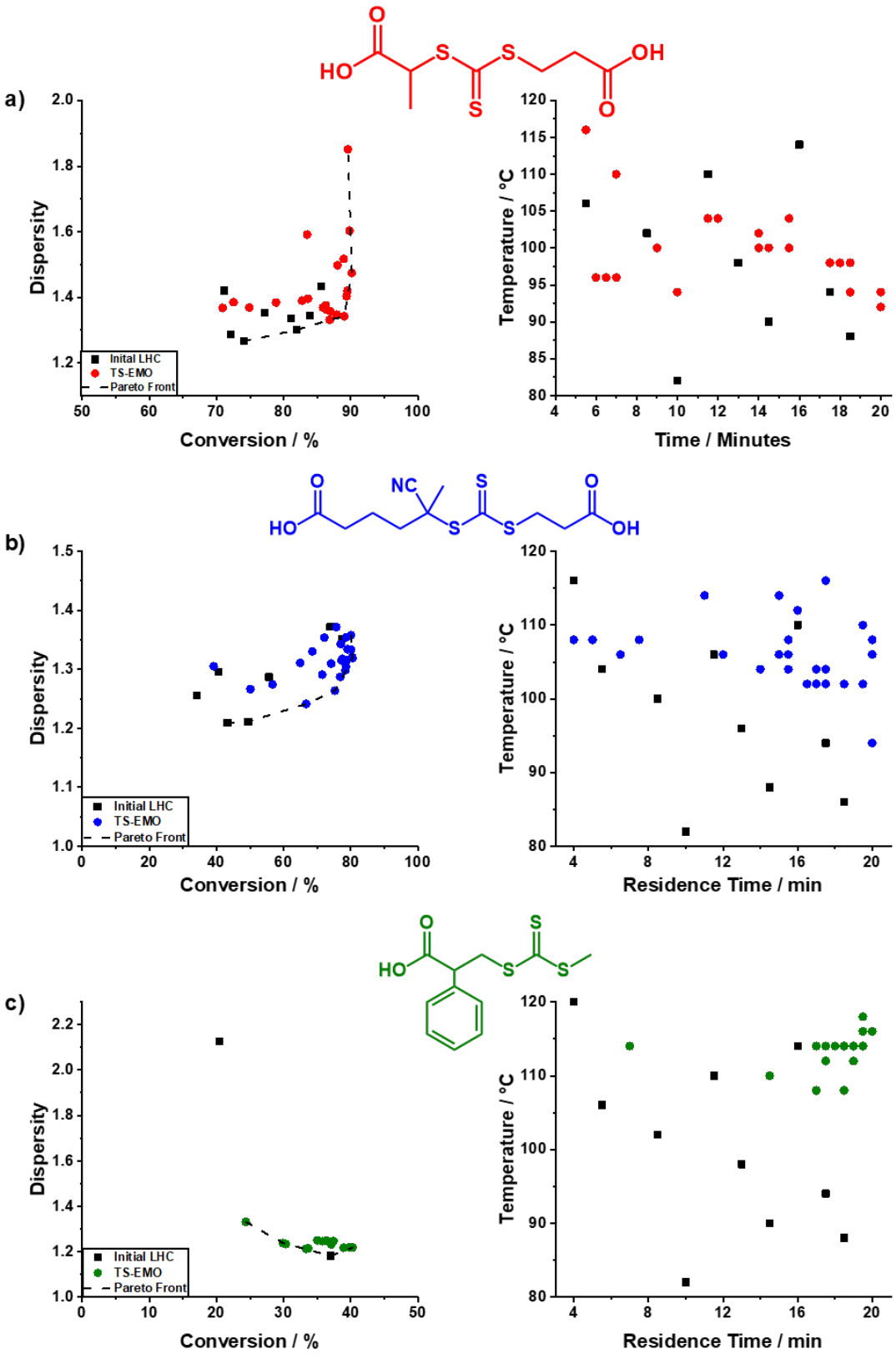

Figure 5.14: Experimental data and reaction conditions generated during the multi-objective optimisation of the RAFT polymerisation of *tert*-butylacrylamide using a) CCTP, b) DCTTC or c) CPMT as the CTA. A Latin hypercube (LHC) generated 10 inital experiments after which the TS-EMO algorithm generated new reaction conditions based on current reaction data. All reactions were performed for at 30 % w/w and [tBuAm]:[CTA]:[AIBN] = 200:1:0.1.

a)

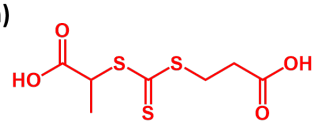

	GP1 (Conversion)	GP2 (Dispersity)
$\Theta_{\text{Residence Time}}$	20.1	31.6
$\Theta_{\text{Temperature}}$	1.2	0.2

b)

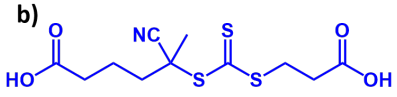

	GP1 (Conversion)	GP2 (Dispersity)
$\Theta_{\text{Residence Time}}$	7.1	31.6
$\Theta_{\text{Temperature}}$	2.6	0.3

c)

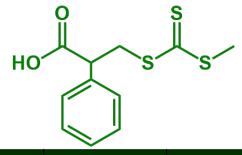

	GP1 (Conversion)	GP2 (Dispersity)
$\Theta_{\text{Residence Time}}$	3.1	3.6
$\Theta_{\text{Temperature}}$	1.4	1.7

Figure 5.15: Hyper parameters generated by the TS-EMO algorithm for the multi-objective optimisation of the RAFT polymerisation of *tert*-butylacrylamide using a) CCTP, b) DCTTC or c) CPMT as the CTA. Lower values indicate a higher contribution to the model.

5.4 Conclusions

In this chapter, a continuous flow platform was used to automate the synthesis and multi-objective optimisation of RAFT polymerisations. Both transient and steady state profiling methods previously described were incorporated into the platform and tested using the RAFT polymerisation of dimethylacrylamide. The transient profiling method was found to have limitations with respect to NMR spectra quality at long residence times and also, had poor temporal control over GPC measurements. Therefore, it was not employed for screening and optimisation experiments. Reaction conditions for the synthesis of $PDMAm_{200}$ were screened using steady state profiling. A total of 45 experiments were performed and an optimum set of reaction conditions (5 minutes and 95 °C) were determined, where conversion was 88 % and dispersity was near its minimum ($Đ = 1.23$). The reaction space was then widened and the same polymerisation was used to perform a multi-objective self-optimisation on the reactor platform by incorporating the TS-EMO algorithm. Initially, ten training experiments generated by LHC sampling were performed, the reaction data obtained allowed the algorithm to predict new reaction conditions to perform. A total of 28 different reaction conditions were autonomously conducted which elucidated optimised reaction conditions that were almost identical to the ones obtain during the screening (5.2 minutes and 92 °C). From the optimisation a Pareto front was observed highlighting the relationship between conversion and dispersity for this polymerisation system. The effect of the reaction conditions on conversion and dispersity where indicated by the hyper-parameters obtained from the TS-EMO algorithm. Residence time was found to have the greatest effect on dispersity whilst temperature had a stronger influence over conversion.

The RAFT polymerisation of *tert*-butylacrylamide in methanol was also screened and optimised

using the platform. A total of 25 experiments were performed during the automatic reaction screen. The estimated optimal reaction conditions (16 minutes, 100 °C) gave a polymer with 89 % conversion and the lowest dispersity of all high conversion experiments (Đ = 1.32). However, due to the large increment changes in reaction conditions during the screen it was likely that a better optimum existed. This was confirmed after performing a self-optimisation of the polymerisation where the estimated reaction conditions were found to be within the Pareto front and a new set of optimum conditions were found (20 minutes, 92 °C). Self-optimisations of the polymerisation using the platform and TS-EMO algorithm were performed for 3 different CTAs. Whilst optimal dispersities varied little (Đ = 1.2 - 1.3), optimal conversions varied significantly with different CTAs (40 % for CPMT, 80% for DCTTC and 90 % for CTTP). Optimal reaction temperatures and residences times were also found to increase as optimal conversion decreased. This was attributed to large induction periods, caused by increasing $R^{\bullet}$ stability, which required more extreme reaction conditions in order to successfully polymerise tBuAm within the defined reaction space.

Chapter 6

Conclusions

Throughout this thesis polymeric materials were synthesised via RAFT polymerisation in a variety of flow reactors, which were described in chapter 2. In Chapter 3, homogeneous and heterogeneous RAFT polymerisations were kinetically investigated in a batch reactor and a basic flow platform. Homogeneous RAFT polymerisations of dimethylacrylamide, using two different CTAs, were initally screened in batch to determine a suitable polymerisation system to transfer to flow. After selecting a suitable polymerisation system, flow kinetic profiles were obtained using both transient and steady state profiling methods. An accelerated rate of polymerisation was observed in flow, which was attributed to improved heat transfer. Although all polymerisations showed good control over reaction kinetics and molecular weight distribution. A large batch of $PDMAm_{113}$ macro-CTA was synthesised using a 20 mL flow reactor and used for further chain extension experiments. The RAFT aqueous dispersion polymerisation of NIPAm was then investigated and target DP was varied from 50 - 200 in order to investigate the self-assembly behaviour of the system. As with the RAFT polymerisation of DMAm, an accelerated rate of polymerisation was observed in flow but pseudo first order kinetics were observed in both reactors. From the kinetic data, a DP around 50 was determined to be the critical chain length at which self assembly occurred. High molecular weight shoulders were observed in batch and flow however the shoulder was much more prominent in flow, likely due to the increased reaction rates observed in flow reactors. The RAFT aqueous dispersion of diacetone acrylamide was then investigated. Batch and flow kinetic profiles once again indicated an accelerated rate of polymerisation in flow. A series of $PDMAm_{113}$-$PDAAm_x$ block copolymer spherical nanoparticles were synthesised in flow and nanoparticle size increased with respect to PDAAm block

length. Higher order morphologies were targeted by increasing the concentration of the reaction solution and reducing the PDMAm DP to 50. Significant fouling was observed when targeting high conversions for DP 200. Therefore, to succesfully collect samples the polymerisation was performed at two shorter residence times. TEM analysis of the resultant nanoparticles indicated a majority worm phase at the shorter residence time and a majority vesicle phase at the longer residence time. However, both samples contained a population of spherical nanoparticles due to fouling in the flow reactor as the reaction progressed. Overall, the results in this chapter indicated that flow reactors can be used to perform both homogenous and heterogeneous RAFT polymerisations without detrimentally affecting the polymerisation kinetics. However, the large amount of fouling present during the synthesis of high order polymer nanoparticles was of concern and warranted further investigation.

In Chapter 4 a PFA flow reactor, better suited to polymeric nanoparticles synthesis due to the chemical resistance of PFA, was used to perform RAFT solution and RAFT aqueous dispersion polymerisations. Acquisition of kinetic profiles was automated by incorporating an NMR spectrometer into the reactor platform. The rate of polymerisation for the synthesis of a PDMAm macro-CTA and its subsequent chain extension with DAAm, to form $PDMAm_x$-$PDAAm_y$ nano-objects, was significantly increased when using a high k_d initiator (VA-044), at 90 °C. High conversions were achieved within 10 minutes for low target DPs. Kinetic profiles obtained for RAFT aqueous dispersion polymerisations were characteristic of RAFT-PISA polymerisations and a DP of approximately 35 was determined to be the critical chain length for self-assembly. A series of well-defined $PDMAm_x$-$PDAAm_y$ block copolymers were synthesised with high conversions (> 90 %) in 20 minutes using the flow platform. These polymers underwent PISA to form spherical, worm and mixed phase nano-objects, as determined by DLS and TEM, depending on their composition. However, pure vesicle phases could not be produced under these reaction conditions, potentially due to temperature responsive behavior upon formation of the vesicle phase. Lowering reaction temperature of the flow reactor for vesicle synthesis caused an inhibition of the polymerisation, which was attributed to the reduced radical flux not being able to quench oxygen permeating the system through the PFA reactor walls. Polymerisations were successfully performed at 70 °C by increasing the concentration of VA-044 and pure vesicle phases (as seen by TEM) were formed in under 20 minutes. However, for polymer compositions around the reported worm-vesicle phase boundary a loss of control over particle formation and aggregate formation was still observed . Through observation of

molecular weight trends, aggregate formation was attributed to a complex amalgam of both the poor hydrophobic core solvation during the worm to vesicle transition during PISA and mixing in the flow reactor system. Overall the work in this chapter indicated that a range of block copolymer nanoparticles could be synthesised at an accelerated rate in flow. However, poor mixing in tubular reactors led to the presence of polymer aggregates when targeting certain block copolymer compositions. This is expected to be of concern for commercial implementation of flow systems and further investigation into reactor design is needed.

In Chapter 5, NMR and GPC analysis were incorporated into a continuous flow platform which was the automated and used to perform the synthesis and multi-objective optimisation of RAFT polymerisations. RAFT polymerisation of dimethylacrylamide was automatically profiled using transient and steady state methods with similar kinetic profiles obtained. Steady state methods were employed for screening and optimisation experiments, due to poor compatability of the transient method with the flow reactor setup. Reaction conditions for the synthesis of $PDMAm_{200}$ were screened and a total of 45 experiments were performed yielding an optimum set of reaction conditions (5 minutes and 95 °C), which gave a polymer with high conversion (88 %) and low dispersity ($Đ = 1.23$). Incorporating a machine learning algorithm (TS-EMO) into the flow reactor allowed for the multi-objective optimisation of the polymerisation. Ten inital training experiments allowed the algorithm to predict new reaction conditions to perform. This process repeated united a total of 28 different reaction conditions were conducted and optimised reaction conditions were elucidated. For the RAFT polymerisation of dimethylacrylamide the optimised conditions were almost identical to conditions obtained during screening experiments (5.2 minutes and 92 °C). From the optimisation a Pareto front was observed highlighting the relationship between conversion and dispersity for this polymerisation system. Hyper-parameters obtained from the TS-EMO algorithm indicated residence time had the greatest effect on dispersity whilst temperature had a stronger influence over conversion. The RAFT polymerisation of *tert*-butylacrylamide in methanol was also screened and optimised using the platform. From the automated screening of 25 reaction conditions, optimal reaction conditions (16 minutes, 100 °C) that gave a polymer with 89 % conversion and the lowest dispersity of all high conversion experiments ($Đ = 1.32$), were estimated. A better optimum was expected to exist due to the small number of experiments screened within the total reaction space. Self-optimisation of the polymerisation showed the estimated reaction conditions were within the Pareto front and a new set of optimum conditions were found (20 minutes, 92 °C). Reaction conditions for a total

of three different CTAs were optimised using the flow platform. Optimal dispersities were found to vary little (Đ = 1.2 - 1.3), however optimal conversions varied significantly with CTA (40 % for CPMT, 80% for DCTTC and 90 % for CTTP). As less optimal CTAs were employed reaction temperatures and residences times were found to increase. This was attributed to large induction periods, caused by increasing $R^{\bullet}$ stability (with CPMT having the most stable $R^{\bullet}$), which required more extreme reaction conditions in order to successfully polymerise tBuAm within the defined reaction space. Overall this chapter demonstrated a versatile automated flow reactor capable of monitoring RAFT solution polymerisations. Incorporating a machine learning algorithm allowed the platform to optimise RAFT polymerisations without human interference. The relationship between conversion and dispersity as well as the effects of residence time and temperature were easily discerned by the automated platform. Further development of automated platforms presents chemists with routes to the facile optimisation of multiple reaction variables simultaneously, even during increasingly complex polymerisation processes such as PISA.

6.1 Future Work

Future research opportunities that can build on this work include:

- Developing flow platforms capable of mixing multiple reaction streams in a controlled manner. This would allow such a platform to optimise overall and individual reactant concentrations, which have to be fixed using the current platform.
- Optimisation or development of new methods for online NMR analysis. The current requirement for multiple monomer peaks limits monomer-solvent selection and also limits the copolymers that can be analysed, as there is often overlap between these signals. Therefore, by optimising the NMR analysis it would greatly increase the number of polymerisation systems that can be monitored by the platform.
- Incorporation of other online analytical techniques. For example incorporating small angle x-ray scattering (SAXS) would allow a platform to analyse and therefore optimise nano-objects generated during PISA.

References

[1] X. Li, E. Mastan, W. J. Wang, B. G. Li and S. Zhu, *Reaction Chemistry and Engineering*, 2016, **1**, 23–59.

[2] M. H. Reis, T. P. Varner and F. A. Leibfarth, *Macromolecules*, 2019, **52**, 3551–3557.

[3] V. D. Pinho, B. Gutmann, L. S. Miranda, R. O. De Souza and C. O. Kappe, *Journal of Organic Chemistry*, 2014, **79**, 1555–1562.

[4] M. B. Plutschack, B. Pieber, K. Gilmore and P. H. Seeberger, *Chemical Reviews*, 2017, **117**, 11796–11893.

[5] K. P. Kuijpers, M. A. Van Dijk, Q. G. Rumeur, V. Hessel, Y. Su and T. Noël, *Reaction Chemistry and Engineering*, 2017, **2**, 109–115.

[6] C. F. Carter, H. Lange, S. V. Ley, I. R. Baxendale, B. Wittkamp, J. G. Goode and N. L. Gaunt, *Organic Process Research and Development*, 2010, **14**, 393–404.

[7] V. Sans, L. Porwol, V. Dragone and L. Cronin, *Chemical Science*, 2015, **6**, 1258–1264.

[8] B. J. Reizman and K. F. Jensen, *Chemical Communications*, 2015, **51**, 13290–13293.

[9] A. D. Clayton, J. A. Manson, C. J. Taylor, T. W. Chamberlain, B. A. Taylor, G. Clemens and R. A. Bourne, *Reaction Chemistry and Engineering*, 2019, **4**, 1545–1554.

[10] N. Holmes, G. R. Akien, A. J. Blacker, R. L. Woodward, R. E. Meadows and R. A. Bourne, *Reaction Chemistry and Engineering*, 2016, **1**, 366–371.

[11] A. M. Schweidtmann, A. D. Clayton, N. Holmes, E. Bradford, R. A. Bourne and A. A. Lapkin, *Chemical Engineering Journal*, 2018, **352**, 277–282.

[12] D. J. Keddie, G. Moad, E. Rizzardo and S. H. Thang, *Macromolecules*, 2012, **45**, 5321–5342.

[13] S. L. Canning, G. N. Smith and S. P. Armes, *Macromolecules*, 2016, **49**, 1985–2001.

[14] A. Blanazs, J. Madsen, G. Battaglia, A. J. Ryan and S. P. Armes, *Journal of the American Chemical Society*, 2011, **133**, 16581–16587.

[15] A. Blanazs, A. J. Ryan and S. P. Armes, *Macromolecules*, 2012, **45**, 5099–5107.

[16] C. Tonhauser and H. Frey, *Macromolecular Rapid Communications*, 2010, **31**, 1938–1947.

[17] M. H. Reis, C. L. Davidson and F. A. Leibfarth, *Polymer Chemistry*, 2018, **9**, 1728–1734.

[18] V. Daniloska, R. Tomovska and J. M. Asua, *Chemical Engineering Journal*, 2012, **184**, 308–314.

[19] C. Rosenfeld, C. Serra, C. Brochon and G. Hadziioannou, *Chemical Engineering Science*, 2007, **62**, 5245–5250.

[20] D. Parida, C. A. Serra, D. K. Garg, Y. Hoarau, F. Bally, R. Muller and M. Bouquey, *Macromolecules*, 2014, **47**, 3282–3287.

[21] A. Kermagoret, B. Wenn, A. Debuigne, C. Jérôme, T. Junkers and C. Detrembleur, *Polymer Chemistry*, 2015, **6**, 3847–3857.

[22] N. Chan, M. F. Cunningham and R. A. Hutchinson, *Polymer Chemistry*, 2012, **3**, 1322–1333.

[23] C. H. Hornung, X. Nguyen, G. Dumsday and S. Saubern, *Macromolecular Reaction Engineering*, 2012, **6**, 458–466.

[24] A. Kuroki, I. Martinez-Botella, C. H. Hornung, L. Martin, E. G. Williams, K. E. Locock, M. Hartlieb and S. Perrier, *Polymer Chemistry*, 2017, **8**, 3249–3254.

[25] E. Baeten, J. J. Haven and T. Junkers, *Polymer Chemistry*, 2017, **8**, 3815–3824.

[26] C. H. Hornung, K. Von Känel, I. Martinez-Botella, M. Espiritu, X. Nguyen, A. Postma, S. Saubern, J. Chiefari and S. H. Thang, *Macromolecules*, 2014, **47**, 8203–8213.

[27] J. Vandenbergh and T. Junkers, *Polymer Chemistry*, 2012, **3**, 2739–2742.

[28] M. Chen and J. A. Johnson, *Chemical Communications*, 2015, **51**, 6742–6745.

[29] N. Corrigan, R. Manahan, Z. T. Lew, J. Yeow, J. Xu and C. Boyer, *Macromolecules*, 2018, **51**, 4553–4563.

[30] M. Rubens, J. H. Vrijsen, J. Laun and T. Junkers, *Angewandte Chemie - International Edition*, 2019, **58**, 3183–3187.

[31] M. Rubens, J. Van Herck and T. Junkers, *ACS Macro Letters*, 2019, **8**, 1437–1441.

[32] N. Zaquen, H. Zu, A. M. Kadir, T. Junkers, P. B. Zetterlund and C. Boyer, *ACS Applied Polymer Materials*, 2019, **1**, 1251–1256.

[33] E. L. Paul, V. A. Atiemo-Obeng and S. M. Kresta, *Handbook of Industrial Mixing: Science and Practice*, Wiley, 2004.

[34] G. Falkovich, *Fluid mechanics*, Cambridge University Press, 2018.

[35] K. D. Nagy, B. Shen, T. F. Jamison and K. F. Jensen, *Organic Process Research and Development*, 2012, **16**, 976–981.

[36] A. A. Kulkarni, *Beilstein Journal of Organic Chemistry*, 2014, **10**, 405–424.

[37] L. Huck, A. De La Hoz, A. Díaz-Ortiz and J. Alcázar, *Organic Letters*, 2017, **19**, 3747–3750.

[38] H. Amii, A. Nagaki and J.-i. Yoshida, *Beilstein Journal of Organic Chemistry*, 2013, **9**, 2793–2802.

[39] T. Illg, P. Löb and V. Hessel, *Bioorganic and Medicinal Chemistry*, 2010, **18**, 3707–3719.

[40] M. Baumann, T. S. Moody, M. Smyth and S. Wharry, *Organic Process Research and Development*, 2020.

[41] I. R. Baxendale, *Journal of Chemical Technology and Biotechnology*, 2013, **88**, 519–552.

[42] B. Pieber and C. O. Kappe, *Organic Letters*, 2016, **18**, 1076–1079.

[43] S. Fuse, N. Tanabe and T. Takahashi, *Chemical Communications*, 2011, **47**, 12661–12663.

[44] F. M. Akwi and P. Watts, *Chemical Communications*, 2018, **54**, 13894–13928.

[45] M. Movsisyan, E. I. Delbeke, J. K. Berton, C. Battilocchio, S. V. Ley and C. V. Stevens, *Chemical Society Reviews*, 2016, **45**, 4892–4928.

[46] F. A. Williams, *AIAA Journal*, 1985, **23**, 1139.

[47] M. Gödde, C. Liebner and H. Hieronymus, *Chemie Ingenieur Technik*, 2009, **81**, 73–78.

[48] C. J. Mallia and I. R. Baxendale, *Organic Process Research and Development*, 2016, **20**, 327–360.

[49] T. Noël and V. Hessel, *ChemSusChem*, 2013, **6**, 405–407.

[50] Y. Su, V. Hessel and T. Noël, *AIChE Journal*, 2015, **61**, 2215–2227.

[51] N. Kockmann, P. Thenée, C. Fleischer-Trebes, G. Laudadio and T. Noël, *Reaction Chemistry and Engineering*, 2017, **2**, 258–280.

[52] K. Jähnisch, V. Hessel, H. Löwe and M. Baerns, *Angewandte Chemie - International Edition*, 2004, **43**, 406–446.

[53] K. Geyer, J. D. C. Codée and P. H. Seeberger, *Chemistry - A European Journal*, 2006, **12**, 8434–8442.

[54] A. Woitalka, S. Kuhn and K. F. Jensen, *Chemical Engineering Science*, 2014, **116**, 1–8.

[55] N. G. Anderson, *Organic Process Research and Development*, 2012, **16**, 852–869.

[56] R. J. Ingham, C. Battilocchio, D. E. Fitzpatrick, E. Sliwinski, J. M. Hawkins and S. V. Ley, *Angewandte Chemie International Edition*, 2015, **54**, 144–148.

[57] J. Yue, F. H. Falke, J. C. Schouten and T. A. Nijhuis, *Lab on a Chip*, 2013, **13**, 4855–4863.

[58] P. Sagmeister, J. Poms, J. D. Williams and C. O. Kappe, *Reaction Chemistry & Engineering*, 2020, **5**, 677–684.

[59] T. A. Beek, *Phytochemical Analysis*, 2020, pca.2921.

[60] J. P. McMullen, M. T. Stone, S. L. Buchwald and K. F. Jensen, *Angewandte Chemie - International Edition*, 2010, **49**, 7076–7080.

[61] N. Holmes, G. R. Akien, R. J. Savage, C. Stanetty, I. R. Baxendale, A. J. Blacker, B. A. Taylor, R. L. Woodward, R. E. Meadows and R. A. Bourne, *Reaction Chemistry and Engineering*, 2016, **1**, 96–100.

[62] R. Leardi, *Analytica Chimica Acta*, 2009, **652**, 161–172.

[63] J. A. Nelder and R. Mead, *The Computer Journal*, 1965, **7**, 308–313.

[64] W. Huyer and A. Neumaier, *ACM Transactions on Mathematical Software*, 2008, **35**, 1–25.

[65] E. Bradford, A. M. Schweidtmann and A. Lapkin, *Journal of Global Optimization*, 2018, **71**, 407–438.

[66] S. A. Weissman and N. G. Anderson, *Organic Process Research and Development*, 2015, **19**, 1605–1633.

[67] C. Houben, N. Peremezhney, A. Zubov, J. Kosek and A. A. Lapkin, *Organic Process Research and Development*, 2015, **19**, 1049–1053.

[68] A. D. Clayton, A. M. Schweidtmann, G. Clemens, J. A. Manson, C. J. Taylor, C. G. Niño, T. W. Chamberlain, N. Kapur, A. J. Blacker, A. A. Lapkin and R. A. Bourne, *Chemical Engineering Journal*, 2020, **384**, 123340.

[69] J. Britton and C. L. Raston, *Chemical Society Reviews*, 2017, **46**, 1250–1271.

[70] L. J. Points, J. W. Taylor, J. Grizou, K. Donkers and L. Cronin, *Proceedings of the National Academy of Sciences of the United States of America*, 2018, **115**, 885–890.

[71] D. Perera, J. W. Tucker, S. Brahmbhatt, C. J. Helal, A. Chong, W. Farrell, P. Richardson and N. W. Sach, *Science*, 2018, **359**, 429–434.

[72] A. B. Henson, P. S. Gromski and L. Cronin, *ACS Central Science*, 2018, **4**, 793–804.

[73] B. J. Reizman and K. F. Jensen, *Accounts of Chemical Research*, 2016, **49**, 1786–1796.

[74] D. Cortés-Borda, K. V. Kutonova, C. Jamet, M. E. Trusova, F. Zammattio, C. Truchet, M. Rodriguez-Zubiri and F. X. Felpin, *Organic Process Research and Development*, 2016, **20**, 1979–1987.

[75] D. E. Fitzpatrick, C. Battilocchio and S. V. Ley, *Organic Process Research and Development*, 2016, **20**, 386–394.

[76] D. Cortés-Borda, E. Wimmer, B. Gouilleux, E. Barré, N. Oger, L. Goulamaly, L. Peault, B. Charrier, C. Truchet, P. Giraudeau, M. Rodriguez-Zubiri, E. Le Grognec and F. X. Felpin, *Journal of Organic Chemistry*, 2018, **83**, 14286–14289.

[77] N. V. Queipo, R. T. Haftka, W. Shyy, T. Goel, R. Vaidyanathan and P. Kevin Tucker, *Progress in Aerospace Sciences*, 2005, **41**, 1–28.

[78] D. N. Jumbam, R. A. Skilton, A. J. Parrott, R. A. Bourne and M. Poliakoff, *Journal of Flow Chemistry*, 2012, **2**, 24–27.

[79] J. S. Moore and K. F. Jensen, *Organic Process Research and Development*, 2012, **16**, 1409–1415.

[80] S. Krishnadasan, R. J. Brown, A. J. DeMello and J. C. DeMello, *Lab on a Chip*, 2007, **7**, 1434–1441.

[81] R. N. Sengupta, A. Gupta and J. Dutta, *Decision Sciences: Theory and Practice*, CRC Press, 2016.

[82] R. T. Marler and J. S. Arora, *Structural and Multidisciplinary Optimization*, 2010, **41**, 853–862.

[83] H. Staudinger, *Berichte der deutschen chemischen Gesellschaft (A and B Series)*, 1920, **53**, 1073–1085.

[84] W. H. Carothers, *Journal of the American Chemical Society*, 1929, **51**, 2548–2559.

[85] P. J. Flory, *Principles of Polymer Chemistry*, Cornell University Press, 1953.

[86] G. Odian, *Principles of Polymerization*, Wiley India Pvt. Limited, 2004.

[87] M. Szwarc, *Nature*, 1956, **178**, 1168–1169.

[88] K. Matyjaszewski and J. Spanswick, *Materials Today*, 2005, **8**, 26–33.

[89] D. H. Solomon, *Journal of Polymer Science Part A: Polymer Chemistry*, 2005, **43**, 5748–5764.

[90] J. S. Wang and K. Matyjaszewski, *Journal of the American Chemical Society*, 1995, **117**, 5614–5615.

[91] M. Sawamoto and M. Kamigaito, *Trends in Polymer Science*, 1996, **4**, 371–377.

[92] J. Chiefari, Y. K. Chong, F. Ercole, J. Krstina, J. Jeffery, T. P. Le, R. T. Mayadunne, G. F. Meijs, C. L. Moad, G. Moad, E. Rizzardo and S. H. Thang, *Macromolecules*, 1998, **31**, 5559–5562.

[93] K. Matyjaszewski and J. Xia, in *Handbook of Radical Polymerization*, John Wiley & Sons, Inc., 2003, pp. 523–628.

[94] Y. Wang, N. Soerensen, M. Zhong, H. Schroeder, M. Buback and K. Matyjaszewski, *Macromolecules*, 2013, **46**, 683–691.

[95] D. Konkolewicz, K. Schröder, J. Buback, S. Bernhard and K. Matyjaszewski, *ACS Macro Letters*, 2012, **1**, 1219–1223.

[96] W. Jakubowski and K. Matyjaszewski, *Angewandte Chemie International Edition*, 2006, **45**, 4482–4486.

[97] K. Matyjaszewski, W. Jakubowski, K. Min, W. Tang, J. Huang, W. A. Braunecker and N. V. Tsarevsky, *Proceedings of the National Academy of Sciences of the United States of America*, 2006, **103**, 15309–15314.

[98] A. J. Magenau, N. C. Strandwitz, A. Gennaro and K. Matyjaszewski, *Science*, 2011, **332**, 81–84.

[99] K. Matyjaszewski, S. Coca, S. G. Gaynor, M. Wei and B. E. Woodworth, *Macromolecules*, 1997, **30**, 7348–7350.

[100] G. Moad, E. Rizzardo and S. H. Thang, *Australian Journal of Chemistry*, 2012, **65**, 985–1076.

[101] S. Perrier, *Macromolecules*, 2017, **50**, 7433–7447.

[102] A. Blanazs, S. P. Armes and A. J. Ryan, *Macromolecular Rapid Communications*, 2009, **30**, 267–277.

[103] N. S. Cameron, M. K. Corbierre and A. Eisenberg, *Canadian Journal of Chemistry*, 1999, **77**, 1311–1326.

[104] N. J. Warren and S. P. Armes, *Journal of the American Chemical Society*, 2014, **136**, 10174–10185.

[105] X. Zhang, S. Boissé, W. Zhang, P. Beaunier, F. D'Agosto, J. Rieger and B. Charleux, *Macromolecules*, 2011, **44**, 4149–4158.

[106] W. Zhang, F. D'Agosto, O. Boyron, J. Rieger and B. Charleux, *Macromolecules*, 2012, **45**, 4075–4084.

[107] W. Zhang, F. D'Agosto, P. Y. Dugas, J. Rieger and B. Charleux, *Polymer*, 2013, **54**, 2011–2019.

[108] S. Boissé, J. Rieger, K. Belal, A. Di-Cicco, P. Beaunier, M. H. Li and B. Charleux, *Chemical Communications*, 2010, **46**, 1950–1952.

[109] T. Junkers, *Macromolecular Chemistry and Physics*, 2017, **218**, 1600421.

[110] D. Wilms, J. Klos and H. Frey, *Macromolecular Chemistry and Physics*, 2008, **209**, 343–356.

[111] N. Micic, A. Young, J. Rosselgong and C. H. Hornung, *Processes*, 2014, **2**, 58–70.

[112] D. R. D'Hooge, P. H. Van Steenberge, M. F. Reyniers and G. B. Marin, *Progress in Polymer Science*, 2016, **58**, 59–89.

[113] V. W. K. R. Barnikol and G. V. Schulz, *Die Makromolekulare Chemie*, 1963, **68**, 211–215.

[114] M. Müller, M. F. Cunningham, R. A. Hutchinson, M. F. Cuningham and R. A. Hutchinson, *Macromolecular Reaction Engineering*, 2008, **2**, 31–36.

[115] T. Honda, M. Miyazaki, H. Nakamura and H. Maeda, *Lab on a Chip*, 2005, **5**, 812–818.

[116] M. Miyazaki, T. Honda, H. Nakamura and H. Maeda, *Chemical Engineering & Technology*, 2007, **30**, 300–304.

[117] A. Nagaki, A. Miyazaki and J. I. Yoshida, *Macromolecules*, 2010, **43**, 8424–8429.

[118] K. Iida, T. Q. Chastek, K. L. Beers, K. A. Cavicchi, J. Chun and M. J. Fasolka, *Lab on a Chip*, 2009, **9**, 339–345.

[119] C. Tonhauser, D. Wilms, F. Wurm, E. Berger-Nicoletti, M. Maskos, H. Lowe and H. Frey, *Macromolecules*, 2010, **43**, 5582–5588.

[120] T. Meyer and J. T. Keurentjes, *Handbook of Polymer Reaction Engineering*, Wiley-VCH, 2008, pp. 1–1102.

[121] C. Serra, N. Sary, G. Schlatter, G. Hadziioannou and V. Hessel, *Lab on a Chip*, 2005, **5**, 966–973.

[122] F. Bally, C. A. Serra, C. Brochon and G. Hadziioannou, *Macromolecular Rapid Communications*, 2011, **32**, 1820–1825.

[123] T. Iwasaki and J. I. Yoshida, *Macromolecules*, 2005, **38**, 1159–1163.

[124] T. Iwasaki, N. Kawano and J. I. Yoshida, *Organic Process Research and Development*, 2006, **10**, 1126–1131.

[125] Y. Song, M. Shang, G. Li, Z.-H. Luo and Y. Su, *AIChE Journal*, 2018, **64**, 1828–1840.

[126] L. Brocken, P. D. Price, J. Whittaker and I. R. Baxendale, *Reaction Chemistry and Engineering*, 2017, **2**, 662–668.

[127] M. Ghosh and T. H. Forsyth, in *Emulsion Polymerization*, 1975, vol. 16, pp. 298–303.

[128] J. W. Vanderhoff, in *Emulsion Polymers and Emulsion Polymerization*, 1981, pp. 199–208.

[129] I. Aizpurua, J. I. Amalvy and M. J. Barandiaran, *Colloids and Surfaces A: Physicochemical and Engineering Aspects*, 2000, **166**, 59–66.

[130] K. Ouzineb, C. Graillat and T. McKenna, *Journal of Applied Polymer Science*, 2004, **91**, 2195–2207.

[131] A. L. Rollin, I. Patterson, P. Bataille and R. Huneault, *The Canadian Journal of Chemical Engineering*, 1977, **55**, 565–571.

[132] N. K. Singha, *Functional Polymers by Reversible Deactivation Radical Polymerisation: Synthesis and Applications*, Smithers Information Limited, 2017.

[133] T. E. Enright, M. F. Cunningham and B. Keoshkerian, *Macromolecular Reaction Engineering*, 2010, **4**, 186–196.

[134] T. Fukuyama, Y. Kajihara, I. Ryu and A. Studer, *Synthesis (Germany)*, 2012, **44**, 2555–2559.

[135] C. Rosenfeld, C. Serra, C. Brochon, V. Hessel and G. Hadziioannou, *Chemical Engineering Journal*, 2008, **135**, S242–S246.

[136] C. Rosenfeld, C. Serra, C. Brochon and G. Hadziioannou, *Lab on a Chip*, 2008, **8**, 1682–1687.

[137] T. E. Enright, M. F. Cunningham and B. Keoshkerian, *Macromolecular Rapid Communications*, 2005, **26**, 221–225.

[138] T. Wu, Y. Mei, J. T. Cabral, C. Xu and K. L. Beers, *Journal of the American Chemical Society*, 2004, **126**, 9880–9881.

[139] T. Wu, Y. Mei, C. Xu, H. C. M. Byrd and K. L. Beers, *Macromolecular Rapid Communications*, 2005, **26**, 1037–1042.

[140] T. Q. Chastek, K. Iida, E. J. Amis, M. J. Fasolka and K. L. Beers, *Lab on a Chip*, 2008, **8**, 950–957.

[141] N. Chan, S. Boutti, M. F. Cunningham and R. A. Hutchinson, *Macromolecular Reaction Engineering*, 2009, **3**, 222–231.

[142] N. Chan, M. F. Cunningham and R. A. Hutchinson, *Macromolecular Reaction Engineering*, 2010, **4**, 369–380.

[143] T. Noda, A. J. Grice, M. E. Levere and D. M. Haddleton, *European Polymer Journal*, 2007, **43**, 2321–2330.

[144] B. Wenn, M. Conradi, A. D. Carreiras, D. M. Haddleton and T. Junkers, *Polymer Chemistry*, 2014, **5**, 3053–3060.

[145] Y. M. Chuang, B. Wenn, S. Gielen, A. Ethirajan and T. Junkers, *Polymer Chemistry*, 2015, **6**, 6488–6497.

[146] B. P. Fors and C. J. Hawker, *Angewandte Chemie International Edition*, 2012, **51**, 8850–8853.

[147] A. Melker, B. P. Fors, C. J. Hawker and J. E. Poelma, *Journal of Polymer Science, Part A: Polymer Chemistry*, 2015, **53**, 2693–2698.

[148] N. Chan, M. F. Cunningham and R. A. Hutchinson, *Journal of Polymer Science, Part A: Polymer Chemistry*, 2013, **51**, 3081–3096.

[149] Y. Shen, S. Zhu, F. Zeng and R. H. Pelton, *Macromolecules*, 2000, **33**, 5427–5431.

[150] Y. Shen, S. Zhu and R. Pelton, *Macromolecular Rapid Communications*, 2000, **21**, 956–959.

[151] Y. Shen and S. Zhu, *AIChE Journal*, 2002, **48**, 2609–2619.

[152] N. Chan, M. F. Cunningham and R. A. Hutchinson, *Macromolecular Rapid Communications*, 2011, **32**, 604–609.

[153] C. Diehl, P. Laurino, N. Azzouz and P. H. Seeberger, *Macromolecules*, 2010, **43**, 10311–10314.

[154] C. H. Hornung, C. Guerrero-Sanchez, M. Brasholz, S. Saubern, J. Chiefari, G. Moad, E. Rizzardo and S. H. Thang, *Organic Process Research and Development*, 2011, **15**, 593–601.

[155] C. H. Hornung, X. Nguyen, S. Kyi, J. Chiefari and S. Saubern, *Australian Journal of Chemistry*, 2013, **66**, 192–198.

[156] S. C. Koch and M. Busch, *Chemie-Ingenieur-Technik*, 2011, **83**, 1720–1727.

[157] J. Vandenbergh, T. De Moraes Ogawa and T. Junkers, *Journal of Polymer Science, Part A: Polymer Chemistry*, 2013, **51**, 2366–2374.

[158] C. H. Hornung, A. Postma, S. Saubern and J. Chiefari, *Polymer*, 2014, **55**, 1427–1435.

[159] C. H. Hornung, A. Postma, S. Saubern and J. Chiefari, *Macromolecular Reaction Engineering*, 2012, **6**, 246–251.

[160] J. Vandenbergh, T. Tura, E. Baeten and T. Junkers, *Journal of Polymer Science, Part A: Polymer Chemistry*, 2014, **52**, 1263–1274.

[161] B. Wenn and T. Junkers, *Macromolecules*, 2016, **49**, 6888–6895.

[162] M. Rubens, P. Latsrisaeng and T. Junkers, *Polymer Chemistry*, 2017, **8**, 6496–6505.

[163] F. Lauterbach, M. Rubens, V. Abetz and T. Junkers, *Angewandte Chemie International Edition*, 2018, **57**, 14260–14264.

[164] N. Corrigan, D. Rosli, J. W. J. Jones, J. Xu and C. Boyer, *Macromolecules*, 2016, **49**, 6779–6789.

[165] N. Corrigan, A. Almasri, W. Taillades, J. Xu and C. Boyer, *Macromolecules*, 2017, **50**, 8438–8448.

[166] N. Corrigan, L. Zhernakov, M. H. Hashim, J. Xu and C. Boyer, *Reaction Chemistry & Engineering*, 2019, **4**, 1216–1228.

[167] N. Zaquen, J. Yeow, T. Junkers, C. Boyer and P. B. Zetterlund, *Macromolecules*, 2018, **51**, 5165–5172.

[168] N. Zaquen, W. A. Azizi, J. Yeow, R. P. Kuchel, T. Junkers, P. B. Zetterlund and C. Boyer, *Polymer Chemistry*, 2019, **10**, 2406–2414.

[169] N. Zaquen, A. M. Kadir, A. Iasa, N. Corrigan, T. Junkers, P. B. Zetterlund and C. Boyer, *Macromolecules*, 2019, **52**, 1609–1619.

[170] J. J. Haven, J. Vandenbergh and T. Junkers, *Chemical Communications*, 2015, **51**, 4611–4614.

[171] J. J. Haven and T. Junkers, *European Journal of Organic Chemistry*, 2017, **2017**, 6474–6482.

[172] J. Haven and T. Junkers, *Polymers*, 2018, **10**, 1228.

[173] M. Rubens and T. Junkers, *Polymer Chemistry*, 2019, **10**, 6315–6323.

[174] F. Lauterbach and V. Abetz, *Macromolecular Rapid Communications*, 2020, 2000029.

[175] J. P. Russum, C. W. Jones and F. J. Schork, *Macromolecular Rapid Communications*, 2004, **25**, 1064–1068.

[176] J. P. Russum, C. W. Jones and F. J. Schork, *Industrial and Engineering Chemistry Research*, 2005, **44**, 2484–2493.

[177] J. P. Russum, C. W. Jones and F. J. Schork, *AIChE Journal*, 2006, **52**, 1566–1576.

[178] Z. Li, W. Chen, Z. Zhang, L. Zhang, Z. Cheng and X. Zhu, *Polymer Chemistry*, 2015, **6**, 1937–1943.

[179] J. Peng, C. Tian, L. Zhang, Z. Cheng and X. Zhu, *Polymer Chemistry*, 2017, **8**, 1495–1506.

[180] J. S. Moore and K. F. Jensen, *Angewandte Chemie - International Edition*, 2014, **53**, 470–473.

[181] C. A. Hone, N. Holmes, G. R. Akien, R. A. Bourne and F. L. Muller, *Reaction Chemistry and Engineering*, 2017, **2**, 103–108.

[182] K. C. Aroh and K. F. Jensen, *Reaction Chemistry and Engineering*, 2018, **3**, 94–101.

[183] K. Golbig, A. Kursawe, M. Hohmann, S. Taghavi-Moghadam and T. Schwalbe, *Chemical Engineering Communications*, 2005, **192**, 620–629.

[184] F. W. Giacobbe, *Journal of Applied Polymer Science*, 1990, **39**, 1121–1132.

[185] S. T. Knox, S. Parkinson, R. Stone and N. J. Warren, *Polymer Chemistry*, 2019, **10**, 4774–4778.

[186] M. A. Vargas, M. Cudaj, K. Hailu, K. Sachsenheimer and G. Guthausen, *Macromolecules*, 2010, **43**, 5561–5568.

[187] D. E. Fitzpatrick, C. Battilocchio and S. V. Ley, *ACS Central Science*, 2016, **2**, 131–138.

[188] S. G. Newman and K. F. Jensen, *Green Chemistry*, 2013, **15**, 1456–1472.

[189] C. M. Bates and F. S. Bates, *Macromolecules*, 2017, **50**, 3–22.

[190] T. Junkers, *Journal of Flow Chemistry*, 2017, **7**, 106–110.

[191] M. Chen, M. J. MacLeod and J. A. Johnson, *ACS Macro Letters*, 2015, **4**, 566–569.

[192] J. Gardiner, C. H. Hornung, J. Tsanaktsidis and D. Guthrie, *European Polymer Journal*, 2016, **80**, 200–207.

[193] T. Junkers and R. Hoogenboom, *European Polymer Journal*, 2016, **80**, 175–176.

[194] B. Charleux, G. Delaittre, J. Rieger and F. D'Agosto, *Macromolecules*, 2012, **45**, 6753–6765.

[195] N. J. Warren, O. O. Mykhaylyk, D. Mahmood, A. J. Ryan and S. P. Armes, *Journal of the American Chemical Society*, 2014, **136**, 1023–1033.

[196] N. J. Warren, M. J. Derry, O. O. Mykhaylyk, J. R. Lovett, L. P. Ratcliffe, V. Ladmiral, A. Blanazs, L. A. Fielding and S. P. Armes, *Macromolecules*, 2018, **51**, 8357–8371.

[197] N. J. Warren, O. O. Mykhaylyk, A. J. Ryan, M. Williams, T. Doussineau, P. Dugourd, R. Antoine, G. Portale and S. P. Armes, *Journal of the American Chemical Society*, 2015, **137**, 1929–1937.

[198] B. Klumperman, E. T. Van Den Dungen, J. P. Heuts and M. J. Monteiro, *Macromolecular Rapid Communications*, 2010, **31**, 1846–1862.

[199] T. Junkers, L. Zang, E. H. Wong, N. Dingenouts and C. Barner-Kowollik, *Journal of Polymer Science, Part A: Polymer Chemistry*, 2011, **49**, 4841–4850.

[200] M. Benaglia, J. Chiefari, Y. K. Chong, G. Moad, E. Rizzardo and S. H. Thang, *Journal of the American Chemical Society*, 2009, **131**, 6914–6915.

[201] B. Y. Chong, J. Krstina, T. P. Le, G. Moad, A. Postma, E. Rizzardo and S. H. Thang, *Macromolecules*, 2003, **36**, 2256–2272.

[202] C. L. Moad, G. Moad, E. Rizzardo and S. H. Thang, *Macromolecules*, 1996, **29**, 7717–7726.

[203] F. Zhong, Y. Zhou and M. Chen, *Polymer Chemistry*, 2019, **10**, 4879–4886.

[204] G. Moad, E. Rizzardo and S. H. Thang, *Polymer*, 2008, **49**, 1079–1131.

[205] K. Jain, R. Vedarajan, M. Watanabe, M. Ishikiriyama and N. Matsumi, *Polymer Chemistry*, 2015, **6**, 6819–6825.

[206] X. Ma and Y. Xing, *Polymer Bulletin*, 2006, **57**, 207–217.

[207] G. E. Parkes, H. J. Hutchins-Crawford, C. Bourdin, S. Reynolds, L. J. Leslie, M. J. Derry, J. L. Harries and P. D. Topham, *Polymer Chemistry*, 2020, **11**, 2869–2882.

[208] X. Wang, J. Zhou, X. Lv, B. Zhang and Z. An, *Macromolecules*, 2017, **50**, 7222–7232.

[209] S. J. Byard, M. Williams, B. E. McKenzie, A. Blanazs and S. P. Armes, *Macromolecules*, 2017, **50**, 1482–1493.

[210] H. Shi, T. Qiu, H. D. Ou-Yang, H. Xu, Q. Lu, Y. Zheng, K. Liu, L. He, L. Guo and X. Li, *Journal of Colloid and Interface Science*, 2019, **545**, 220–230.

[211] P. Biais, P. Beaunier, F. Stoffelbach and J. Rieger, *Polymer Chemistry*, 2018, **9**, 4483–4491.

[212] G. Mellot, P. Beaunier, J. M. Guigner, L. Bouteiller, J. Rieger and F. Stoffelbach, *Macromolecular Rapid Communications*, 2019, **40**, 1800315.

[213] W. Zhou, Q. Qu, Y. Xu and Z. An, *ACS Macro Letters*, 2015, **4**, 495–499.

[214] I. Canton, N. J. Warren, A. Chahal, K. Amps, A. Wood, R. Weightman, E. Wang, H. Moore and S. P. Armes, *ACS Central Science*, 2016, **2**, 65–74.

[215] K. A. Simon, N. J. Warren, B. Mosadegh, M. R. Mohammady, G. M. Whitesides and S. P. Armes, *Biomacromolecules*, 2015, **16**, 3952–3958.

[216] M. Sponchioni, C. T. O'Brien, C. Borchers, E. Wang, M. N. Rivolta, N. J. Penfold, I. Canton and S. P. Armes, *Chemical Science*, 2020, **11**, 232–240.

[217] M. J. Derry, O. O. Mykhaylyk and S. P. Armes, *Angewandte Chemie - International Edition*, 2017, **56**, 1746–1750.

[218] M. J. Derry, T. Smith, P. S. O'Hora and S. P. Armes, *ACS Applied Materials and Interfaces*, 2019, **11**, 33364–33369.

[219] S. Varlas, J. C. Foster, P. G. Georgiou, R. Keogh, J. T. Husband, D. S. Williams and R. K. O'Reilly, *Nanoscale*, 2019, **11**, 12643–12654.

[220] P. Plouffe, A. Macchi and D. M. Roberge, *Organic Process Research and Development*, 2014, **18**, 1286–1294.

[221] R. L. Hartman, J. P. McMullen and K. F. Jensen, *Angewandte Chemie - International Edition*, 2011, **50**, 7502–7519.

[222] E. M. Schuster and P. Wipf, *Israel Journal of Chemistry*, 2014, **54**, 361–370.

[223] G. Gody, R. Barbey, M. Danial and S. Perrier, *Polymer Chemistry*, 2015, **6**, 1502–1511.

[224] J. Morsbach, A. H. Müller, E. Berger-Nicoletti and H. Frey, *Macromolecules*, 2016, **49**, 5043–5050.

[225] S. Kaga, N. P. Truong, L. Esser, D. Senyschyn, A. Sanyal, R. Sanyal, J. F. Quinn, T. P. Davis, L. M. Kaminskas and M. R. Whittaker, *Biomacromolecules*, 2017, **18**, 3963–3970.

[226] S. C. Ligon, B. Husár, H. Wutzel, R. Holman and R. Liska, *Chemical Reviews*, 2014, **114**, 577–589.

[227] J. Yeow, R. Chapman, A. J. Gormley and C. Boyer, *Chemical Society Reviews*, 2018, **47**, 4357–4387.

[228] C. Decker and A. D. Jenkins, *Macromolecules*, 1985, **18**, 1241–1244.

[229] D. R. McKean, U. Schaedeli and S. A. MacDonald, *Journal of Polymer Science Part A: Polymer Chemistry*, 1989, **27**, 3927–3935.

[230] M. J. Derry, L. A. Fielding, N. J. Warren, C. J. Mable, A. J. Smith, O. O. Mykhaylyk and S. P. Armes, *Chemical Science*, 2016, **7**, 5078–5090.

[231] C. Tanford, *Journal of Physical Chemistry*, 1972, **76**, 3020–3024.

[232] T. G. Hiss and E. L. Cussler, *AIChE Journal*, 1973, **19**, 698–703.

[233] I. Kim and S. Li, *Polymer Reviews*, 2019, **59**, 561–587.

[234] S. Salehpour and M. A. Dubé, *Macromolecular Reaction Engineering*, 2012, **6**, 85–92.

[235] B. Wan, C. A. Zordan, X. Lu and G. McGeorge, *AAPS PharmSciTech*, 2016, **17**, 1173–1181.

[236] M. Goldbach, E. Danieli, J. Perlo, B. Kaptein, V. M. Litvinov, B. Blümich, F. Casanova and A. L. Duchateau, *Tetrahedron Letters*, 2016, **57**, 122–125.

[237] L. S. Santos, *European Journal of Organic Chemistry*, 2008, **2008**, 235–253.

[238] R. Hoogenboom, M. W. Fijten, C. H. Abeln and U. S. Schubert, *Macromolecular Rapid Communications*, 2004, **25**, 237–242.

[239] D. C. Fabry, E. Sugiono and M. Rueping, *Reaction Chemistry and Engineering*, 2016, **1**, 129–133.

[240] S. V. Ley, D. E. Fitzpatrick, R. J. Ingham and R. M. Myers, *Angewandte Chemie - International Edition*, 2015, **54**, 3449–3464.

[241] B. J. Reizman, Y. M. Wang, S. L. Buchwald and K. F. Jensen, *Reaction Chemistry and Engineering*, 2016, **1**, 658–666.

[242] Z. Amara, E. S. Streng, R. A. Skilton, J. Jin, M. W. George and M. Poliakoff, *European Journal of Organic Chemistry*, 2015, **2015**, 6141–6145.

[243] V. Darcos, S. Monge and D. M. Haddleton, *Journal of Polymer Science, Part A: Polymer Chemistry*, 2004, **42**, 4933–4940.

[244] H. Çatalgil-Giz, A. Giz, A. M. Alb, A. Öncül Koç and W. F. Reed, *Macromolecules*, 2002, **35**, 6557–6571.

[245] M. E. Levere, I. Willoughby, S. O'Donohue, A. De Cuendias, A. J. Grice, C. Fidge, C. R. Becer and D. M. Haddleton, *Polymer Chemistry*, 2010, **1**, 1086–1094.

[246] C. Rosenfeld, C. Serra, S. O'Donohue and G. Hadziioannou, *Macromolecular Reaction Engineering*, 2007, **1**, 547–552.

[247] G. Moad, E. Rizzardo and S. H. Thang, *Australian Journal of Chemistry*, 2006, **59**, 669–692.

[248] A. Adamo, R. L. Beingessner, M. Behnam, J. Chen, T. F. Jamison, K. F. Jensen, J. C. M. Monbaliu, A. S. Myerson, E. M. Revalor, D. R. Snead, T. Stelzer, N. Weeranoppanant, S. Y. Wong and P. Zhang, *Science*, 2016, **352**, 61–67.

[249] D. Konkolewicz, B. S. Hawkett, A. Gray-Weale and S. Perrier, *Macromolecules*, 2008, **41**, 6400–6412.

[250] C. Houben and A. A. Lapkin, *Current Opinion in Chemical Engineering*, 2015, **9**, 1–7.

Appendix A

Appendix

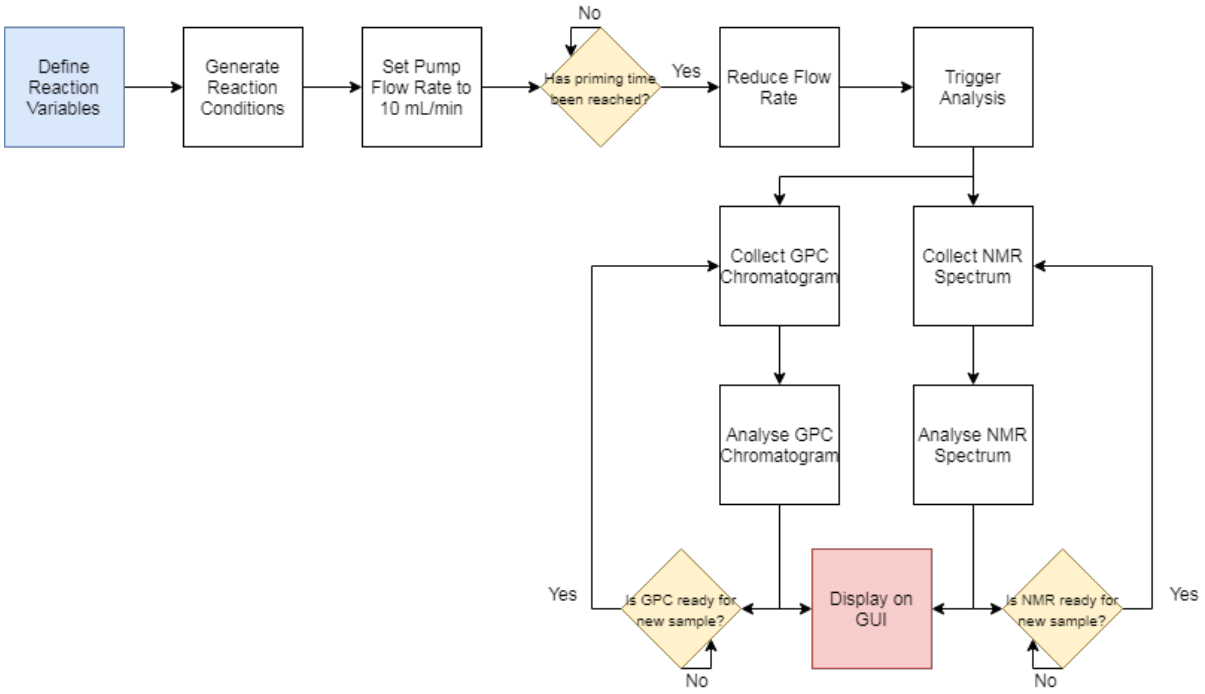

Figure A.1: Flowchart of the algorithm used for transient kinetic profiling on the automated flow reactor.

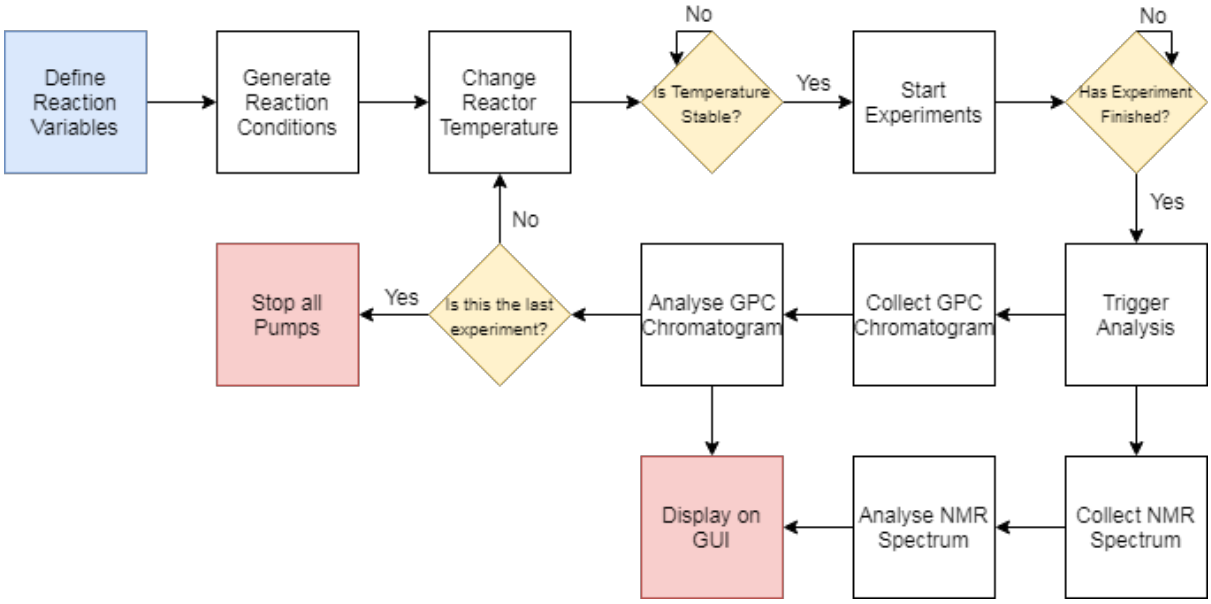

Figure A.2: Flowchart of the algorithm used for steady state kinetic profiling.

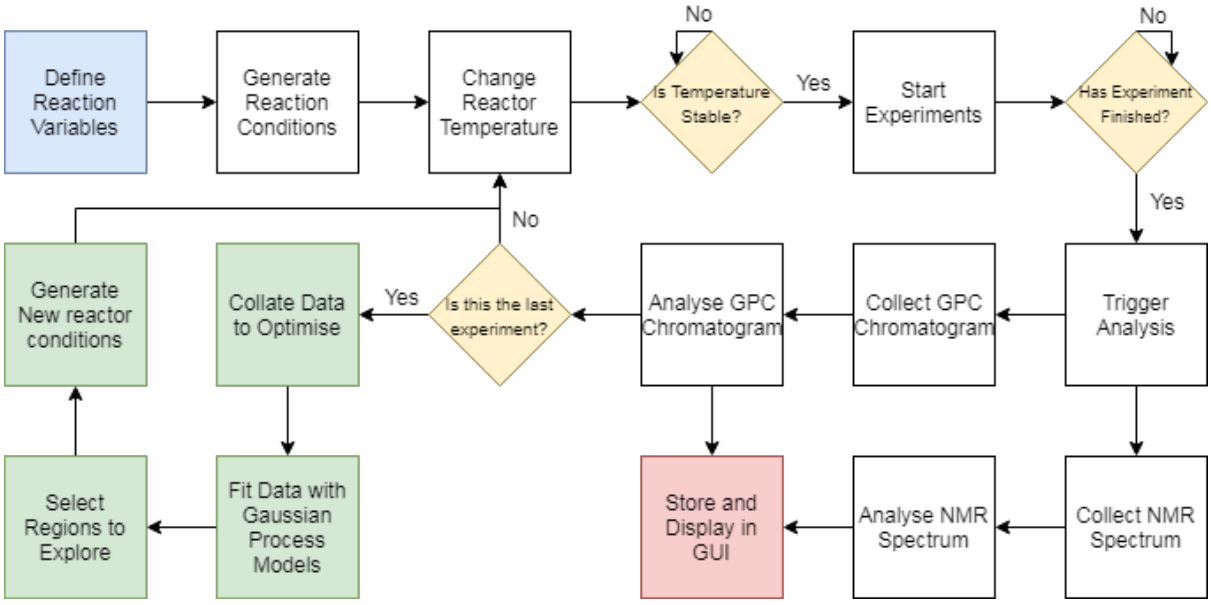

Figure A.3: Flowchart of the algorithm used for multi-objective optimisation.

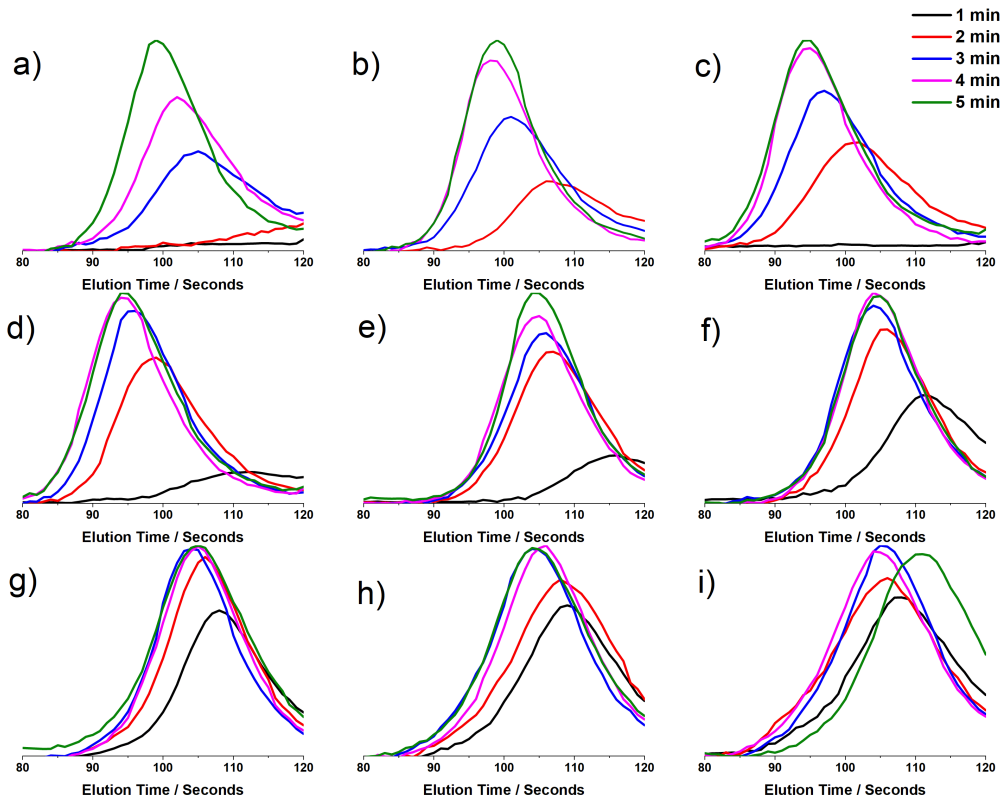

Figure A.4: GPC chromatograms obtained during the automated screen of $PDMAm_{200}$ at a) 80 °C, b) 85 °C, c) 90 °C, d) 95 °C, e) 100 °C, f) 105 °C, g) 110 °C, h) 115 °C and i) 120 °C. All reactions were performed for at 30 % w/w and [DMAm]:[CCTP]:[VA-044] = 200:1:0.02.

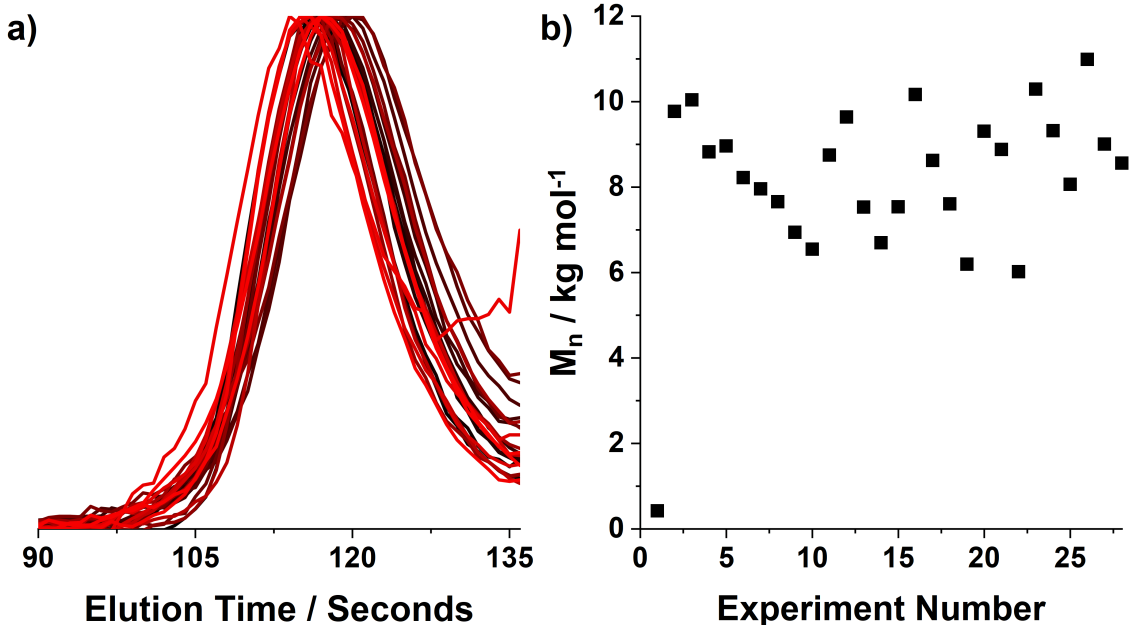

Figure A.5: a) GPC chromatograms (black to red) and b) calculated molecular weights obtained during self-optimisation of the RAFT polymerisation of dimethylacrylamide. All reactions were performed for at 30 % w/w and [DMAm]:[CCTP]:[VA-044] = 200:1:0.02.

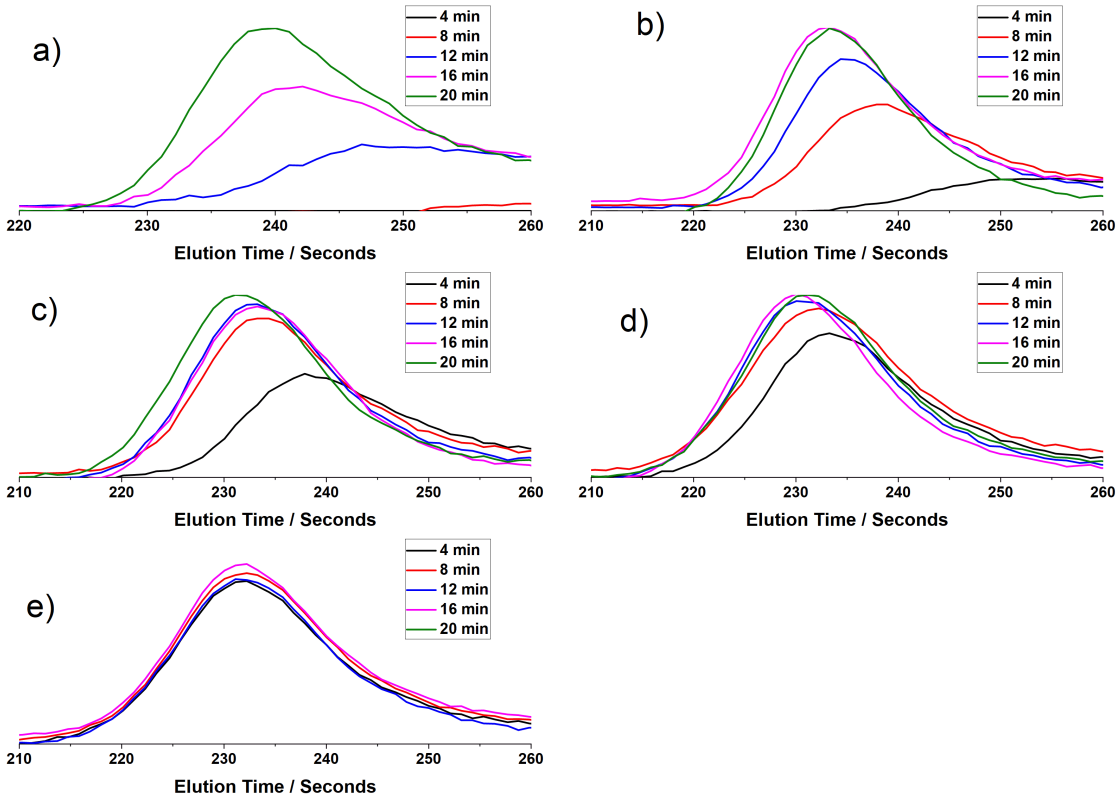

Figure A.6: GPC chromatograms obtained during the automated screen of $PtBuAm_{200}$ at a) 80 °C, b) 90 °C, c) 100 °C, d) 110 °C and e) 120 °C. All reactions were performed for at 30 % w/w and [tBuAm]:[CCTP]:[AIBN] = 200:1:0.1.

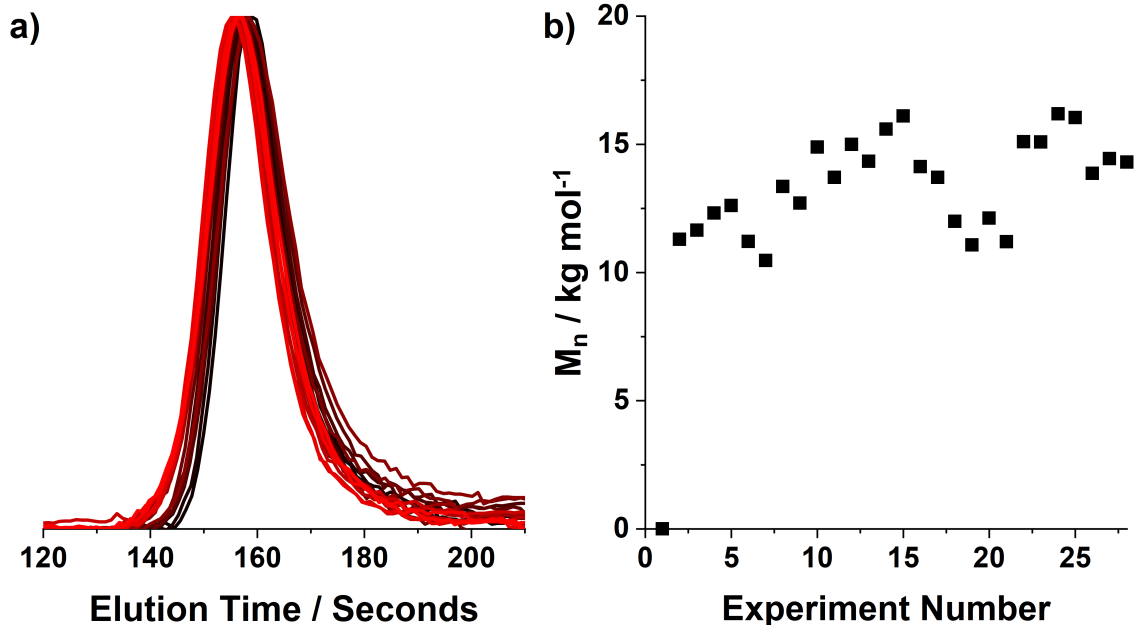

Figure A.7: a) GPC chromatograms (black to red) and b) calculated molecular weights obtained during self-optimisation of the RAFT polymerisation of *tert*-butylacrylamide. All reactions were performed for at 30 % w/w and [tBuAm]:[CCTP]:[AIBN] = 200:1:0.1.

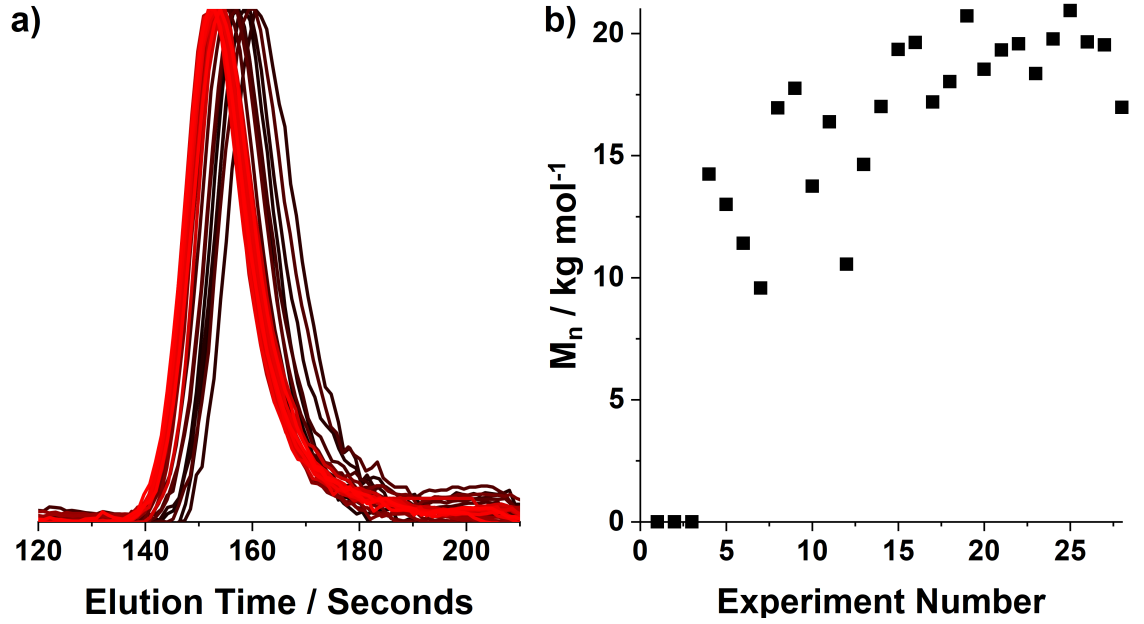

Figure A.8: a) GPC chromatograms (black to red) and b) calculated molecular weights obtained during self-optimisation of the RAFT polymerisation of *tert*-butylacrylamide. All reactions were performed for at 30 % w/w and [tBuAm]:[DCTTC]:[AIBN] = 200:1:0.1.

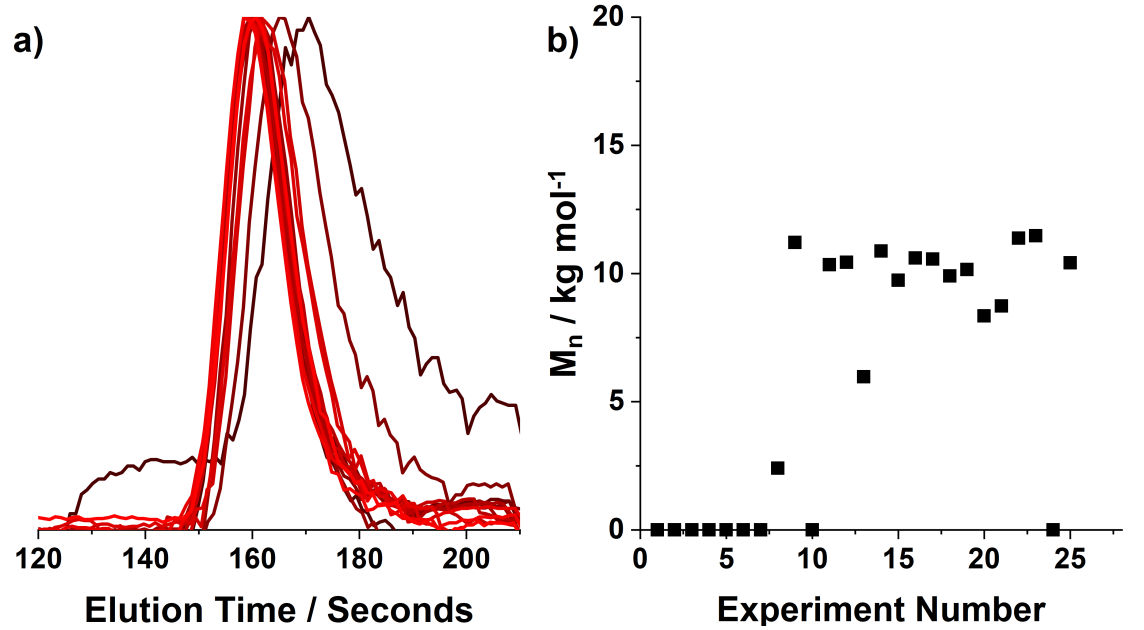

Figure A.9: a) GPC chromatograms (black to red) and b) calculated molecular weights obtained during self-optimisation of the RAFT polymerisation of *tert*-butylacrylamide. All reactions were performed for at 30 % w/w and [tBuAm]:[CPMT]:[AIBN] = 200:1:0.1.